Search for α condensed states in ^{13}C using α inelastic scattering

Kento Inaba

Doctoral Dissertation

Department of Physics, Kyoto University

January, 2022

Abstract

α condensation in atomic nuclei is of great interest in the modern nuclear physics. In α condensates, all α clusters are condensed into the same lowest-energy orbit like the atomic Bose-Einstein condensation. Since they have a very narrow momentum distribution around zero, their density becomes much lower than the saturation density. Very recently, it was proposed that the α condensation reduces the internal energy of cold dilute nuclear matter. Because it is inferred that the energy gain due to the α condensation is suppressed in the asymmetric nuclear matter, the α condensation induces the strong isospin dependence of the equation of state of the dilute nuclear matter. However, it is not trivial that the α condensation really occur in the dilute nuclear matter, therefore it must be confirmed by experiments.

Although we cannot directly investigate infinite nuclear matter in the laboratory, we can get some clues to the α condensation in dilute nuclear matter through experimental searches for α condensates in finite nuclei (α condensed states) over a wide range of the mass number and isospin. If the α condensed states universally exist in various nuclei, it will demonstrate that the α condensate is a trivial conformation in dilute nuclear many-body systems. Many theoretical and experimental efforts have been devoted to establish the α condensed states and to reveal their nature. However, the scope of these studies has been limited to self-conjugated $A = 4k$ nuclei. Few studies have discussed the α condensation in $A \neq 4k$ nuclei with non-zero isospin, so far.

In the present work, we searched for the α condensed state in ^{13}C as the first step for the systematic exploration into non self-conjugated $A \neq 4k$ nuclei. Since the isoscalar monopole ($IS0$) and dipole ($IS1$) transitions induce density changes of nuclei, these transitions are suitable to excite α condensed states with dilute densities from the ground state. Therefore, we measured the α inelastic scattering off ^{13}C at $E_\alpha = 388$ MeV at forward angles including 0° where the cross sections for the $IS0$ and $IS1$ transitions are large in order to precisely measure the strengths of these transitions.

We found a bump structure around $E_x = 12.5$ MeV in ^{13}C due to the $IS0$ transition. A peak-fit analysis suggested that this bump consisted of several $1/2^-$ states. It could be speculated that these $1/2^-$ states were candidates for the α condensed state, but the $3\alpha + n$ orthogonality condition model suggests that the α condensed state is unlikely to emerge as the negative parity states. We also found the two $1/2^+$ or $3/2^+$ states at $E_x = 14.5$ and 16.1 MeV in ^{13}C populated by the $IS1$ transition. We proposed that the 16.1-MeV state is a possible candidate for the α condensed state predicted by the cluster-model calculations on the basis of the good correspondence between the experimental and calculated level structures. However, the theoretical $IS1$ transition strengths for these states are significantly smaller than the measured values. Further experimental information is strongly desired to establish the α condensed state in ^{13}C.

Contents

Chapter 1

Introduction

1.1 Cluster structure in nuclei

An atomic nucleus is a quantum many-body system consisting of protons and neutrons. One of the most notable properties of nuclei is the appearance of magic numbers. Nuclei with proton numbers Z or neutron numbers N of 2, 8, 20, 28, 50, and 126 have larger binding energies and are more stable than other nuclei. These properties are similar to those of the noble gas elements which are more stabilized than other elements in the periodic table. This analogy suggests that nucleons form a shell structure in nuclei as electrons in atoms. Mayer and Jensen proposed the jj-coupling shell model in 1949 [1–4], which nicely explained the magic numbers, spin and parity of the ground state, magnetic moment, and other properties of nuclei. In the shell-model picture of nuclei, constituent particles of nuclei are nucleons, and nucleons occupy single-particle orbits formed by the mean-field potential.

Various properties of nuclei are described using the degrees of freedom of nucleons with independent-particle motions in the mean-field potential. However, an atomic nucleus is a complicated many-body system having a huge number of degrees of freedom, and the shell-model approach is an approximation to describe an aspect of nuclei. Another aspect of nuclei, which cannot be described by the shell model, is the cluster structures. It is widely known that several nucleons get together to form clusters as tightly bound subunits in nuclei. The shell model cannot explain the properties of nuclei arising from relative motion of the clusters, but a cluster model of nuclei which explicitly takes into account the clustering degrees of freedom reasonably describes them. This fact is the manifestation of the so-called dual nature of nuclei. It is thus important to examine exotic structures arsing from the clustering degrees of

freedom for better understanding of atomic nuclei.

The history of the cluster model goes back to the dawn of the nuclear physics, before the discovery of the neutron. Rutherford and Gamow proposed an idea that α particles exist as stable components in nuclei [5]. Wefelmeier proposed a cluster model of nuclei in the early days, called as the alpha-particle model at that time, in which nuclei was composed of a collection of α particles [6]. Although this model was primitive for describing the nuclear structures, it made some success in explaining the binding energies of light self-conjugated ($N = Z$) nuclei with mass numbers $A = 4k$ [6, 7]. Later, Brink and Bloch developed a more realistic microscopic cluster model taking into account the nucleon degrees of freedom [8]. The wave function of a nucleus consisting of k clusters is expressed in the Brink-Bloch model as

$$\Psi(\boldsymbol{R}_1, \boldsymbol{R}_2, \cdots, \boldsymbol{R}_k) = \mathcal{N}_0 \mathcal{A}[\psi(\mathrm{C}_1, \boldsymbol{R}_1)\psi(\mathrm{C}_2, \boldsymbol{R}_2) \cdots \psi(\mathrm{C}_k, \boldsymbol{R}_k)], \tag{1.1}$$

where $\psi(\mathrm{C}_i, \boldsymbol{R}_i)$ denotes the antisymmetrized wave function for the cluster C_i at the spatial point $\boldsymbol{R}_i$. $\mathcal{N}_0$ is a normalization constant and $\mathcal{A}$ is the antisymmetrizer of nucleons between different clusters. One of the victories of the microscopic cluster model is that it successfully describes the level structure of the natural-parity states in ^{12}C. The 0_2^+ state at $E_x = 7.65$ MeV in ^{12}C was reproduced by the microscopic cluster model [9–11] although the shell-model calculations could not reproduce this state at such a low excitation energy [12–14]. Therefore, the 0_2^+ state is considered to have well developed cluster structure unlike the shell-model-like structure.

When do the clustering degrees of freedom manifest in nuclei? The cluster structures are expected to develop in nuclei when their energies are close to the cluster-decay thresholds. This threshold rule is established on the fact that the interaction between α clusters is relatively week, while protons and neutrons are tightly bound in the α clusters. The Ikeda diagram schematically demonstrates this threshold rule in light self-conjugated $A = 4k$ nuclei as shown in Fig.1.1 [15]. The Ikeda diagram suggests that nuclei with shell-model-like structures in the ground state change to different cluster structures near various cluster-decay thresholds. The 0_2^+ state in ^{12}C is a typical example of the α-cluster state, which is located about 400 keV above the 3α-decay threshold. Many theoretical and experimental studies have been devoted to explore the cluster states in various nuclei near or above the threshold energies (see, e.g., Ref. [9, 16, 17]).

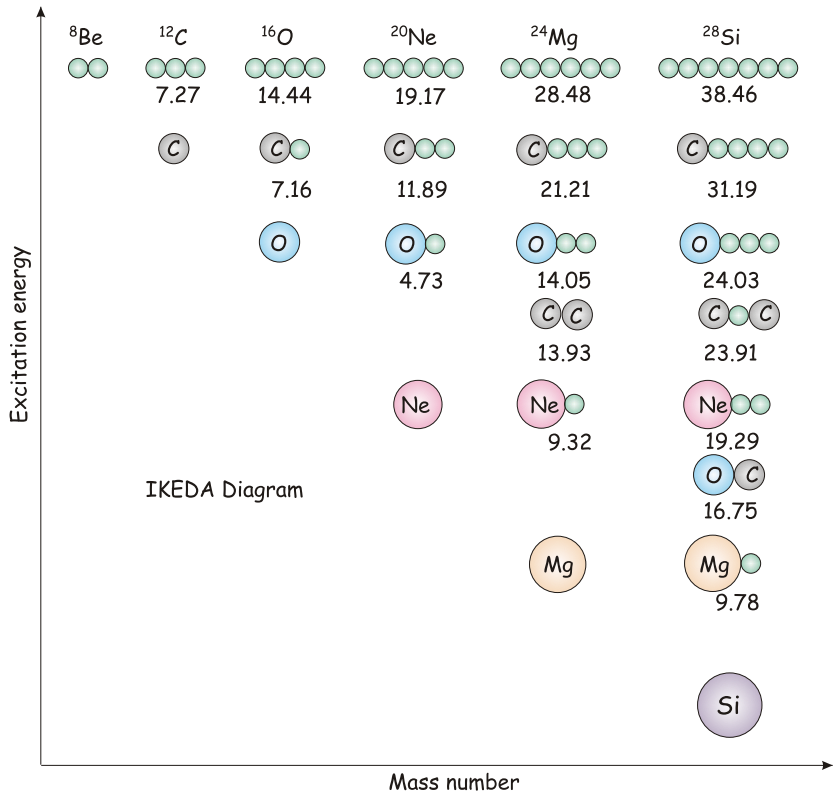

Figure 1.1: Ikeda diagram showing the relation between threshold energy to each decay mode and the cluster structure. Taken from Fig. 1 in Ref. [18]. The small circles without alphabets show the α particles. The threshold energy to each decay mode from the ground state is shown in the unit of MeV.

1.2 Nuclear clusters in astrophysics

Clustering in nuclei is crucial not only for describing nuclear structures but also for the stellar nucleosynthesis. After a star is formed by gravitational attraction, hydrogen burning will start once its central temperature and density reach $T \sim 1.0$–1.5×10^7 K and $\rho \sim 10^2$ g/cm^3. There are two types of the hydrogen burning processes. One is the proton-proton chain, which is the main process of hydrogen burning in stars with $M \lesssim 1.1\mathrm{M}_\odot$ and in first stars where no heavy elements exist. The other is the CNO cycle, which is dominant in stars with $M \gtrsim 1.1\mathrm{M}_\odot$. Four protons convert into one α particle with two positrons, two electron neutrinos, and released energy of 26.73 MeV in both processes of the hydrogen burning. A large number of α particles is produced in stars by the process. However, α particles cannot form any binary bound states with themselves, with protons, nor with neutrons since there

are no stable nuclei with $A = 5$ or 8. Therefore, nuclei of mass $A \geq 9$ are rarely produced in stars by the hydrogen burning. It was a serious puzzle in physics until 1950's how heavy elements such as ^{12}C and ^{16}O were synthesized in the universe.

The decisive key to solve this puzzle is the triple-α reaction. In the triple-α reaction, two α particles constitute a narrow resonance in ^{8}Be, and another α particle collides with the resonance to form ^{12}C. However, the non-resonant direct triple-α reaction cannot produce ^{12}C as much as observed in the universe. Sir Fred Hoyle pointed out in 1954 that there must be a narrow 3α resonance with the spin and parity of 0^+ slightly above the 3α-decay threshold to explain the cosmic abundance of ^{12}C [19]. This predicted resonance formed by a $^{8}\mathrm{Be} + \alpha$ collision can decay into the ground state in ^{12}C and enhance the triple-α reaction rate. Later, this 0^+ resonance was observed by experiments [20, 21] just above the 3α and $^{8}\mathrm{Be} + \alpha$ decay thresholds as shown in Fig. 1.2. Now, this state is known as the Hoyle state. The Hoyle state decays to the ground state by γ emission via the 2^+_1 state or by direct e^+e^- creation. The ^{12}C and ^{16}O nuclei are produced by helium burning such as the triple-α reaction and $^{12}\mathrm{C}(\alpha,\gamma)^{16}\mathrm{O}$ reaction. Then, the stellar nucleosynthesis will proceed to heavier nuclei.

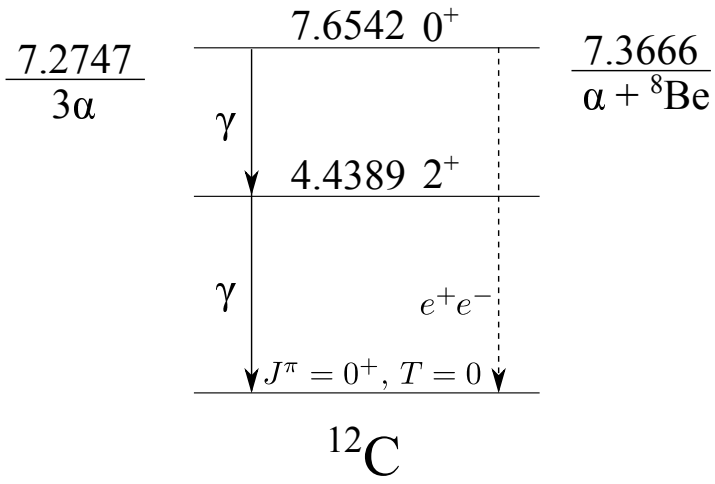

Figure 1.2: Energy level diagram for the relevant states to the triple-α reaction in ^{12}C. The 3α and $^{8}\mathrm{Be} + \alpha$ decay thresholds are also presented.

Particles in stars are in thermal equilibrium and have a velocity distribution according to the Maxwell-Boltzmann statistics. Since the central temperature in a normal star is $T \sim 10^{7-8}$ K, the mean particle energy is about as low as a few keV. Therefore, the existence of a resonant state slightly above the cluster decay threshold is essential not only in the triple-α reaction but also in the entire nucleosynthesis. The Cluster-Nucleosynthesis diagram [22]

schematically explains the nuclear reactions involving various clusters in nucleosynthesis as shown in Fig. 1.3. The reaction process starts with the triple-α reaction in the upper left of Fig. 1.3, and it proceeds to the lower right until the Fe production. It should be mentioned that this Cluster-Nucleosynthesis diagram is very similar to the Ikeda diagram (Fig. 1.1). The cluster structures in nuclei play the important role in nucleosynthesis after helium burning.

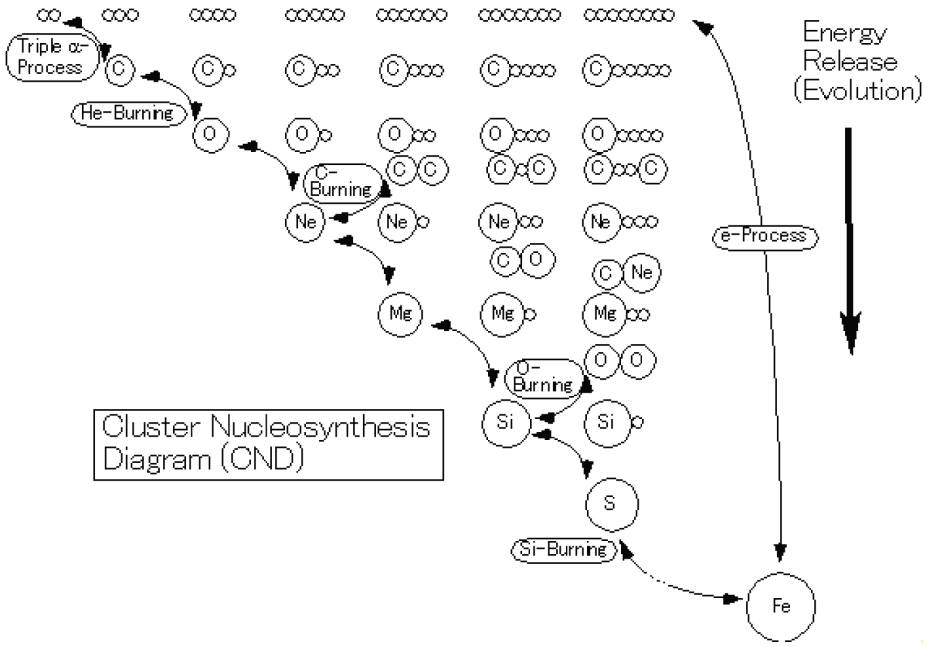

Figure 1.3: Cluster-Nucleosynthesis diagram for nucleosynthesis along the stellar evolution. Taken from Fig. 1 in Ref. [23]. The small open circles indicate α particles. The processes going to lower levels imply energy release.

1.3 α condensation in $A = 4k$ nuclei

As discussed in Sec. 1.1, the 0_2^+ state in ^{12}C is considered to have well-developed 3α-cluster structure. In the early days, it was suggested that the 0_2^+ state might have a linear configuration of three α clusters [24,25]. In recent years, it has been pointed out that this state is the α condensed state in which the three α clusters occupy the same $0S$ orbit like the atomic Bose-Einstein condensation (BEC) [26–28]. According to the 3α orthogonality condition model (OCM) calculation [28], the 3α clusters in the 0_2^+ state are condensed into the $0S$ orbit with a high occupancy about 70%. This calculation suggests that the momentum distribution of

the α clusters has a sharp peak like a δ-function around 0 fm^{-1} as shown in Fig. 1.4(a). The density distribution of the α clusters is obtained by the Fourier transform of the momentum distribution. Reflecting this δ-function-like momentum distribution, the 0_2^+ state has more spatially expanded and lower density distribution than that of the ground state as shown in Fig. 1.4(b). Therefore, the 0_2^+ state is considered to be a low-density cluster gas state whose radius is about twice as large as the radius of the ground state.

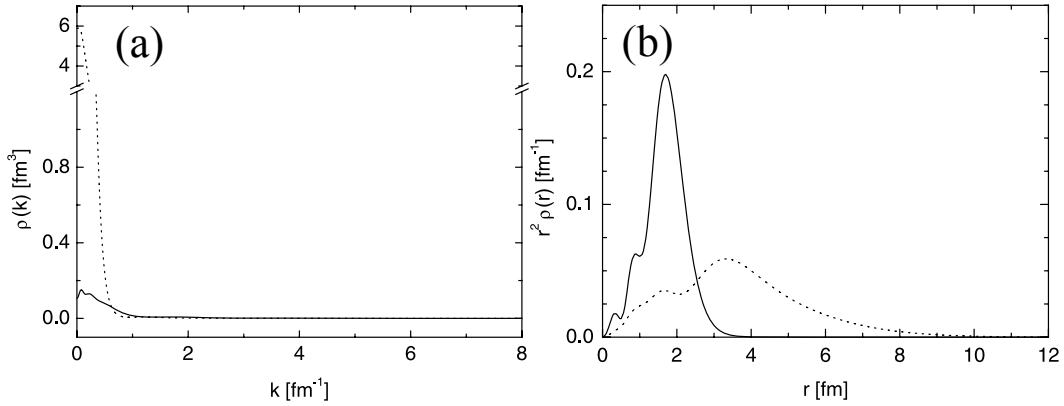

Figure 1.4: (a) Momentum and (b) density distribution of the α clusters in the ground state and the 0_2^+ state in ^{12}C obtained by the 3α OCM calculation. (a) and (b) are taken from Figs. 2 and 7 in Ref. [28], respectively. The solid and dashed lines correspond to the ground state and the 0_2^+ state, respectively.

Does the cluster-gas state with similar properties to the 0_2^+ state exist in heavier self-conjugated $A = 4k$ nuclei? Alpha clusters are loosely confined in the cluster-gas state by a barrier formed by the short-range nuclear potential and the long-range Coulomb potential. As the number of the α clusters in the gas state is increased, the mean distance between the α clusters are getting larger. Then, the repulsive contribution from the long-range Coulomb interaction is beating the attractive one from the short-range nuclear force. Since the potential felt by the α clusters becomes shallow, the α condensed state can no longer metastably exist in nuclei at a critical number of the α clusters $k = k_{cr}$. According to the theoretical calculation with the Gross-Pitaevskii and Hill-Wheeler equations by Yamada and Schuck [29], the $k\alpha$ condensed state can exist in nuclei up to $k_{cr} \sim 10$, namely ^{40}Ca.

Although candidates for the $k\alpha$ condensed state have been established in light nuclei such as ^{8}Be and ^{12}C [30–33], there is still no sufficient experimental evidence in heavier nuclei. Figure 1.5 shows the predicted energies of the $k\alpha$ condensed states measured from each $k\alpha$-decay threshold [29]. The excitation energy of the $k\alpha$ condensed state becomes higher as the

value of k increases. For example, the 5α condensed state in ^{20}Ne is predicted at $E_x = 22.1$ MeV, and the 6α condensed state in ^{24}Mg is predicted at $E_x = 33.4$ MeV. It is not easy to identify the α condensed state in such a high excitation-energy region since the level density of nuclei becomes high. Experimental searches for the $k\alpha$ condensed states are being intensively carried out in nuclei such as ^{16}O [34–37], ^{20}Ne [38], ^{24}Mg [39], and ^{28}Si [40].

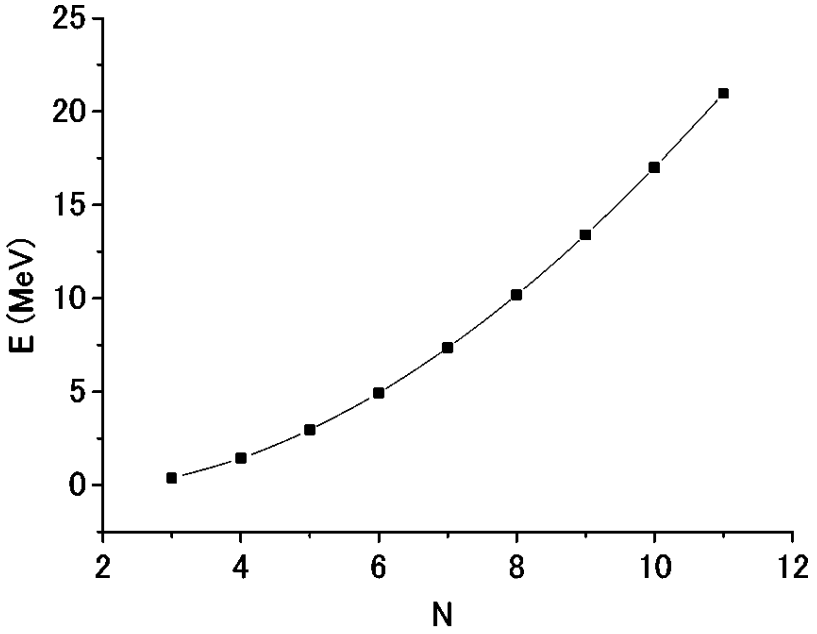

Figure 1.5: Energies of the $k\alpha$ condensed states measured from each $k\alpha$-decay threshold. Taken from Fig. 2 in Ref. [29]. N in the figure corresponds to k in the text.

1.4 Effects of the α condensation on the nuclear matter

Construction of the equation of state (EoS) of nuclear matter is one of the ultimate goal in nuclear physics because it is not only the benchmark for our understanding of the strongly interacting fermionic many-body systems but also the essentials for a clarification of internal structures of the neutron stars and core-collapse supernovae. Conventionally, the internal energy per nucleon $E_{\rm int}(n,\ \delta,\ T)$ of nuclear matter at given density n and temperature T can be expanded in powers of isospin asymmetry $\delta = (n_n - n_p)/(n_n + n_p)$ as

$$E_{\rm int}(n,\ \delta,\ T) = E_{\rm int}(n,\ 0,\ T) + E_{\rm sym}(n,\ T)\delta^2 + \mathcal{O}(\delta^4), \tag{1.2}$$

where $E_{\rm sym}$ is called the symmetry energy. Equation (1.2) is known as the EoS of nuclear matter. Since the astrophysical phenomena such as the neutron stars and supernovae cover broad ranges of densities and charge asymmetries, comprehension on the isospin dependence of the EoS over a wide-density range of $n/n_0 \sim 0$–10 is necessary.

Very recently, it has been pointed out that the α condensation causes a drastic change in the property of dilute nuclear matter [41–44]. Below the nuclear saturation density ($n_0 \approx 0.16$ fm^{-3}), nuclear matter can no longer be homogeneous and minimize its energy by forming light clusters such as deuteron, triton, ^{3}He, and α particle. Since the α particle has the largest binding energy of 28 MeV and is the most stable species among these clusters, almost all of the constituent clusters are the α particles in dilute nuclear matter around $\delta \sim 0$ at low temperatures below about 1 MeV [42, 45]. Since the α particles are bosons, the BEC of the α particles, *i.e.* α condensation, can occur when the temperature is lower than the critical point.

One of the remarkable effects of the α condensation is a reduction of the internal energy of dilute nuclear matter. Figure 1.6 shows the internal energy $E_{\rm int}$ per nucleon in the nuclear matter at $T = 0$ MeV as a function of the baryon density $n_{\rm B}$ with (thick curves) and without (thin curves) taking into account the α condensation calculated by the generalized nonlinear relativistic mean-field (gNL-RMF) model with the FSUGold interaction [42]. $E_{\rm int}$ with the α condensation becomes lower than that without the α condensation at lower densities. This reduction of $E_{\rm int}$ is explained by the fact that the system gains additional binding energy by forming α clusters. It should be noted that, at low-density limit, $E_{\rm int}$ with the α condensation increases with δ, whereas $E_{\rm int}$ without the α condensation converges at 0 MeV independent of δ. This introduces strong isospin dependence of cold dilute nuclear matter.

The above discussions are based on the assumption that the α condensation occurs in cold dilute nuclear matter, however, this is not trivial. We must confirm the existence of the α condensation in dilute nuclear matter by experiments. Since we cannot directly access infinite nuclear matter, we should hunt for clues to the α condensation through experimental searches for the α condensed states in finite nuclei. If the α condensed states universally exist in various nuclei over a wide range of the mass number and isospin, it will demonstrate that the α condensate is a trivial confirmation in dilute nuclear many-body systems. In addition, the structual information on the α condensed states such as their energies and decay widths will give an insight into $E_{\rm int}$ in dilute nuclear matter by restricting theoretical models.

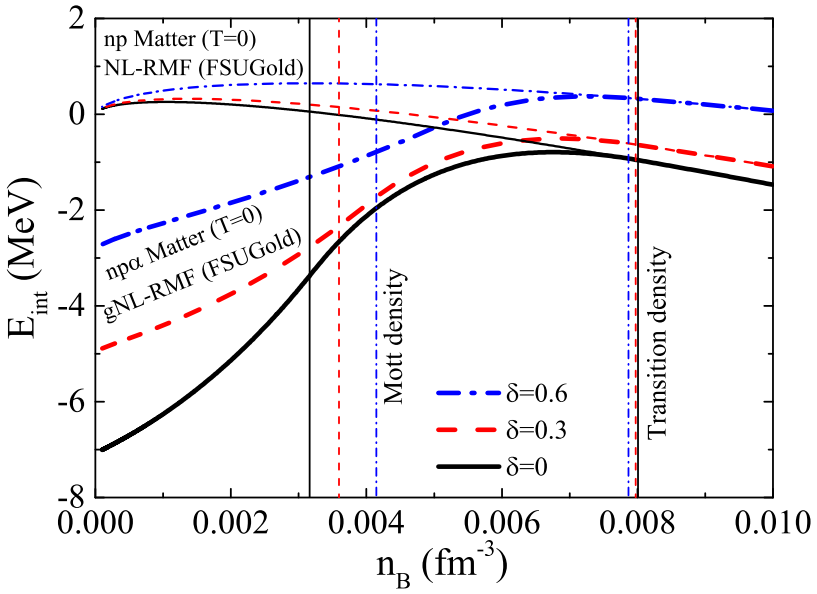

Figure 1.6: Internal energy per nucleon as a function of the baryon density with (thick curves) and without (thin curves) considering the α condensation. Calculated results for various isospin asymmetries $\delta = 0$, 0.3, and 0.6 are displayed. Taken from Fig. 2 in Ref. [42].

1.5 α condensation in $A \neq 4k$ nuclei

There have been a lot of experimental and theoretical investigations of the α condensed states, however, the scope of these studies are limited to self-conjugated $A = 4k$ nuclei. Therefore, it is an urgent issue to investigate the α condensed states in $A \neq 4k$ nuclei in order to check whether the α condensed states universally exist in finite nuclei.

Several pioneering studies of the α condensation in non self-conjugated $A \neq 4k$ nuclei are reviewed in the following sections.

1.5.1 Case in ^{11}B

Kawabata *et al.* [46] measured the transition strengths for the spin-flip $M1$ and Gamow-Teller (GT) transitions from the ground state to the excited states in ^{11}B and its mirror states in ^{11}C. This measurement was originally performed to evaluate the cross sections for the neutral-current and charged-current transitions by the stellar neutrino, but the measurement revealed that the spin-flip $M1$ and GT strengths for the $3/2^-_3$ states are abnormally quenched in comparison with the other states. In addition, the $3/2^-_3$ state was not well described by the shell-model calculations, although the other states including the ground state were

successfully described. On the basis of these facts, the $3/2^-_3$ state in ^{11}B was suggested to have a non-shell-model-like structure in Ref. [46].

Soon after this measurement, Kawabata *et al.* [47] reported that the $3/2^-_3$ state is excited from the ground state with the large isoscalar monopole ($IS0$) strength. The experimental value of the $IS0$ transition strength is $B(IS0,\ \text{g.s.} \rightarrow 3/2^-_3) = 96 \pm 16$ (fm^4) [47], which is comparable to that from the ground state to the 0^+_2 state in ^{12}C, $B(IS0,\ \text{g.s.} \rightarrow 0^+_2) = 121 \pm 9$ (fm^4) [48]. This large $IS0$ transition strength is successfully explained by the antisymmetrized molecular dynamics (AMD) calculation although the shell-model calculation cannot reproduce such a large $IS0$ transition. The excitation energy of the $3/2^-_3$ state in ^{11}B is $E_x = 8.56$ MeV, which is close to the α decay threshold at $E_x = 8.66$ MeV. This situation is similar to the 0^+_2 state in ^{12}C where the 0^+_2 state is located at about 400-keV above the α-decay threshold. Therefore, the $3/2^-_3$ state in ^{11}B has been proposed to have a spatially developed $2\alpha + t$ cluster structure akin to the 0^+_2 state in ^{12}C [47]. This fact implies that the dilute nature of the 0^+_2 state is preserved even if one α cluster is replaced by a triton. Actually, the various nuclear-model calculations have pointed out the dilute nature of the $3/2^-_3$ state [49–51]. It was speculated that this state was the α condensed state with an additional P-wave triton. However, the theoretical calculations showed that this state could not be regarded as the α condensed state with a triton since the 2α clusters did not fully condense into the same $0S$ orbit. Instead, the α condensed state in which the constituent clusters were condensed into the $0S$ orbit was predicted to be the $1/2^+$ state locating at $E_x = 11.85$ MeV about 750 keV above the $2\alpha + t$ threshold [49]. This predicted $1/2^+_2$ state has never been experimentally established, and the existence of the α condensed state in ^{11}B is still under discussion.

1.5.2 Case in ^{13}C

It is interesting to see whether the α condensed nature of the 0^+_2 state in ^{12}C still remains when an extra neutron is added to the 0^+_2 state. Two state-of-the-art theoretical studies on the α condensed state in ^{13}C were published in Refs. [52, 53]. One is based on the full four-body $3\alpha + n$ OCM calculation [52]. The total wave function of ^{13}C in the $3\alpha + n$ OCM, $\Psi(^{13}\text{C})_{\text{OCM}}$, is expressed by the product of the internal wave functions of 3α clusters $\phi(\alpha)$ and the relative wave function among the 3α clusters and the excess neutron $\Phi(^{13}\text{C})$ as

$$\Psi(^{13}\text{C})_{\text{OCM}} = \Phi(^{13}\text{C})\phi(\alpha_1)\phi(\alpha_2)\phi(\alpha_3). \tag{1.3}$$

This $3\alpha+n$ OCM explicitly incorporates the clustering degrees of freedom, and its model space fully covers various cluster configurations such as $3\alpha + n$, $^9\mathrm{Be} + \alpha$, $^{12}\mathrm{C} + n$, and $^8\mathrm{Be} +^5$ He as well as a part of the shell-model-like configurations. The $3\alpha + n$ OCM calculation predicts that several $1/2^{\pm}$ excited states in ^{13}C with spatially developed cluster structures emerge near the $3\alpha + n$ threshold at $E_x = 12.2$ MeV. An excess P-wave neutron couples to the $^{12}\mathrm{C}(0_2^+)$ core in the $1/2^-$ states, whereas an S-wave neutron couples to the core in the $1/2^+$ states. This calculation suggests that the $1/2_5^+$ state predicted at $E_x = 14.9$ MeV is the α condensed state with an excess neutron where the three α clusters and the excess neutron occupy the $(0S)_\alpha^3(0S)_\nu$ configuration.

The other study is based on the AMD calculation [53]. The AMD approach treats nucleon degrees of freedom independently without an *a priori* assumption of existence of clusters. The wave function in the AMD approach $\Psi(^{13}\mathrm{C})_{\mathrm{AMD}}$ is given by a Slater determinant of single-nucleon Gaussian wave functions ϕ_i as

$$\Psi(^{13}\mathrm{C})_{\mathrm{AMD}} = \mathcal{A}\{\phi_1\phi_2\cdots\phi_{13}\}. \tag{1.4}$$

The central positions and intrinsic-spin orientations for all nucleons are determined independently by energy variation. Although the AMD explicitly takes only the nucleon degree of freedom into account, it can describe various cluster structures as a result of an energy variation if the system favors a specific cluster structure. Since the AMD wave function can also describe the shell-model configurations, the AMD is superior in the description of both the cluster and mean-field features for the ground and excited states of nuclei. The AMD proposes that the $1/2_2^+$ state predicted at $E_x = 15.4$ MeV is the α condensed state [53]. The density distributions of the ground state and the $1/2_2^+$ state calculated by the AMD are shown in Fig. 1.7. Compared to the ground state with a shell-model-like compact structure, the $1/2_2^+$ state has a spatially expanded and dilute density distribution.

Figure 1.8 compares the experimental level diagrams [48] for the $1/2^{\pm}$ states in ^{13}C with those calculated by the OCM [52], AMD [53], and shell model with the SFO interaction [96]. The existence of the $1/2^{\pm}$ states with spatially developed cluster structure predicted near the $3\alpha + n$ threshold by the OCM and AMD calculations has not been experimentally confirmed yet. Therefore, it is important to conduct an experimental search for these $1/2^{\pm}$ states in order to confirm whether the α condensed state still exists in ^{13}C, irrespective of additional one neutron. Since the shell-model calculation also predicts several $1/2^{\pm}$ states near the $3\alpha+n$ threshold, we should determine whether the observed states have shell-model-like or cluster

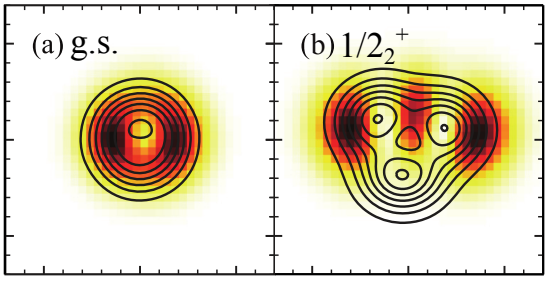

Figure 1.7: Density distributions of (a) the ground state and (b) the $1/2_2^+$ state in ^{13}C calculated by the AMD [53]. The contour plots indicate the matter density distribution while the color plots indicate the valence neutron density distribution. Taken from Fig. 3 in Ref. [53].

configurations by the detailed comparison with the theoretical models.

1.6 Probes for cluster states

Transition strengths between the ground and excited states are given by the overlap between the wave functions for both states. We can get some clues to the structure of nuclei from the transition strengths since they provide information on the nuclear wave function.

It has been pointed out that the $IS0$ transition strength is a key observable to explore the spatially developed cluster states [47, 54]. The $IS0$ transition operator is given by

$$O^{IS0} = \sum_{i=1}^{A} r_i^2, \tag{1.5}$$

where the summation runs over all nucleons i. Because this operator causes a density change in nuclei, it is useful to populate dilute cluster states from the ground state. It should be noted the reason why the $IS0$ transition operator can excite spatially developed cluster states in spite of large difference in the structure between spatially developed cluster states and the compact ground state. On the basis of the Bayman-Bohr theorem [55], Yamada *et al.* [54] pointed out that the clustering degrees of freedom inherently exist even in the ground state, which is reasonably described with the shell-model wave function because the shell-model wave function for the ground state is mathematically equivalent to the α cluster-model wave function at the $SU(3)$ limit. This is called "dual nature of the ground state" [54]. It is naturally expected that spatially developed cluster states can be excited by stimulating

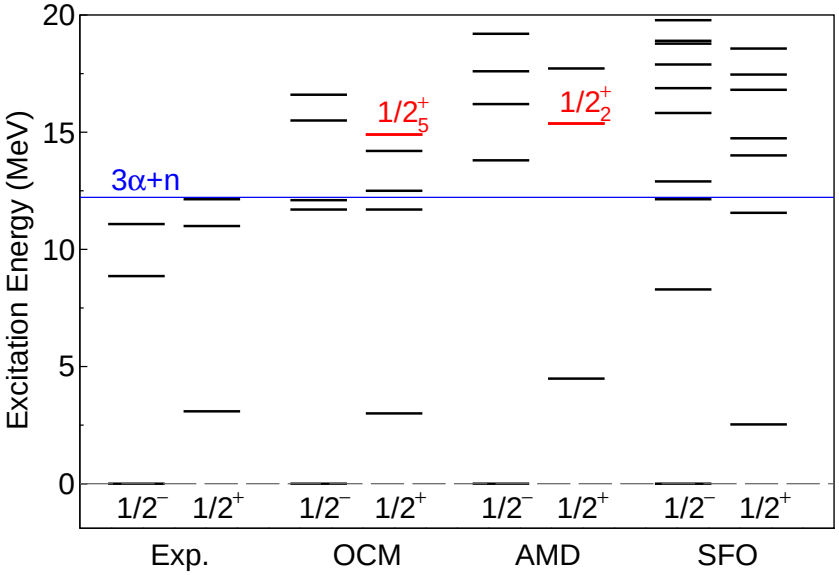

Figure 1.8: Experimental level diagrams [48] for the $1/2^{\pm}$ states in ^{13}C compared with those calculated by the OCM [52], AMD [53], and shell model with the SFO interaction [96]. The solid blue line shows the $3\alpha + n$ threshold at $E_x = 12.2$ MeV. The theoretical candidates for the α condensed states are presented by the red texts.

relative motions of the α clusters in the ground state with the $IS0$ transition operator.

It has been recently pointed out that the isoscalar dipole ($IS1$) transition is also useful probes for exploring cluster states in addition to the $IS0$ transition [56–58]. The $IS1$ transition operator is given as

$$O_{\mu}^{IS1} = \sum_{i=1}^{A} r_i^3 Y_{1\mu}(\Omega_i). \tag{1.6}$$

Since the $IS1$ transition is also compressional mode, the cluster states can be excited in the same mechanism as the $IS0$ transition.

1.7 Alpha inelastic scattering

The α inelastic scattering is a useful probe to extract isoscalar transition strengths with various transferred angular momenta [34, 59–71]. Since the spin (S) and isospin (T) of the α particle are zero, the natural-parity isoscalar transitions ($\Delta S = \Delta T = 0$) are selectively

induced in the α inelastic scattering if the Coulomb interaction is neglected. The reaction process in the α inelastic scattering is well described by the distorted-wave Born-approximation (DWBA) calculation with the single-folding potential. Thus, the cross sections are approximately proportional to the transition strengths. Since the α inelastic scattering is a surface reaction, the angular distribution of the cross section is not sensitive to the details of the internal wave function but is characterized by the transferred angular momentum. Therefore, the multipole decomposition analysis (MDA) works well to extract the different ΔL components from the measured cross sections [62–70]. In the MDA, experimental double differential cross sections $[d^2\sigma/d\Omega dE_x]^{\rm exp}$ are fitted by the calculated cross sections for the ΔL transitions $[d^2\sigma/d\Omega dE_x]^{\rm DWBA}_{\Delta L}$ to search for the best parameters $a_{\Delta L}(E_x)$ as

$$\left[\frac{d^2\sigma(\theta_{\rm c.m.},E_x)}{d\Omega dE_x}\right]^{\rm exp} = \sum_{\Delta L} a_{\Delta L}(E_x)\left[\frac{d^2\sigma(\theta_{\rm c.m.},E_x)}{d\Omega dE_x}\right]^{\rm DWBA}_{\Delta L}. \tag{1.7}$$

Because the angular distributions of the cross sections are quite different near $\theta_{\rm c.m.} = 0^\circ$ depending on the transferred angular momenta as shown in Fig.1.9, it is desirable to measure the α inelastic scattering at forward angles including 0 degrees in order to conduct the MDA.

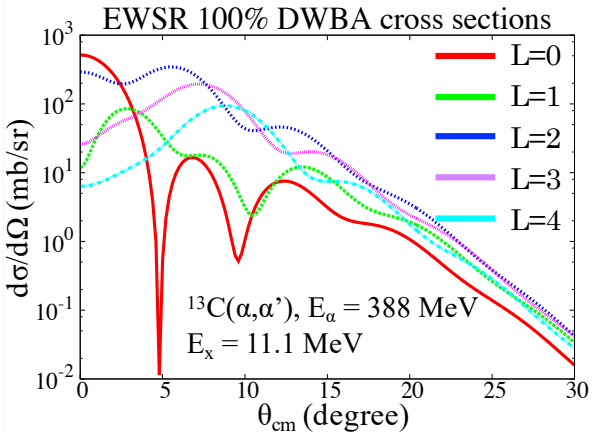

Figure 1.9: Angular distribution of the differential cross sections in the $^{13}{\rm C}(\alpha,\alpha')$ reaction at $E_x = 388$ MeV calculated by the DWBA. The red, green, blue, purple, and light blue lines show the cross sections for the $\Delta L = 0, 1, 2, 3$, and 4 transitions assuming that one state at $E_x = 11.1$ MeV exhausts 100% of the energy-weighted sum-rule (EWSR) strength, respectively.

1.8 Aim of the present work

α condensation in atomic nuclei is one of the hottest topics in the modern nuclear physics. Although it was pointed out that the α condensation induces the strong isospin dependence of the EoS of the dilute nuclear matter in Ref. [42], it is not trivial that the α condensation actually occurs in the dilute nuclear matter. Since we cannot directly access infinite nuclear matter in the laboratory, we should investigate the α condensation in finite nuclei over a wide range of the mass number and isospin in order to establish the existence of the α condensate in dilute nuclear matter. If the α condensed states exist universally in various nuclei, we can establish that the α condensate is a trivial conformation in dilute nuclear many-body system.

Many theoretical and experimental efforts have been devoted to establish the α condensed states and to reveal their nature. However, the scope of these studies has been limited to self-conjugated $A = 4k$ nuclei. Few studies have discussed the α condensation in $A \neq 4k$ nuclei with excess neutrons or protons, so far. Therefore, it is an urgent issue to search for the α condensed states in various nuclei not only in $A = 4k$ nuclei but also in $A \neq 4k$ nuclei. The systematic research of the excitation energies and decay widths of the α condensed states will help construction of theoretical models to describe the α condensation, and shed light on low-density nuclear matter.

In the present work, we searched for the α condensed state in ^{13}C as the first step for the systematic exploration into non self-conjugated $A \neq 4k$ nuclei. Since the $IS0$ and $IS1$ transitions induce the density change of nuclei, these transitions are suitable to excite the α condensed state. Therefore, we measured the α inelastic scattering off ^{13}C at $E_\alpha = 388$ MeV at forward angles including 0° where the cross sections for the $IS0$ and $IS1$ transitions are large in order to precisely measure the strengths of these transitions. We analyzed the measured cross sections with the DWBA calculations with the single-folding potentials and determined the isoscalar transition strengths in ^{13}C. We extracted the strength distributions for the isoscalar $\Delta L = 0$–3 transitions by the MDA. We compared the experimental level diagram and transition strengths for the $1/2^\pm$ states excited through the $IS0$ and $IS1$ transitions with theoretical predictions by the shell-model, $3\alpha+n$ OCM, and AMD calculations. We discussed the structures of these states and the existence of the α condensed state in ^{13}C. We tried to investigate whether the α condensed nature discussed in self-conjugated $A = 4k$ nuclei is still maintained even with the excess neutron.

Chapter 2

Experiment

2.1 Overview

We measured the cross sections for the α elastic and inelastic scattering off ^{13}C and ^{12}C at a beam energy of $E_\alpha = 388$ MeV and scattering angles of $\theta_{\rm lab} = 0°$–$20.2°$ in the laboratory frame. The experiment was performed at Research Center for Nuclear Physics (RCNP), Osaka University. An incident He^{2+} beam was accelerated by a series of cyclotrons at RCNP and transported to a self-supporting target. Scattered alpha particles were momentum-analyzed with the high-resolution magnetic spectrometer Grand Raiden [72], and were detected with the focal plane detectors.

2.2 Beam line

A plane view of the RCNP cyclotron facility is given in Fig. 2.1. A He^{2+} beam was extracted from the external ECR ion source (Neomafios) in the AVF cyclotron area. The AVF cyclotron accelerated the beam up to $E_\alpha = 86$ MeV, then, the beam was accelerated again by the ring cyclotron up to $E_\alpha = 388$ MeV. The fully accelerated beam was transported to the target in a scattering chamber in the west experimental hall through the WS beam line [73]. The beam was achromatically focused on the target. The size of the beam spot was about 1 mm in diameter on the target.

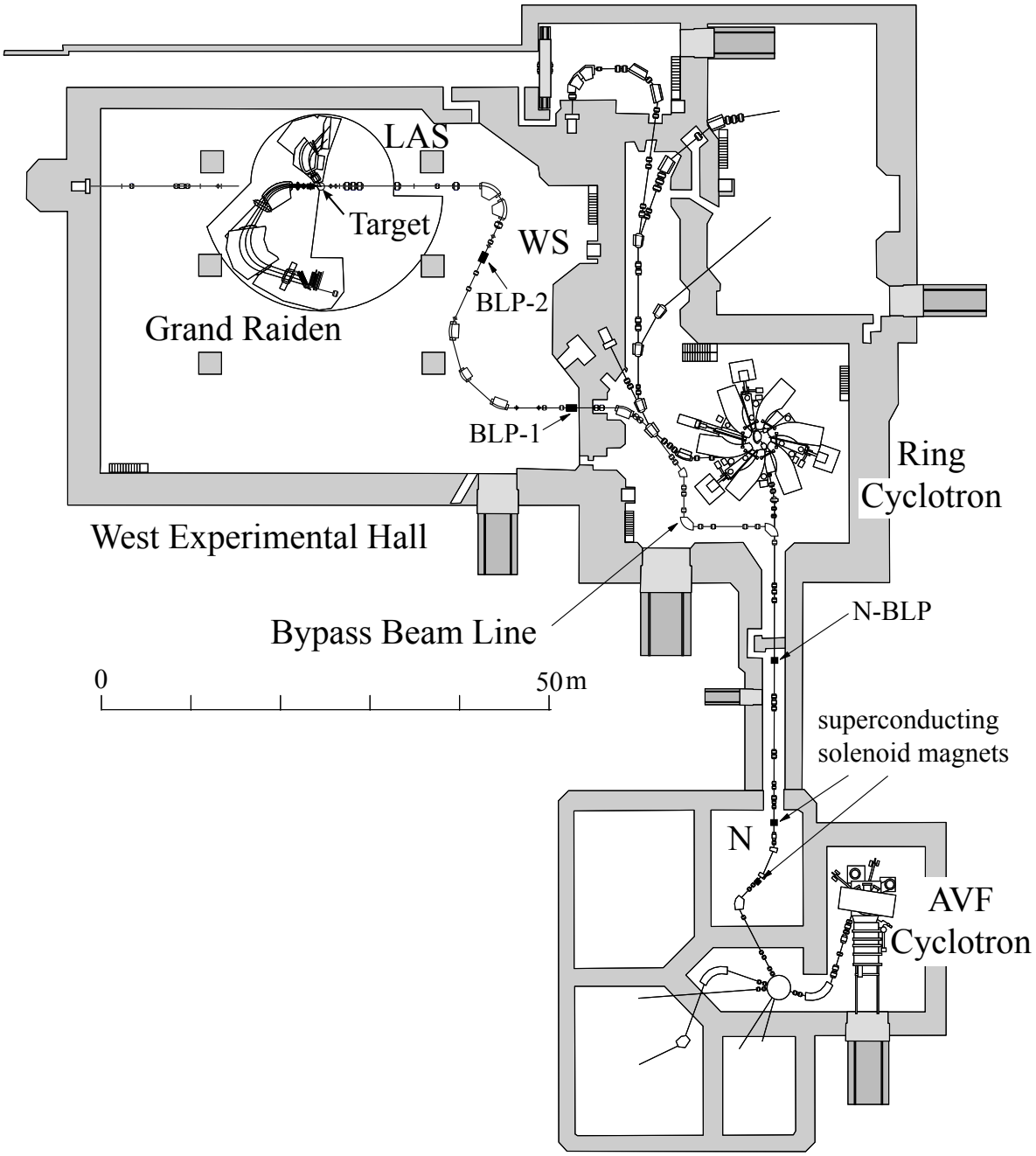

Figure 2.1: Plane view of the RCNP cyclotron facility.

2.3 Targets

Self-supporting ^{13}C and $^{\rm nat}$C targets were used in this experiment. These targets were prepared by a thermal cracking method [74]. We used two $^{\rm nat}$C targets with different thicknesses depending on the measuring angle. Table 2.1 summarizes the target nuclei, thicknesses, and isotope enrichments.

Table 2.1: Thicknesses and isotope enrichments of the targets used in the present measurement.

Nucleus	Thickness (mg/cm^2)	Enrichment (%)	Measuring angle (°)
^{12}C	0.5	98.9[a]	0–5.9
^{12}C	2.8	98.9[a]	6.0–20.2
^{13}C	1.5	98	0–20.2

[a] Natural abundance.

2.4 Grand Raiden spectrometer

Figure 2.2 shows the experimental setup of the Grand Raiden spectrometer for the measurement at $\theta_{\rm lab} = 0°$. The Grand Raiden spectrometer consists of three dipole magnets (D1, D2, DSR), two quadrupole magnets (Q1, Q2), one sextupole magnet (SX), and one multipole magnet (MP). These magnets are arranged as QSQD(M)D(+D) from upstream as presented in Fig. 2.2. The MP is used to correct ion-optical aberrations. The DSR is an optional dipole magnet, which is usually used for measurements of the spin-rotation parameters or polarization transfer observables. In the present measurement at $\theta_{\rm lab} = 0°$, the DSR was utilized as a steering magnet to guide the incident He^{2+} beam toward a Faraday cup (0deg-FC) in the beam dump as shown in Fig. 2.2. The design specifications of the Grand Raiden spectrometer are summarized in Table 2.2.

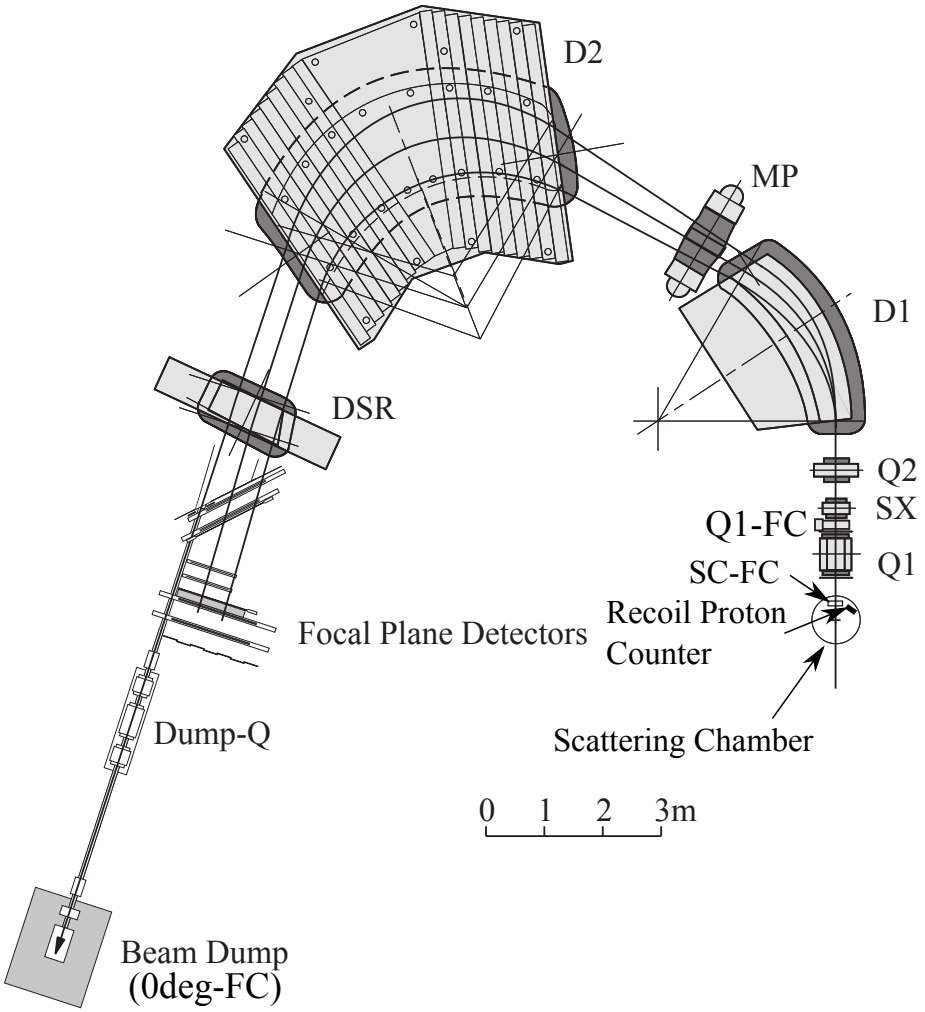

Figure 2.2: Overview of the Grand Raiden spectrometer at $\theta_{\rm lab} = 0°$.

Table 2.2: Design specifications of the Grand Raiden spectrometer.

Configuration	QSQD(M)D(+D)
Mean orbit radius	3 m
Total deflection angle	162°
Focal plane length	150 cm
Tilting angle of focal plane	45°
Maximum magnetic field strength	1.8 T
Maximum magnetic rigidity	5.4 T · m
Horizontal magnification $(x\|x)$	−0.42
Vertical magnification $(y\|y)$	5.98
Momentum dispersion $(x\|\delta)$	15.45 m
Momentum range	5%
Momentum resolution	3.71×10^4
Acceptance of horizontal angle	±20 mr
Acceptance of vertical angle	±70 mr
Solid angle	∼ 5.6 msr

2.5 Detectors

2.5.1 Focal plane detectors

The standard focal plane detectors consisted of two multi-wire drift chambers (MWDC1 and MWDC2) and two plastic scintillation counters (PS1 and PS2). The detector layout for the measurement at $\theta_{\rm lab} = 0°$ is shown in Fig. 2.3. The MWDCs, PS1, and PS2 were aligned along the focal plane, which were inclined at 45° with respect to the central trajectories of the Grand Raiden spectrometer. The focal plane polarimeter consisting of the four multi-wire proportional chambers (MWPCs) and the scintillator hodoscope (HS-X) was not used in this experiment. The MWDCs were used to determine the three-dimensional trajectories of scattered particles on the focal plane. The PSs were used to make trigger signals and to identify the scattered α particles. The sizes of the PSs were 1200 mm (W) × 120 mm (H) × 10 mm (T). The scintillation photons were detected by the photo-multiplier tubes (PMTs) attached on both sides of each PS.

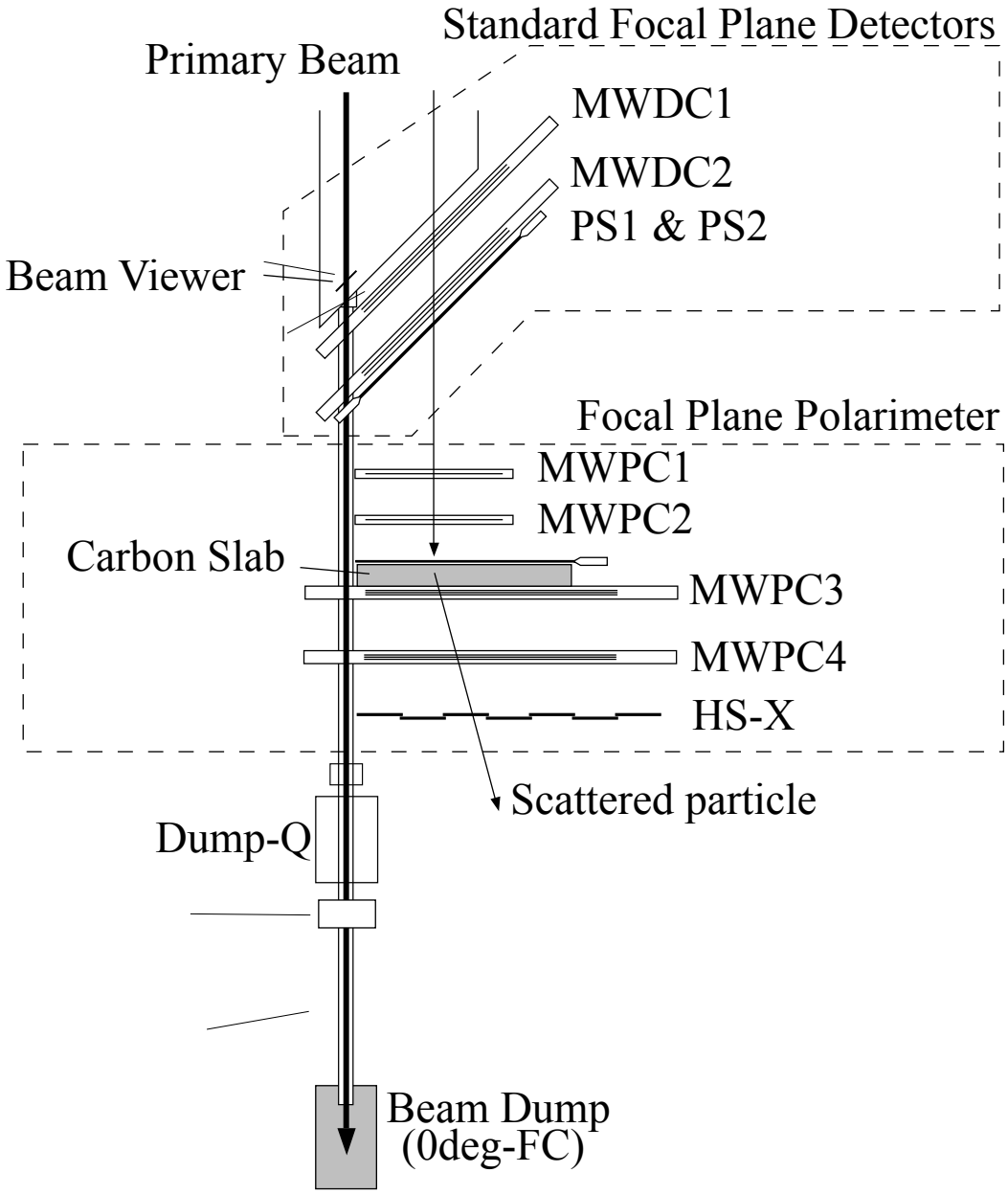

Figure 2.3: Focal plane detector system for the measurement at $\theta_{\rm lab} = 0°$.

Table 2.3: Design specifications of the MWDCs at the focal plane of the Grand Raiden spectrometer.

	MWDC
Active area	1150 mm (W) × 120 mm (H)
Wire configuration	X (0°), U (−48.19°)
Cathode-anode gap	10 mm
Anode sense wires	20 μm ϕ Au-W
Anode potential wires	50 μm ϕ Au-Cu/Be
Anode wire spacing	2 mm
Sense wire spacing	6 mm (X), 4 mm (U)
Number of sense wires	192 (X), 208 (U)
Supplied voltage	−4.7 kV (cathode)
	−240 V (potential)
	0 V(sense)
Gas mixture	Argon (71.4%) + Iso-butane (28.6%)
	+ Iso-propyl-alcohol
Gas seal	12.5 μm aramid film
Pre-amplifier	LeCroy 2735DC
Digitizer	LeCroy 3377 drift chamber TDC

2.5.2 Multi-wire drift chambers

Design specifications of the MWDCs are summarized in Table 2.3. Each MWDC consists of two anode planes, horizontal (X) plane and 48.2°-tilted (U) plane. A schematic view of the MWDC for the X plane is shown in Fig. 2.4. The spacing between the cathode plane and the anode wires is 10 mm. The anode wires consist of the sense and potential wires. They are arranged at the 2 mm intervals in the anode planes. The spacing of the sense wires are 6 mm in the X plane and 4 mm in the U plane as shown in Fig. 2.5. High volatges of −4.7 kV were supplied to the cathode planes, and −240 V were supplied to the potential wires in the present experiment. A gas mixture of argon (71.4%), iso-butane (28.6%), and iso-propyl-alcohol (vapor pressure at 2°C) was used. Signals from the anode wires were pre-amplified and discriminated by LeCroy 2735DC modules. Timing information was digitized by using LeCroy 3377 drift chamber time-to-digital converter (TDC) modules.

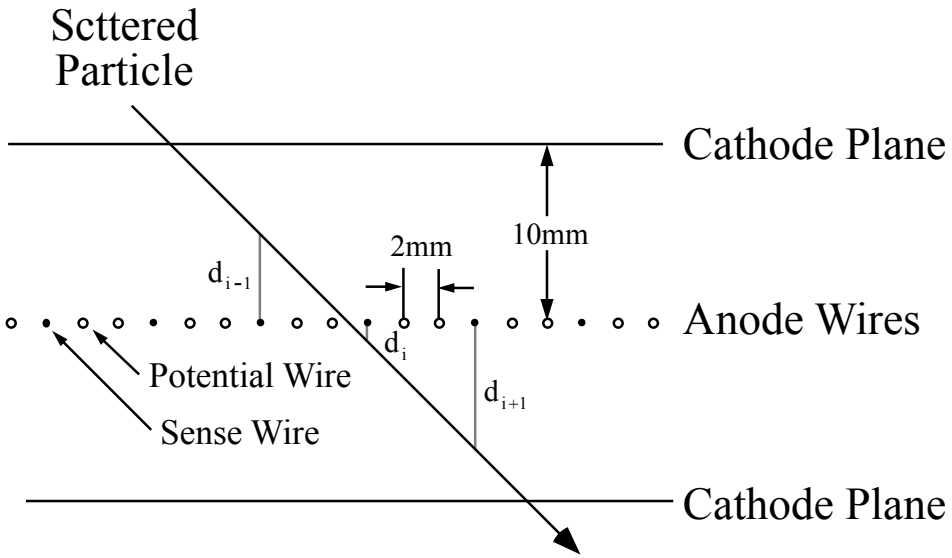

Figure 2.4: Schematic view of the MWDC for the X plane.

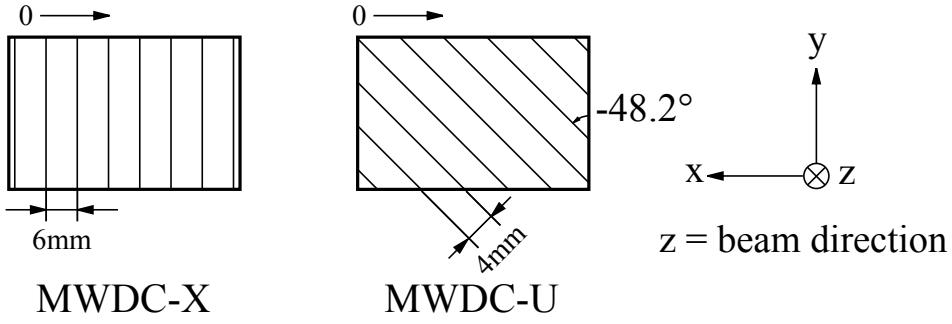

Figure 2.5: Wire configuration of the MWDC for the X and U planes.

2.5.3 Recoil proton counter

One of the visible backgrounds in this measurement was α+p elastic scattering due to hydrogen contaminants in the ^{13}C target. Since the cross sections for the elastic scattering were large compared to the inelastic scattering at forward angles, even a small amount of the hydrogen contaminates the excitation-energy spectra. We developed a recoil proton counter (RPC) to detect recoil protons to tag the background events caused by the $\alpha + p$ elastic scattering. The RPC was an E–ΔE telescope consisting of two plastic scintillation counters. The sizes of both scintillators were 240 mm high and 35 mm wide, and the thicknesses were 1 mm and 9 mm, respectively. The scintillation photons were detected by the PMTs attached on the top and bottom sides of each plastic scintillator. Figure 2.6 shows the RPC used in this experiment. The RPC was installed in the scattering chamber as shown in Fig. 2.7. Installation angle of the RPC was remotely changed to catch recoil protons depending on the setting angle of the Grand Raiden spectrometer.

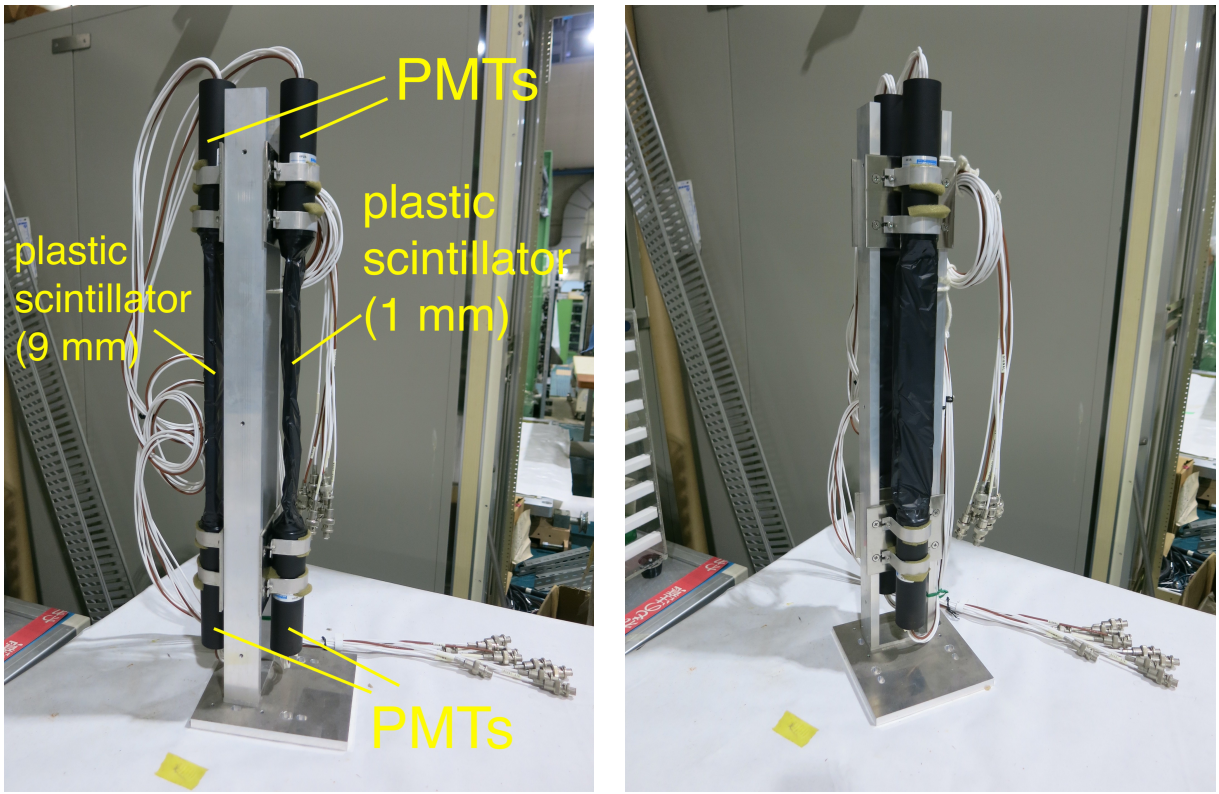

Figure 2.6: Pictures of the RPC. (left) Side view. (right) Front view.

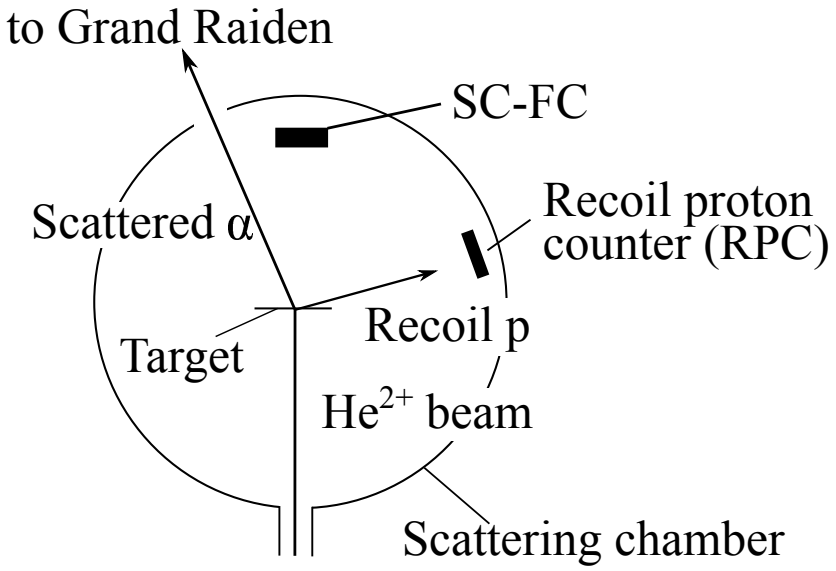

Figure 2.7: Schematic view of detector layout in the scattering chamber with the RPC.

2.6 Faraday cups

We used three different Faraday cups depending on the setting angle of the Grand Raiden spectrometer. Two of the three Faraday cups were located behind the Q1 magnet (Q1-FC) and in the scattering chamber (SC-FC), and were used for the measurement at $\theta_{\rm lab} = 1.7$–5.9° and $\theta_{\rm lab} = 6.0$–20.2°, respectively.

In the measurement at $\theta_{\rm lab} = 0^\circ$, the He^{2+} beam was guided to the focal plane through the Grand Raiden spectrometer in the same way as scattered alpha particles. The beam passed through the beam duct at the high-momentum side of the focal plane detectors. The beam current was measured by a Faraday cup (0deg-FC) in the beam dump as shown in Fig. 2.2. The excitation-energy region measurable with this setup was limited to $E_x \geq 7$ MeV due to the geometrical relationship between the beam duct and the sensitive area of the focal plane detectors. Therefore, we prepared another experimental setup to extend the measurable excitation-energy region down to $E_x = 2.5$ MeV. As shown in Fig. 2.8, an alternative beam stopper was installed upstream of the MWDCs to make the beam position as close as possible to the sensitive area of focal plane detectors. Since this beam stopper could not measure the beam current, the absolute value of the cross sections was not determined. The determination of the cross sections for the low-lying states will be discussed in Sec. 3.8.

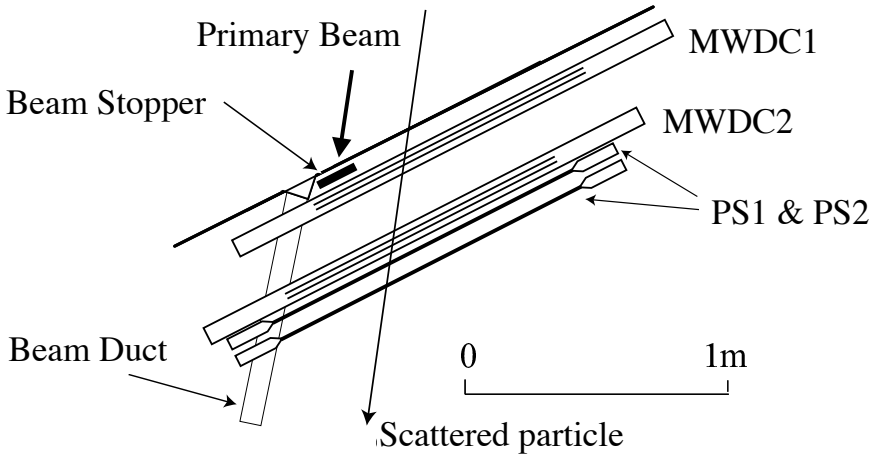

Figure 2.8: Same as Fig. 2.3 but for the low-lying measurement. The beam stopper was installed upstream of the MWDCs.

2.6.1 Beam-line polarimeter

The beam-line polarimeters (BLP-1 and BLP-2) were located at the WS beam line as shown in Fig. 2.1. Each BLP system consisted of four pairs of plastic scintillation detectors in the horizontal and vertical planes. Figure 2.9 shows the two pairs of the scintillators in the horizontal plane. The scintillation detectors of each pair were placed at the angles of 14.4° and 40.0° with respect to the beam direction. An aramid film with a thickness of 4 μm was used as the analyzer target to calibrate the charge collection efficiency. Elastically scattered alpha particles from the aramid target and recoil protons were detected by the detectors at 14.4° and 40.0°, respectively. The $\alpha + p$ elastic scattering was identified by detecting both alpha particle and proton in coincidence. The charge collection efficiency of the three Faraday-cups were calibrated within 3% uncertainties by comparing the output from each Faraday-cup with the counting rate of the coincidence signals from the BLP detectors.

2.7 Data acquisition system

The schematic diagram of the trigger circuit is illustrated in Fig. 2.10. Event triggers were generated by the coincidence of the PS1 and PS2 signals. Since two PMTs were attached to the left and right sides of each scintillation counter, the PS1 and PS2 signals were generated with the coincidence of both PMTs' signals. The overview of the data acquisition (DAQ) system is illustrated in Fig. 2.11. Each event consisted of the drift-time data from the MWDCs

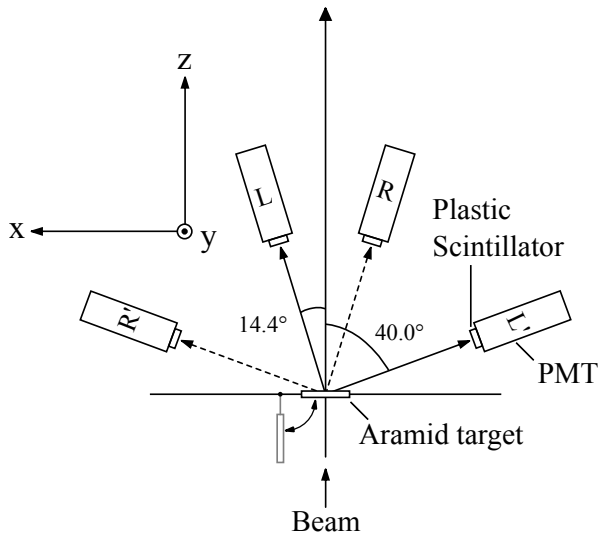

Figure 2.9: Schematic view of the BLP illustrating the two pairs of the scintillators in the horizontal plane.

digitized by LeCroy3377 TDC, the charge and timing signals from the trigger scintillators encoded with the LeCroy FERA and FERET systems, and the input register. In order to check the consistency of data flow, the event header, event number, and input register words were attached to every event by the Flow Controlling Event Tagger (FCET) [75]. The digitized data were transferred in parallel via ECL bus lines to the high-speed memory (HSM) modules (LeCroy 1191 Dual Port Memory) in the VME crate. The stored data in the HSMs were transferred via Ethernet to the DAQ server provided by an IBM RS/6000 work station. The typical dead time for encoding events was shorter than 30 μs/event.

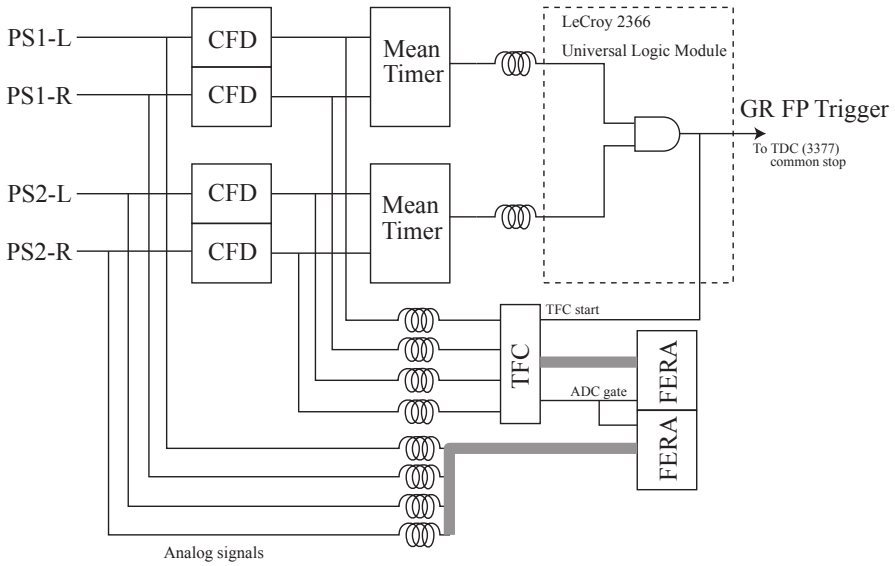

Figure 2.10: Schematic diagram of the trigger circuit and a part of circuit for analogue signals from the PSs.

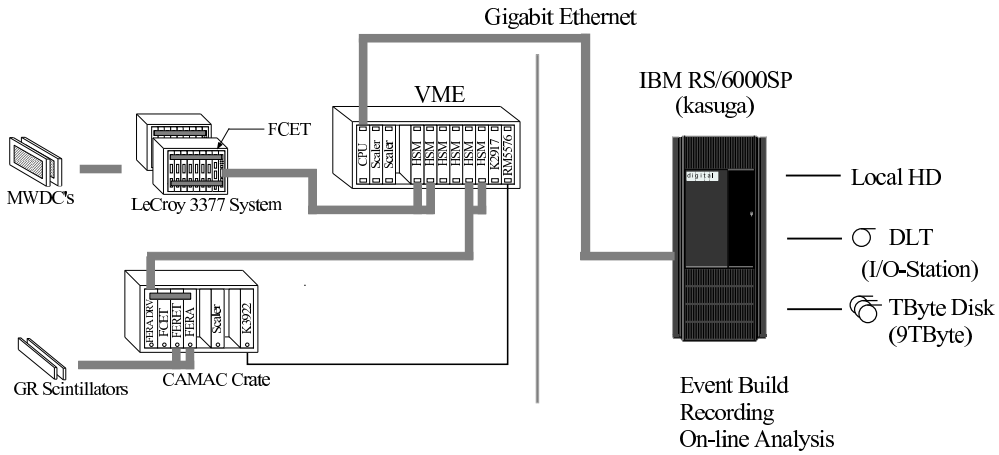

Figure 2.11: Overview of the DAQ system in the WS course of RCNP.

Chapter 3

Data reduction

3.1 Outline

The analyzer program KAWABATA-ANALYZER developed by T. Kawabata was used. The data analysis was performed in the following procedure:

1. Track reconstruction of scattered particle

   Position and angle of scattered particle on the focal plane were reconstructed by using the MWDCs.

2. Particle identification

   Events of the α inelastic scattering were selected.

3. Determination of scattering angle and momentum of scattered particle

   Scattering angle and momentum of scattered particle were obtained using ion-optical parameters of the Grand Raiden spectrometer. Calibration of the scattering angle was conducted by the sieve-slit measurement. Calibration of the excitation energy was also performed for every run by comparing the measured excitation-energy spectra with the known energy levels in ^{13}C.

4. Background subtraction

   The contributions from the contaminants of ^{12}C and hydrogen in the ^{13}C target were subtracted.

5. Determination of solid angles

The solid angles were determined by entrance slits of the Grand Raiden spectrometer and software gates.

6. Estimation of efficiencies

   The tracking efficiency of the MWDCs and the data acquisition efficiency were estimated for every run.

7. Determination of differential cross sections

   The differential cross sections for the α inelastic and elastic scattering were determined.

3.2 Track reconstruction of scattered particles

Three-dimensional trajectories of scattered particles were reconstructed using the position and angle information on the focal plane obtained by the MWDCs. Ionized electrons generated by a scattered particle drifted in the electric field made by the cathode plane and potential wires as shown in Fig. 2.4. The vertical drift lengths of d_{i-1}, d_i, and d_{i+1} were determined from the drift times obtained with LeCroy3377 TDCs. They were converted into a particle position on the anode-wire plane. The particle position on the X-plane of the MWDC1 (X1) and MWDC2 (X2) defined an X-tracking plane, and those on the U planes (U1 and U2) defined a U-tracking plane. Thus the three-dimensional trajectory of a scattered particle was determined from the intersection of the two planes as shown in Fig. 3.1.

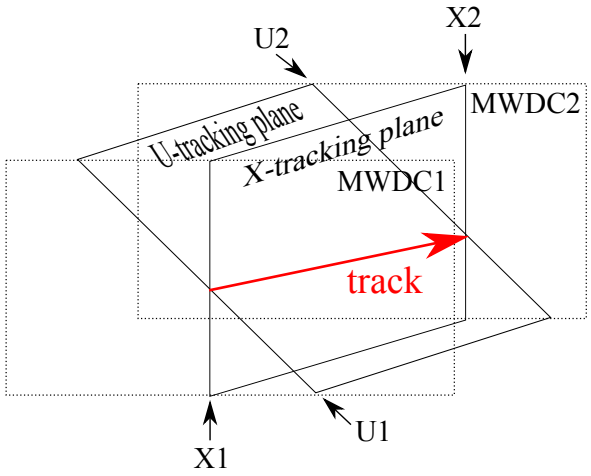

Figure 3.1: Schematic view of the determination of the particle trajectory.

The drift lengths were calibrated by using the continuum spectrum in a highly excited

region in ^{13}C, where a uniform distribution of the scattered α particles could be expected. A schematic image of the drift-time spectrum is shown in Fig. 3.2. The lower edge of the spectrum corresponds to the maximum drift length in the MWDC and the sharp peak at the higher edge is attributed to the steep gradient of the electric field near the anode wires. The drift time T was converted to the drift length L assuming the uniform distribution of L as

$$L = L_{\max} \times \frac{\int_T^b f(t)dt}{\int_a^b f(t)dt}, \tag{3.1}$$

where $L_{\max}$ is the maximum drift length (10 mm in this case) and $f(t)$ is a distribution function of the TDC. a and b are the minimum and the maximum drift time in the distribution of the TDC.

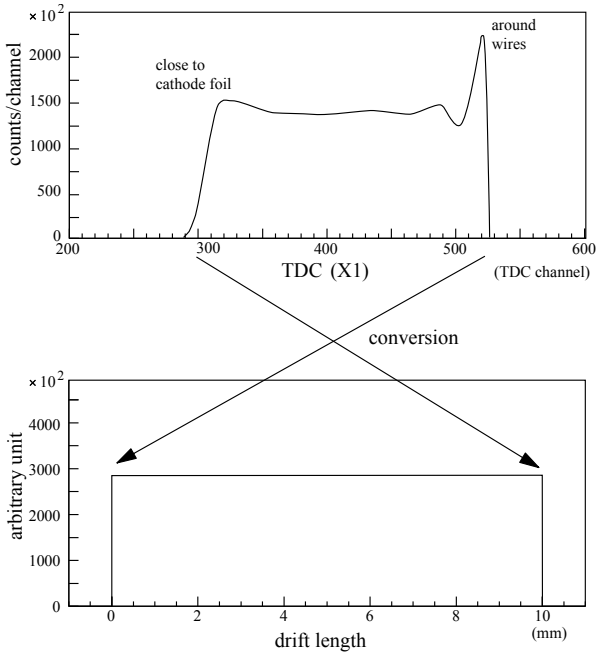

Figure 3.2: Schematic image of the conversion procedure from a drift-time spectrum obtained with LeCroy3377 TDCs to a drift-length spectrum in the X plane of the MWDC1.

Since the focal plane of the Grand Raiden spectrometer was tilted on 45° with respect to the central orbit and the MWDCs were aligned along the focal plane, charged particles entering the MWDCs hit several adjacent wires on each plane of the MWDCs. The group of these adjacent wires was defined as a "cluster". Small clusters consisting of a single hit wire were excluded from the present analysis since the background events such as X- and γ-rays usually cause single-wire hits.

3.3 Particle identification

The two plastic scintillation counters PS1 and PS2 were utilized for the particle identification (PID). The PID was performed applying two gates on the data. One was the gate for the time difference between the DAQ trigger and the signal synchronized to the acceleration by the AVF cyclotron (RF signal), which corresponded to the time of flight (TOF) from the target to the focal plane. The other was the gate for the energy deposit in the PS1 and PS2.

3.3.1 PID by TOF

The TOF from the target to the focal plane depends on the flight path, the momentum, and the rest mass of scattered particle as

$$\mathrm{TOF} = \frac{L}{c}\sqrt{1 + c^2\left(\frac{m_0}{P}\right)^2}, \tag{3.2}$$

where L, m_0, and P denotes the flight pass, the rest mass, and the momentum of the particle, respectively. c is the speed of light. We can identify the particle using the correlation between the TOF and momentum of the particle if L is constant. However, L through the Grand Raiden spectrometer depends on the scattering angle and the momentum of the particle. Therefore, a correction to the TOF should be performed to remove the dependence on the scattering angle on the focal plane (θ_{fp}) and the horizontal position at the focal plane (x_{fp}) which corresponds to the momentum of the particle. Figure 3.3(a) shows two dimensional scatter plot of the TOF versus θ_{fp}, and Fig. 3.3(b) shows that of the TOF versus and x_{fp}. Assuming that the TOF has linear dependence on θ_{fp} and quadratic dependence on x_{fp}, a correction to the TOF was performed to remove these dependence as shown in Figs. 3.3(c) and (d). The raw and corrected TOF are shown in the left and right panels in Fig. 3.4, respectively. Since the RF signals were downscaled to its half frequency of the original frequency 15.4 MHz by a rate divider circuit, two prominent peaks due to the alpha particles were observed in the gray regions of Fig. 3.4.

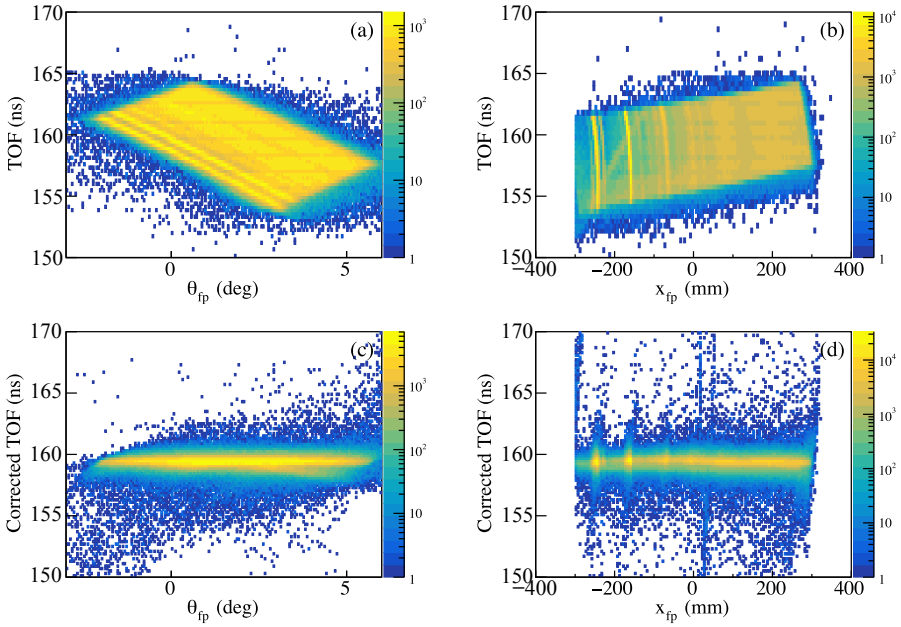

Figure 3.3: Typical two dimensional scatter plots of the TOF versus the horizontal scattering angle on the focal plane $\theta_{\rm fp}$ and the TOF versus the horizontal position at the focal plane $x_{\rm fp}$. (a) and (b) show the TOF before the correction, where as (c) and (d) show that after the correction.

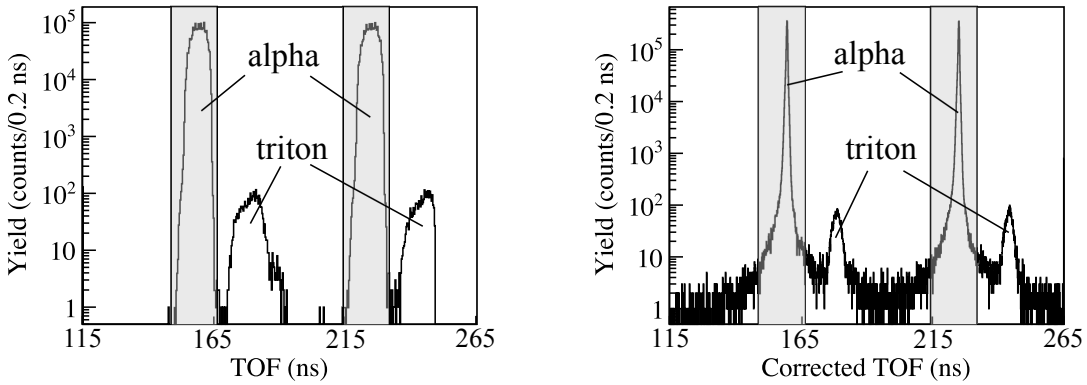

Figure 3.4: Typical TOF spectra (a) before and (b) after the correction. The gray regions in the histograms correspond to the alpha particles.

3.3.2 PID by the energy deposit

Charged particles lose their energies in matter primarily by ionization. The average energy loss is given by the Bethe-Bloch formula [76]

$$-\frac{dE}{dx} = 2\pi N_{\rm A} r_e^2 m_e \rho \frac{Z}{A}\frac{z^2}{\beta^2}\left\{\log\left(\frac{2m_e\beta^2\gamma^2 W_{\rm max}}{I^2}\right) - 2\beta^2 - \delta - 2\frac{C}{Z}\right\}. \tag{3.3}$$

Here $W_{\rm max}$ is the maximum kinetic energy which can be imparted to a free electron in a single collision. The other variables are defined as

r_e: Classical electron radius (2.817×10^{-13} cm),

M_e: Electron mass,

$N_{\rm A}$: Avogadro constant (6.022×10^{23} mol^{-1}),

I: Mean excitation energy,

Z: Atomic number of the absorbing material,

A: Atomic weight of the absorbing material,

ρ: Density of the absorbing material,

z: Charge of the incident particle,

β: Velocity of the incident particle,

C: Shell correction.

The charged particles excite atoms and molecules in the scintillating materials, which cause a light emission due to de-excitation. The attenuation of photons along the flight path x from the emission point to the PMTs is approximately described as

$$I(x) = I_0 \exp(-x/l), \tag{3.4}$$

where I_0 denotes the number of initial photons by de-excitation processes. l denotes the attenuation length of the scintillator. When the distance between the emission point and the PMTs on the left and right sides are x_L and x_R, respectively, the geometric mean $\bar{I}$ of the number of photons detected by the PMTs on the both sides of the scintillator is described as

$$\begin{aligned}\bar{I} &= \sqrt{I_0\exp(-x_L/l)\cdot I_0\exp(-x_R/l)} \\ &= I_0\exp(-(x_L+x_R)/2l)) = I_0\exp(-L/2l),\end{aligned} \tag{3.5}$$

where $L = x_L + x_R$ denotes the length of the scintillator. Equation (3.5) shows that $\bar{I}$ is independent of the position where a charged particle hits. Therefore, $\bar{I}$ is a good measure of energy deposition by the particles into the scintillator. Typical energy-deposit spectra for the PS1 measured with an analog-to-digital converter (ADC) module are shown in Fig. 3.5. The ADC values from the left and right PMTs decrease as a function of the distance between the hit position and the PMT as shown in Fig. 3.5(a) and (b). However, the geometric mean of the left and right ADC values shown in Fig. 3.5(c) is almost independent from the position of the emission point.

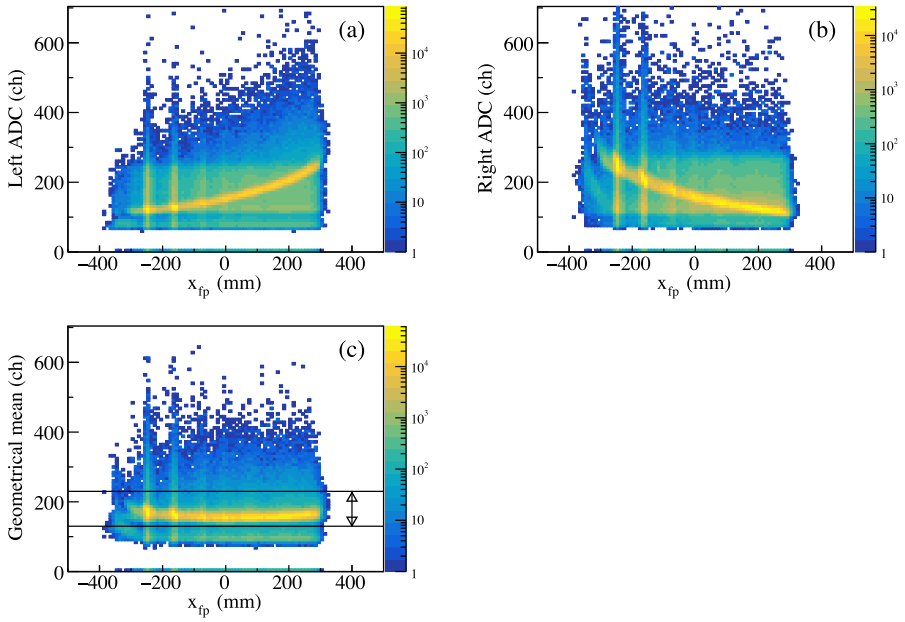

Figure 3.5: Typical two dimensional scatter plots of the energy deposit at the PS1 versus the horizontal position $x_{\rm fp}$ on the focal plane. (a) and (b) show ADC values from the left and right PMTs. (c) shows the geometrical mean of the ADC values from the left and right PMTs. The region indicated by the arrow corresponds to the alpha particles.

The loci with the higher ADC values in Fig. 3.5(c) (the region indicated by the arrows) were attributed to alpha particles, whereas those with the lower ADC values were due to tritons. In this measurement, tritons were easy to eliminate by gating on the TOF (see Fig. 3.4) as shown in Fig. 3.6. Figure 3.7 shows the spectra of the geometric mean of the ADC values from the left and right PMTs. The peak due to tritons in Fig. 3.7(a) disappears in Fig. 3.7(b) by gating on the TOF. In addition to the gate by the TOF, an additional gate on the energy deposit selecting the gray area in Fig. 3.7(b) was also applied for the better

PID.

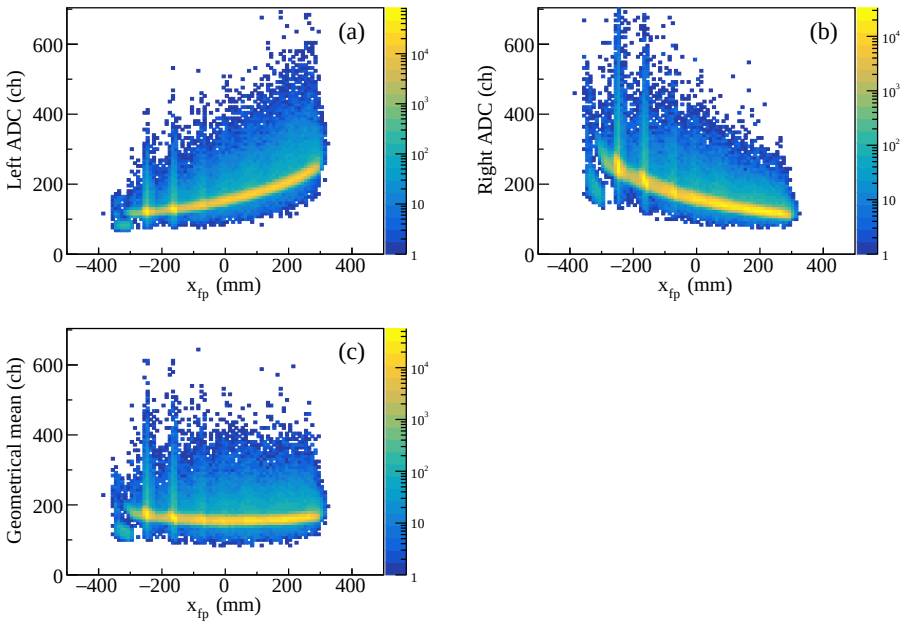

Figure 3.6: Same as Fig. 3.5, but gated by the TOF.

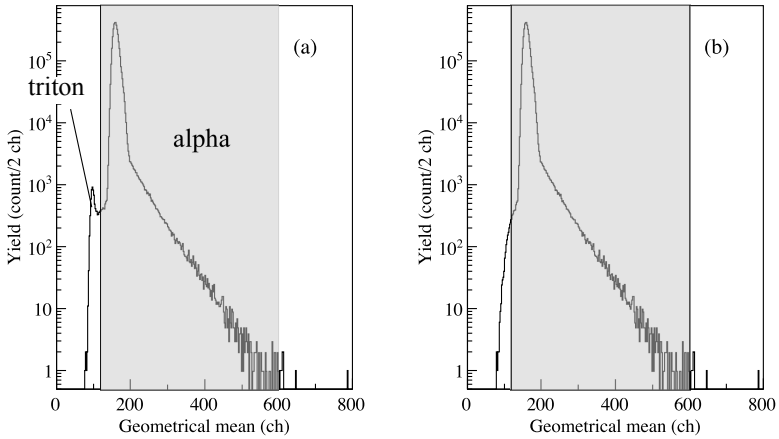

Figure 3.7: Typical spectra of the geometric mean of the ADC values from the left and right PMTs measured by the PS1 (a) without and (b) with the gate for the TOF. The gray region in the histograms correspond to the alpha particles.

3.4 Determination of scattering angle and momentum of scattered particle

Since we can measure the position and angle of scattered particles on the focal plane only, these information should be converted into those on the target using the ion optical calculation of the Grand Raiden spectrometer. For example, the horizontal position on the focal plane $x_{\rm fp}$ is associated with the information on the target as

$$x_{\rm fp} = \sum_{i,j,k,l,m} (x|x^i y^j \theta^k \phi^l \delta^m) x^i_{\rm tgt} y^j_{\rm tgt} \theta^k_{\rm tgt} \phi^l_{\rm tgt} \delta^m. \tag{3.6}$$

Here, $x_{\rm tgt}$ and $y_{\rm tgt}$ are the horizontal and vertical positions on the target. $\theta_{\rm tgt}$ and $\phi_{\rm tgt}$ are the horizontal and vertical scattering angles on the target with respect to the central orbit of the Grand Raiden spectrometer. δ is the fractional momentum deviation from the central orbit. The horizontal variables (x, θ) are not coupled with the vertical ones (y, ϕ) in the first order calculation. Therefore, the variables on the focal plane can be related to those on the target using the transfer matrix in the first order calculation as

$$\begin{pmatrix} x_{\rm fp} \\ \theta_{\rm fp} \\ y_{\rm fp} \\ \phi_{\rm fp} \\ \delta \end{pmatrix} = \begin{pmatrix} (x|x) & (x|\theta) & 0 & 0 & (x|\delta) \\ (\theta|x) & (\theta|\theta) & 0 & 0 & (\theta|\delta) \\ 0 & 0 & (y|y) & (y|\phi) & 0 \\ 0 & 0 & (\phi|y) & (\phi|\phi) & 0 \\ 0 & 0 & 0 & 0 & 1 \end{pmatrix} \begin{pmatrix} x_{\rm tgt} \\ \theta_{\rm tgt} \\ y_{\rm tgt} \\ \phi_{\rm tgt} \\ \delta \end{pmatrix}. \tag{3.7}$$

The matrix elements $(x|x)$ and $(y|y)$ are called the horizontal and vertical magnifications, and $(x|\delta)$ is called the momentum dispersion. In the normal magnetic-field setting of the Grand Raiden spectrometer, these values are $(x|x) = -0.42$, $(y|y) = 5.98$, and $(x|\delta) = 15.45$ m. The values of $(x|\theta)$ and $(y|\phi)$ are 0 m/deg in the normal magnetic-field setting of the Grand Raiden spectrometer because the horizontal and vertical focus conditions are realized. Since a typical size of the beam spot is about 1 mm in diameter on the target, $(x|x)x_{\rm tgt}$ is negligibly small compared to $(x|\delta)\delta$. Therefore, δ can be determined by measuring $x_{\rm fp}$ only as

$$\delta = \frac{1}{(x|\delta)} x_{\rm fp}. \tag{3.8}$$

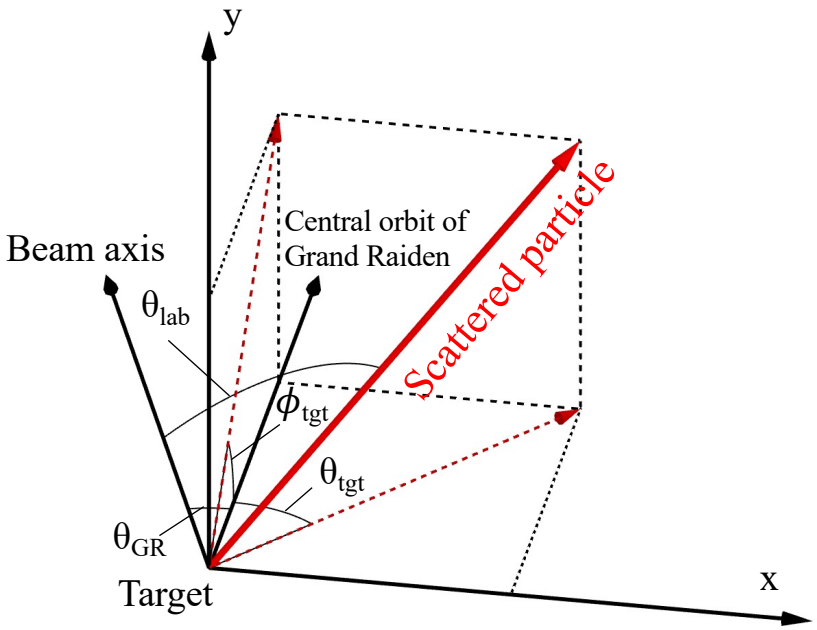

Figure 3.8: Schematic view of the relation among the scattering angle and its the vertical and horizontal projections on the target.

Owing to the Liouville's theorem, which conserves a phase-space volume of a particle ensemble, the determinant of the transfer matrix must be unity. Therefore, $(\theta|\theta)$ and $(\phi|\phi)$ are given by $(\theta|\theta) = 1/(x|x)$ and $(\phi|\phi) = 1/(y|y)$, respectively. Because the value of $(\theta|x)$ is -77.96 deg/m, $(\theta|x)x_{\rm tgt}$ is negligible for calculating $\theta_{\rm tgt}$ due to the small value of $x_{\rm tgt}$. Accordingly, $\theta_{\rm tgt}$ and $\phi_{\rm tgt}$ can be calculated from the information on the focal plane only as

$$\theta_{\rm tgt} = (x|x)\left[\theta_{\rm fp} - \frac{(\theta|\delta)}{(x|\delta)}x_{\rm fp}\right], \tag{3.9}$$

$$\phi_{\rm tgt} = (y|y)[\phi_{\rm fp} - (\phi|y)y_{\rm fp}]. \tag{3.10}$$

Scattering angle on the target in the laboratory frame $\theta_{\rm lab}$ is calculated by combining $\theta_{\rm tgt}$ and $\phi_{\rm tgt}$ as

$$\theta_{\rm lab} = \tan^{-1}\sqrt{\tan^2(\theta_{\rm tgt} + \theta_{\rm GR}) + \tan^2(\phi_{\rm tgt})}, \tag{3.11}$$

where $\theta_{\rm GR}$ is the angle of the central orbit of the Grand Raiden spectrometer with respect to the beam axis. Figure 3.8 shows a schematic view of the relation among $\theta_{\rm lab}$, $\theta_{\rm GR}$, $\theta_{\rm tgt}$, and $\phi_{\rm tgt}$.

Not only horizontal angular resolution but also vertical angular resolution are important

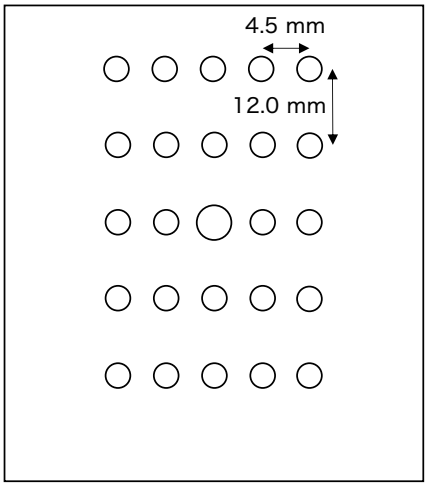

Figure 3.9: Drawing of the sieve slit used for the calibration of the scattering angle. The large hole at the center of the slit was designed to be aligned on the central trajectory of the Grand Raiden spectrometer.

to determine $\theta_{\rm lab}$ precisely at forward angles near $\theta_{\rm GR} = 0^\circ$. However, in the normal magnetic-field setting of the Grand Raiden spectrometer, the vertical angular resolution is deteriorated due to the large value of $(y|y)$ in Eq. (3.10). In order to improve the vertical angular resolution, we operated the Grand Raiden spectrometer in the under-focus mode at $0^\circ \leq \theta_{\rm GR} \leq 6.8^\circ$. The vertical focus point was moved downstream from the normal position without changing the horizontal focus condition by adjusting the field gradients of the Q1 and Q2 magnets in the under-focus mode. Because the vertical focus condition $(y|\phi) = 0$ was not held on the focal plane in this mode, $y_{\rm fp}$ was related to $y_{\rm tgt}$ and $\phi_{\rm tgt}$ as

$$y_{\rm fp} = (y|y)y_{\rm tgt} + (y|\phi)\phi_{\rm tgt}. \tag{3.12}$$

If $(y|\phi)$ is large enough to make $(y|\phi)\phi_{\rm tgt}$ dominant in Eq.(3.12), $\phi_{\rm tgt}$ can be determined more precisely than in the normal mode in principle. However, higher-order effects should be also considered in reality. Therefore, we obtained an empirical formula to determine the vertical angle from the information on the focal plane in the under-focus mode with a sieve-slit measurement.

A drawing of the sieve slit utilized in this experiment is shown in Fig. 3.9. The large hole at the center of the slit was designed to be aligned with the central orbit of the Grand Raiden spectrometer. The hole spacing in the horizontal and vertical directions corresponded

to $\Delta\theta_{\rm tgt} = 0.45^\circ$ and $\Delta\phi_{\rm tgt} = 1.08^\circ$, respectively. We measured α particle, which were elastically scattered from a gold target and passed through the 5×5 holes on the sieve slit. The sieve-slit measurement was performed for various δ by changing the magnetic rigidity of the Grand Raiden spectrometer. We surveyed the correspondences between the positions and angles on the focal plane and the scattering angles on the target. Assuming that $\theta_{\rm tgt}$ and $\phi_{\rm tgt}$ were expressed as polynomial functions of $x_{\rm fp}, y_{\rm fp}, \theta_{\rm fp}$, and $\phi_{\rm fp}$, we determined the coefficients of the polynomial by a least-squares method.

Figure 3.10(a) shows two dimensional scatter plots of $\phi_{\rm fp}$ versus $\theta_{\rm fp}$ measured with the sieve slit. Since the vertical angular resolution was deteriorated due to a large value of $(y|y)$, the vertically aligned holes of the sieve slit could not be distinguished. However, they were clearly distinguished by using $y_{\rm fp}$ instead as shown in Fig. 3.10(b). This fact shows that $(y|\phi)$ in Eq.(3.12) is large enough and we can determine $\phi_{\rm tgt}$ more precisely from $y_{\rm fp}$ than from $\phi_{\rm fp}$. The horizontal and vertical scattering angles on the target reconstructed with the polynomial are shown in Fig. 3.10(b). The image of the sieve slit was successfully obtained in Fig. 3.10(b).

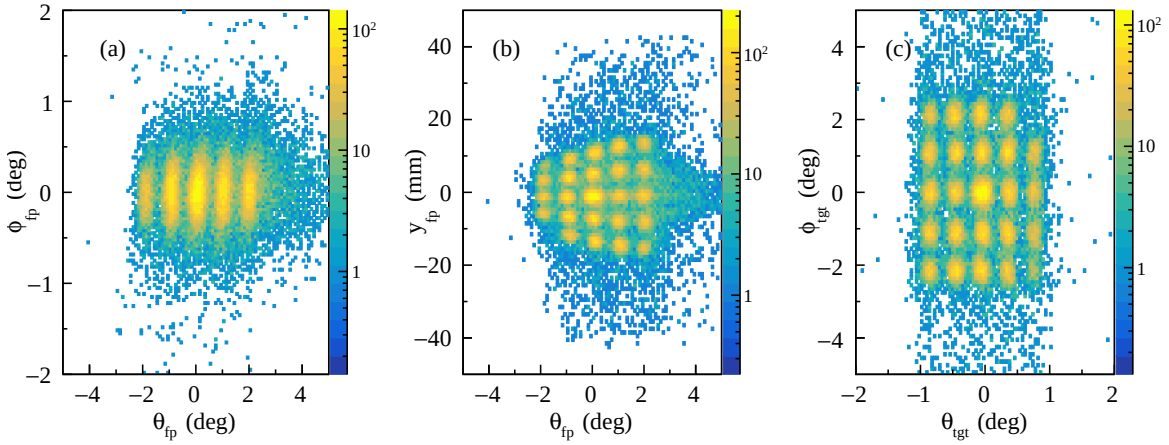

Figure 3.10: Two dimensional scatter plots of (a) the vertical scattering angles versus the horizontal scattering angles and (b) the vertical positions versus the horizontal scattering angles of alpha particles passing through the 5×5 holes on the sieve slit measured on the focal plane. (c) Two dimensional scatter plots of the vertical and horizontal scattering angles reconstructed from the positions and angles on the focal plane.

The excitation energy E_x was determined by using kinematical relation for the two-body reaction as

$$E_x = \sqrt{(E_\alpha - E'_\alpha + Mc^2)^2 - (P_\alpha - P'_\alpha)^2 c^2} - Mc^2, \tag{3.13}$$

where E_α and P_α are the total energy and momentum of an incident α particle whereas E'_α

and P'_α are those of a scattered α particle. M is the rest mass of the target nucleus. The kinetic energy of the incident α particle was $T_\alpha = 388$ MeV (E_α is derived by $E_\alpha = T_\alpha + m_\alpha c^2$) in this experiment.

Since there was small fluctuation of the magnetic field during the measurement, the excitation energy was calibrated using the peak position for the known discrete excited states in the measured spectra for every run.

3.5 Background subtraction

Background arising from the beam halo was reduced by tuning parameters of the accelerator using an empty target frame. In addition, background due to elastic and inelastic scatterings off contaminants in the target was necessary to be removed from the excitation-energy spectra.

A two-dimensional scatter plot of the scattering angle versus the excitation energy of ^{13}C measured at $1.7^\circ \leq \theta_{\rm lab} \leq 3.2^\circ$ is shown in Fig. 3.12(a). The $\alpha + p$ elastic scattering events due to the hydrogen contaminants are overlapped with the inelastic events due to the discrete states in ^{13}C and ^{12}C. The RPC was utilized to detect recoil protons and to tag the background events caused by the $\alpha + p$ elastic scattering as discussed in Sec. 2.5.3. The PID of recoil particles was performed by using the E–ΔE correlation and the TOF determined by the time difference between the RPC event and the RF signal. Since the TOF depends on the kinetic energy of recoil protons, we corrected the energy dependence using the energy deposit measured with the RPC. Figure 3.11 shows a typical example of the PID using a correlation between the corrected TOF and the energy deposit with the RPC. Recoil-proton events were clearly identified using the RPC.

The background due to the hydrogen contaminants was removed by rejecting the events in which the RPC detected the recoil protons as shown in Fig. 3.12(b). Figure 3.13(a) shows an excitation-energy spectra for the ^{13}C(α, α') reaction at $\theta_{\rm lab} = 2.5^\circ$. The red histogram corresponds to the $\alpha + p$ elastic scattering events. The contribution from the $\alpha + p$ events was eliminated by using the RPC as shown in Fig. 3.13(b).

In addition to the background due to the $\alpha + p$ scattering, the 2^+_1 state in ^{12}C was also observed in Fig. 3.13(a). In order to subtract the background events due to the ^{12}C contaminant in the ^{13}C target, the background measurements with the $^{\rm nat}$C targets were carried out as discussed in Sec. 2.3. The blue histogram in Fig. 3.13(b) shows the normalized excitation-energy spectra measured with the $^{\rm nat}$C target at $\theta_{\rm lab} = 2.5^\circ$. The normalization factors for the

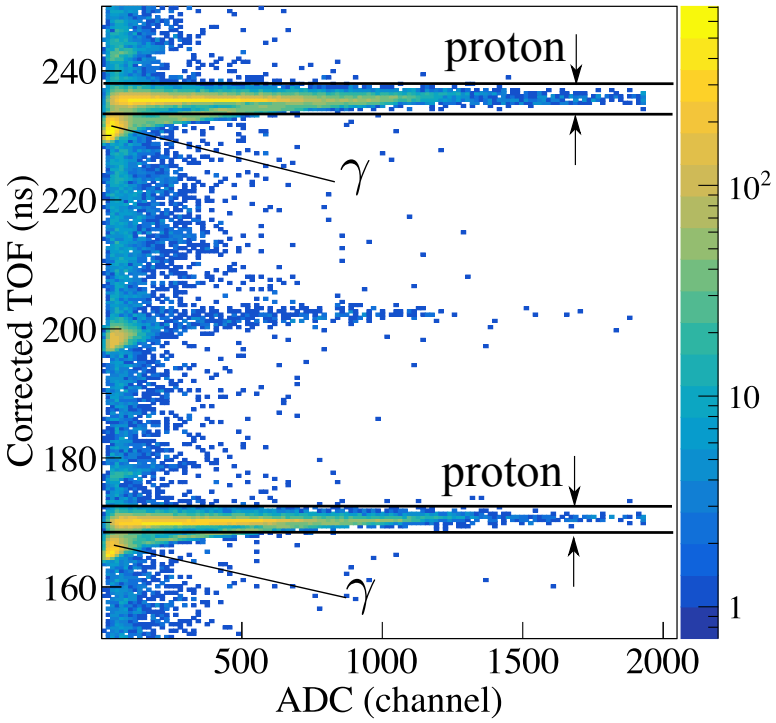

Figure 3.11: Typical example of PID of recoil particles using a correlation between the corrected TOF and the energy deposit measured with the RPC. Two horizontally long loci indicated by the arrows correspond to recoil protons. γ rays produced by nuclear reactions are also detected.

background spectra were determined by taking into account the beam intensities, the target thicknesses, the tracking efficiencies, and the DAQ efficiencies. The background-free spectra for the ^{13}C(α, α') reaction were successfully obtained by subtracting contributions from the $\alpha + p$ scattering and $^{\rm nat}$C as shown in Fig. 3.13 (c).

Since the background measurement with the $^{\rm nat}$C target was not performed for the low-lying states in the excitation-energy region of $E_x \leq 7$ MeV at $\theta_{\rm lab} = 0°$, the ^{12}C contribution to the measurement for the ^{13}C(α, α') reaction was evaluated only at $E_x \geq 7$ MeV. Therefore, the background due to the first excited state at $E_x = 4.44$ MeV in ^{12}C was not subtracted at $\theta_{\rm lab} = 0°$, but its contribution was clearly distinguished from the discrete states of ^{13}C in the excitation-energy spectrum.

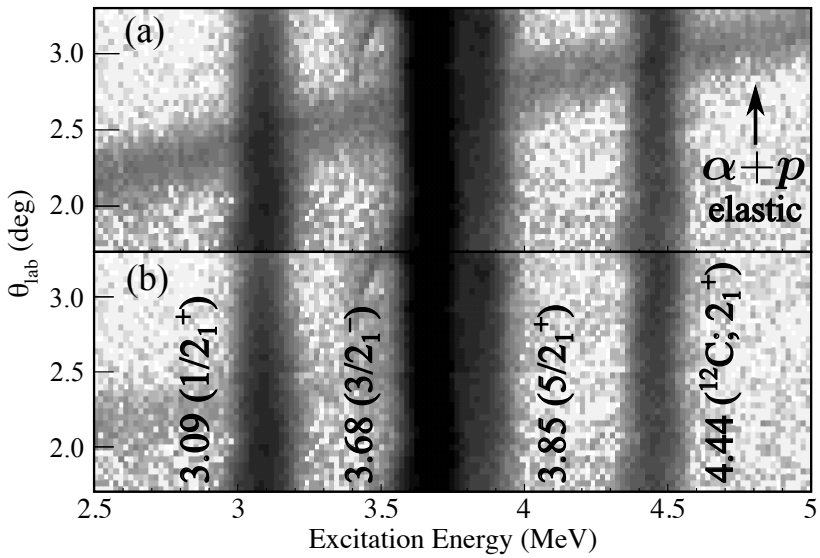

Figure 3.12: Two-dimensional scatter plots of the scattering angle in the laboratory frame versus the excitation energy of ^{13}C measured (a) without and (b) with the RPC. The four vertical loci correspond to the $1/2_1^+, 3/2_1^-, 5/2_1^+$ states at $E_x = 3.09$, 3.68, and 3.85 MeV in ^{13}C and the 2_1^+ state at $E_x = 4.44$ MeV in ^{12}C. The locus indicated by the arrow corresponds to the $\alpha + p$ elastic scattering.

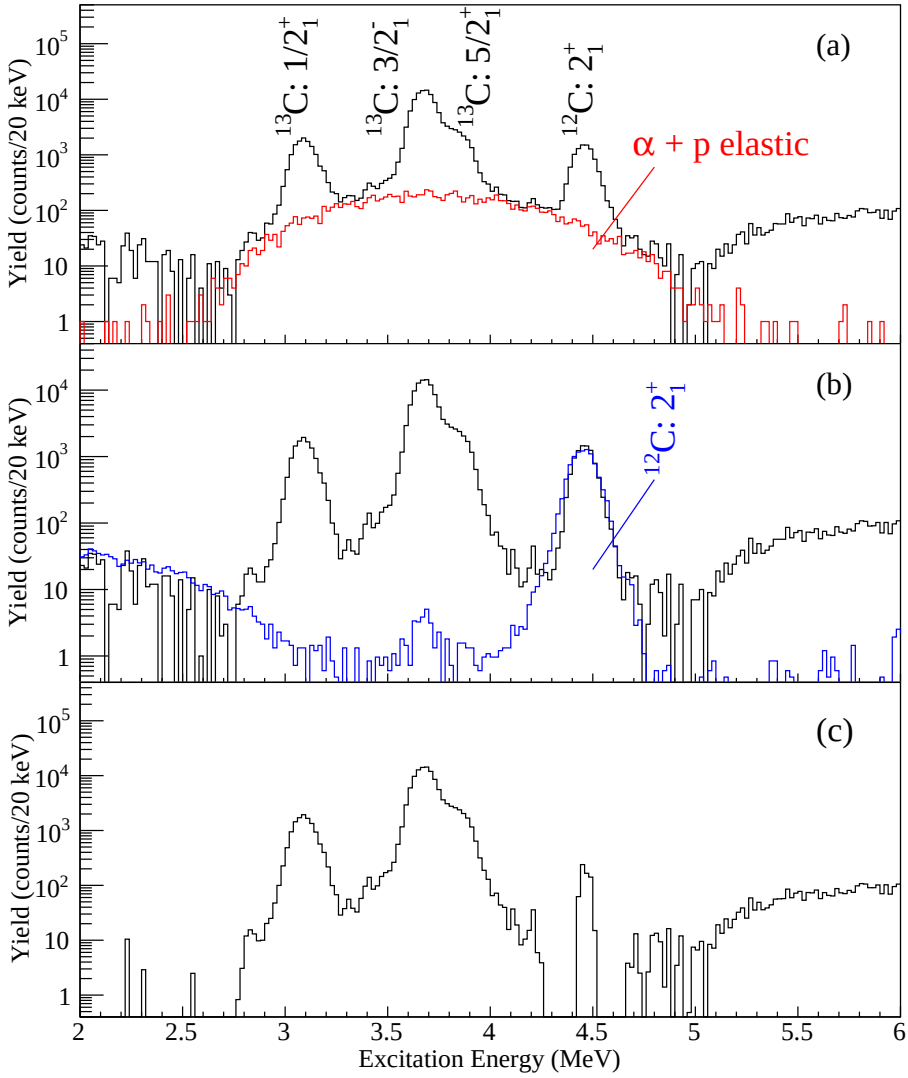

Figure 3.13: Excitation-energy spectra for the ^{13}C(α, α') reaction measured at $E_\alpha = 388$ MeV at $\theta_{\rm lab} = 2.5°$. (a) The open histogram shows the spectrum obtained with the ^{13}C target. The red histogram corresponds to the $\alpha + p$ events. (b) The excitation-energy spectrum obtained by eliminating the $\alpha + p$ events. The blue histogram shows the normalized spectrum obtained with the $^{\rm nat}$C target. (c) Background-free spectrum for the ^{13}C(α, α') reaction.

3.6 Determination of solid angles

The solid angle was determined with an entrance slit of the Grand Raiden spectrometer and software gates. When the Grand Raiden spectrometer was located at $\theta_{\rm GR} \neq 0^\circ$, the vertical angular acceptance $\Delta\phi$ was $\pm$20 mr for the measurements at $2.5^\circ \leq \theta_{\rm GR} \leq 5.1^\circ$ and $\pm$30 mr at $\theta_{\rm GR} \geq 6.8^\circ$. The horizontal angular acceptance $\Delta\theta$ was separated into four angular bins ($-0.8^\circ \leq \theta_{\rm tgt} \leq -0.4^\circ$, $-0.4^\circ \leq \theta_{\rm tgt} \leq 0^\circ$, $0^\circ \leq \theta_{\rm tgt} \leq 0.4^\circ$, and $0.4^\circ \leq \theta_{\rm tgt} \leq 0.8^\circ$) by the software gates. When the Grand Raiden spectrometer was located at $\theta_{\rm GR} = 0^\circ$, the solid angle was divided into two bins as shown in Fig. 3.14. In order to reduce background events in the excitation-energy spectra, the solid angle was gated asymmetrically about $\theta_{\rm tgt}$.

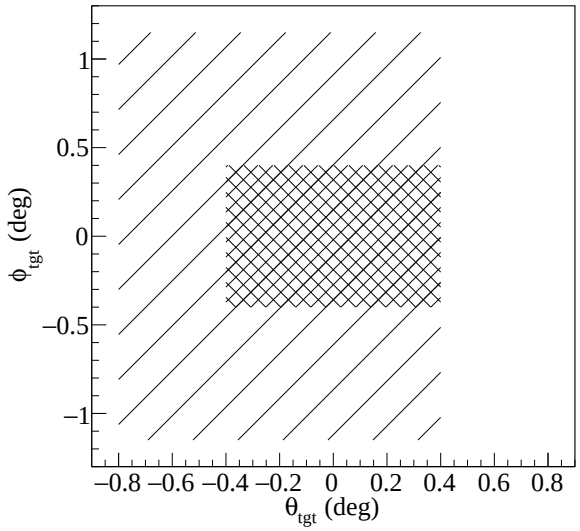

Figure 3.14: Schematic view of the solid angle defined in the present analysis when the Grand Raiden spectrometer was located at $\theta_{\rm GR} = 0^\circ$. The two regions with the different hatches show the two angular acceptances in the present analysis.

The solid angle $\Delta\Omega$ and the average scattering angle $\bar{\theta}_{\rm lab}$ are given by

$$\Delta\Omega = \int_{-\frac{\Delta\theta}{2}}^{+\frac{\Delta\theta}{2}} \int_{-\frac{\Delta\phi}{2}}^{+\frac{\Delta\phi}{2}} d\theta_{\rm tgt} d\phi_{\rm tgt}, \tag{3.14}$$

$$\bar{\theta}_{\rm lab} = \frac{\displaystyle\int_{-\frac{\Delta\theta}{2}}^{+\frac{\Delta\theta}{2}} \int_{-\frac{\Delta\phi}{2}}^{+\frac{\Delta\phi}{2}} \theta_{\rm lab} d\theta_{\rm tgt} d\phi_{\rm tgt}}{\displaystyle\int_{-\frac{\Delta\theta}{2}}^{+\frac{\Delta\theta}{2}} \int_{-\frac{\Delta\phi}{2}}^{+\frac{\Delta\phi}{2}} d\theta_{\rm tgt} d\phi_{\rm tgt}}. \tag{3.15}$$

3.7 Estimation of efficiencies

In order to determine the cross section, it is necessary to estimate the efficiencies of the present measurement. Two types of the efficiencies were taken into account in the analysis: the tracking efficiency of the MWDCs and the DAQ efficiency. The tracking and DAQ efficiencies were evaluated for every run.

The tracking efficiency on each plane of the MWDCs was estimated as

$$\epsilon_{X1} = \frac{N_{X1\cap U1\cap X2\cap U2}}{N_{U1\cap X2\cap U2}}, \tag{3.16}$$

$$\epsilon_{X2} = \frac{N_{X1\cap U1\cap X2\cap U2}}{N_{X1\cap U1\cap U2}}, \tag{3.17}$$

$$\epsilon_{U1} = \frac{N_{X1\cap U1\cap X2\cap U2}}{N_{X1\cap X2\cap U2}}, \tag{3.18}$$

$$\epsilon_{U2} = \frac{N_{X1\cap U1\cap X2\cap U2}}{N_{X1\cap X2\cap U1}}, \tag{3.19}$$

where $N_{X1\cap U1\cap X2\cap U2}$ is the number of events in which the trajectories of scattered particles were determined with all of the four planes of the MWDCs. $N_{U1\cap X2\cap U2}$ ($N_{X1\cap U1\cap U2}$, $N_{X1\cap X2\cap U2}$, and $N_{X1\cap X2\cap U1}$) in the denominator is the number of events in which the trajectories were determined with three planes except the $X1$ ($X2, U1$, and $U2$) plane. In principle, the position information from all of the four planes of the MWDCs were needed to reconstruct the three dimensional particle trajectories. However, the particle trajectories could be approximately determined with the three planes by making up the missing information with an assumption of $\phi_{\rm fp} = 0$. This approximation was reasonable thanks to the ion-optical property of the Grand Raiden spectrometer that the particle trajectories on the focal plane were almost parallel in the vertical direction ($|\phi_{\rm fp}| \leq 5$ mr). The overall tracking efficiency ($\epsilon_{\rm MWDC}$) was calculated by $\epsilon_{\rm MWDC} = \epsilon_{X1} \times \epsilon_{X2} \times \epsilon_{U1} \times \epsilon_{U2}$.

The position dependence of the tracking efficiency was also examined. Since the position on the focal plane could be related to the excitation energy, the efficiency of each plane of the MWDCs could be estimated as a function of excitation energy. Typical tracking efficiencies of the MWDCs are shown in Fig. 3.15.

The DAQ efficiency was determined from the ratio of the number of accepted events to that of requested events. The DAQ efficiency was within the range of 90%–99% depending on the trigger rate in the present measurement.

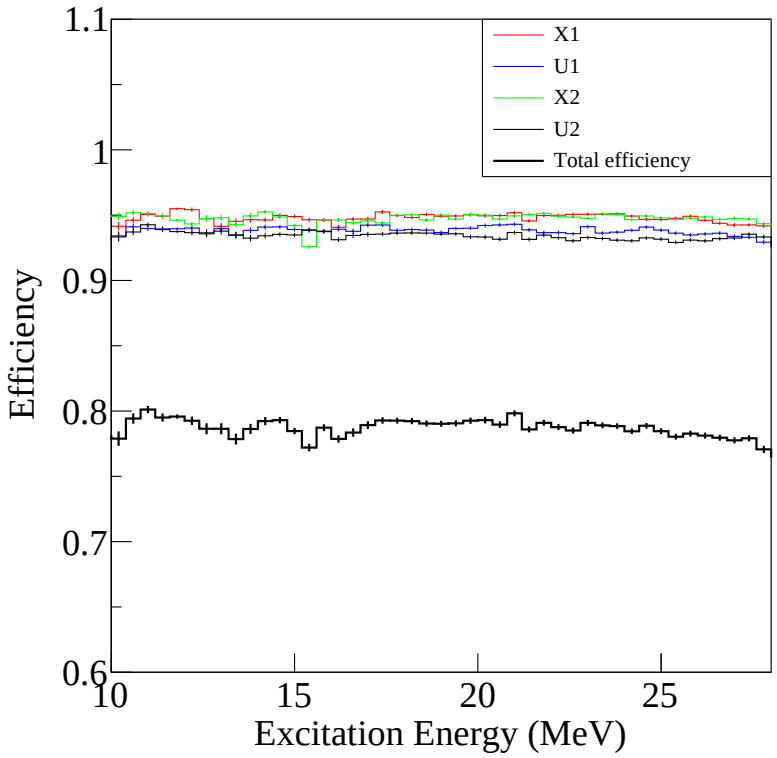

Figure 3.15: Typical detection efficiency of each plane of the MWDCs for the ^{13}C(α, α') reaction at $\theta_{\rm lab} = 3.7^\circ$ as a function of the excitation energy. The red, blue, green, and black histograms show the detection efficiencies for the X1, U1, X2, and U2 planes of the MWDCs at each excitation-energy bin with a width of 0.2 MeV. The thick black histogram shows the total tracking efficiency $\epsilon_{\rm MWDC}$.

3.8 Determination of differential cross sections

The double-differential cross sections for the α inelastic and elastic scatterings in the laboratory frame $[d^2\sigma/d\Omega_{\rm lab}dE_x]$ were obtained by dividing the number of the detected α particles Y by the number of nuclei per unit area in the target $N_{\rm tgt}$, the number of the incident beam particles $N_{\rm beam}$, the detection solid angles $\Delta\Omega_{\rm lab}$, the excitation-energy bin ΔE_x, the tracking efficiency $\epsilon_{\rm MWDC}$, the DAQ efficiency $\epsilon_{\rm DAQ}$, and the charge-collection efficiency $\epsilon_{\rm FC}$ as

$$\frac{d^2\sigma}{d\Omega_{\rm lab}dE_x}(\theta_{\rm lab}) = \frac{Y}{N_{\rm tgt}N_{\rm beam}\Delta\Omega\Delta E} \cdot \frac{1}{\epsilon_{\rm MWDC}\epsilon_{\rm DAQ}\epsilon_{\rm FC}}. \tag{3.20}$$

The absolute values of the cross sections for the low-lying states at $\theta_{\rm GR} = 0^\circ$ could not be determined because the beam stopper installed upstream of the MWDCs did not measure the

beam current as described in Sec. 2.6. Therefore, the cross sections for the low-lying states were normalized using the $1/2^-_2$ state at $E_x = 8.86$ MeV as shown in Fig. 3.16 since this state could be measured in both of the two setups at $\theta_{\rm GR} = 0°$.

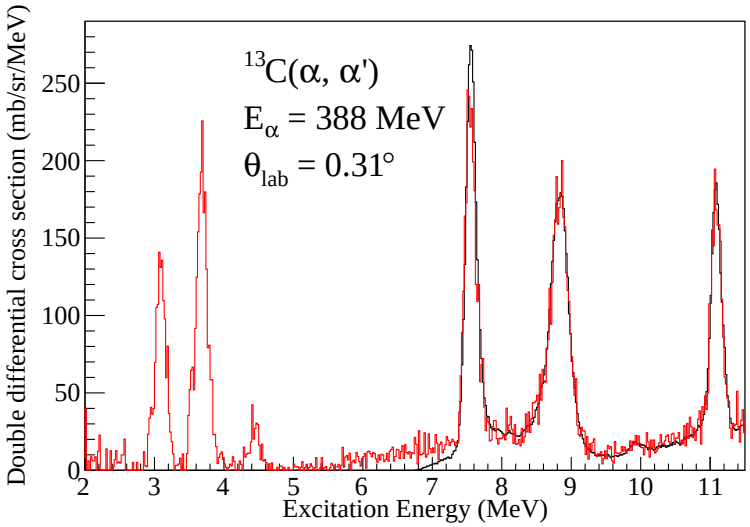

Figure 3.16: Excitation-energy spectra for the ^{13}C(α, α') reaction obtained at $\theta_{\rm lab} = 0.31°$. The black histogram shows the excitation-energy spectrum at $E_x \geq 7$ MeV measured by using the 0deg-FC. The red histogram shows the spectrum for the low-lying states measured by using the beam stopper.

The cross section in the laboratory frame $[d^2\sigma/d\Omega_{\rm lab}dE_x]$ was converted to that in the center-of-mass frame $[d^2\sigma/d\Omega_{\rm c.m.}dE_x]$ by taking into account the difference in the solid angle between the laboratory and center-of-mass frame as

$$\frac{d^2\sigma}{d\Omega_{\rm c.m.}dE}(\theta_{\rm c.m.}) = \frac{d\Omega_{\rm lab}}{d\Omega_{\rm c.m.}}\frac{d^2\sigma}{d\Omega_{\rm lab}dE}(\theta_{\rm lab}). \tag{3.21}$$

The ratio $d\Omega_{\rm c.m.}/d\Omega_{\rm lab}$ and $\theta_{\rm c.m.}$ were calculated from the relativistic kinematics.

Chapter 4

Analysis and results

4.1 Excitation-energy spectra

Typical excitation-energy spectra for the ^{13}C(α, α') reaction measured at $\theta_{\rm lab} = 0.31^\circ$ and 2.00° are shown in Fig. 4.1. The open and hatched histograms show the spectra at $\theta_{\rm lab} = 0.31^\circ$ and 2.00°, respectively. Several discrete states in the excitation-energy region of $E_x \leq 11.08$ MeV listed in the compilation [48] are clearly observed in the spectra. The energy resolution for the first excited state at $E_x = 3.09$ MeV was about 140 keV at full width at half maximum, dominated by the energy spread of the He^{2+} beam.

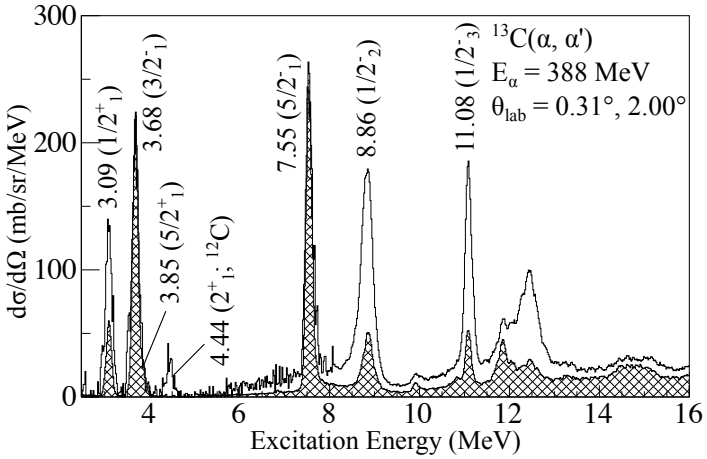

Figure 4.1: Typical excitation-energy spectra for the ^{13}C(α, α') reaction at $E_\alpha = 388$ MeV. The open and hatched histograms show the spectrum at $\theta_{\rm lab} = 0.31^\circ$ and 2.00°, respectively.

In addition to the discrete states at $E_x \leq 11.08$ MeV, we observed a prominent bump

structure around $E_x = 12.5$ MeV in the spectrum at $\theta_{\rm lab} = 0.31^\circ$. The detailed level structures at 10.5 MeV $\leq E_x \leq$ 13.0 MeV were examined by fitting the measured spectra with the known states in Ref. [48] and several new states. The shape of the excited states was assumed to be the Voigtian shape in which the Lorentzian profile was convoluted with the Gaussian profile as

$$V(E;\,\sigma,\Gamma) = \int_{-\infty}^{\infty} G(E';\,\sigma) L(E - E';\,\Gamma) dE'. \tag{4.1}$$

Here, G is the Gaussian profile describing the beam shape and L is the Lorentzian profile. E and Γ denote the energy and width of the excited state. σ denotes the energy spread of the beam. A quadratic polynomial was used to describe continuum states. The energies and widths of the known states were fixed at the values listed in Ref. [48], whereas those of the new states were determined to fit the five spectra obtained at $\theta_{\rm lab} = 0.31$–2.78° simultaneously. Five new states were introduced to reasonably well fit the measured spectra. Although we included all the states listed in Ref. [48] in the peak-fit analysis at first as tabulated in the left three columns in Table 4.1, several states with almost zero yields were neglected in the following analysis. The fit results are drawn by the solid lines in Fig. 4.2. The energies and widths of the excited states used in the peak-fit analysis are summarized in the fourth and fifths columns of Table 4.1. The isoscalar transition strengths $B(IS\lambda)$ and the energy-weighted sum-rule (EWSR) fractions for these states determined by the DWBA analysis are also given in Table 4.1. The details of the DWBA analysis will be described in Sec. 4.2.

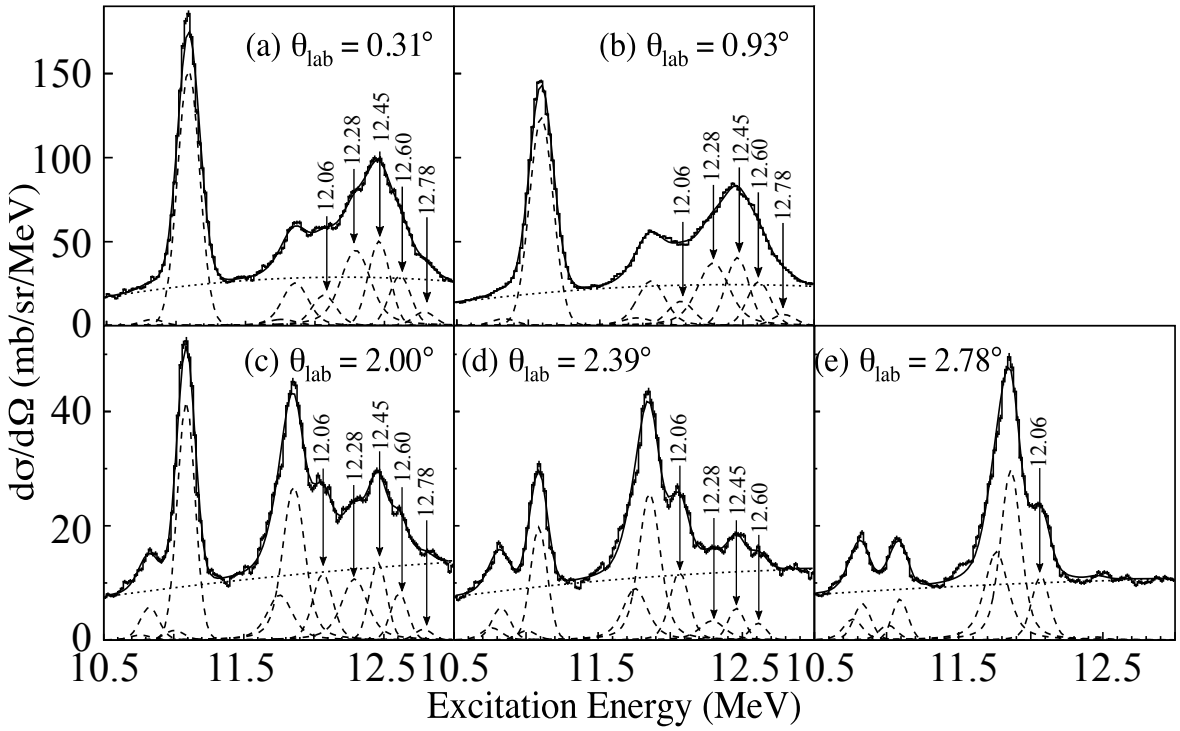

Figure 4.2: Excitation-energy spectra in the region of 10.5 MeV $\leq E_x \leq$ 13.0 MeV measured at $\theta_{\rm lab} = 0.31$–$2.78°$. Only statistical errors were taken into account in the peak-fit analysis. The solid lines show the result of the fit. The dashed lines show the fitting curves for the excited states. The dotted lines show the assumed continuum states. The new states included in the peak-fit analysis are indicated by the vertical arrows.

Table 4.1: Excitation energies and widths of the excited states at 10.5 MeV $\leq E_x \leq$ 13.0 MeV taken from Ref [48] and those used in the peak-fit analysis. Isoscalar transition strengths $B(IS\lambda)$ and EWSR fractions determined by the DWBA analysis are also tabulated.

	Ref. [48]		Present				
J^π	E_x (MeV)	Γ (keV)	E_x (MeV)	Γ (keV)	Multipolarity	$B(IS\lambda)$ (fm$^{2\lambda}$)[a]	EWSR fraction (%)
$7/2^-$	10.753 ± 0.004	55 ± 2	10.753	55	$IS4$	370 ± 140	0.08 ± 0.03
$5/2^-$	10.818 ± 0.005	24 ± 3	10.818	24	$IS2$	1.7 ± 0.1	0.27 ± 0.02
$1/2^+$	10.996 ± 0.006	37 ± 4	10.996	37	$IS1$	< 2.3	< 0.5
$1/2^-$	11.080 ± 0.005	< 4	11.080	4	$IS0$	19.2 ± 0.3	3.2 ± 0.1
$3/2^-$	11.748 ± 0.010	110 ± 15	11.748	110	$IS2$	5.6 ± 1.6	1.0 ± 0.3
$7/2^+$	11.848 ± 0.004	68 ± 4	11.848	68	$IS3$	740 ± 80	4.8 ± 0.5
$5/2^+$	11.950 ± 0.040	500 ± 80					
			12.055 ± 0.001	38 ± 4	$IS0$[b] $IS2$[b]	1.7 ± 0.3 2.2 ± 0.1	0.32 ± 0.06 0.40 ± 0.02
$3/2^+$	12.106 ± 0.005	540 ± 70					
$5/2^-$	12.130 ± 0.050	80 ± 30					
$1/2^+$	12.140 ± 0.070	430 ± 70			$IS1$	< 1.8[c]	< 0.5[c]
$3/2^-$	12.187 ± 0.010	150 ± 40					
			12.282 ± 0.005	122 ± 22	$IS0$	4.1 ± 0.4	0.77 ± 0.08
$7/2^-$	12.438 ± 0.012	140 ± 30					
			12.450 ± 0.003	$\ll 70$[d]	$IS0$	4.9 ± 0.4	0.93 ± 0.08
			12.601 ± 0.003	$\ll 70$[d]	$IS0$	3.1 ± 0.2	0.59 ± 0.03
			12.775 ± 0.004	$\ll 70$[d]	$IS0$	0.92 ± 0.05	0.18 ± 0.01

[a] The units of $B(IS0)$ and $B(IS1)$ are fm^4 and fm^6, respectively.

[b] Both the $IS0$ and $IS2$ transitions contributed to this state. See text for detail.

[c] Although this state was not included in the peak-fit analysis, the upper limits of the 95% confidence intervals for the $B(IS1)$ and EWSR fraction were evaluated. See text for detail.

[d] Much smaller enough than the energy resolution ($\sigma \sim 70$ keV) in the present measurement.

4.2 DWBA analysis

We calculated cross sections for the ^{13}C(α, α') reaction at $E_\alpha = 388$ MeV in the framework of the DWBA using a computer code ECIS-95 [77]. The calculated cross sections were compared with the measured cross sections to determine the isoscalar transition strengths in ^{13}C. The optical-model potential for the α elastic scattering was used as the distorting potential. The same distorting potential was applied to the entrance and exit channels. The optical-model potential was obtained using the single-folding model, where an effective αN interaction was folded with the ground-state density distribution of the target nucleus.

4.2.1 Density distribution of nucleus

The charge distributions $\rho_c(r)$ for the ground states of ^{12}C and ^{13}C were derived from the electron-scattering data [78]. $\rho_c(r)$ of ^{12}C was parameterized in the form of the sum of Gaussian [78] as

$$\rho_c(r) = \sum_i A_i \left\{ \exp\left[-\frac{r - R_i^2}{\gamma} \right] + \exp\left[-\frac{r + R_i^2}{\gamma} \right] \right\}, \tag{4.2}$$

$$A_i = ZeQ_i \left[2\pi^{3/2}\gamma^3 \left(1 + \frac{2R_i^2}{\gamma^2} \right) \right]^{-1}, \tag{4.3}$$

where R_i and Q_i are the position and the amplitude of the Gaussians. R_i, Q_i, and γ were determined to reproduce the cross sections of the electron elastic scattering under the constraint of $\sum_i Q_i = 1$. $\rho_c(r)$ of ^{13}C was parameterized in the form of the modified harmonic oscillator as

$$\rho_c(r) = \rho_0[1 + \alpha(r/a)^2]\exp[-(r/a)^2]. \tag{4.4}$$

Here, a and α are free parameters to be determined to reproduce the measured cross sections of the electron elastic scattering. ρ_0 is a normalization constant determined to satisfy

$$4\pi \int \rho_c(r) r^2 dr = Ze. \tag{4.5}$$

The charge distributions were used as the proton-density distributions $\rho_p(r)$ for the ground states in the present analysis. The difference between the charge distribution and the point-proton distribution was included in the effective interaction and was not explicitly considered

in the present analysis. The neutron-density distribution $\rho_n(r)$ of ^{12}C was assumed to be same as $\rho_p(r)$ of ^{12}C. On the other hand, $\rho_n(r)$ of ^{13}C was assumed to be $\rho_n(r) = \rho_p(r')$ with $r' = (6/7)^{1/3}r$. Figure 4.3 shows the density distributions for the ground state of ^{12}C and ^{13}C used in the present analysis.

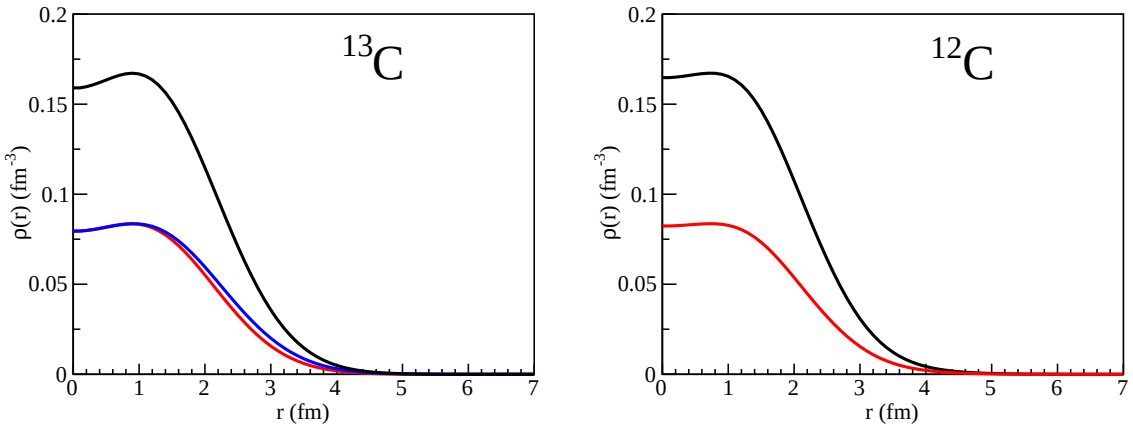

Figure 4.3: Density distributions for the ground state of ^{13}C and ^{12}C used in the present analysis. The red and blue lines show the proton and neutron-density distributions, respectively. The black line shows the matter-density distribution given by $\rho_p(r) + \rho_n(r)$.

4.2.2 Optical-model potential and effective αN interaction

The optical-model potential $U(r)$ was given as

$$U(r) = \int d\boldsymbol{r'} \rho(r') u(|\boldsymbol{r} - \boldsymbol{r'}|), \tag{4.6}$$

where $\boldsymbol{r'}$ and $\boldsymbol{r}$ denote the position of a nucleon in the target nucleus and of an incident α particle, respectively. $\rho(r')$ is the matter-density distribution of the ground state given by $\rho_p(r') + \rho_n(r')$, and $u(|\boldsymbol{r} - \boldsymbol{r'}|)$ is the effective interaction between a nucleon and an α particle. Figure 4.4 shows the definition of the spatial coordinates $\boldsymbol{r}$ and $\boldsymbol{r'}$.

Many previous analyses of the α inelastic scattering [34, 47, 61–70] employed the density-dependent effective αN interaction proposed by Satchler and Khoa [79]. However, the recent systematic analysis of the α inelastic scattering demonstrated that the cross sections for the $IS0$ transition tended to be overestimated when the density-dependent interaction was used [59]. Therefore, we used the density-independent interaction parameterized by the

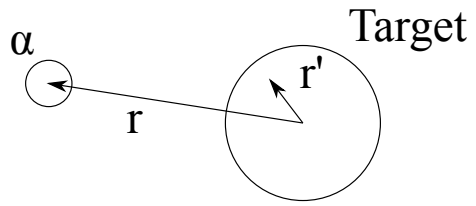

Figure 4.4: Definition of the spacial coordinates.

Gaussian functions as

$$u(|\boldsymbol{r}-\boldsymbol{r'}|) = -ve^{-|\boldsymbol{r}-\boldsymbol{r'}|^2/\alpha_v^2} - iwe^{-|\boldsymbol{r}-\boldsymbol{r'}|^2/\alpha_w^2}, \tag{4.7}$$

in the present DWBA analysis. Here, v and w are the depth parameters. α_v and α_w are the range parameters of the interaction. Very recently, a sophisticated interaction obtained by the G-matrix folding model has been used with the matter-density distribution calculated with the AMD for theoretical studies of the α inelastic scattering [80–84]. However, we used the Gaussian form interaction in the present analysis for simplicity.

The interaction parameters in Eq. (4.7) were determined to reproduce the measured cross section of the α elastic scattering off ^{12}C as shown in Fig. 4.5(a) since the ambiguity in the assumption about the neutron-density distribution of ^{13}C caused uncertainty in the determination of the interaction. The depth and range parameters were determined to be $v = 20.4$ MeV, $w = 9.35$ MeV, $\alpha_v = 1.97$ fm, and $\alpha_w = 2.18$ fm. Figure 4.5(b) shows the comparison between the measured elastic cross section for ^{13}C and the calculated cross section using the same interaction parameters with ^{12}C. The measured cross section for ^{13}C is well reproduced by the single-folding potential, indicating that the assumption on the neutron-density distribution of ^{13}C and application of the same effective interaction for ^{12}C and ^{13}C are reasonable.

4.2.3 Transition densities and potentials

The transition potentials for the α inelastic scattering were calculated by folding the effective αN interaction with the transition densities. The transition densities $\delta\rho^{(\lambda)}(r)$ for the $\Delta L = \lambda$

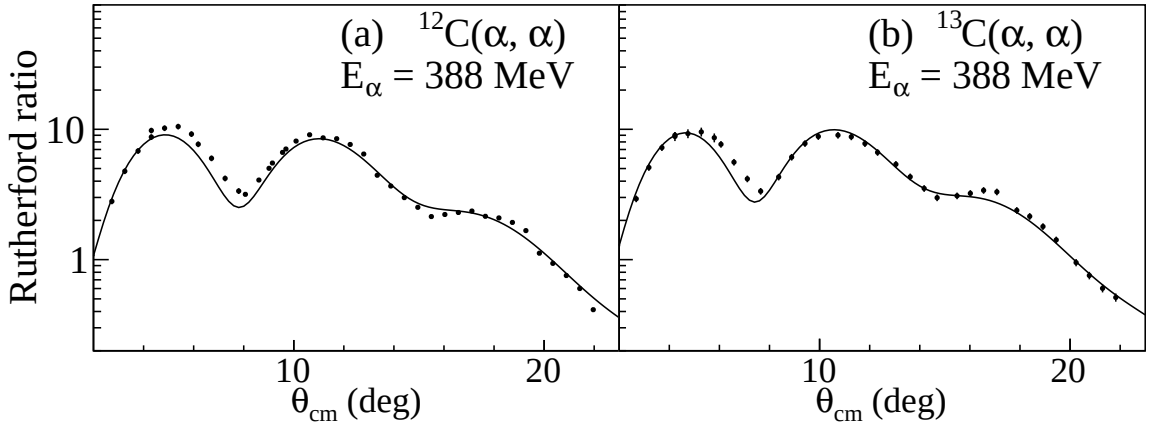

Figure 4.5: Angular distributions of the cross sections for the α elastic scattering off (a) ^{12}C and (b) ^{13}C at $E_\alpha = 388$ MeV relative to the Rutherford cross sections (Rutherford ratio). The measured cross sections (the solid circles) are compared with the calculations using the single-folding potentials (the solid lines).

transitions were obtained by the macroscopic model [85, 86] as

$$\delta\rho^{(0)}(r) = -\alpha_0 \left(3 + r\frac{d}{dr}\right)\rho(r) \quad (\lambda = 0), \tag{4.8}$$

$$\delta\rho^{(1)}(r) = -\frac{\beta_1}{\sqrt{3}R}\left[3r^2\frac{d}{dr} + 10r - \frac{5}{3}\langle r^2\rangle\frac{d}{dr} + \epsilon\left(r\frac{d^2}{dr^2} + 4\frac{d}{dr}\right)\right]\rho(r) \quad (\lambda = 1), \tag{4.9}$$

$$\delta\rho^{(\lambda)}(r) = -\delta_\lambda\frac{d}{dr}\rho(r) \quad (\lambda \geq 2), \tag{4.10}$$

where $\epsilon = (4/E_{\rm ISGQR} + 5/E_{\rm ISGMR})\hbar^2/3mA$. $E_{\rm ISGQR} = 65A^{-1/3}$ MeV and $E_{\rm ISGMR} = 80A^{-1/3}$ MeV are the mean excitation energies of the isoscalar giant quadrupole and monopole resonances. α_0 is the deformation parameter, and β_1 is the collective coupling parameter for the isoscalar dipole resonance. δ_λ is the deformation length. R is the half-density radius of the Fermi mass distribution. The transition potential $\delta U_\lambda(r)$ for the $\Delta L = \lambda$ transition was obtained by folding the transition density with the effective αN interaction as

$$\delta U_\lambda(r) = \int \delta\rho^{(\lambda)}(r')u(|\boldsymbol{r} - \boldsymbol{r'}|)dr'. \tag{4.11}$$

The isoscalar transition matrix elements $M(IS\lambda)$ were calculated from the transition

densities as

$$M(IS0) = \sqrt{4\pi} \int \delta\rho^{(0)}(r) r^4 dr, \tag{4.12}$$

$$M(IS1) = \int \delta\rho^{(1)}(r) r^5 dr, \tag{4.13}$$

$$M(IS\lambda) = \int \delta\rho^{(\lambda)}(r) r^{\lambda+2} dr, \qquad (\lambda \geq 2). \tag{4.14}$$

The isoscalar transition strengths $B(IS\lambda)$ were obtained from $M(IS\lambda)$ using the relation as

$$B(IS\lambda) = \frac{1}{2J_i + 1} |M(IS\lambda)|^2, \tag{4.15}$$

where J_i is the spin of the initial state. The transition strengths were deduced by determining α_0, β_1/R, and δ_λ to reproduce the measured cross sections. If one excited state at the excitation energy E_x exhausts 100% of the EWSR strengths for the $\Delta L = \lambda$ transition, α_0, β_1/R, and δ_λ are given by the sum rule limits in Refs. [85, 86] as

$$\alpha_0^2 = \frac{2\pi\hbar^2}{mAE_x\langle r^2 \rangle}, \tag{4.16}$$

$$\left(\frac{\beta_1}{R}\right)^2 = \frac{6\pi\hbar^2}{mAE_x} \frac{1}{11\langle r^4 \rangle - 25/3\langle r^2 \rangle^2 - 10\epsilon\langle r^2 \rangle}, \tag{4.17}$$

$$\delta_\lambda^2 = \frac{\lambda(2\lambda+1)^2}{(\lambda+2)} \frac{2\pi\hbar^2}{mAE_x} \frac{\langle r^{2\lambda-2} \rangle}{\langle r^{\lambda-1} \rangle^2}. \tag{4.18}$$

The measured transition strengths were converted into the EWSR fractions using the sum-rule limits given by Eqs. (4.16)–(4.18).

4.2.4 Coulomb excitation

Although the isoscalar transitions are selectively induced by the strong interaction in the α inelastic scattering, the isovector transitions can be induced through the Coulomb interaction. Especially, the isovector $E1$ transition is not negligible. Therefore, the cross sections for the $\Delta L = 1$ transitions were calculated by taking into account the interference between the isoscalar and isovector transitions. The isovector $E1$ strengths were determined from the photonuclear cross section or radiative-decay widths [48, 87–89]. Assuming that the $E1$ transition dominates the photonuclear reaction, the photonuclear cross section was related to

the $E1$ strengths function as

$$\sigma(E) = \frac{16\pi^3}{9}\frac{E}{\hbar c}\frac{dB(E1)}{dE}. \tag{4.19}$$

The photonuclear cross section for ^{13}C reported in Refs. [88,89] is shown in Fig. 4.6(a), while the $E1$ strength distribution obtained by Eq. (4.19) is shown in Fig. 4.6(b).

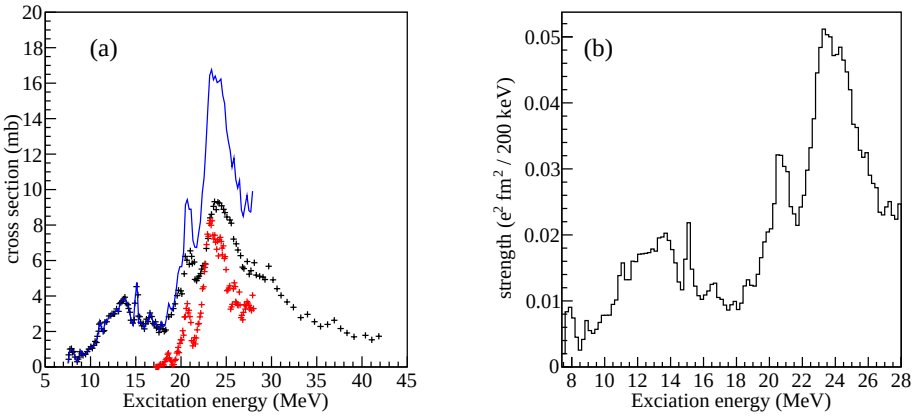

Figure 4.6: (a) Photonuclear cross section for ^{13}C. The black points show the sum of the cross sections for the (γ, n), (γ, np), $(\gamma, n\alpha)$, and $(\gamma, 2n)$ reactions [88], whereas the red points show the cross section for the $\sigma(\gamma, p)$ reaction [89]. The solid blue line shows the sum of the cross section for these five reactions. (b) $E1$ strength distribution obtained using Eq. (4.19).

It should be commented that the validity of the DWBA analysis with the macroscopic model for the isoscalar $\Delta L = 0, 2$, and 3 transitions have been investigated by comparing the known electromagnetic transition strength $B(E\lambda)$ with the measured $B(IS\lambda)$ in Refs. [59,90]. However, $B(IS1)$ cannot be compared with reliable strengths determined by the electromagnetic probes. The leading term of the electric dipole operator is expressed as

$$O^{E1}_{\mu} = \sum_{i=1}^{A} e(1/2 - t_{iz}) r_i Y_{1\mu}(\Omega_i), \tag{4.20}$$

$$= \frac{1}{2} e \sum_{i=1}^{A} r_i Y_{1\mu}(\Omega_i) - e \sum_{i=1}^{A} t_{iz} r_i Y_{1\mu}(\Omega_i), \tag{4.21}$$

where the isospin is $t_z = +1/2$ for neutron and $t_z = -1/2$ for proton. Since the isoscalar term (the first term of the right-hand side of Eq. (4.21)) is proportional to the center-of-mass coordinate of the nucleus, the first-order isoscalar dipole transition cannot induce an intrinsic excitation of the nucleus. Therefore, the first-order electric dipole operator is purely

isovector. Because the isoscalar dipole transition is induced by the next-order term of the dipole operator as given by Eq. (1.6), it is generally weaker than the isovector transition for electromagnetic probes. Accordingly, for the isoscalar $\Delta L = 1$ transition, uncertainty still remains in the DWBA analysis.

4.2.5 Results of the DWBA analysis

Figure 4.7 shows the comparison between the DWBA cross sections and the measured cross sections for the low-lying states at $E_x \leq 8.86$ MeV as well as those for the high-lying states at 10.5 MeV $\leq E_x \leq$ 13.0 MeV obtained by the peak-fit analysis. The measured cross sections for the low-lying states are reasonably well reproduced by the DWBA calculations for the corresponding $\Delta L = \lambda$ transition. The steep increment of the cross section at forward angles for the 3.09-MeV state is fairly well reproduced by taking into account the isovector $E1$ transition by the Coulomb excitation as shown in Fig. 4.7(a). For the several states at $E_x \geq 10.5$ MeV whose energies are close to each other, we could not reliably separate these states in the peak-fit analysis. Therefore, the sum of the cross sections for these states are plotted in Figs. 4.7(f), (g), and (h). These summed cross sections were fitted by the DWBA cross sections for the different ΔL transitions, and their transition strengths were separately determined.

The transition strengths and EWSR fractions determined by the present DWBA analysis for the low-lying states and the $1/2^-_3$ state at $E_x = 11.08$ MeV of ^{13}C are listed in Table 4.2 with the electromagnetic transition strength $B(E\lambda)$ from the ground state determined with the (e, e') reaction [48]. $B(E\lambda)$ for the mirror states in ^{13}N determined from the radiative-decay widths [48] are also tabulated in Table 4.2. It is worthy to compare the present experimental $B(IS\lambda)$ values with the known $B(E\lambda)$ values. $B(E\lambda)$ and $B(IS\lambda)$ are obtained by the neutron and proton transition matrix elements as

$$B(E\lambda) = \frac{1}{2J_i + 1}|M_p(E\lambda)|^2 e^2, \tag{4.22}$$

$$B(IS\lambda) = \frac{1}{2J_i + 1}|M_p(E\lambda) + M_n(E\lambda)|^2. \tag{4.23}$$

The proton transition matrix element for the $3/2^-_1$ state of ^{13}C is calculated by Eq. (4.22) to be $M_p(E2;\ ^{13}\mathrm{C}) = 5.2 \pm 0.2$ fm^2, and that for the mirror state in ^{13}N to be $M_p(E2;\ ^{13}\mathrm{N}) = 7.9$ fm^2 (its uncertainty is not given in Ref. [48]). Since the good mirror symmetry is conserved between ^{13}C and ^{13}N, we can assume $M_n(E2;\ ^{13}\mathrm{C}) = M_p(E2;\ ^{13}\mathrm{N})$. On this assumption,

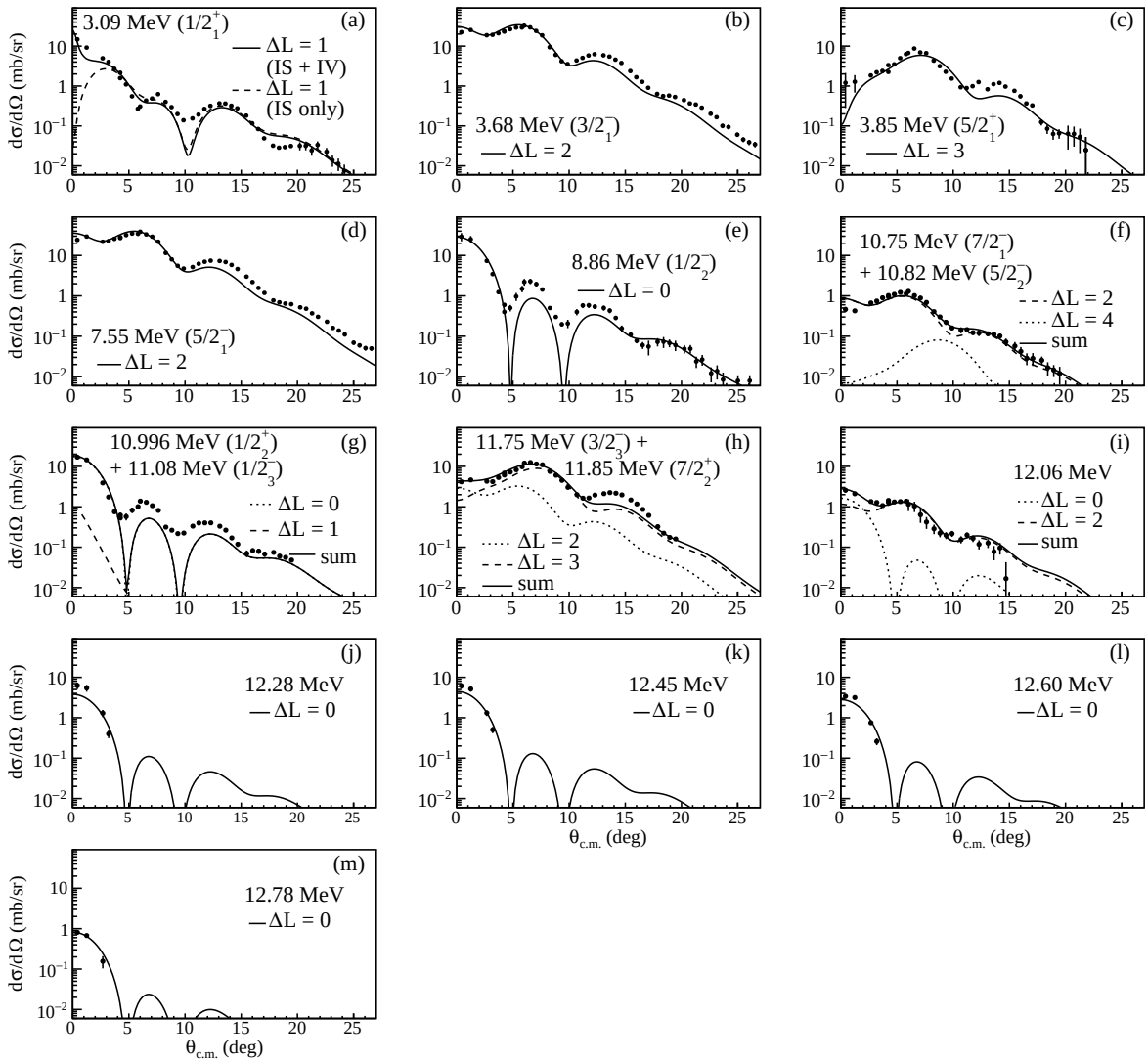

Figure 4.7: Comparison between the DWBA cross sections and the measured cross sections in the ^{13}C(α, α') reaction. The solid circles show the measured cross sections. The solid, dashed, and dotted lines show the fit result with the cross sections calculated by the DWBA. In the panel (a), the solid line shows the calculated cross section taking into account the interference between the $IS1$ and isovector $E1$ transitions, whereas the dashed line shows the cross section for the $IS1$ transition only.

the isoscalar transition strength for the $3/2^-_1$ state of ^{13}C is estimated to be $|M_p(E2;\ ^{13}\mathrm{C}) + M_p(E2;\ ^{13}\mathrm{N})|^2/2 = 84.5$ fm^4, which is larger than $B(IS2)$ determined by the α inelastic scattering by a factor of 1.5. This might be due to the large error of $M_p(E2;\ ^{13}\mathrm{N})$.

Table 4.2: $B(IS\lambda)$ strengths and EWSR fractions for the low-lying states and the $1/2^-_3$ state at $E_x = 11.08$ MeV of ^{13}C determined by the DWBA analysis with $B(E\lambda)$ determined from the (e, e') reaction [48]. $B(E\lambda)$ strengths for the mirror states in ^{13}N determined from the radiative-decay widths [48] are also presented.

J^π	E_x (MeV)	Multi. (λ)	$B(IS\lambda)$ (fm$^{2\lambda}$)[a]	fraction (%)	$B(E\lambda;\ ^{13}\mathrm{C})$ (e^2fm$^{2\lambda}$)	E_x (MeV)	$B(E\lambda;\ ^{13}\mathrm{N})$ (e^2fm$^{2\lambda}$)
$1/2^+_1$	3.09	1	9.6 ± 0.5	0.63 ± 0.03	$(1.7 \pm 0.4) \times 10^{-2}$	2.36	$(3.6 \pm 0.3) \times 10^{-2}$
$3/2^-_1$	3.68	2	56.0 ± 2.0	3.12 ± 0.11	13.3 ± 1.5	3.50	31.4[c]
$5/2^+_1$	3.85	3	472 ± 26	1.01 ± 0.06	38.6 ± 5.9	3.55	
$5/2^-_1$	7.55	2	66.3 ± 2.4	7.56 ± 0.27	17.6 ± 0.9	7.38	
$1/2^-_2$	8.86	0	29.6 ± 2.3	3.95 ± 0.31	2.2 ± 0.8[b]	8.92	
$1/2^-_3$	11.08	0	19.2 ± 0.3	3.2 ± 0.1	3.4 ± 0.8[b]	10.83	

[a] The units of $B(IS0)$ and $B(IS1)$ are fm^4 and fm^6, respectively.
[b] The value of $|M(C0)|^2/(2J_i+1)$ is listed in the unit of fm^4, where $M(C0)$ is the monopole matrix element.
[c] Uncertainty is not given in Ref. [48].

If all the nucleons of a nucleus participate in a collective transition in phase (namely, the isoscalar transition), the contribution of the protons to the transition matrix element is Z/A of the total matrix element. Therefore, under this assumption, the isoscalar transition strength could be estimated from the electromagnetic transition strength as $B(IS\lambda)/B(E\lambda) = (A/Z)^2$ ($= 4.7$ in case of ^{13}C). This relation holds relatively well for the $3/2^-_1$, $5/2^-_1$, and $1/2^-_3$ states of ^{13}C, where the ratios $r = B(IS\lambda)/B(E\lambda)$ are 4.2 ± 0.5, 3.8 ± 0.2, and 5.6 ± 1.3, respectively. However, the ratios are far from 4.7 for the $5/2^+_1$ state ($r = 12.2 \pm 2.0$) and the $1/2^-_2$ state ($r = 13.5 \pm 5.0$). This fact suggests that the neutron transition matrix elements for these states are much larger than the proton transition matrix elements. We note that this discussion cannot be applied to the dipole transitions since the relation between $B(IS1)$ and $B(E1)$ is not straightforward as described in Sec. 4.2.4.

The transition strengths and EWSR fractions for the high-lying states are separately listed in Table 4.1. The systematic uncertainties in the present DWBA analysis were evaluated by a similar method to Ref. [91]. The 68% confidence interval for the transition strength was determined by changing the amplitude of the transition density over the range satisfying

$$\tilde{\chi}^2 \leq \tilde{\chi}^2_{\mathrm{min}} + 1. \tag{4.24}$$

Here, the renormalized chi-square $\tilde{\chi}^2$ is defined as $\tilde{\chi}^2 \equiv \chi^2/(\chi^2_{\mathrm{min}}/\nu)$ where χ^2_{min} and ν are

the minimum chi-square value and the number degrees of freedom in the fit analysis. Some excited states at 10.5 MeV $\leq E_x \leq$ 13.0 MeV included in the peak-fit analysis are discussed individually below.

The 10.996 and 11.08-MeV states

The $1/2^+$ state at $E_x = 10.996$ MeV and the $1/2^-$ state at $E_x = 11.08$ MeV are listed in Ref. [48]. The 10.996-MeV state was less populated than the 11.08-MeV state in the present experiment. However, we included both states in the peak-fit analysis to reproduce the excitation-energy spectra. The experimental summed cross section was fitted by the DWBA cross sections for the $\Delta L = 0$ and 1 transitions as shown in Fig. 4.7(g). The measured cross section is dominated by the $IS0$ transition, and the dotted line for the $\Delta L = 0$ transition almost overlaps with the solid line for the summed cross section. The $E1$ strength for the 10.996-MeV state was taken from the photonuclear experiment [88], assuming that the 10.996-MeV state corresponds to a peak structure observed at $E_x = 11.0$ MeV in Ref. [88]. Since the $IS1$ strength in the present DWBA analysis was zero within its uncertainty, an upper limit of the 95% confidence interval for the $IS1$ strength was evaluated. The spin and parity of the 11.08-MeV state are unambiguously $1/2^-$ although Milin and von Oertzen proposed that this state should be the $3/2^+$ state as the band head of the $K = 3/2^+$ rotational band [92]. The 10.996-MeV state has been rarely resolved from the prominent 11.08-MeV state except in the ^{9}Be(α, n) reaction [93, 94] and the ^{9}Be$(^6$Li$, d)$ reaction [95].

The 12.14-MeV state

The $1/2^+$ state at $E_x = 12.14$ MeV is listed in Ref. [48]. However, this state was not identified in the present experiment. An upper limit of the 95% confidence interval for the $IS1$ strength was evaluated. The interference between the $E1$ and $IS1$ transitions was neglected in the DWBA calculation since no peak structure corresponding to the 12.14-MeV state was observed in the photonuclear experiment [88]. This state with a broad width of 430 keV has never been clearly observed except in the ^{9}Be(α, n) reaction [93, 94].

The bump structure around $E_x = 12.5$ MeV

We could not reproduce the observed bump structure around $E_x = 12.5$ MeV with a single Voigtian function. We needed to introduce five new states at least in the peak-fit analysis. The centroid energies of the five new states were $E_x = 12.06, 12.28, 12.45, 12.60,$ and 12.78

MeV. These energies agreed with the centroids of the observed structures in Fig. 4.2. When we added the sixth and more states in the peak-fit analysis, the chi-square of the fit was improved. However, no correspondence between the additional states and the visible structures was observed. Therefore, we did not include these additional states in the present analysis. The energy spectrum at this energy region is so complicated that the accurate peak assignment is not easy, but we can conclude that the observed bump around $E_x = 12.5$ MeV consists several $1/2^-$ states from the result of the peak fit and the DWBA analysis.

The cross sections for the four states at $E_x = 12.28, 12.45, 12.60$, and 12.78 MeV were well fitted by the DWBA cross sections for the $\Delta L = 0$ transition as shown in Figs. 4.7(j), (k), (l), and (m), respectively. Therefore, the spin and parity of these states were assigned to be $1/2^-$. On the other hand, it was necessary to consider both the $\Delta L = 0$ and 2 transitions to reproduce the cross section for the 12.06-MeV state as seen in Fig. 4.7(i). This indicates that a $1/2^-$ state and a $3/2^-$ or $5/2^-$ state exist around $E_x = 12.06$ MeV although these states were not separated in the peak-fit analysis.

4.3 Multipole decomposition analysis

4.3.1 Formalism

The cross sections for the α inelastic scattering have characteristic angular distributions depending on the transferred angular momenta. Therefore, the observed cross sections $[d^2\sigma/d\Omega\, dE_x]^{\rm exp}$ can be decomposed into each multipole component by the MDA as

$$\left[\frac{d^2\sigma}{d\Omega dE_x}\right]^{\rm exp} = \sum_{\lambda,\ \lambda\neq 1}^{\lambda_{\rm max}} a_\lambda(E_x) \left[\frac{d^2\sigma}{d\Omega dE_x}\right]^{\rm DWBA}_{IS\lambda} + \left[\frac{d^2\sigma(\beta_1/R)}{d\Omega dE_x}\right]^{\rm DWBA}_{IS1+E1}. \qquad (4.25)$$

$\left[d^2\sigma/d\Omega dE_x\right]^{\rm DWBA}_{IS\lambda}$ is the calculated cross section for the $\Delta L = \lambda$ transition which exhausts 100% of the EWSR strength, whereas $\left[d^2\sigma(\beta_1/R)/d\Omega dE_x\right]^{\rm DWBA}_{IS1+E1}$ is the cross section for the $\Delta L = 1$ transition taking into account the interference between the $IS1$ and isovector $E1$ transitions. β_1/R, whose square is proportional to $B(IS1)$, denotes the ratio of the collective coupling parameter for the $IS1$ transition to the half-density radius of the Fermi mass distribution in Eq. (4.9). $a_\lambda(E_x)$ is a parameter corresponding to the EWSR fraction for the $\Delta L = \lambda$ transition.

We determined $a_\lambda(E_x)$ and β_1/R to minimize χ^2 in the MDA under the constraint of

$a_\lambda(E_x) \geq 0$.

The MDA was performed for every 200-keV excitation-energy bin up to $E_x = 25.0$ MeV. The interference between the $E1$ and $IS1$ transitions was accounted for energy bins centered at $E_x = 3.1$ MeV and at $E_x \geq 7.5$ MeV, where the radiative-decay widths or the photonuclear cross sections were available. The maximum transferred angular momentum for the MDA was determined to be $\lambda_{\max} = 8$. This value is well above the critical value of $\lambda_{\max} = 5$ where the χ^2/ν value was almost converged as shown in Fig. 4.8.

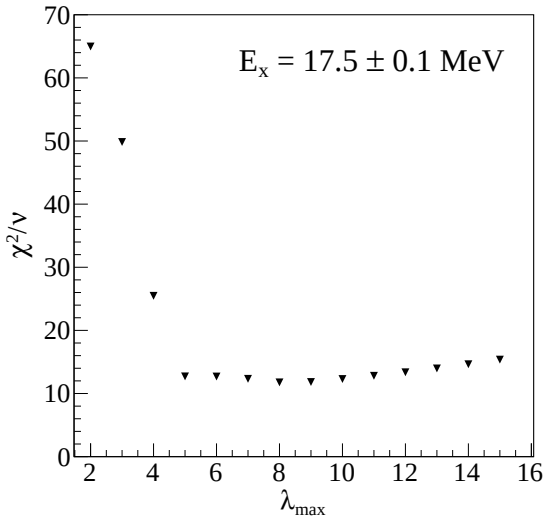

Figure 4.8: Reduced chi-square χ^2/ν in the MDA for an energy bin centered at $E_x = 17.5$ MeV as a function of the maximum transferred angular momentum $\lambda_{\max}$.

4.3.2 Results of the MDA

Figure 4.9 shows the strength distributions for the isoscalar $\Delta L = 0$–3 transitions compared with the excitation-energy spectra at $\theta_{\rm lab} = 0.93°$ and 3.17°. The $IS0$ transition is dominant at $\theta_{\rm lab} = 0.93°$, whereas the other transitions are stronger than the $IS0$ transition at $\theta_{\rm lab} = 3.17°$. The uncertainties of the transition strengths were estimated from the 68% confidence intervals for $\alpha_\lambda(E_x)$ and β_1/R, which were determined by using Eq. (4.24). When the confidence interval for one parameter was evaluated, the other parameters were freely changed to minimize χ^2.

Since the spin and parity of the ground state in ^{13}C are $1/2^-$, the spin and parity of a excited state populated by a $\Delta L = \lambda$ transition are $J = |1/2 \pm \lambda|$ and $\pi = (-)^{(\lambda+1)}$. It

should be noted that the known discrete states labeled in Fig. 4.9 are correctly observed in the corresponding $\Delta L = \lambda$ strength distributions. This demonstrates the reliability of the present MDA. Since the present DWBA calculations did not completely reproduce the cross sections for the discrete states, residues in the MDA were decomposed into incorrect strength distributions. Therefore, spurious small peaks were observed in different strength distributions near strong discrete states. Actually, small peaks in the $\Delta L = 0, 1$, and 3 strength distributions were observed at the same energy with the $5/2^-_1$ state at $E_x = 7.55$ MeV. These peaks were accompanied by the large uncertainties in the MDA.

Several narrow peaks are observed in the $\Delta L = 0$ strength distribution as shown in Fig. 4.9(a). In addition to the two peaks corresponding to the $1/2^-_2$ state at $E_x = 8.86$ MeV and the $1/2^-_3$ state at $E_x = 11.08$ MeV, a bump structure is observed at $E_x = 12.5$ MeV. This bump corresponds to the $1/2^-$ states newly found around $E_x = 12.5$ MeV. The measured angular distribution of the cross section at $E_x = 12.5$ MeV fitted by the MDA is shown in Fig. 4.10(a). The steep increase of the measured cross section at forward angles is well reproduced by the $\Delta L = 0$ transition.

In the $\Delta L = 1$ strength distribution shown in Fig. 4.9(b), not only a narrow peak due to the $1/2^+_1$ state at $E_x = 3.09$ MeV but also two bumps at $E_x = 14.5$ and 16.1 MeV are observed. These bumps correspond to shoulders at the low-energy sides of the broad structures observed at $E_x = 15.0$ and 16.3 MeV in the excitation-energy spectrum at $\theta_{\rm lab} = 3.17^\circ$ presented in Fig. 4.9(f). The measured angular distributions of the cross sections for the excitation-energy bins at $E_x = 14.5$ and 16.1 MeV are shown in Figs. 4.10(b) and (c), respectively. The sizable contributions of the $IS1$ transition to the cross sections are visible. The asymmetric shape of the bump at $E_x = 16.1$ MeV in the $\Delta L = 1$ strength distribution is due to the error of the present MDA. Since a visible peak exists around $E_x = 16.3$ MeV in the $\Delta L = 2$ strength distribution, the obtained $\Delta L = 1$ strength for the 16.3-MeV bin is affected by this peak.

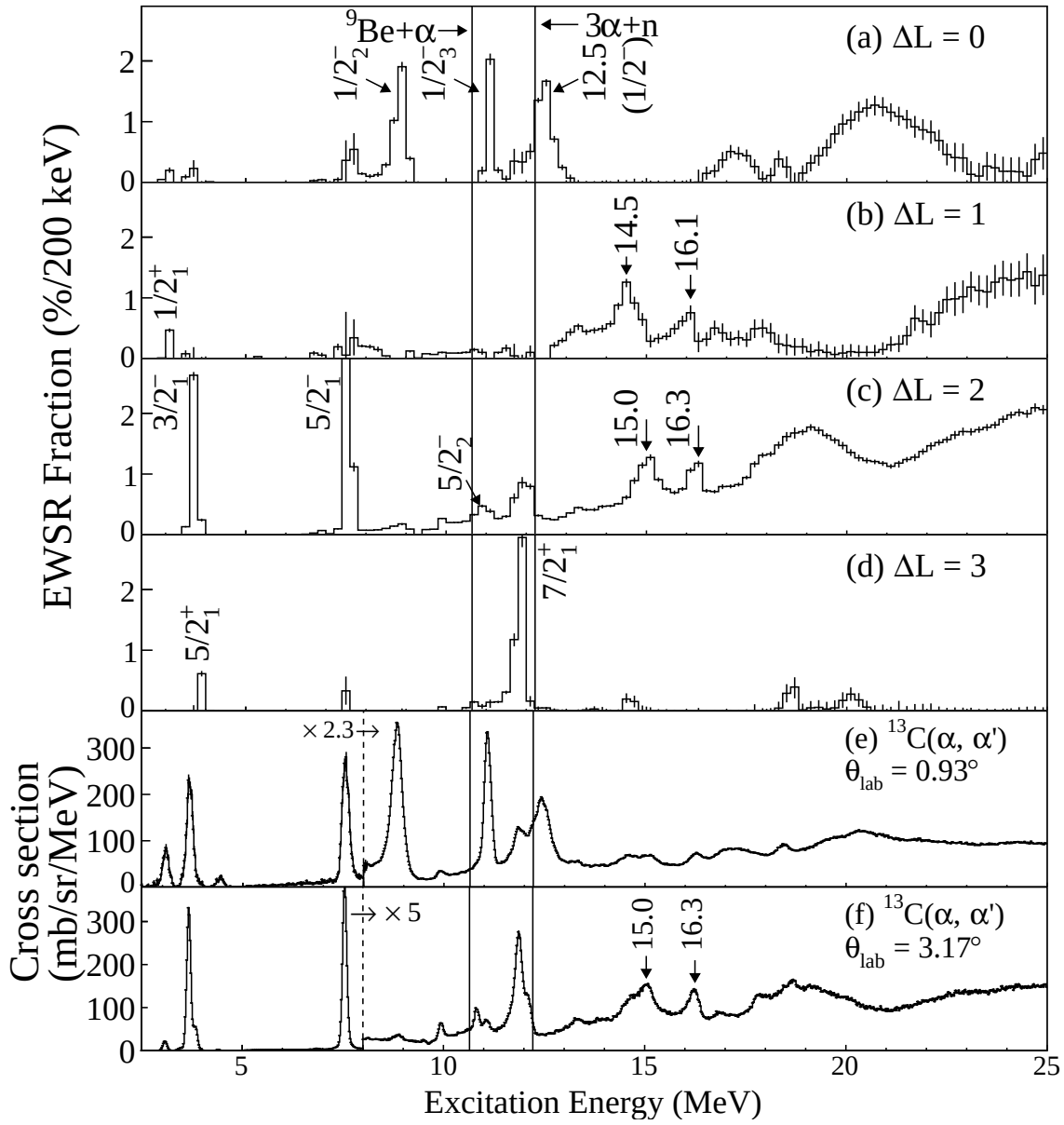

Figure 4.9: Strength distributions for the isoscalar $\Delta L = 0$–3 transitions in the ^{13}C(α, α') reaction obtained by the MDA. The threshold energies for the ^{9}Be+α and $3\alpha + n$ channels are shown by the vertical lines. The excitation-energy spectra measured at $\theta_{\rm lab} = 0.93°$ and 3.17° are also shown in the panels (e) and (f) for comparison. The excitation-energy spectra at $E_x \geq 8.0$ MeV are scaled by factors of 2.3 and 5 in the panels (e) and (f), respectively.

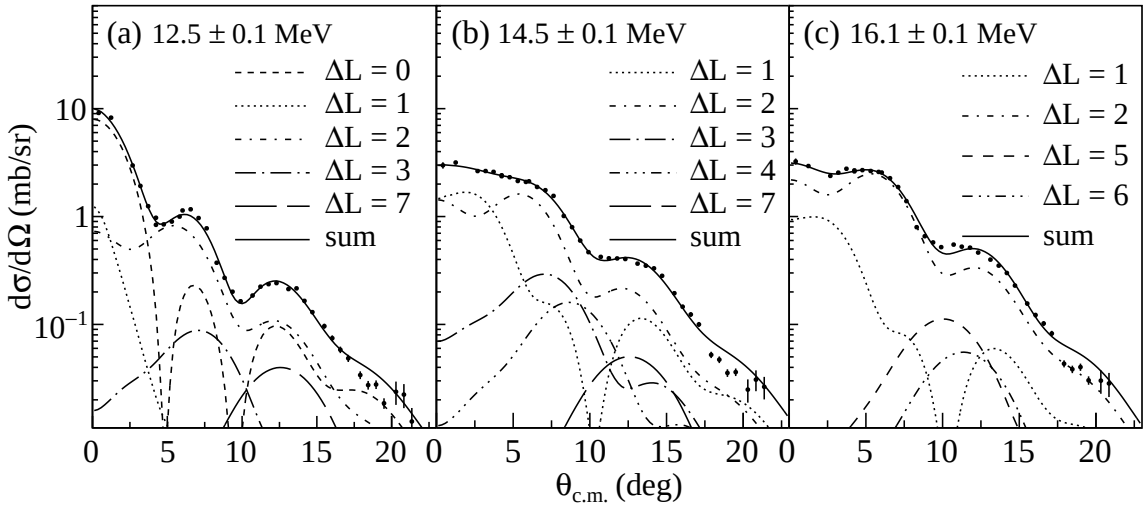

Figure 4.10: Measured angular distributions of the cross sections at several excitation-energy bins with their widths of 200 keV fitted by the MDA. The solid circles show the measured cross sections, whereas the solid lines show the theoretical cross sections fitted to the experimental data. The decomposed cross sections with $a_\lambda(E_x) \neq 0$ are also plotted.

Chapter 5

Discussion

5.1 $1/2^-$ states

The experimental level diagram for the $1/2^-$ states is compared with those obtained by several theoretical models in Fig. 5.1(a). According to the experimental compilation [48], there exists a state at $E_x = 14.39$ MeV with the spin and parity of $1/2^-$ or $5/2^-$. Since this state was not observed in the present measurement, this state is presented by the dashed line. Although the number of the $1/2^-$ states observed around $E_x = 12.5$ MeV is larger than that theoretically predicted, the shell-model calculation with the SFO interaction [96] best reproduces the experimental level diagram among these theoretical models. This shell-model calculation was carried out in the *psd* configuration space up to $2\hbar\omega$ using the code NuShellX [97]. However, the shell model could not reproduce the experimental $IS0$ strengths. The experimental EWSR fractions for the $IS0$ transitions are shown in Fig. 5.2(a). The measured EWSR fractions are at least about 0.2%, however, the theoretical values calculated by the shell model are about 10^{-4}%.

The $3\alpha + n$ OCM [52] and AMD [53] calculations systematically overestimate the energies of the $1/2^-$ states. They do not satisfactorily reproduce the observed energy levels. However, it should be noted that the OCM and AMD calculations reproduce the sizable EWSR fractions for the $IS0$ strengths as shown in Figs. 5.2(b) and (c). The OCM calculation explicitly takes into account the clustering degrees of freedom, and the AMD can also incorporate them. However, the conventional shell-model calculation cannot describe the clustering degrees of freedom due to the limitation of the configuration space. This fact suggests that the clustering degrees of freedom are crucial to describe the sizable $IS0$ strengths for these

$1/2^-$ states although the shell-model-like configurations are also needed to reproduce their energies. Therefore, theoretical calculations covering both the cluster-model and shell-model configuration spaces are necessary, and such calculations might solve the situation that the number of the predicted $1/2^-$ states is fewer than the experiment.

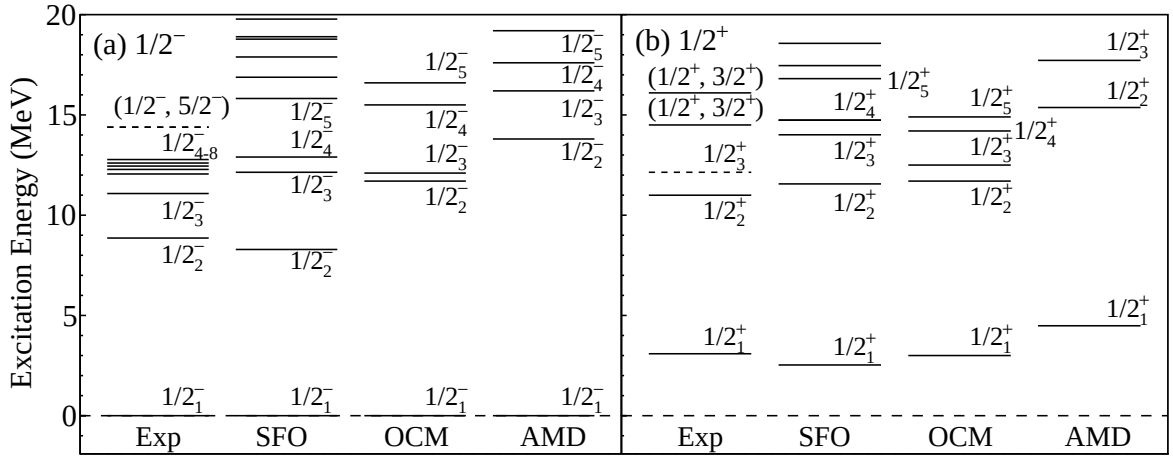

Figure 5.1: Experimental level diagrams for (a) the $1/2^-$ states and (b) the $1/2^+$ states in ^{13}C compared with the theoretical predictions by the shell model with the SFO interaction [96], OCM [52], and AMD [53].

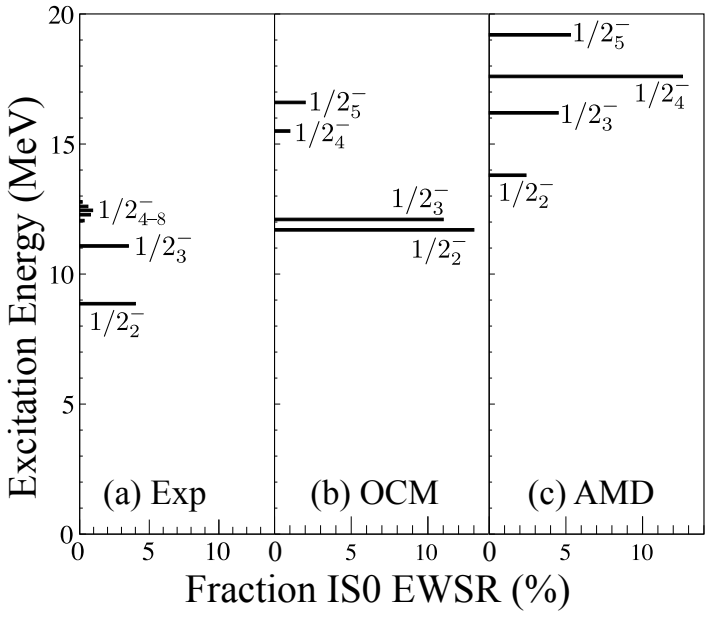

Figure 5.2: Measured EWSR fractions for the $IS0$ transitions compared with those predicted by the OCM [52] and AMD [53] calculations.

It is worth discussing the $1/2^-$ states in ^{13}N because a good mirror symmetry is conserved between ^{13}C and ^{13}N. The two $1/2^-$ states as the isobaric mirror states for the $1/2^-_2$ and $1/2^-_3$ states in ^{13}C were clearly observed in the ^{13}C(^{3}He, t)^{13}N reaction at $\theta_{\rm lab} = 0^\circ$ as seen in Fig. 5.3(a). In addition to these two $1/2^-$ states, a small bump at $E_x = 13.5$ MeV was observed at forward angles. Since this bump is considered to be excited by the Gamow-Teller transition, its spin and parity are $1/2^-$ or $3/2^-$. It is naturally expected that the mirror state for this 13.5-MeV state is observed in the ^{13}C(α, α') reaction. The $1/2^-$ states observed around $E_x = 12.5$ MeV in ^{13}C are inferred to be the mirror state of the 13.5-MeV state in ^{13}N.

The proton decay from the excited states in ^{13}N to the low-lying $T = 0$ states in ^{12}C were also measured in Ref. [98]. In Table 5.1, the measured branching ratios for the proton decay are compared with the theoretical predictions given by

$$\frac{\Gamma_i}{\Gamma} = \frac{S_i P_i}{\sum_i S_i P_i}, \tag{5.1}$$

where S_i and P_i are the spectroscopic (S) factors and the penetrabilities for the ^{13}N(J^π) $\rightarrow$ ^{12}C(J^π) + n channels, respectively. i is the label for each decay channel. The S factors were taken from the OCM [52] and AMD [53] calculations for ^{13}C, assuming the mirror symmetry between ^{13}C and ^{13}N. The S factors for ^{13}C were also calculated by the shell model with the SFO interaction [96]. The channel radii to calculate the penetrabilities were given by the sum of the rms radii of proton and the final states in ^{12}C taken from the generator coordinate method calculation [99]. The excitation energies for the theoretical $1/2^-_2$ and $1/2^-_3$ states were taken from the experimental values, and those for the $1/2^-_4$ and $1/2^-_5$ states were assumed to be 13.5 MeV.

The measured branching ratio from the $1/2^-_2$ state in ^{13}N to the 0^+_1 state in ^{12}C is larger than that to the 2^+_1 state in ^{12}C. This is due to the larger decay energy for the 0^+_1 state than the 2^+_1 state. All the theoretical calculations reasonably well reproduce this result. On the other hand, the measured branching ratios from the $1/2^-_3$ state in ^{13}N to the 2^+_1 and 0^+_2 states in ^{12}C are much larger than that to the 0^+_1 state in ^{12}C despite the larger decay energy for the 0^+_1 state. This result is reproduced by the OCM calculation and the shell-model calculation with the SFO interaction although the AMD calculation fails to reproduce the small branching ratio from the $1/2^-_3$ state in ^{13}N to the 0^+_1 state in ^{12}C. This discrepancy might be due to the insufficient model space in the AMD calculation to describe the cluster structures in ^{13}C as

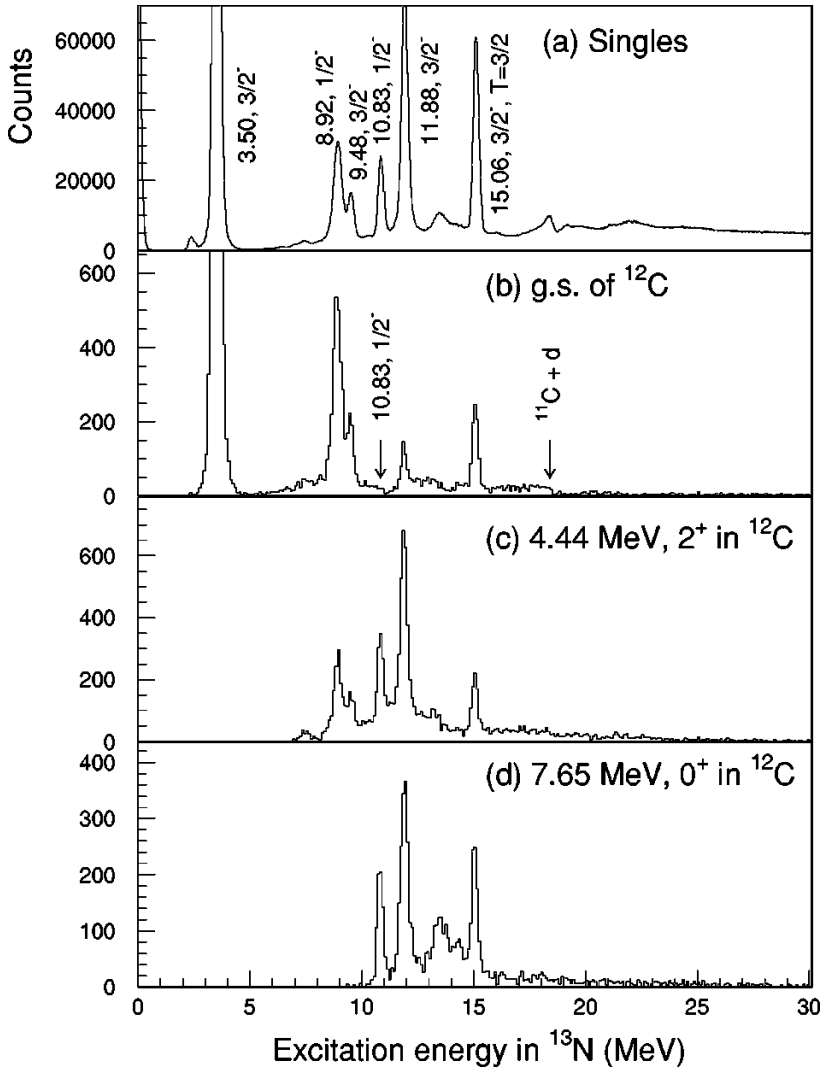

Figure 5.3: (a) Excitation-energy spectra for the ^{13}C(^{3}He, t)^{13}N reaction at $\theta_{\rm lab} = 0^{\circ}$ and $E_{^3\rm He} = 450$ MeV. The excitation-energy spectra obtained for the proton-decay events to the three final states in ^{12}C are also shown for comparison: (b) the ground state, (c) the 4.44-MeV 2^+_1 state, and (d) the 7.65-MeV 0^+_2 state. Taken from Fig. 8 in Ref. [98].

Table 5.1: Branching ratios (BR) for the proton decay measured in the ^{13}C(^{3}He, t)^{13}N reaction [98] compared with the theoretical predictions by the $3\alpha + n$ OCM [52], AMD [53], and shell model with the SFO interaction [96]. S denotes the spectroscopic factor.

		Experiment [98]	$3\alpha + n$ OCM		AMD		SFO	
^{13}N(J^π)	^{12}C(J^π)	BR	$S \times 10^2$	BR	$S \times 10^2$	BR	$S \times 10^2$	BR
$1/2^-_2$	0^+_1	0.60 ± 0.09	2.1	0.57	3.8	0.87	0.46	0.80
	2^+_1	0.30 ± 0.05	6.8	0.43	2.5	0.13	0.50	0.20
$1/2^-_3$	0^+_1	0.05 ± 0.01	1.0	0.08	2.1	0.49	0.08	0.05
	2^+_1	0.54 ± 0.09	20	0.73	3.3	0.35	1.4	0.39
	0^+_2	0.43 ± 0.16	22	0.19	6.7	0.17	8.3	0.56
$1/2^-_4$	0^+_1		0.35	0.09	3.3	0.22	2.9	0.15
	2^+_1		0.35	0.06	5.0	0.20	0.63	0.02
	0^+_2		5.2	0.85	14	0.58	25	0.83
$1/2^-_5$	0^+_1		1.0	0.05	2.5	0.25	0.23	0.92
	2^+_2		7.7	0.24	2.9	0.18	0.01	0.03
	0^+_2		23	0.71	9.2	0.57	0.02	0.05

discussed in Ref. [53].

As seen in Figs. 5.3(b), (c), and (d), the small bump at $E_x = 13.5$ MeV is prominent in the excitation-energy spectrum of ^{13}N for the proton-decay events to the 0^+_2 state, but not prominent in those to the 0^+_1 and 2^+_1 states. This means that the observed states around $E_x = 13.5$ MeV have larger decay widths to the 0^+_2 state than to the 0^+_1 and 2^+_1 states although the numerical values are not given in Ref. [98]. The OCM calculation predicts that the $1/2^-_4$ and $1/2^-_5$ states have larger decay widths to the 0^+_2 state in ^{12}C than to the 0^+_1 and 2^+_1 states as shown in Table 5.1. Therefore, the 13.5-MeV state in ^{13}N and its possible mirror state in ^{13}C might correspond to the $1/2^-_4$ and $1/2^-_5$ state in the OCM calculation although their predicted energies were higher than the experiment by a few MeV. Since the $1/2^-$ states around $E_x = 12.5$ MeV in ^{13}C locate slightly above the $3\alpha + n$ decay threshold and its mirror state has larger decay width to the α condensed state in ^{12}C, these $1/2^-$ states in ^{13}C might be the candidates for the α condensed state in which an excess neutron in the $p_{1/2}$ orbit is coupled to the 0^+_2 state in ^{12}C. However, the OCM calculation suggests that the wave functions of the $1/2^-_{2,3,4,5}$ states are dominated by the $^9\mathrm{Be} + \alpha$ configuration rather than the $^{12}\mathrm{C}(0^+_2) + n$ configuration [52]. Since the odd-parity α–n force is attractive [100], the excess neutron in the $p_{1/2}$ orbit glues two α clusters among the three α clusters in the 0^+_2 state to form the $^9\mathrm{Be} + \alpha$ structure in the $1/2^-$ states. Therefore, the three α clusters are not fully condensed into the same s orbit, and the $3\alpha + n$ condensed state is unlikely to emerge as the negative parity states.

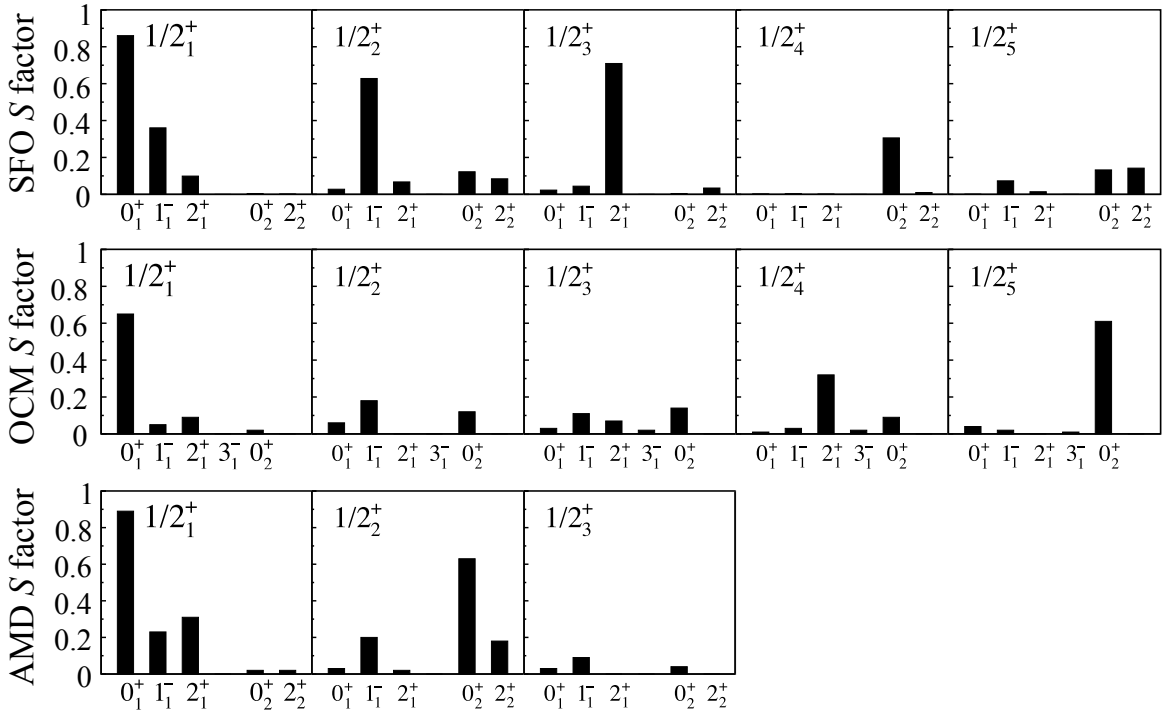

Figure 5.4: S factors for the $^{12}\mathrm{C}+n$ channels of the $1/2^+$ states calculated by the shell model with the SFO interaction [96], OCM [52], and AMD [53]. The $^{12}\mathrm{C}(3^-_1)+n$ channel was not included in the AMD calculation, whereas the $^{12}\mathrm{C}(2^+_2)+n$ channel was not taken into account in the OCM calculation.

It is expected that the excitation energy of the state having a dilute structure in $Z > N$ nuclei is smaller than that of the mirror state since the radial expansion of the proton distribution reduces the energy difference between the mirror states due to the Coulomb interaction. However, the energy difference of the 13.5-MeV state in ^{13}N and the 12.5-MeV state in ^{13}C contradicts this speculation. Further theoretical investigation of the Coulomb shift between these mirror states is required.

5.2 Positive-parity states excited by $\Delta L = 1$ transitions

The experimental level diagram for the positive-parity states excited by the $\Delta L = 1$ transitions is compared with theoretical predictions in Fig. 5.1(b). Since the $1/2^+_3$ state at $E_x = 12.14$ MeV listed in Ref. [48] was not observed in this experiment, this state is presented by the dashed line. The two states at $E_x = 14.5$ and 16.1 MeV are observed in the $\Delta L = 1$ strength

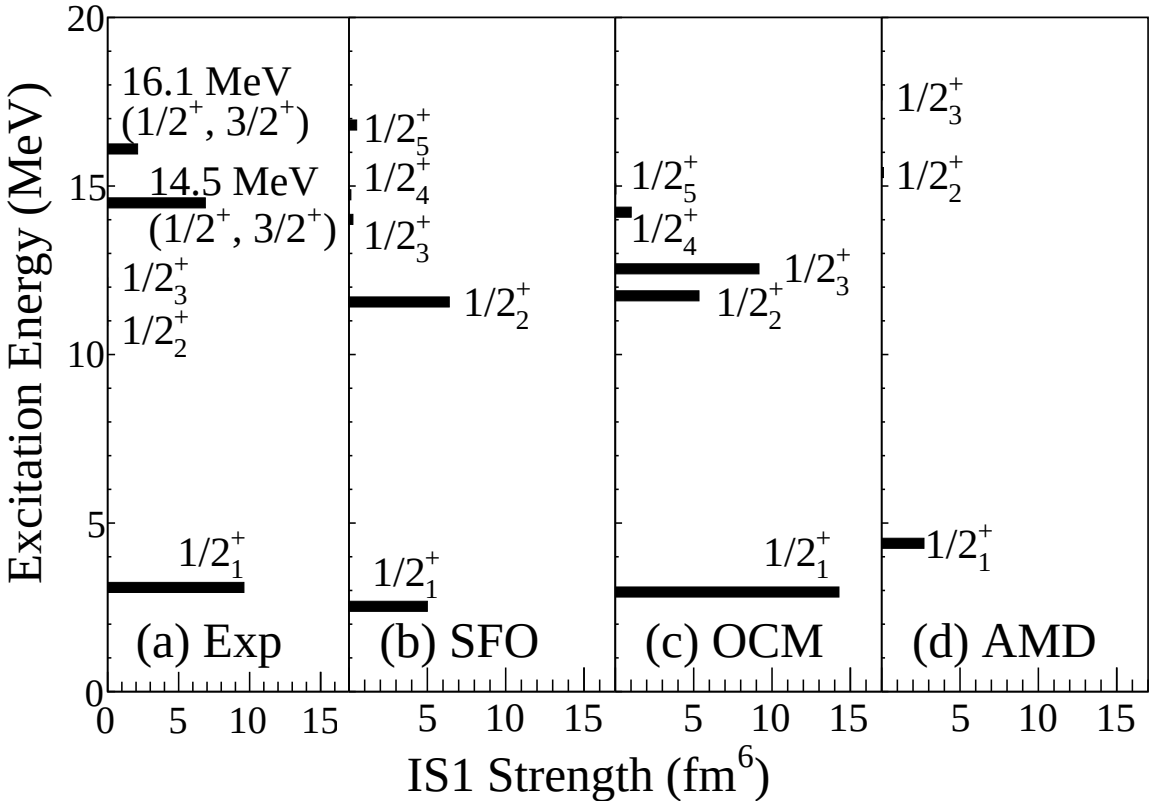

Figure 5.5: Measured $IS1$ strengths and those predicted by the shell model with the SFO interaction [96], OCM [52], and AMD [53].

distribution in Fig. 4.9(b). The spin and parity of these states are either $1/2^+$ or $3/2^+$. If we assume that the spin and parity of both the 14.5-MeV and 16.1-MeV states are $1/2^+$, the theoretical level diagrams predicted by the shell-model and OCM calculations are in good agreement with the experiment except that the experimental $1/2^+_3$ state does not appear in the shell-model calculation. The AMD calculation also reproduces the excitation energy of the $1/2^+_1$ state, however, the excitation energies of the $1/2^+_2$ and $1/2^+_3$ states predicted in the AMD calculation are much larger than those in the shell-model and the OCM calculations.

The S factors of the $1/2^+$ states for the $^{12}\mathrm{C}+n$ channels calculated by the shell model, OCM, and AMD are compared in Fig. 5.4. Since the configuration space of the present shell-model calculation with the SFO interaction was limited to the *psd* shells, the shell model did not include the $^{12}\mathrm{C}(3^-_1)+n$ channel, in which an F-wave neutron must be taken into account. The AMD calculation did not include this channel either. The OCM calculation predicts that

the $^{12}\mathrm{C}(3^-_1) + n$ channel makes a minor contribution to the $1/2^+$ states.

All the calculations agree that the $1/2^+_1$ state has a shell-model-like structure in which an $s_{1/2}$ neutron couples to the 0^+_1 state in ^{12}C. Yamada and Funaki pointed out that the $1/2^+_5$ state in the OCM calculation is the theoretical candidate for the α condensed state [52]. The energy of the $1/2^+_2$ state in the AMD calculation is close to that of the $1/2^+_5$ state in the OCM calculation. The $1/2^+_2$ state in the AMD calculation also has the largest S factor for the $^{12}\mathrm{C}(0^+_2) + n$ channel. Therefore, we suggest that the $1/2^+_{2,3,4}$ states in the OCM calculation are missed in the AMD calculation, and the $1/2^+_2$ state in the AMD calculation corresponds to the $1/2^+_5$ state in the OCM calculation. Actually, Chiba and Kimura pointed out the $1/2^+_2$ state in the AMD calculation is the candidate for the α condensed state [53].

It is worth mentioning that there is a good agreement in the dominant channel between the shell-model and the OCM calculations if the $1/2^+_3$ state in the OCM calculation is ignored. The $1/2^+_3$ state in the shell-model calculation and the $1/2^+_4$ state in the OCM calculation have the largest S factor in the $^{12}\mathrm{C}(2^+_1) + n$ channel. The $1/2^+_4$ state in the shell-model calculation and the $1/2^+_5$ state in the OCM calculation gave the largest S factor in the $^{12}\mathrm{C}(0^+_2) + n$ channel. The energies of the $1/2^+_3$ and $1/2^+_4$ states in the shell-model calculation are close to those of the $1/2^+_4$ and $1/2^+_5$ states in the OCM calculation. These states might correspond to the 14.5-MeV and 16.1-MeV states observed in the $\Delta L = 1$ strength distribution. Therefore, the 16.1-MeV state is speculated to be the experimental candidate for the α condensed state.

The experimental $IS1$ strengths are presented in Fig. 5.5(a). Since the $IS1$ strengths for the $1/2^+_2$ and $1/2^+_3$ states were consistent with zero in the present study, the upper limits of the 95% confidence interval were given as listed in Table 4.1. The $IS1$ strengths for the 14.5-MeV and 16.1-MeV states were evaluated by subtracting a continuum component of the $\Delta L = 1$ strengths in Fig. 4.9(b) to be 6.9 ± 0.7 fm^6 and 2.1 ± 0.8 fm^6, respectively. The theoretical $IS1$ strengths calculated by the shell model, OCM, and AMD are compared with the experimental values in Fig. 5.5. It should be noted that the $IS1$ strength distributions calculated by the shell model and the OCM are similar if the $1/2^+_3$ state in the OCM calculation is ignored as in the level diagram and the S factors. The measured $IS1$ strength for the $1/2^+_1$ state is reasonably reproduced well in all the theoretical calculations. However, the sizable $IS1$ strengths for the $1/2^+_2$ state predicted by the shell-model and OCM calculations do not agree with the experiment. An experimental counterpart of the $1/2^+_3$ state in the OCM calculation was not observed in the present study.

Although we have suggested that the 16.1-MeV state is a possible candidate for the α

condensed state on the basis of the observed level structure, the measured $IS1$ strengths of this experimental candidate is much larger than the theoretical predictions. One plausible explanation for the suppressed $IS1$ strengths in the theoretical calculations is that both of the core excitation from the 0^+_1 state to the 0^+_2 state in ^{12}C and the neutron excitation from the $p_{1/2}$ orbit to the $s_{1/2}$ orbit are necessary to excite the α condensed state from the ground state in ^{13}C. This discrepancy in the $IS1$ strength raises a doubt about the identification of the α condensed state, therefore, further experimental information is strongly desired to clarify the present situation. The spin and parity of the 14.5-MeV and 16.1-MeV states need to be determined. The decay modes of these states should also be measured because the α condensed state is expected to decay by emitting a neutron via the 0^+_2 state in ^{12}C.

Further theoretical investigation of the α condensed states is also needed. Although the energies of the α condensed states in $A = 4k$ nuclei are systematically predicted in Ref. [29], there is no such theoretical predictions in $A \neq 4k$ nuclei over isotopic chains. Survival of α clusters in neutron-rich nuclei is also an important issue. It is not trivial whether the α cluster structures are kept even in various nuclei. It should be noted that Ref. [29] calculates the α condensed states with assuming *a priori* existence of α clusters, but competition between the clustering degrees of freedom and the single-particle degrees of freedom is crucial for survival of the α cluster structures, especially in non-self conjugate nuclei with excess neutrons or protons. Theoretical studies of how much excess neutrons can be added to the α condensed states with keeping its condensed nature, namely, "the neutron drip line for the α condensed states", should be performed taking into account the single-particle degrees of freedom.

Chapter 6

Summary

Studying of clustering in atomic nuclei has a long history dating back to the discovery of the neutron. Over the years, many researches have revealed that the clustering phenomena play crucial roles to describe stellar nucleosynthesis, neutron stars, nuclear structures, and so on. Nevertheless, our understanding of clustering phenomena in atomic nuclei is still far from complete since atomic nuclei are complicated many-body systems having huge number of degrees of freedom. In recent years, the 0_2^+ state at $E_x = 7.65$ MeV in ^{12}C has attracted attention as an exotic cluster state, called the 3α condensed state, in which the Bose-Einstein condensation of 3α particles is realized in this state. It is interesting problem whether such an α condensed state exists in nuclei other than ^{12}C.

Very recently, it was theoretically proposed that the α condensation induces the strong isospin dependence of the EoS of the cold dilute nuclear matter [42]. However, it is not trivial that the α condensation actually occurs in dilute nuclear matter, therefore, this must be confirmed by experiments. Although we cannot directly access infinite nuclear matter in the laboratory, the systematic study of the α condensed states in finite nuclei with various mass numbers and isospins will give us some clues to the α condensation in dilute nuclear matter. If the α condensed states universally exist in various nuclei, it will demonstrate that the α condensate is a trivial conformation in dilute nuclear many-body systems. Many experimental and theoretical efforts have been devoted to establish the α condensed states and to reveal the natures of them. However, the scope of these studies has been limited to self-conjugated $A = 4k$ nuclei. Few studies have discussed the α condensate with excess neutrons or protons in the $k\alpha$ system, so far.

In the present work, we searched for the α condensed state in ^{13}C as the first step for

the systematic exploration into non self-conjugated $A \neq 4k$ nuclei. Since the $IS0$ and $IS1$ transitions can induce density change of nuclei, these transitions are suitable to excite the α condensed state with dilute density from the ground state. Therefore, we measured the angular distribution of the cross section for the ^{13}C(α, α') reaction at $E_\alpha = 388$ MeV at forward angles including 0° where the cross sections for the $IS0$ and $IS1$ transitions are large in order to precisely measure the strengths of these transitions. The measured cross sections were analyzed by employing the DWBA calculation with the single-folding potentials to determine the isoscalar transition strengths in ^{13}C. The measured angular distributions of the cross sections for the observed discrete states were reasonably well reproduced by the DWBA calculations. This result demonstrated the reliability of the present DWBA analysis.

We found a bump structure around $E_x = 12.5$ MeV in ^{13}C due to the $IS0$ transition. The peak-fit analysis suggested that this bump consisted of several $1/2^-$ states. We performed the MDA in order to determine the strength distributions for the isoscalar $\Delta L = 0$–3 transitions. The known discrete states were correctly observed in the corresponding $\Delta L = \lambda$ strength distributions. We found the two bumps at $E_x = 14.5$ and 16.1 MeV in the $\Delta L = 1$ strength distribution. The spin and parities of these states were assigned to be $1/2^+$ or $3/2^+$.

We compared the experimental level diagram and the $IS0$ and $IS1$ strengths for the $1/2^-$ and $1/2^+$ states with those predicted by the shell model with the SFO interaction [96], OCM [52], and AMD [53]. The shell-model calculation best reproduces the experimental level diagram of the $1/2^-$ states among these calculations, but it cannot explain the observed sizable $IS0$ strengths. The clustering degrees of freedom are crucial to account for the sizable $IS0$ strengths for these states. Therefore, the theoretical calculations covering both the cluster-model and shell-model configuration spaces are necessary to well describe these $1/2^-$ states.

The small bump observed around $E_x = 13.5$ MeV in ^{13}N, which is the possible mirror states of the $1/2^-$ states around $E_x = 12.5$ MeV near the $3\alpha + n$ decay threshold in ^{13}C, dominantly decays to the 0^+_2 state in ^{12}C [98]. This fact implies that the $1/2^-$ states around $E_x = 12.5$ MeV are the candidates for the α condensed state in which a $p_{1/2}$ neutron couples to the ^{12}C(0^+_2) core. However, the OCM calculation suggests that the wave functions of the $1/2^-_{2,3,4,5}$ states are dominated by the $^9\mathrm{Be} + \alpha$ configuration due to the attractive odd-parity α–n force, and thus the α condensed state is unlikely to emerge as the negative parity states in ^{13}C.

It is expected that the excitation energy of a state having a dilute structure in $Z > N$ nuclei is smaller than that of the mirror state due to a reduction of the energy difference by

the Coulomb interaction. However, the energy difference of the 13.5-MeV state in ^{13}N and the 12.5-MeV state in ^{13}C contradicts this speculation. Further theoretical investigation of the Coulomb shift between these mirror states is required.

The experimental level diagram for the $1/2^+$ states populated by the $IS1$ transitions is reasonably well reproduced by the shell-model and OCM calculations if we assume the spin and parity of both the 14.5-MeV and 16.1-MeV states to be $1/2^+$. On the other hand, the excitation energies of the $1/2^+_2$ and $1/2^+_3$ states predicted in the AMD calculation are much larger than those in the shell-model and the OCM calculations. We suggest that the AMD calculation misses the $1/2^+_{2,3,4}$ states predicted by the OCM calculation. All the calculations reasonably well reproduce the measured $IS1$ strength for the $1/2^+_1$ state, which is suggested to have a shell-model-like structure in these calculations. We propose that the 16.1-MeV state is a possible candidate for the α condensed state predicted by the OCM and AMD calculations on the basis of the good correspondence between the experimental and calculated level structures. However, the measured $IS1$ strength for the 16.1-MeV state is much larger than the theoretical predictions. This discrepancy in the $IS1$ strength raises a doubt about the identification of the α condensed state.

We need further experimental information to establish the α condensed state in ^{13}C. The spins of the 14.5-MeV and 16.1-MeV states should be determined. The decay modes of these states should be also investigated since the α condensed state is expected to decay by emitting a neutron via the 0^+_2 state in ^{12}C. A new experiment measuring the decay neutrons from the 14.5-MeV and 16.1-MeV states in coincidence with inelastically scattered α particles is highly desired.

Acknowledgement

First and foremost, I would like to express my great gratitude to Prof. T. Kawabata. For almost six years since I started the graduate school until now, he has been patiently and carefully teaching me various essential skills for an experimental researcher such as how to plan an experiment, how to read the data, how to discuss the result, and how to communicate my point of view to others. Although he is a very active person and is extremely busy every day, he never gave up on me and stayed by my side until my doctoral dissertation was completed. I would like to thank him with great sincerity for making it possible to publish my work on the search for the α condensed state in ^{13}C and to summarize the results in the dissertation.

Experimental data for ^{12}C and ^{13}C used in the present work were obtained in the E253 experiment. Since this experiment was performed about 15 years ago as a master thesis's experiment for Dr. Y. Sasamoto, I could not participate in the experiment. I would like to thank her and all the collaborators of E253 for providing me with the experimental data. The angular distributions of the cross sections for the α elastic scattering off ^{12}C and ^{13}C were provided by her. I am grateful to Prof. I. Sugai for preparing the high quality $^{\rm nat}$C and ^{13}C targets. I also thank the RCNP cyclotron crews for the stable operation of the cyclotron facilities and for providing a high quality beam for background-free measurements at forward angles including 0 degrees. Mr. M. Murata kindly checked on parameters of the accelerators for the E253 experiment and took the trouble to measure the thickness of scintillators of the recoil proton counter. Thanks to him, the accuracy of information described in the dissertation was ensured.

Prof. T. Yamada and Prof. Y. Funaki provided the theoretical $IS1$ transition strengths from the ground state to the $1/2^+$ excited states in ^{13}C calculated by the $3\alpha + n$ OCM. The calculated results are highly important to discuss the existence of the α condensed state in ^{13}C. They kindly took an opportunity to have a meeting with me even though it was their

day off although they should be so busy with their works at the university. I really appreciate their discussions over and over again before the publication of the present work.

Dr. Y. Chiba and Prof. M. Kimura had a very fruitful discussion on the AMD calculation for ^{13}C. Dr. Chiba, especially, had a meeting with me and provided the theoretical S factors for the $1/2^+$ states in ^{13}C. It is needless to say that his sincere support improved the quality of the present work.

Dr. H. Fujimura provided me with her doctoral dissertation for the measurement of ^{13}N(^{3}He, t) reaction. Her dissertation was very helpful in discussing the excitation energies and the decay branching ratios of the mirror states in ^{13}N. I would like to thank her for her kindness in spite of my urgent request for her dissertation.

Prof. M. Fujiwara patiently corrected the structure of my paper and my poor English even though he was not my direct supervisor. I am very grateful for many honest comments on my paper (e.g., difficult to read, this doesn't make any sense, etc.). Thanks to these comments, I could greatly improved the readability of the paper. He also occasionally sent me encouragement by e-mail and phone. I greatly appreciate his patient support.

I also thank my colleagues, Dr. S. Adachi, Dr. T. Furuno, Mr. M. Murata, Ms. M. Tsumura, Ms. A. Sakaue, Mr. T. Morimoto, Mr. T. Takeda, Mr. Y. Takahashi, Mr. Y. Fujikawa, Mr. S. Okamoto, Mr. T. Doi, Mr. K. Sakanashi, Ms. K. Himi, and Mr. S. Tsuji for making my researcher life so exciting. I will never forget many enjoyable memories of experiments and discussions having with them.

I would like to appreciate Prof. T. Nagae and other Lab members at Kyoto University. The atmosphere at Kyoto University, where professors and students can discuss on equal footing, was very comfortable for me. It was my precious time chatting about physics and recent news with them at lunch and drinking party.

Finally, I would like to express my gratitude to my family, Sumako, Yuzo, Madoka, Yukihiro, and Toshiko for always looking out for me. I cannot finish the graduate school nor complete my dissertation without their warm support.

Appendix A

Data tables of cross sections

A.1 Cross sections for elastic scattering

Table A.1: $^{13}C(\alpha, \alpha)$ elastic, $E_\alpha = 386$ MeV

$\theta_{\text{c.m.}}$ (deg)	$d\sigma/d\Omega$ (mb/sr)	error (mb/sr)
2.7	2.22×10^4	1.30×10^3
3.2	1.93×10^4	1.13×10^3
3.7	1.50×10^4	8.77×10^2
4.2	1.10×10^4	6.46×10^2
4.7	7.14×10^3	5.59×10^2
5.3	4.80×10^3	3.76×10^2
5.8	2.98×10^3	2.34×10^2
6.1	2.22×10^3	1.29×10^2
6.6	1.16×10^3	6.80×10^2
7.1	6.35×10^2	3.72×10^1
7.6	3.83×10^2	2.25×10^1
8.4	3.44×10^2	2.01×10^1
8.9	3.84×10^2	2.24×10^1
9.4	3.87×10^2	2.26×10^1

Table A.1: (Continued)

$\theta_{\text{c.m.}}$ (deg)	$d\sigma/d\Omega$ (mb/sr)	error (mb/sr)
9.9	3.52×10^2	2.06×10^1
10.7	2.66×10^2	1.56×10^1
11.3	2.13×10^2	1.25×10^1
11.8	1.57×10^2	9.17
12.3	1.14×10^2	6.65
13.0	7.31×10^1	4.28
13.6	4.94×10^1	2.90
14.2	3.43×10^1	2.02
14.7	2.52×10^1	1.49
15.5	2.12×10^1	1.24
16.0	1.93×10^1	1.13
16.5	1.79×10^1	1.05
17.1	1.54×10^1	9.00×10^{-1}
17.9	9.26	5.42×10^{-1}

Table A.1: (Continued)

$\theta_{\text{c.m.}}$ (deg)	$d\sigma/d\Omega$ (mb/sr)	error (mb/sr)
18.4	7.44	4.36×10^{-1}
18.9	5.56	3.26×10^{-1}
19.4	3.93	2.32×10^{-1}
20.2	2.25	1.44×10^{-1}
20.8	1.62	1.07×10^{-1}
21.3	1.17	8.08×10^{-2}
21.8	9.02×10^{-1}	6.51×10^{-2}

Table A.2: ^{12}C(α, α) elastic, $E_\alpha = 386$ MeV

$\theta_{\text{c.m.}}$ (deg)	$d\sigma/d\Omega$ (mb/sr)	error (mb/sr)
2.73	2.03×10^4	1.02×10^3
3.25	1.73×10^4	8.68×10^2
3.78	1.35×10^4	6.77×10^2
4.31	1.02×10^4	5.13×10^2
4.31	1.15×10^4	5.76×10^2
4.84	7.52×10^3	3.78×10^2
5.38	5.06×10^3	2.55×10^2
5.91	3.05×10^3	1.54×10^2
6.18	2.13×10^3	1.07×10^2
6.71	1.19×10^3	6.01×10^1
7.26	6.15×10^2	3.11×10^1
7.80	3.69×10^2	1.88×10^1
8.07	3.04×10^2	9.16
8.61	3.02×10^2	9.11
9.15	3.20×10^2	9.64

Table A.2: (Continued)

$\theta_{\text{c.m.}}$ (deg)	$d\sigma/d\Omega$ (mb/sr)	error (mb/sr)
9.69	3.26×10^2	9.83
9.01	3.09×10^2	9.35
9.55	3.25×10^2	9.82
10.1	3.19×10^2	9.63
10.6	2.89×10^2	8.75
11.2	2.25×10^2	6.79
11.7	1.83×10^2	5.54
12.3	1.38×10^2	4.19
12.8	9.83×10^1	2.99
13.3	5.74×10^1	1.74
13.9	4.04×10^1	1.24
14.4	2.83×10^1	8.71×10^{-1}
15.0	2.06×10^1	6.42×10^{-1}
15.5	1.52×10^1	4.66×10^{-1}
16.0	1.37×10^1	4.23×10^{-1}
16.8	1.25×10^1	3.86×10^{-1}
17.1	1.13×10^1	3.49×10^{-1}
17.7	9.08	2.77×10^{-1}
18.2	7.83	2.40×10^{-1}
18.7	6.45	1.98×10^{-1}
19.3	4.98	1.54×10^{-1}
19.8	3.00	9.06×10^{-2}
20.3	2.26	6.83×10^{-2}
20.9	1.64	4.99×10^{-2}
21.4	1.18	3.61×10^{-2}
22.0	7.36×10^{-1}	2.25×10^{-2}

A.2 Cross sections for low-lying states

Table A.3: $^{13}C(\alpha, \alpha')$ inelastic, $E_x = 3.09$ MeV $(1/2^+_1)$, $E_\alpha = 386$ MeV

$\theta_{\text{c.m.}}$ (deg)	$d\sigma/d\Omega$ (mb/sr)	error (mb/sr)
0.4	1.48×10^{1}	7.78×10^{-1}
1.2	9.19	3.73×10^{-1}
2.7	4.96	7.35×10^{-2}
3.2	4.01	6.18×10^{-2}
3.7	2.70	4.46×10^{-2}
4.2	2.15	5.49×10^{-2}
4.7	1.10	3.46×10^{-2}
5.3	5.52×10^{-1}	2.23×10^{-2}
5.8	2.69×10^{-1}	1.43×10^{-2}
6.0	3.07×10^{-1}	1.59×10^{-2}
6.5	4.33×10^{-1}	1.92×10^{-2}
7.1	4.87×10^{-1}	2.10×10^{-2}
7.6	6.25×10^{-1}	2.42×10^{-2}
8.3	4.00×10^{-1}	1.22×10^{-2}
8.8	2.96×10^{-1}	1.00×10^{-2}
9.3	1.99×10^{-1}	7.78×10^{-3}
9.9	1.39×10^{-1}	6.23×10^{-3}
10.7	1.54×10^{-1}	7.34×10^{-3}
11.2	1.92×10^{-1}	8.40×10^{-3}
11.7	2.66×10^{-1}	1.03×10^{-2}
12.3	3.19×10^{-1}	1.15×10^{-2}
13.1	3.67×10^{-1}	1.24×10^{-2}

Table A.3: (Continued)

$\theta_{\text{c.m.}}$ (deg)	$d\sigma/d\Omega$ (mb/sr)	error (mb/sr)
13.6	3.63×10^{-1}	1.23×10^{-2}
14.1	3.21×10^{-1}	1.14×10^{-2}
14.6	2.76×10^{-1}	1.04×10^{-2}
15.4	1.81×10^{-1}	8.88×10^{-3}
16.0	1.16×10^{-1}	6.83×10^{-2}
16.5	8.36×10^{-2}	5.65×10^{-3}
17.0	4.89×10^{-2}	4.17×10^{-3}
17.8	3.20×10^{-2}	3.06×10^{-3}
18.4	2.85×10^{-2}	2.87×10^{-3}
18.9	2.94×10^{-2}	2.92×10^{-3}
19.4	3.14×10^{-2}	3.03×10^{-3}
20.2	3.17×10^{-2}	7.28×10^{-3}
20.7	3.18×10^{-2}	7.29×10^{-3}
21.3	2.42×10^{-2}	6.34×10^{-3}
21.8	3.44×10^{-2}	7.51×10^{-3}
22.6	2.25×10^{-2}	5.61×10^{-3}
23.1	1.38×10^{-2}	4.33×10^{-3}
23.6	1.13×10^{-2}	3.91×10^{-3}
24.2	7.54×10^{-3}	3.18×10^{-3}
25.0	2.98×10^{-3}	1.53×10^{-3}
25.5	2.24×10^{-3}	1.32×10^{-3}
26.0	4.48×10^{-3}	1.89×10^{-3}
26.5	5.23×10^{-3}	2.05×10^{-3}

Table A.4: $^{13}C(\alpha,\alpha')$ inelastic, $E_x = 3.68$ MeV $(3/2^-_1)$, $E_\alpha = 386$ MeV

$\theta_{\text{c.m.}}$ (deg)	$d\sigma/d\Omega$ (mb/sr)	error (mb/sr)
0.4	2.24×10^{1}	9.62×10^{-1}
1.2	2.54×10^{1}	6.92×10^{-1}
2.7	1.87×10^{1}	2.37×10^{-1}
3.2	1.92×10^{1}	2.42×10^{-1}
3.7	2.10×10^{1}	2.63×10^{-1}
4.2	2.36×10^{1}	2.91×10^{-1}
4.7	2.65×10^{1}	3.94×10^{-1}
5.3	2.92×10^{1}	4.27×10^{-1}
5.8	2.93×10^{1}	5.43×10^{-1}
6.0	3.24×10^{1}	4.68×10^{-1}
6.5	2.95×10^{1}	4.88×10^{-1}
7.1	2.40×10^{1}	4.49×10^{-1}
7.6	1.86×10^{1}	3.00×10^{-1}
8.3	9.37	1.91×10^{-1}
8.8	6.03	1.13×10^{-1}
9.3	4.17	8.08×10^{-2}
9.9	3.55	6.30×10^{-2}
10.7	4.36	7.93×10^{-2}
11.2	5.07	9.10×10^{-2}
11.7	5.82	1.13×10^{-1}
12.3	6.27	1.22×10^{-1}
13.1	5.89	9.91×10^{-2}
13.6	5.47	9.43×10^{-2}

Table A.4: (Continued)

$\theta_{\text{c.m.}}$ (deg)	$d\sigma/d\Omega$ (mb/sr)	error (mb/sr)
14.1	4.58	8.52×10^{-2}
14.7	3.78	7.32×10^{-2}
15.4	2.37	6.51×10^{-2}
16.0	1.66	4.34×10^{-2}
16.5	1.27	3.73×10^{-2}
17.0	9.03×10^{-1}	3.35×10^{-2}
17.8	6.33×10^{-1}	2.08×10^{-2}
18.4	5.60×10^{-1}	1.88×10^{-2}
18.9	5.76×10^{-1}	1.97×10^{-2}
19.4	5.31×10^{-1}	1.78×10^{-2}
20.2	4.43×10^{-1}	3.44×10^{-2}
20.7	3.66×10^{-1}	2.99×10^{-2}
21.3	3.45×10^{-1}	2.92×10^{-2}
21.8	2.87×10^{-1}	2.61×10^{-2}
22.6	2.01×10^{-1}	1.88×10^{-2}
23.1	1.65×10^{-1}	1.67×10^{-2}
23.7	1.00×10^{-1}	1.26×10^{-2}
24.2	9.42×10^{-2}	1.21×10^{-2}
25.0	6.03×10^{-2}	7.56×10^{-3}
25.5	4.55×10^{-2}	6.44×10^{-3}
26.0	3.88×10^{-2}	5.93×10^{-3}
26.5	3.44×10^{-2}	5.50×10^{-3}

Table A.5: $^{13}C(\alpha, \alpha')$ inelastic, $E_x = 3.85$ MeV $(5/2^+_1)$, $E_\alpha = 386$ MeV

$\theta_{\text{c.m.}}$ (deg)	$d\sigma/d\Omega$ (mb/sr)	error (mb/sr)
0.4	1.20	9.22×10^{-1}
1.2	1.28	5.95×10^{-1}
2.7	1.84	1.11×10^{-1}
3.2	2.21	1.18×10^{-1}
3.7	2.39	1.25×10^{-1}
4.2	2.25	1.16×10^{-1}
4.2	3.34	2.12×10^{-1}
4.7	3.49	1.99×10^{-1}
5.3	5.00	2.31×10^{-1}
5.8	6.32	2.58×10^{-1}
6.0	6.74	3.47×10^{-1}
6.5	8.71	3.86×10^{-1}
7.1	6.96	3.20×10^{-1}
7.6	6.67	4.30×10^{-1}
8.3	4.33	1.68×10^{-1}
8.8	3.14	1.26×10^{-1}
9.3	2.27	9.46×10^{-2}
9.9	1.54	6.87×10^{-2}
10.7	9.32×10^{-1}	6.41×10^{-2}

Table A.5: (Continued)

$\theta_{\text{c.m.}}$ (deg)	$d\sigma/d\Omega$ (mb/sr)	error (mb/sr)
11.2	8.89×10^{-1}	6.00×10^{-2}
11.7	9.90×10^{-1}	6.50×10^{-2}
12.3	1.25	6.70×10^{-2}
13.1	8.30×10^{-1}	5.52×10^{-2}
13.6	1.11	6.37×10^{-2}
14.1	1.20	6.70×10^{-2}
14.7	9.69×10^{-1}	5.75×10^{-2}
15.4	7.59×10^{-1}	5.84×10^{-2}
16.0	5.53×10^{-1}	6.42×10^{-2}
16.5	3.67×10^{-1}	3.47×10^{-2}
17.0	3.26×10^{-1}	2.86×10^{-2}
17.8	1.24×10^{-1}	2.17×10^{-2}
18.4	8.52×10^{-2}	2.21×10^{-2}
18.9	6.30×10^{-2}	1.81×10^{-2}
19.4	6.51×10^{-2}	1.73×10^{-2}
20.2	6.38×10^{-2}	3.82×10^{-2}
20.7	6.33×10^{-2}	3.31×10^{-2}
21.3	5.31×10^{-2}	3.23×10^{-2}
21.8	2.47×10^{-2}	2.82×10^{-2}

Table A.6: $^{13}C(\alpha, \alpha')$ inelastic, $E_x = 7.55$ MeV $(5/2^-_1)$, $E_\alpha = 386$ MeV

$\theta_{\text{c.m.}}$ (deg)	$d\sigma/d\Omega$ (mb/sr)	error (mb/sr)
0.4	2.43×10^1	1.57
1.2	2.94×10^1	2.00
2.7	2.18×10^1	7.07×10^{-1}
3.2	2.27×10^1	6.43×10^{-1}
3.7	2.57×10^1	8.29×10^{-1}
4.2	2.83×10^1	9.20×10^{-1}
4.8	3.19×10^1	5.66×10^{-1}
5.3	3.48×10^1	6.33×10^{-1}
5.8	3.43×10^1	8.73×10^{-1}
6.0	3.87×10^1	7.98×10^{-1}
6.5	3.32×10^1	1.73
7.1	2.92×10^1	1.13
7.6	2.19×10^1	1.49
8.3	1.15×10^1	2.49×10^{-1}
8.8	8.00	1.80×10^{-1}
9.3	5.55	2.35×10^{-1}
9.9	4.75	1.79×10^{-1}
10.7	5.17	1.67×10^{-1}
11.2	6.23	2.71×10^{-1}
11.7	6.98	2.68×10^{-1}
12.3	7.44	2.62×10^{-1}
13.1	7.31	3.06×10^{-1}
13.6	6.88	3.03×10^{-1}
14.1	5.83	2.35×10^{-1}
14.7	4.62	1.65×10^{-1}
15.5	3.00	1.47×10^{-1}
16.0	2.20	9.93×10^{-2}
16.5	1.57	5.82×10^{-2}
17.1	1.18	4.26×10^{-2}
17.9	7.71×10^{-1}	3.53×10^{-2}
18.4	6.91×10^{-1}	2.08×10^{-2}
18.9	6.45×10^{-1}	2.59×10^{-2}
19.5	6.22×10^{-1}	1.86×10^{-2}
20.2	5.20×10^{-1}	3.31×10^{-2}
20.8	4.81×10^{-1}	3.16×10^{-2}
21.3	3.69×10^{-1}	2.72×10^{-2}
21.8	3.03×10^{-1}	2.43×10^{-2}
22.6	2.29×10^{-1}	1.93×10^{-2}
23.2	1.61×10^{-1}	1.58×10^{-2}
23.7	1.38×10^{-1}	1.45×10^{-2}
24.2	1.11×10^{-1}	1.29×10^{-2}
25.0	6.92×10^{-2}	7.76×10^{-3}
25.5	5.96×10^{-2}	7.15×10^{-3}
26.1	5.08×10^{-2}	6.53×10^{-3}
26.6	4.99×10^{-2}	6.44×10^{-3}

Table A.6: (Continued)

Table A.7: $^{13}C(\alpha, \alpha')$ inelastic, $E_x = 8.86$ MeV $(1/2^-_2)$, $E_\alpha = 386$ MeV

$\theta_{\text{c.m.}}$ (deg)	$d\sigma/d\Omega$ (mb/sr)	error (mb/sr)
0.4	2.91×10^{1}	6.74
1.2	2.51×10^{1}	5.21
2.7	7.34	6.30×10^{-1}
3.2	3.46	2.59×10^{-1}
3.7	1.24	9.84×10^{-2}
4.2	5.98×10^{-1}	6.58×10^{-2}
4.8	5.03×10^{-1}	9.10×10^{-2}
5.3	9.63×10^{-1}	2.18×10^{-1}
5.8	1.50	2.71×10^{-1}
6.0	2.21	4.22×10^{-1}
6.5	2.29	3.46×10^{-1}
7.1	1.96	2.56×10^{-1}
7.6	1.44	1.60×10^{-1}
8.3	5.00×10^{-1}	4.47×10^{-2}
8.8	3.00×10^{-1}	2.92×10^{-2}
9.4	1.98×10^{-1}	2.43×10^{-2}
9.9	2.07×10^{-1}	4.85×10^{-2}
10.7	4.00×10^{-1}	6.92×10^{-2}
11.2	5.79×10^{-1}	8.18×10^{-2}
11.8	5.84×10^{-1}	8.13×10^{-2}
12.3	5.41×10^{-1}	6.89×10^{-2}
13.1	5.01×10^{-1}	7.19×10^{-2}
13.6	4.32×10^{-1}	6.08×10^{-2}
14.1	2.85×10^{-1}	3.22×10^{-2}
14.7	1.56×10^{-1}	2.84×10^{-2}
15.5	1.10×10^{-1}	1.35×10^{-2}
16.0	7.72×10^{-2}	1.04×10^{-2}
16.5	6.01×10^{-2}	1.17×10^{-2}
17.1	5.56×10^{-2}	2.22×10^{-2}
17.9	7.28×10^{-2}	1.67×10^{-2}
18.4	7.33×10^{-2}	2.22×10^{-2}
18.9	6.82×10^{-2}	1.49×10^{-2}
19.5	6.03×10^{-2}	1.74×10^{-2}
20.3	4.88×10^{-2}	1.16×10^{-2}
20.8	4.91×10^{-2}	1.16×10^{-2}
21.3	2.38×10^{-2}	7.41×10^{-3}
21.8	2.65×10^{-2}	7.88×10^{-3}
22.6	1.21×10^{-2}	4.86×10^{-3}
23.2	1.38×10^{-2}	5.30×10^{-3}
23.7	8.48×10^{-3}	4.11×10^{-3}
24.2	5.27×10^{-3}	2.97×10^{-3}
25.0	7.90×10^{-3}	2.89×10^{-3}
25.5	4.22×10^{-3}	1.99×10^{-3}
26.1	7.92×10^{-3}	2.89×10^{-3}
26.6	4.34×10^{-3}	2.05×10^{-3}

A.3 Cross sections for high-lying states

Table A.8: $^{13}C(\alpha, \alpha')$ inelastic, $E_x = 10.75$ MeV $(7/2^-)$ +10.82 MeV $(5/2^-)$, $E_\alpha = 386$ MeV

$\theta_{\text{c.m.}}$ (deg)	$d\sigma/d\Omega$ (mb/sr)	error (mb/sr)
0.4	4.63×10^{-1}	6.80×10^{-2}
1.2	4.26×10^{-1}	4.15×10^{-2}
2.7	6.69×10^{-1}	4.39×10^{-2}
3.2	7.43×10^{-1}	4.54×10^{-2}
3.7	8.95×10^{-1}	5.04×10^{-2}
4.2	1.02	8.04×10^{-2}
4.2	9.55×10^{-1}	1.08×10^{-1}
4.8	1.09	1.05×10^{-1}
5.3	1.22	1.12×10^{-1}
5.8	1.14	1.30×10^{-1}
6.0	1.29	1.25×10^{-1}
6.6	1.02	1.37×10^{-1}
7.1	8.82×10^{-1}	1.11×10^{-1}
7.6	6.87×10^{-1}	9.47×10^{-2}
8.3	4.07×10^{-1}	3.45×10^{-2}
8.8	3.01×10^{-1}	2.84×10^{-2}
9.4	2.23×10^{-1}	3.30×10^{-2}
9.9	1.60×10^{-1}	1.99×10^{-2}
10.7	1.43×10^{-1}	2.40×10^{-2}
11.2	1.46×10^{-1}	1.73×10^{-2}
11.8	1.23×10^{-1}	1.55×10^{-2}
12.3	1.20×10^{-1}	1.99×10^{-2}
13.1	1.15×10^{-1}	1.35×10^{-2}
13.6	1.12×10^{-1}	1.56×10^{-2}
14.2	1.01×10^{-1}	1.46×10^{-2}
14.7	7.23×10^{-2}	1.54×10^{-2}
15.5	5.73×10^{-2}	1.45×10^{-2}
16.0	4.21×10^{-2}	1.19×10^{-2}
16.6	2.85×10^{-2}	9.26×10^{-3}
17.1	2.82×10^{-2}	9.90×10^{-3}
17.9	2.54×10^{-2}	6.06×10^{-3}
18.4	1.66×10^{-2}	6.09×10^{-3}
18.9	1.46×10^{-2}	4.78×10^{-3}
19.5	1.19×10^{-2}	5.59×10^{-3}

Table A.9: $^{13}C(\alpha, \alpha')$ inelastic, $E_x = 10.996$ MeV $(1/2^+)$ +11.08 MeV $(1/2^-)$, $E_\alpha = 386$ MeV

$\theta_{\text{c.m.}}$ (deg)	$d\sigma/d\Omega$ (mb/sr)	error (mb/sr)
0.4	1.69×10^{1}	6.01×10^{-1}
1.2	1.45×10^{1}	4.86×10^{-1}
2.7	3.90	1.77×10^{-1}
3.2	1.75	1.07×10^{-1}
3.7	7.54×10^{-1}	8.37×10^{-2}
4.2	5.27×10^{-1}	6.38×10^{-2}
4.2	6.21×10^{-1}	9.66×10^{-2}
4.8	5.70×10^{-1}	1.11×10^{-1}
5.3	8.23×10^{-1}	1.25×10^{-1}
5.8	1.01	9.05×10^{-2}
6.0	1.38	9.96×10^{-2}
6.6	1.29	9.61×10^{-2}
7.1	1.07	9.27×10^{-2}
7.6	8.13×10^{-1}	7.64×10^{-2}
8.3	3.14×10^{-1}	3.40×10^{-2}
8.8	2.63×10^{-1}	2.45×10^{-2}
9.4	2.17×10^{-1}	2.42×10^{-2}
9.9	2.24×10^{-1}	1.99×10^{-2}

Table A.9: (Continued)

$\theta_{\text{c.m.}}$ (deg)	$d\sigma/d\Omega$ (mb/sr)	error (mb/sr)
10.7	3.32×10^{-1}	2.39×10^{-2}
11.2	3.96×10^{-1}	2.85×10^{-2}
11.8	3.99×10^{-1}	2.87×10^{-2}
12.3	4.00×10^{-1}	2.79×10^{-2}
13.1	3.30×10^{-1}	3.15×10^{-2}
13.6	2.64×10^{-1}	2.77×10^{-2}
14.2	1.70×10^{-1}	1.85×10^{-2}
14.7	1.19×10^{-1}	1.71×10^{-2}
15.5	6.97×10^{-2}	1.33×10^{-2}
16.0	8.23×10^{-2}	1.24×10^{-2}
16.6	7.98×10^{-2}	1.21×10^{-2}
17.1	6.76×10^{-2}	1.06×10^{-2}
17.9	7.43×10^{-2}	7.79×10^{-3}
18.4	5.99×10^{-2}	7.08×10^{-3}
18.9	5.58×10^{-2}	6.51×10^{-3}
19.5	4.78×10^{-2}	5.80×10^{-3}

Table A.10: ^{13}C(α, α') inelastic, $E_x = 11.75$ MeV $(3/2^-)$ +11.85 MeV $(7/2^+)$, $E_\alpha = 386$ MeV

$\theta_{\text{c.m.}}$ (deg)	$d\sigma/d\Omega$ (mb/sr)	error (mb/sr)
0.4	4.15	2.53×10^{-1}
1.2	4.63	2.55×10^{-1}
2.7	4.29	2.29×10^{-1}
3.2	4.20	2.47×10^{-1}
3.7	5.31	3.51×10^{-1}
4.2	6.85	3.71×10^{-1}
4.2	6.11	2.80×10^{-1}
4.8	7.26	3.14×10^{-1}
5.3	8.24	3.64×10^{-1}
5.8	9.77	3.96×10^{-1}
6.0	1.21×10^{1}	8.64×10^{-1}
6.6	1.25×10^{1}	1.02
7.1	1.15×10^{1}	7.44×10^{-1}
7.6	1.10×10^{1}	4.22×10^{-1}
8.3	7.49	2.69×10^{-1}
8.8	6.04	2.20×10^{-1}
9.4	4.51	1.69×10^{-1}
9.9	3.03	1.20×10^{-1}

Table A.10: (Continued)

$\theta_{\text{c.m.}}$ (deg)	$d\sigma/d\Omega$ (mb/sr)	error (mb/sr)
10.7	2.00	8.79×10^{-2}
11.2	1.64	7.54×10^{-2}
11.8	1.65	7.72×10^{-2}
12.3	1.95	9.03×10^{-2}
13.1	2.12	8.94×10^{-2}
13.6	2.25	9.64×10^{-2}
14.2	2.17	9.30×10^{-2}
14.7	1.97	8.63×10^{-2}
15.5	1.48	6.93×10^{-2}
16.0	1.17	5.70×10^{-2}
16.6	8.61×10^{-1}	4.50×10^{-2}
17.1	6.12×10^{-1}	3.44×10^{-2}
17.9	3.22×10^{-1}	1.97×10^{-2}
18.4	2.22×10^{-1}	1.56×10^{-2}
19.0	1.75×10^{-1}	1.31×10^{-2}
19.5	1.60×10^{-1}	1.25×10^{-2}

Table A.11: ^{13}C(α, α') inelastic, $E_x = 12.06$ MeV, $E_\alpha = 386$ MeV

$\theta_{\text{c.m.}}$ (deg)	$d\sigma/d\Omega$ (mb/sr)	error (mb/sr)
0.4	2.57	3.16×10^{-1}
1.2	2.11	2.42×10^{-1}
2.7	1.35	1.12×10^{-1}
3.2	1.28	8.16×10^{-2}
3.7	1.07	8.86×10^{-2}
4.2	1.44	1.39×10^{-1}
4.2	1.29	1.28×10^{-1}
4.8	1.32	1.33×10^{-1}
5.3	1.34	1.38×10^{-1}
5.8	1.38	1.66×10^{-1}
6.0	1.15	3.69×10^{-1}
6.6	1.04	2.98×10^{-1}
7.1	6.35×10^{-1}	2.37×10^{-1}
7.6	4.20×10^{-1}	1.37×10^{-1}
8.3	2.86×10^{-1}	7.53×10^{-2}
8.8	2.23×10^{-1}	4.71×10^{-2}
9.4	1.97×10^{-1}	3.83×10^{-2}
9.9	2.16×10^{-1}	3.67×10^{-2}
10.7	1.55×10^{-1}	3.12×10^{-2}
11.2	2.00×10^{-1}	3.20×10^{-2}
11.8	1.65×10^{-1}	3.08×10^{-2}
12.3	1.18×10^{-1}	3.02×10^{-2}
13.1	1.27×10^{-1}	3.15×10^{-2}
13.6	7.73×10^{-2}	3.01×10^{-2}
14.2	9.61×10^{-2}	3.05×10^{-2}
14.7	1.67×10^{-2}	2.59×10^{-2}

Table A.12: ^{13}C(α, α') inelastic, $E_x = 12.28$ MeV, $E_\alpha = 386$ MeV

$\theta_{\text{c.m.}}$ (deg)	$d\sigma/d\Omega$ (mb/sr)	error (mb/sr)
0.4	6.26	1.16
1.2	5.45	1.05
2.7	1.30	$2.63 \times 10-1$
3.2	3.98×10^{-1}	8.57×10^{-2}

Table A.13: ^{13}C(α, α') inelastic, $E_x = 12.45$ MeV, $E_\alpha = 386$ MeV

$\theta_{\text{c.m.}}$ (deg)	$d\sigma/d\Omega$ (mb/sr)	error (mb/sr)
0.4	6.15	9.42×10^{-1}
1.2	5.16	7.66×10^{-1}
2.7	1.31	2.13×10^{-1}
3.2	5.03×10^{-1}	8.97×10^{-2}

Table A.14: ^{13}C(α, α') inelastic, $E_x = 12.60$ MeV, $E_\alpha = 386$ MeV

$\theta_{\text{c.m.}}$ (deg)	$d\sigma/d\Omega$ (mb/sr)	error (mb/sr)
0.4	3.40	3.40×10^{-1}
1.2	3.15	2.65×10^{-1}
2.7	7.52×10^{-1}	7.70×10^{-2}
3.2	2.58×10^{-1}	4.92×10^{-2}

Table A.15: ^{13}C(α, α') inelastic, $E_x = 12.78$ MeV, $E_\alpha = 386$ MeV

$\theta_{\text{c.m.}}$ (deg)	$d\sigma/d\Omega$ (mb/sr)	error (mb/sr)
0.4	8.12×10^{-1}	9.87×10^{-2}
1.2	6.76×10^{-1}	5.48×10^{-2}
2.7	1.56×10^{-1}	5.24×10^{-2}

A.4 Cross section for excitation-energy bins with 200-keV widths.

Table A.16: Angular distribution for the $^{13}C(\alpha, \alpha')$ reaction at $E_\alpha = 386$ MeV.

E_x (MeV)	$\theta_{\text{c.m.}}$ (deg)	$d\sigma/d\Omega$ (mb/sr)	error (mb/sr)
3.1	1.24	6.94	2.36×10^{-1}
3.1	2.67	4.44	2.26×10^{-2}
3.1	3.19	3.65	2.06×10^{-2}
3.1	3.71	2.53	1.70×10^{-2}
3.1	4.23	1.48	1.30×10^{-2}
3.1	4.23	2.00	3.23×10^{-2}
3.1	4.75	1.02	2.29×10^{-2}
3.1	5.28	5.12×10^{-1}	1.61×10^{-2}
3.1	5.80	2.52×10^{-1}	1.13×10^{-2}
3.1	6.00	2.78×10^{-1}	1.20×10^{-2}
3.1	6.53	4.02×10^{-1}	1.43×10^{-2}
3.1	7.07	4.64×10^{-1}	1.55×10^{-2}
3.1	7.60	6.08×10^{-1}	1.78×10^{-2}
3.1	8.26	3.90×10^{-1}	8.12×10^{-3}
3.1	8.80	2.89×10^{-1}	6.99×10^{-3}
3.1	9.33	1.92×10^{-1}	5.69×10^{-3}
3.1	9.86	1.35×10^{-1}	4.77×10^{-3}
3.1	10.66	1.36×10^{-1}	5.44×10^{-3}
3.1	11.19	1.76×10^{-1}	6.19×10^{-3}
3.1	11.72	2.46×10^{-1}	7.33×10^{-3}
3.1	12.26	2.98×10^{-1}	8.08×10^{-3}
3.1	13.05	3.23×10^{-1}	8.21×10^{-3}
3.1	13.59	3.22×10^{-1}	8.19×10^{-3}
3.1	14.12	2.92×10^{-1}	7.81×10^{-3}
3.1	14.65	2.46×10^{-1}	7.16×10^{-3}
3.1	15.44	1.33×10^{-1}	6.08×10^{-3}

Table A.16: Continued.

E_x (MeV)	$\theta_{\text{c.m.}}$ (deg)	$d\sigma/d\Omega$ (mb/sr)	error (mb/sr)
3.1	17.04	4.28×10^{-2}	3.44×10^{-3}
3.1	17.83	2.01×10^{-2}	2.17×10^{-3}
3.1	18.36	1.91×10^{-2}	2.12×10^{-3}
3.1	18.89	1.87×10^{-2}	2.10×10^{-3}
3.1	19.42	2.36×10^{-2}	2.36×10^{-3}
3.1	20.21	2.12×10^{-2}	5.69×10^{-3}
3.1	20.74	1.82×10^{-2}	5.27×10^{-3}
3.1	21.27	1.36×10^{-2}	4.58×10^{-3}
3.1	21.80	2.27×10^{-2}	5.94×10^{-3}
3.1	22.59	1.38×10^{-2}	4.20×10^{-3}
3.1	23.12	7.52×10^{-3}	3.10×10^{-3}
3.1	23.65	8.78×10^{-3}	3.35×10^{-3}
3.1	24.17	5.03×10^{-3}	2.54×10^{-3}
3.1	24.96	1.00×10^{-5}	1.00×10^{-5}
3.1	25.49	7.46×10^{-4}	7.51×10^{-4}
3.1	26.01	2.99×10^{-3}	1.50×10^{-3}
3.1	26.54	2.99×10^{-3}	1.51×10^{-3}
3.3	0.41	1.20	1.84×10^{-1}
3.3	1.24	8.08×10^{-1}	8.24×10^{-2}
3.3	2.67	2.40×10^{-1}	5.18×10^{-3}
3.3	3.19	2.21×10^{-1}	5.30×10^{-3}
3.3	3.71	1.55×10^{-1}	4.29×10^{-3}
3.3	4.23	1.04×10^{-1}	3.42×10^{-3}
3.3	4.23	1.08×10^{-1}	7.34×10^{-3}
3.3	4.75	5.40×10^{-2}	5.19×10^{-3}
3.3	5.28	4.12×10^{-2}	4.54×10^{-3}
3.3	5.80	5.36×10^{-2}	5.17×10^{-3}

Table A.16: Continued.

E_x (MeV)	$\theta_{\text{c.m.}}$ (deg)	$d\sigma/d\Omega$ (mb/sr)	error (mb/sr)
3.3	7.07	4.96×10^{-2}	5.71×10^{-3}
3.3	7.60	2.78×10^{-2}	4.82×10^{-3}
3.3	8.27	1.00×10^{-5}	1.00×10^{-5}
3.3	8.80	1.00×10^{-5}	1.00×10^{-5}
3.3	9.33	8.90×10^{-5}	1.10×10^{-3}
3.3	9.86	6.11×10^{-3}	1.15×10^{-3}
3.3	10.66	8.20×10^{-3}	1.34×10^{-3}
3.3	11.19	6.90×10^{-3}	1.23×10^{-3}
3.3	11.73	1.26×10^{-2}	1.66×10^{-3}
3.3	12.26	1.11×10^{-2}	1.55×10^{-3}
3.3	13.06	2.69×10^{-2}	2.37×10^{-3}
3.3	13.59	2.53×10^{-2}	2.29×10^{-3}
3.3	14.12	1.83×10^{-2}	1.95×10^{-3}
3.3	14.65	1.45×10^{-2}	1.74×10^{-3}
3.3	15.45	2.37×10^{-2}	2.56×10^{-3}
3.3	15.98	1.46×10^{-2}	2.01×10^{-3}
3.3	16.51	7.43×10^{-3}	1.44×10^{-3}
3.3	17.04	4.40×10^{-3}	1.11×10^{-3}
3.3	17.83	6.30×10^{-3}	1.21×10^{-3}
3.3	18.36	5.60×10^{-3}	1.15×10^{-3}
3.3	18.89	6.31×10^{-3}	1.22×10^{-3}
3.3	19.42	5.38×10^{-3}	1.12×10^{-3}
3.3	20.21	7.56×10^{-3}	3.39×10^{-3}
3.3	20.74	6.05×10^{-3}	3.04×10^{-3}
3.3	21.27	3.03×10^{-3}	2.15×10^{-3}
3.3	21.80	3.03×10^{-3}	2.16×10^{-3}
3.3	22.59	1.00×10^{-2}	3.60×10^{-3}
3.3	23.12	2.51×10^{-3}	1.78×10^{-3}
3.3	23.65	2.51×10^{-3}	1.79×10^{-3}

Table A.16: Continued.

E_x (MeV)	$\theta_{\text{c.m.}}$ (deg)	$d\sigma/d\Omega$ (mb/sr)	error (mb/sr)
3.3	25.49	2.24×10^{-3}	1.30×10^{-3}
3.3	26.02	1.49×10^{-3}	1.06×10^{-3}
3.3	26.54	2.24×10^{-3}	1.30×10^{-3}
3.5	0.41	4.21	3.28×10^{-1}
3.5	1.24	4.08	1.77×10^{-1}
3.5	2.67	1.76	1.40×10^{-2}
3.5	3.19	1.27	1.20×10^{-2}
3.5	3.71	1.32	1.22×10^{-2}
3.5	4.23	1.95	1.48×10^{-2}
3.5	4.23	1.32	2.58×10^{-2}
3.5	4.75	1.74	2.97×10^{-2}
3.5	5.28	1.44	2.70×10^{-2}
3.5	5.80	1.53	2.78×10^{-2}
3.5	6.00	2.09	3.27×10^{-2}
3.5	6.53	1.39	2.67×10^{-2}
3.5	7.07	1.28	2.55×10^{-2}
3.5	7.60	8.55×10^{-1}	2.09×10^{-2}
3.5	8.27	5.11×10^{-1}	9.38×10^{-3}
3.5	8.80	2.88×10^{-1}	7.01×10^{-3}
3.5	9.33	1.89×10^{-1}	5.67×10^{-3}
3.5	9.86	1.42×10^{-1}	4.90×10^{-3}
3.5	10.66	2.88×10^{-1}	7.99×10^{-3}
3.5	11.19	2.88×10^{-1}	7.99×10^{-3}
3.5	11.73	3.94×10^{-1}	9.40×10^{-3}
3.5	12.26	4.04×10^{-1}	9.52×10^{-3}
3.5	13.06	5.74×10^{-1}	1.10×10^{-2}
3.5	13.59	4.49×10^{-1}	9.75×10^{-3}
3.5	14.12	3.86×10^{-1}	9.04×10^{-3}
3.5	14.65	3.01×10^{-1}	7.96×10^{-3}

Table A.16: Continued.

E_x (MeV)	$\theta_{\text{c.m.}}$ (deg)	$d\sigma/d\Omega$ (mb/sr)	error (mb/sr)
3.5	16.51	1.88×10^{-1}	7.26×10^{-3}
3.5	17.04	1.01×10^{-1}	5.32×10^{-3}
3.5	17.83	1.06×10^{-1}	5.09×10^{-3}
3.5	18.36	8.43×10^{-2}	4.51×10^{-3}
3.5	18.89	9.63×10^{-2}	4.84×10^{-3}
3.5	19.42	9.03×10^{-2}	4.68×10^{-3}
3.5	20.22	1.03×10^{-1}	1.28×10^{-2}
3.5	20.75	8.47×10^{-2}	1.16×10^{-2}
3.5	21.27	8.63×10^{-2}	1.18×10^{-2}
3.5	21.80	9.10×10^{-2}	1.21×10^{-2}
3.5	22.59	5.38×10^{-2}	8.66×10^{-3}
3.5	23.12	3.63×10^{-2}	6.93×10^{-3}
3.5	23.65	1.63×10^{-2}	4.60×10^{-3}
3.5	24.18	2.26×10^{-2}	5.46×10^{-3}
3.5	24.97	1.12×10^{-2}	2.93×10^{-3}
3.5	25.49	1.34×10^{-2}	3.26×10^{-3}
3.5	26.02	7.47×10^{-3}	2.40×10^{-3}
3.5	26.54	9.72×10^{-3}	2.74×10^{-3}
3.7	0.41	1.68×10^{1}	6.12×10^{-1}
3.7	1.24	1.98×10^{1}	3.75×10^{-1}
3.7	2.67	1.69×10^{1}	4.43×10^{-2}
3.7	3.19	1.80×10^{1}	4.58×10^{-2}
3.7	3.71	1.99×10^{1}	4.82×10^{-2}
3.7	4.23	2.21×10^{1}	5.10×10^{-2}
3.7	4.23	2.21×10^{1}	1.09×10^{-1}
3.7	4.75	2.48×10^{1}	1.16×10^{-1}
3.7	5.28	2.83×10^{1}	1.26×10^{-1}
3.7	5.80	2.83×10^{1}	1.26×10^{-1}
3.7	6.00	3.06×10^{1}	1.25×10^{-1}

Table A.16: Continued.

E_x (MeV)	$\theta_{\text{c.m.}}$ (deg)	$d\sigma/d\Omega$ (mb/sr)	error (mb/sr)
3.7	7.60	1.85×10^{1}	9.71×10^{-2}
3.7	8.27	9.21	4.25×10^{-2}
3.7	8.80	6.06	3.37×10^{-2}
3.7	9.33	4.23	2.77×10^{-2}
3.7	9.86	3.59	2.55×10^{-2}
3.7	10.66	4.13	3.14×10^{-2}
3.7	11.20	4.81	3.42×10^{-2}
3.7	11.73	5.47	3.68×10^{-2}
3.7	12.26	5.90	3.84×10^{-2}
3.7	13.06	5.34	3.47×10^{-2}
3.7	13.59	5.06	3.37×10^{-2}
3.7	14.12	4.29	3.09×10^{-2}
3.7	14.65	3.55	2.80×10^{-2}
3.7	15.45	2.14	2.53×10^{-2}
3.7	15.98	1.49	2.09×10^{-2}
3.7	16.51	1.12	1.80×10^{-2}
3.7	17.04	8.30×10^{-1}	1.54×10^{-2}
3.7	17.84	4.90×10^{-1}	1.13×10^{-2}
3.7	18.36	4.40×10^{-1}	1.06×10^{-2}
3.7	18.89	4.49×10^{-1}	1.08×10^{-2}
3.7	19.42	4.11×10^{-1}	1.03×10^{-2}
3.7	20.22	3.22×10^{-1}	2.34×10^{-2}
3.7	20.75	2.51×10^{-1}	2.05×10^{-2}
3.7	21.28	2.32×10^{-1}	1.96×10^{-2}
3.7	21.80	1.83×10^{-1}	1.73×10^{-2}
3.7	22.60	1.13×10^{-1}	1.26×10^{-2}
3.7	23.12	9.77×10^{-2}	1.17×10^{-2}
3.7	23.65	6.52×10^{-2}	9.42×10^{-3}
3.7	24.18	5.78×10^{-2}	8.79×10^{-3}

Table A.16: Continued.

E_x (MeV)	$\theta_{\text{c.m.}}$ (deg)	$d\sigma/d\Omega$ (mb/sr)	error (mb/sr)
3.7	26.02	2.76×10^{-2}	4.69×10^{-3}
3.7	26.55	1.57×10^{-2}	3.49×10^{-3}
3.9	0.41	2.45	2.35×10^{-1}
3.9	1.24	2.48	1.34×10^{-1}
3.9	2.67	2.11	1.55×10^{-2}
3.9	3.19	2.55	1.71×10^{-2}
3.9	3.71	3.08	1.89×10^{-2}
3.9	4.23	3.41	1.98×10^{-2}
3.9	4.23	3.59	4.17×10^{-2}
3.9	4.75	4.06	4.43×10^{-2}
3.9	5.28	4.80	4.81×10^{-2}
3.9	5.80	5.70	5.25×10^{-2}
3.9	6.00	6.89	5.97×10^{-2}
3.9	6.53	7.83	6.38×10^{-2}
3.9	7.07	6.51	5.81×10^{-2}
3.9	7.60	6.01	5.58×10^{-2}
3.9	8.27	3.71	2.59×10^{-2}
3.9	8.80	2.88	2.27×10^{-2}
3.9	9.33	2.14	1.94×10^{-2}
3.9	9.87	1.46	1.60×10^{-2}
3.9	10.66	8.88×10^{-1}	1.41×10^{-2}
3.9	11.20	8.07×10^{-1}	1.34×10^{-2}
3.9	11.73	7.66×10^{-1}	1.30×10^{-2}
3.9	12.26	8.49×10^{-1}	1.38×10^{-2}
3.9	13.06	1.05	1.49×10^{-2}
3.9	13.59	1.16	1.57×10^{-2}
3.9	14.12	1.04	1.49×10^{-2}
3.9	14.65	8.91×10^{-1}	1.37×10^{-2}
3.9	15.45	7.06×10^{-1}	1.42×10^{-2}

Table A.16: Continued.

E_x (MeV)	$\theta_{\text{c.m.}}$ (deg)	$d\sigma/d\Omega$ (mb/sr)	error (mb/sr)
3.9	17.04	2.85×10^{-1}	8.93×10^{-3}
3.9	17.84	1.38×10^{-1}	5.79×10^{-3}
3.9	18.37	1.10×10^{-1}	5.16×10^{-3}
3.9	18.90	9.25×10^{-2}	4.72×10^{-3}
3.9	19.43	8.19×10^{-2}	4.44×10^{-3}
3.9	20.22	7.55×10^{-2}	1.09×10^{-2}
3.9	20.75	5.90×10^{-2}	9.64×10^{-3}
3.9	21.28	6.05×10^{-2}	9.75×10^{-3}
3.9	21.81	4.39×10^{-2}	8.26×10^{-3}
3.9	22.60	3.38×10^{-2}	6.70×10^{-3}
3.9	23.13	3.01×10^{-2}	6.28×10^{-3}
3.9	23.65	1.76×10^{-2}	4.76×10^{-3}
3.9	24.18	1.38×10^{-2}	4.22×10^{-3}
3.9	24.97	1.04×10^{-2}	2.85×10^{-3}
3.9	25.50	6.71×10^{-3}	2.27×10^{-3}
3.9	26.02	3.73×10^{-3}	1.69×10^{-3}
3.9	26.55	8.22×10^{-3}	2.51×10^{-3}
4.1	0.41	1.99×10^{-1}	1.19×10^{-1}
4.1	1.24	9.59×10^{-2}	4.76×10^{-2}
4.1	2.67	9.00×10^{-2}	3.30×10^{-3}
4.1	3.19	5.08×10^{-2}	2.54×10^{-3}
4.1	3.71	5.45×10^{-2}	3.06×10^{-3}
4.1	4.23	3.88×10^{-2}	2.76×10^{-3}
4.1	4.23	4.07×10^{-2}	5.87×10^{-3}
4.1	4.75	3.26×10^{-2}	4.29×10^{-3}
4.1	5.28	5.72×10^{-2}	5.43×10^{-3}
4.1	5.80	7.88×10^{-2}	6.33×10^{-3}
4.1	6.00	1.03×10^{-1}	7.27×10^{-3}
4.1	6.54	1.46×10^{-1}	8.60×10^{-3}

Table A.16: Continued.

E_x (MeV)	$\theta_{\text{c.m.}}$ (deg)	$d\sigma/d\Omega$ (mb/sr)	error (mb/sr)
4.1	8.27	3.90×10^{-2}	2.53×10^{-3}
4.1	8.80	3.08×10^{-2}	2.25×10^{-3}
4.1	9.33	1.97×10^{-2}	1.83×10^{-3}
4.1	9.87	1.83×10^{-2}	1.76×10^{-3}
4.1	10.66	1.75×10^{-2}	1.98×10^{-3}
4.1	11.20	1.49×10^{-2}	1.80×10^{-3}
4.1	11.73	1.01×10^{-2}	1.49×10^{-3}
4.1	12.26	8.39×10^{-3}	1.36×10^{-3}
4.1	13.06	3.39×10^{-2}	2.66×10^{-3}
4.1	13.59	2.98×10^{-2}	2.49×10^{-3}
4.1	14.12	2.76×10^{-2}	2.40×10^{-3}
4.1	14.65	1.63×10^{-2}	1.85×10^{-3}
4.1	15.45	2.59×10^{-2}	2.67×10^{-3}
4.1	15.98	2.04×10^{-2}	2.37×10^{-3}
4.1	16.51	1.19×10^{-2}	1.81×10^{-3}
4.1	17.04	6.05×10^{-3}	1.30×10^{-3}
4.1	17.84	7.69×10^{-3}	1.34×10^{-3}
4.1	18.37	5.13×10^{-3}	1.10×10^{-3}
4.1	18.90	4.20×10^{-3}	9.93×10^{-4}
4.1	19.43	1.63×10^{-3}	6.19×10^{-4}
4.1	20.22	4.53×10^{-3}	2.62×10^{-3}
4.1	20.75	4.53×10^{-3}	2.64×10^{-3}
4.1	21.28	3.03×10^{-3}	2.15×10^{-3}
4.1	21.81	1.00×10^{-5}	1.00×10^{-5}
4.1	22.60	3.75×10^{-3}	2.18×10^{-3}
4.1	23.13	1.25×10^{-3}	1.26×10^{-3}
4.1	23.65	1.25×10^{-3}	1.26×10^{-3}
4.1	24.18	1.00×10^{-5}	1.00×10^{-5}
4.1	24.97	2.23×10^{-3}	1.30×10^{-3}

Table A.16: Continued.

E_x (MeV)	$\theta_{\text{c.m.}}$ (deg)	$d\sigma/d\Omega$ (mb/sr)	error (mb/sr)
4.1	26.55	1.50×10^{-3}	1.06×10^{-3}
4.3	0.41	9.12×10^{-1}	1.61×10^{-1}
4.3	1.24	8.02×10^{-1}	8.58×10^{-2}
4.3	2.67	8.04×10^{-2}	7.10×10^{-3}
4.3	3.19	1.00×10^{-5}	1.00×10^{-5}
4.3	3.71	1.00×10^{-5}	1.00×10^{-5}
4.3	4.23	4.96×10^{-2}	5.43×10^{-3}
4.3	4.23	2.35×10^{-2}	1.12×10^{-2}
4.3	4.75	1.64×10^{-1}	1.16×10^{-2}
4.3	5.28	2.39×10^{-2}	9.49×10^{-3}
4.3	5.80	2.52×10^{-2}	8.35×10^{-3}
4.3	6.00	7.23×10^{-2}	9.45×10^{-3}
4.3	6.54	2.68×10^{-2}	6.99×10^{-3}
4.3	7.07	1.00×10^{-5}	1.00×10^{-5}
4.3	7.60	1.00×10^{-5}	1.00×10^{-5}
4.3	8.27	2.95×10^{-3}	1.19×10^{-3}
4.3	8.80	7.28×10^{-4}	7.33×10^{-4}
4.3	9.33	1.96×10^{-3}	6.51×10^{-4}
4.3	9.87	1.58×10^{-3}	6.06×10^{-4}
4.3	10.67	1.00×10^{-5}	1.00×10^{-5}
4.3	11.20	1.00×10^{-5}	1.00×10^{-5}
4.3	11.73	1.00×10^{-5}	1.00×10^{-5}
4.3	12.26	1.00×10^{-5}	1.00×10^{-5}
4.3	13.06	1.24×10^{-3}	5.49×10^{-4}
4.3	13.59	4.46×10^{-4}	3.60×10^{-4}
4.3	14.12	5.48×10^{-4}	3.60×10^{-4}
4.3	14.65	1.00×10^{-5}	1.00×10^{-5}
4.3	15.45	7.42×10^{-4}	4.77×10^{-4}
4.3	15.98	2.22×10^{-4}	2.76×10^{-4}

Table A.16: Continued.

E_x (MeV)	$\theta_{\text{c.m.}}$ (deg)	$d\sigma/d\Omega$ (mb/sr)	error (mb/sr)
4.3	17.84	1.00×10^{-5}	1.00×10^{-5}
4.3	18.37	1.00×10^{-5}	1.00×10^{-5}
4.3	18.90	2.31×10^{-4}	2.34×10^{-4}
4.3	19.43	1.00×10^{-5}	1.00×10^{-5}
4.3	20.22	1.51×10^{-3}	1.51×10^{-3}
4.3	20.75	1.51×10^{-3}	1.52×10^{-3}
4.3	21.28	1.51×10^{-3}	1.52×10^{-3}
4.3	21.81	1.00×10^{-5}	1.00×10^{-5}
4.3	22.60	1.00×10^{-5}	1.00×10^{-5}
4.3	23.13	1.00×10^{-5}	1.00×10^{-5}
4.3	23.66	1.00×10^{-5}	1.00×10^{-5}
4.3	24.18	1.00×10^{-5}	1.00×10^{-5}
4.3	24.97	1.00×10^{-5}	1.00×10^{-5}
4.3	25.50	1.00×10^{-5}	1.00×10^{-5}
4.3	26.03	1.00×10^{-5}	1.00×10^{-5}
4.3	26.55	1.00×10^{-5}	1.00×10^{-5}
4.5	0.41	2.24	2.39×10^{-1}
4.5	1.24	1.61	1.15×10^{-1}
4.5	2.67	1.00×10^{-5}	1.00×10^{-5}
4.5	3.19	1.00×10^{-5}	1.00×10^{-5}
4.5	3.71	1.00×10^{-5}	1.00×10^{-5}
4.5	4.23	1.00×10^{-5}	1.00×10^{-5}
4.5	4.23	6.65×10^{-3}	3.34×10^{-2}
4.5	4.75	1.00×10^{-5}	1.00×10^{-5}
4.5	5.28	2.81×10^{-2}	3.76×10^{-2}
4.5	5.80	9.84×10^{-2}	3.80×10^{-2}
4.5	6.00	1.00×10^{-5}	1.00×10^{-5}
4.5	6.54	1.00×10^{-5}	1.00×10^{-5}
4.5	7.07	2.68×10^{-2}	3.85×10^{-2}

Table A.16: Continued.

E_x (MeV)	$\theta_{\text{c.m.}}$ (deg)	$d\sigma/d\Omega$ (mb/sr)	error (mb/sr)
4.5	8.80	9.31×10^{-3}	8.27×10^{-3}
4.5	9.33	1.40×10^{-2}	5.99×10^{-3}
4.5	9.87	6.46×10^{-4}	4.15×10^{-3}
4.5	10.67	1.00×10^{-5}	1.00×10^{-5}
4.5	11.20	1.00×10^{-5}	1.00×10^{-5}
4.5	11.73	1.00×10^{-5}	1.00×10^{-5}
4.5	12.26	1.00×10^{-5}	1.00×10^{-5}
4.5	13.06	1.00×10^{-5}	1.00×10^{-5}
4.5	13.59	1.00×10^{-5}	1.00×10^{-5}
4.5	14.12	1.00×10^{-5}	1.00×10^{-5}
4.5	14.66	6.72×10^{-4}	5.10×10^{-4}
4.5	15.45	1.00×10^{-5}	1.00×10^{-5}
4.5	15.98	1.92×10^{-4}	3.91×10^{-4}
4.5	16.51	1.00×10^{-5}	1.00×10^{-5}
4.5	17.05	1.00×10^{-5}	1.00×10^{-5}
4.5	17.84	1.00×10^{-5}	1.00×10^{-5}
4.5	18.37	1.00×10^{-5}	1.00×10^{-5}
4.5	18.90	1.00×10^{-5}	1.00×10^{-5}
4.5	19.43	1.00×10^{-5}	1.00×10^{-5}
4.5	20.22	1.00×10^{-5}	1.00×10^{-5}
4.5	20.75	1.51×10^{-3}	1.52×10^{-3}
4.5	21.28	1.00×10^{-5}	1.00×10^{-5}
4.5	21.81	1.00×10^{-5}	1.00×10^{-5}
4.5	22.60	1.00×10^{-5}	1.00×10^{-5}
4.5	23.13	1.00×10^{-5}	1.00×10^{-5}
4.5	23.66	1.00×10^{-5}	1.00×10^{-5}
4.5	24.19	1.00×10^{-5}	1.00×10^{-5}
4.5	24.98	1.00×10^{-5}	1.00×10^{-5}
4.5	25.50	1.00×10^{-5}	1.00×10^{-5}

Table A.16: Continued.

E_x (MeV)	$\theta_{\text{c.m.}}$ (deg)	$d\sigma/d\Omega$ (mb/sr)	error (mb/sr)
4.7	0.41	1.55×10^{-1}	7.22×10^{-2}
4.7	1.24	1.02×10^{-1}	3.06×10^{-2}
4.7	2.67	1.94×10^{-2}	2.24×10^{-3}
4.7	3.19	1.00×10^{-5}	1.00×10^{-5}
4.7	3.71	1.00×10^{-5}	1.00×10^{-5}
4.7	4.23	1.00×10^{-5}	1.00×10^{-5}
4.7	4.23	7.82×10^{-3}	5.02×10^{-3}
4.7	4.75	9.28×10^{-3}	5.69×10^{-3}
4.7	5.28	1.00×10^{-5}	1.00×10^{-5}
4.7	5.80	1.53×10^{-3}	7.05×10^{-3}
4.7	6.00	1.70×10^{-2}	9.90×10^{-3}
4.7	6.54	6.66×10^{-2}	1.15×10^{-2}
4.7	7.07	6.33×10^{-2}	1.10×10^{-2}
4.7	7.60	3.38×10^{-2}	1.10×10^{-2}
4.7	8.27	1.00×10^{-5}	1.00×10^{-5}
4.7	8.80	1.00×10^{-5}	1.00×10^{-5}
4.7	9.34	1.00×10^{-5}	1.00×10^{-5}
4.7	9.87	2.24×10^{-2}	6.29×10^{-3}
4.7	10.67	2.88×10^{-2}	7.69×10^{-3}
4.7	11.20	1.78×10^{-2}	8.78×10^{-3}
4.7	11.73	3.38×10^{-3}	9.50×10^{-3}
4.7	12.26	1.00×10^{-5}	1.00×10^{-5}
4.7	13.06	1.00×10^{-5}	1.00×10^{-5}
4.7	13.59	1.00×10^{-5}	1.00×10^{-5}
4.7	14.13	1.00×10^{-5}	1.00×10^{-5}
4.7	14.66	1.00×10^{-5}	1.00×10^{-5}
4.7	15.45	1.00×10^{-5}	1.00×10^{-5}
4.7	15.98	1.00×10^{-5}	1.00×10^{-5}
4.7	16.52	1.00×10^{-5}	1.00×10^{-5}

Table A.16: Continued.

E_x (MeV)	$\theta_{\text{c.m.}}$ (deg)	$d\sigma/d\Omega$ (mb/sr)	error (mb/sr)
4.7	18.37	1.00×10^{-5}	1.00×10^{-5}
4.7	18.90	1.00×10^{-5}	1.00×10^{-5}
4.7	19.43	3.68×10^{-4}	3.31×10^{-4}
4.7	20.23	1.00×10^{-5}	1.00×10^{-5}
4.7	20.75	1.00×10^{-5}	1.00×10^{-5}
4.7	21.28	1.00×10^{-5}	1.00×10^{-5}
4.7	21.81	1.00×10^{-5}	1.00×10^{-5}
4.7	22.60	1.00×10^{-5}	1.00×10^{-5}
4.7	23.13	1.00×10^{-5}	1.00×10^{-5}
4.7	23.66	1.00×10^{-5}	1.00×10^{-5}
4.7	24.19	1.00×10^{-5}	1.00×10^{-5}
4.7	24.98	1.00×10^{-5}	1.00×10^{-5}
4.7	25.50	1.00×10^{-5}	1.00×10^{-5}
4.7	26.03	1.00×10^{-5}	1.00×10^{-5}
4.7	26.56	1.00×10^{-5}	1.00×10^{-5}
4.9	0.41	1.05×10^{-1}	5.34×10^{-2}
4.9	1.24	8.17×10^{-2}	2.71×10^{-2}
4.9	2.67	1.39×10^{-2}	1.77×10^{-3}
4.9	3.19	2.70×10^{-2}	1.82×10^{-3}
4.9	3.71	8.99×10^{-3}	1.40×10^{-3}
4.9	4.23	4.23×10^{-2}	2.24×10^{-3}
4.9	4.23	1.00×10^{-5}	1.00×10^{-5}
4.9	4.75	1.08×10^{-2}	2.64×10^{-3}
4.9	5.28	1.19×10^{-2}	2.60×10^{-3}
4.9	5.80	1.10×10^{-2}	2.60×10^{-3}
4.9	6.00	1.00×10^{-5}	1.00×10^{-5}
4.9	6.54	1.00×10^{-5}	1.00×10^{-5}
4.9	7.07	1.00×10^{-5}	1.00×10^{-5}
4.9	7.60	1.07×10^{-3}	4.00×10^{-3}

Table A.16: Continued.

E_x (MeV)	$\theta_{\text{c.m.}}$ (deg)	$d\sigma/d\Omega$ (mb/sr)	error (mb/sr)
4.9	9.34	4.97×10^{-4}	6.53×10^{-4}
4.9	9.87	2.00×10^{-3}	8.41×10^{-4}
4.9	10.67	1.00×10^{-5}	1.00×10^{-5}
4.9	11.20	2.62×10^{-3}	1.94×10^{-3}
4.9	11.73	1.00×10^{-5}	1.00×10^{-5}
4.9	12.27	1.61×10^{-2}	3.56×10^{-3}
4.9	13.06	1.80×10^{-2}	5.36×10^{-3}
4.9	13.59	2.86×10^{-2}	6.13×10^{-3}
4.9	14.13	2.38×10^{-2}	6.75×10^{-3}
4.9	14.66	2.90×10^{-2}	7.00×10^{-3}
4.9	15.46	4.80×10^{-5}	6.95×10^{-3}
4.9	15.99	1.00×10^{-5}	1.00×10^{-5}
4.9	16.52	1.00×10^{-5}	1.00×10^{-5}
4.9	17.05	1.00×10^{-5}	1.00×10^{-5}
4.9	17.84	1.00×10^{-5}	1.00×10^{-5}
4.9	18.37	2.00×10^{-5}	1.71×10^{-3}
4.9	18.90	8.48×10^{-4}	1.43×10^{-3}
4.9	19.43	9.05×10^{-4}	1.10×10^{-3}
4.9	20.23	4.53×10^{-3}	2.62×10^{-3}
4.9	20.76	1.00×10^{-5}	1.00×10^{-5}
4.9	21.29	1.00×10^{-5}	1.00×10^{-5}
4.9	21.81	1.00×10^{-5}	1.00×10^{-5}
4.9	22.61	1.00×10^{-5}	1.00×10^{-5}
4.9	23.13	1.00×10^{-5}	1.00×10^{-5}
4.9	23.66	1.00×10^{-5}	1.00×10^{-5}
4.9	24.19	1.00×10^{-5}	1.00×10^{-5}
4.9	24.98	1.00×10^{-5}	1.00×10^{-5}
4.9	25.51	1.00×10^{-5}	1.00×10^{-5}
4.9	26.03	1.00×10^{-5}	1.00×10^{-5}

Table A.16: Continued.

E_x (MeV)	$\theta_{\text{c.m.}}$ (deg)	$d\sigma/d\Omega$ (mb/sr)	error (mb/sr)
5.1	1.24	1.54×10^{-1}	3.74×10^{-2}
5.1	2.67	5.99×10^{-2}	2.67×10^{-3}
5.1	3.19	4.95×10^{-2}	2.35×10^{-3}
5.1	3.71	3.66×10^{-2}	2.07×10^{-3}
5.1	4.23	9.97×10^{-2}	3.36×10^{-3}
5.1	4.23	5.29×10^{-2}	5.14×10^{-3}
5.1	4.75	4.55×10^{-2}	4.75×10^{-3}
5.1	5.28	3.10×10^{-2}	3.92×10^{-3}
5.1	5.80	2.90×10^{-2}	3.80×10^{-3}
5.1	6.00	7.18×10^{-3}	4.17×10^{-3}
5.1	6.54	1.00×10^{-5}	1.00×10^{-5}
5.1	7.07	1.00×10^{-5}	1.00×10^{-5}
5.1	7.60	1.00×10^{-5}	1.00×10^{-5}
5.1	8.27	5.01×10^{-3}	9.34×10^{-4}
5.1	8.80	6.75×10^{-3}	1.07×10^{-3}
5.1	9.34	4.11×10^{-3}	9.03×10^{-4}
5.1	9.87	6.41×10^{-3}	1.05×10^{-3}
5.1	10.67	4.32×10^{-3}	9.93×10^{-4}
5.1	11.20	2.81×10^{-3}	8.12×10^{-4}
5.1	11.73	2.47×10^{-3}	7.83×10^{-4}
5.1	12.27	3.90×10^{-3}	1.02×10^{-3}
5.1	13.06	1.49×10^{-3}	8.57×10^{-4}
5.1	13.60	6.49×10^{-4}	8.84×10^{-4}
5.1	14.13	1.00×10^{-5}	1.00×10^{-5}
5.1	14.66	8.32×10^{-4}	1.11×10^{-3}
5.1	15.46	5.50×10^{-3}	2.26×10^{-3}
5.1	15.99	1.53×10^{-3}	2.16×10^{-3}
5.1	16.52	3.34×10^{-3}	2.48×10^{-3}
5.1	17.05	2.12×10^{-3}	2.59×10^{-3}

Table A.16: Continued.

E_x (MeV)	$\theta_{\text{c.m.}}$ (deg)	$d\sigma/d\Omega$ (mb/sr)	error (mb/sr)
5.1	18.90	6.87×10^{-3}	2.66×10^{-3}
5.1	19.43	3.70×10^{-3}	2.54×10^{-3}
5.1	20.23	2.26×10^{-2}	5.89×10^{-3}
5.1	20.76	1.66×10^{-2}	5.04×10^{-3}
5.1	21.29	4.54×10^{-3}	2.63×10^{-3}
5.1	21.82	4.54×10^{-3}	2.63×10^{-3}
5.1	22.61	2.50×10^{-3}	1.78×10^{-3}
5.1	23.14	1.00×10^{-5}	1.00×10^{-5}
5.1	23.66	1.25×10^{-3}	1.26×10^{-3}
5.1	24.19	1.00×10^{-5}	1.00×10^{-5}
5.1	24.98	1.00×10^{-5}	1.00×10^{-5}
5.1	25.51	1.00×10^{-5}	1.00×10^{-5}
5.1	26.03	7.46×10^{-4}	7.51×10^{-4}
5.1	26.56	1.00×10^{-5}	1.00×10^{-5}
5.3	0.41	2.24×10^{-1}	7.25×10^{-2}
5.3	1.24	2.11×10^{-1}	3.95×10^{-2}
5.3	2.67	9.91×10^{-2}	3.32×10^{-3}
5.3	3.19	1.05×10^{-1}	3.42×10^{-3}
5.3	3.71	9.28×10^{-2}	3.21×10^{-3}
5.3	4.23	1.68×10^{-1}	4.34×10^{-3}
5.3	4.23	7.48×10^{-2}	6.14×10^{-3}
5.3	4.75	1.04×10^{-1}	7.13×10^{-3}
5.3	5.28	6.08×10^{-2}	5.43×10^{-3}
5.3	5.80	5.31×10^{-2}	5.08×10^{-3}
5.3	6.00	3.52×10^{-2}	4.22×10^{-3}
5.3	6.54	1.77×10^{-3}	3.95×10^{-3}
5.3	7.07	9.20×10^{-3}	4.07×10^{-3}
5.3	7.61	1.47×10^{-2}	4.58×10^{-3}
5.3	8.27	1.00×10^{-2}	1.31×10^{-3}

Table A.16: Continued.

E_x (MeV)	$\theta_{\text{c.m.}}$ (deg)	$d\sigma/d\Omega$ (mb/sr)	error (mb/sr)
5.3	9.87	1.27×10^{-2}	1.46×10^{-3}
5.3	10.67	1.42×10^{-2}	1.76×10^{-3}
5.3	11.20	9.46×10^{-3}	1.44×10^{-3}
5.3	11.73	8.21×10^{-3}	1.34×10^{-3}
5.3	12.27	7.34×10^{-3}	1.27×10^{-3}
5.3	13.07	5.01×10^{-3}	1.04×10^{-3}
5.3	13.60	4.99×10^{-3}	1.04×10^{-3}
5.3	14.13	6.90×10^{-3}	1.21×10^{-3}
5.3	14.66	7.59×10^{-3}	1.26×10^{-3}
5.3	15.46	3.24×10^{-3}	9.93×10^{-4}
5.3	15.99	1.89×10^{-3}	7.80×10^{-4}
5.3	16.52	1.05×10^{-3}	6.17×10^{-4}
5.3	17.05	2.65×10^{-3}	9.16×10^{-4}
5.3	17.85	9.83×10^{-4}	7.39×10^{-4}
5.3	18.38	2.17×10^{-3}	9.64×10^{-4}
5.3	18.91	1.04×10^{-3}	1.02×10^{-3}
5.3	19.44	1.26×10^{-3}	1.29×10^{-3}
5.3	20.23	9.05×10^{-3}	3.71×10^{-3}
5.3	20.76	1.36×10^{-2}	4.56×10^{-3}
5.3	21.29	1.36×10^{-2}	4.58×10^{-3}
5.3	21.82	1.51×10^{-2}	4.81×10^{-3}
5.3	22.61	1.00×10^{-2}	3.58×10^{-3}
5.3	23.14	2.50×10^{-3}	1.78×10^{-3}
5.3	23.67	3.76×10^{-3}	2.18×10^{-3}
5.3	24.19	2.51×10^{-3}	1.79×10^{-3}
5.3	24.98	7.44×10^{-4}	7.49×10^{-4}
5.3	25.51	7.45×10^{-4}	7.50×10^{-4}
5.3	26.04	1.00×10^{-5}	1.00×10^{-5}
5.3	26.56	7.47×10^{-4}	7.52×10^{-4}

Table A.16: Continued.

E_x (MeV)	$\theta_{\text{c.m.}}$ (deg)	$d\sigma/d\Omega$ (mb/sr)	error (mb/sr)
5.5	2.67	1.16×10^{-1}	3.57×10^{-3}
5.5	3.19	1.22×10^{-1}	3.68×10^{-3}
5.5	3.71	1.56×10^{-1}	4.16×10^{-3}
5.5	4.23	2.07×10^{-1}	4.80×10^{-3}
5.5	4.23	1.65×10^{-1}	8.90×10^{-3}
5.5	4.75	1.47×10^{-1}	8.44×10^{-3}
5.5	5.29	1.03×10^{-1}	7.07×10^{-3}
5.5	5.81	8.98×10^{-2}	6.58×10^{-3}
5.5	6.01	6.54×10^{-2}	5.84×10^{-3}
5.5	6.54	3.51×10^{-2}	5.49×10^{-3}
5.5	7.07	3.05×10^{-2}	4.82×10^{-3}
5.5	7.61	2.98×10^{-2}	4.53×10^{-3}
5.5	8.27	1.16×10^{-2}	1.40×10^{-3}
5.5	8.81	1.50×10^{-2}	1.59×10^{-3}
5.5	9.34	1.43×10^{-2}	1.56×10^{-3}
5.5	9.87	2.04×10^{-2}	1.85×10^{-3}
5.5	10.67	1.38×10^{-2}	1.73×10^{-3}
5.5	11.20	1.40×10^{-2}	1.75×10^{-3}
5.5	11.74	1.43×10^{-2}	1.76×10^{-3}
5.5	12.27	1.08×10^{-2}	1.53×10^{-3}
5.5	13.07	8.41×10^{-3}	1.33×10^{-3}
5.5	13.60	7.59×10^{-3}	1.26×10^{-3}
5.5	14.13	6.78×10^{-3}	1.19×10^{-3}
5.5	14.66	4.34×10^{-3}	9.51×10^{-4}
5.5	15.46	3.55×10^{-3}	9.92×10^{-4}
5.5	15.99	3.00×10^{-3}	9.13×10^{-4}
5.5	16.52	2.74×10^{-3}	8.72×10^{-4}
5.5	17.05	2.74×10^{-3}	8.72×10^{-4}
5.5	17.85	8.76×10^{-4}	4.66×10^{-4}

Table A.16: Continued.

E_x (MeV)	$\theta_{\text{c.m.}}$ (deg)	$d\sigma/d\Omega$ (mb/sr)	error (mb/sr)
5.5	19.44	8.25×10^{-4}	4.68×10^{-4}
5.5	20.23	1.00×10^{-5}	1.00×10^{-5}
5.5	20.76	3.02×10^{-3}	2.15×10^{-3}
5.5	21.29	6.05×10^{-3}	3.03×10^{-3}
5.5	21.82	4.54×10^{-3}	2.63×10^{-3}
5.5	22.61	8.75×10^{-3}	3.33×10^{-3}
5.5	23.14	1.00×10^{-2}	3.58×10^{-3}
5.5	23.67	5.01×10^{-3}	2.52×10^{-3}
5.5	24.19	2.51×10^{-3}	1.78×10^{-3}
5.5	24.99	2.23×10^{-3}	1.30×10^{-3}
5.5	25.51	1.49×10^{-3}	1.06×10^{-3}
5.5	26.04	1.00×10^{-5}	1.00×10^{-5}
5.5	26.56	7.46×10^{-4}	7.52×10^{-4}
5.7	0.41	5.91×10^{-1}	1.08×10^{-1}
5.7	1.24	4.19×10^{-1}	5.24×10^{-2}
5.7	2.67	1.61×10^{-1}	4.23×10^{-3}
5.7	3.19	1.60×10^{-1}	4.22×10^{-3}
5.7	3.71	1.69×10^{-1}	4.33×10^{-3}
5.7	4.23	2.44×10^{-1}	5.22×10^{-3}
5.7	4.23	2.05×10^{-1}	9.94×10^{-3}
5.7	4.75	1.69×10^{-1}	9.05×10^{-3}
5.7	5.29	1.67×10^{-1}	8.96×10^{-3}
5.7	5.81	1.24×10^{-1}	7.73×10^{-3}
5.7	6.01	6.46×10^{-2}	5.74×10^{-3}
5.7	6.54	4.31×10^{-2}	4.78×10^{-3}
5.7	7.07	1.00×10^{-5}	1.00×10^{-5}
5.7	7.61	1.71×10^{-2}	4.49×10^{-3}
5.7	8.27	1.50×10^{-2}	1.59×10^{-3}
5.7	8.81	2.35×10^{-2}	1.99×10^{-3}

Table A.16: Continued.

E_x (MeV)	$\theta_{\text{c.m.}}$ (deg)	$d\sigma/d\Omega$ (mb/sr)	error (mb/sr)
5.7	10.67	1.84×10^{-2}	2.00×10^{-3}
5.7	11.20	1.71×10^{-2}	1.93×10^{-3}
5.7	11.74	1.51×10^{-2}	1.81×10^{-3}
5.7	12.27	1.13×10^{-2}	1.56×10^{-3}
5.7	13.07	1.28×10^{-2}	1.63×10^{-3}
5.7	13.60	8.03×10^{-3}	1.33×10^{-3}
5.7	14.13	6.42×10^{-3}	1.15×10^{-3}
5.7	14.66	5.16×10^{-3}	1.04×10^{-3}
5.7	15.46	4.38×10^{-3}	1.10×10^{-3}
5.7	15.99	4.12×10^{-3}	1.07×10^{-3}
5.7	16.52	3.29×10^{-3}	9.55×10^{-4}
5.7	17.05	2.74×10^{-3}	8.72×10^{-4}
5.7	17.85	1.38×10^{-3}	5.71×10^{-4}
5.7	18.38	2.08×10^{-3}	7.00×10^{-4}
5.7	18.91	1.15×10^{-3}	5.22×10^{-4}
5.7	19.44	6.88×10^{-4}	4.05×10^{-4}
5.7	20.23	1.00×10^{-5}	1.00×10^{-5}
5.7	20.76	1.51×10^{-3}	1.51×10^{-3}
5.7	21.29	1.51×10^{-3}	1.52×10^{-3}
5.7	21.82	1.51×10^{-3}	1.52×10^{-3}
5.7	22.61	1.00×10^{-5}	1.00×10^{-5}
5.7	23.14	1.00×10^{-5}	1.00×10^{-5}
5.7	23.67	1.25×10^{-3}	1.26×10^{-3}
5.7	24.20	1.00×10^{-5}	1.00×10^{-5}
5.7	24.99	2.23×10^{-3}	1.30×10^{-3}
5.7	25.51	7.44×10^{-4}	7.50×10^{-4}
5.7	26.04	7.45×10^{-4}	7.51×10^{-4}
5.7	26.57	1.49×10^{-3}	1.06×10^{-3}
5.9	0.41	7.14×10^{-1}	1.14×10^{-1}

Table A.16: Continued.

E_x (MeV)	$\theta_{\text{c.m.}}$ (deg)	$d\sigma/d\Omega$ (mb/sr)	error (mb/sr)
5.9	3.19	2.04×10^{-1}	4.77×10^{-3}
5.9	3.71	2.03×10^{-1}	4.77×10^{-3}
5.9	4.23	2.48×10^{-1}	5.28×10^{-3}
5.9	4.23	2.11×10^{-1}	1.01×10^{-2}
5.9	4.75	2.01×10^{-1}	9.89×10^{-3}
5.9	5.29	1.47×10^{-1}	8.61×10^{-3}
5.9	5.81	1.26×10^{-1}	8.12×10^{-3}
5.9	6.01	1.10×10^{-1}	8.09×10^{-3}
5.9	6.54	3.60×10^{-2}	6.49×10^{-3}
5.9	7.07	4.03×10^{-2}	6.41×10^{-3}
5.9	7.61	2.62×10^{-2}	5.33×10^{-3}
5.9	8.27	2.44×10^{-2}	2.03×10^{-3}
5.9	8.81	2.50×10^{-2}	2.05×10^{-3}
5.9	9.34	2.66×10^{-2}	2.12×10^{-3}
5.9	9.87	2.81×10^{-2}	2.18×10^{-3}
5.9	10.67	2.81×10^{-2}	2.47×10^{-3}
5.9	11.20	2.77×10^{-2}	2.45×10^{-3}
5.9	11.74	2.16×10^{-2}	2.17×10^{-3}
5.9	12.27	2.04×10^{-2}	2.10×10^{-3}
5.9	13.07	9.49×10^{-3}	1.40×10^{-3}
5.9	13.60	8.88×10^{-3}	1.36×10^{-3}
5.9	14.13	7.02×10^{-3}	1.21×10^{-3}
5.9	14.66	7.22×10^{-3}	1.23×10^{-3}
5.9	15.46	6.30×10^{-3}	1.32×10^{-3}
5.9	15.99	4.10×10^{-3}	1.07×10^{-3}
5.9	16.52	4.38×10^{-3}	1.10×10^{-3}
5.9	17.05	1.36×10^{-3}	6.17×10^{-4}
5.9	17.85	2.78×10^{-3}	8.07×10^{-4}
5.9	18.38	2.32×10^{-3}	7.38×10^{-4}

Table A.16: Continued.

E_x (MeV)	$\theta_{\text{c.m.}}$ (deg)	$d\sigma/d\Omega$ (mb/sr)	error (mb/sr)
5.9	20.23	1.00×10^{-5}	1.00×10^{-5}
5.9	20.76	3.02×10^{-3}	2.14×10^{-3}
5.9	21.29	1.00×10^{-5}	1.00×10^{-5}
5.9	21.82	1.00×10^{-5}	1.00×10^{-5}
5.9	22.61	1.25×10^{-3}	1.26×10^{-3}
5.9	23.14	1.25×10^{-3}	1.26×10^{-3}
5.9	23.67	1.00×10^{-5}	1.00×10^{-5}
5.9	24.20	1.00×10^{-5}	1.00×10^{-5}
5.9	24.99	1.00×10^{-5}	1.00×10^{-5}
5.9	25.52	7.44×10^{-4}	7.50×10^{-4}
5.9	26.04	7.45×10^{-4}	7.51×10^{-4}
5.9	26.57	7.46×10^{-4}	7.52×10^{-4}
6.1	0.41	1.05	1.36×10^{-1}
6.1	1.24	6.17×10^{-1}	5.81×10^{-2}
6.1	2.67	2.00×10^{-1}	4.79×10^{-3}
6.1	3.19	2.36×10^{-1}	5.19×10^{-3}
6.1	3.71	2.34×10^{-1}	5.19×10^{-3}
6.1	4.23	2.53×10^{-1}	5.40×10^{-3}
6.1	4.23	2.22×10^{-1}	1.05×10^{-2}
6.1	4.75	2.48×10^{-1}	1.12×10^{-2}
6.1	5.29	1.94×10^{-1}	9.91×10^{-3}
6.1	5.81	1.56×10^{-1}	8.84×10^{-3}
6.1	6.01	1.40×10^{-1}	8.61×10^{-3}
6.1	6.54	8.77×10^{-2}	6.90×10^{-3}
6.1	7.07	6.88×10^{-2}	6.26×10^{-3}
6.1	7.61	2.88×10^{-2}	4.74×10^{-3}
6.1	8.27	1.91×10^{-2}	1.80×10^{-3}
6.1	8.81	2.52×10^{-2}	2.06×10^{-3}
6.1	9.34	2.42×10^{-2}	2.02×10^{-3}

Table A.16: Continued.

E_x (MeV)	$\theta_{\text{c.m.}}$ (deg)	$d\sigma/d\Omega$ (mb/sr)	error (mb/sr)
6.1	11.21	2.46×10^{-2}	2.31×10^{-3}
6.1	11.74	2.29×10^{-2}	2.23×10^{-3}
6.1	12.27	1.73×10^{-2}	1.94×10^{-3}
6.1	13.07	1.69×10^{-2}	1.87×10^{-3}
6.1	13.60	9.67×10^{-3}	1.42×10^{-3}
6.1	14.13	1.03×10^{-2}	1.47×10^{-3}
6.1	14.66	4.12×10^{-3}	9.28×10^{-4}
6.1	15.46	3.01×10^{-3}	9.12×10^{-4}
6.1	15.99	3.84×10^{-3}	1.03×10^{-3}
6.1	16.52	4.67×10^{-3}	1.14×10^{-3}
6.1	17.06	4.12×10^{-3}	1.07×10^{-3}
6.1	17.85	3.94×10^{-3}	9.61×10^{-4}
6.1	18.38	3.02×10^{-3}	8.41×10^{-4}
6.1	18.91	2.80×10^{-3}	8.09×10^{-4}
6.1	19.44	1.16×10^{-3}	5.23×10^{-4}
6.1	20.24	1.00×10^{-5}	1.00×10^{-5}
6.1	20.77	1.51×10^{-3}	1.51×10^{-3}
6.1	21.29	1.00×10^{-5}	1.00×10^{-5}
6.1	21.82	1.00×10^{-5}	1.00×10^{-5}
6.1	22.62	1.25×10^{-3}	1.26×10^{-3}
6.1	23.14	1.00×10^{-5}	1.00×10^{-5}
6.1	23.67	1.00×10^{-5}	1.00×10^{-5}
6.1	24.20	1.00×10^{-5}	1.00×10^{-5}
6.1	24.99	1.00×10^{-5}	1.00×10^{-5}
6.1	25.52	1.00×10^{-5}	1.00×10^{-5}
6.1	26.04	1.00×10^{-5}	1.00×10^{-5}
6.1	26.57	1.00×10^{-5}	1.00×10^{-5}
6.3	0.41	9.30×10^{-1}	1.22×10^{-1}
6.3	1.24	7.33×10^{-1}	6.18×10^{-2}

Table A.16: Continued.

E_x (MeV)	$\theta_{\text{c.m.}}$ (deg)	$d\sigma/d\Omega$ (mb/sr)	error (mb/sr)
6.3	3.71	2.64×10^{-1}	5.41×10^{-3}
6.3	4.23	2.66×10^{-1}	5.43×10^{-3}
6.3	4.23	2.57×10^{-1}	1.11×10^{-2}
6.3	4.75	2.43×10^{-1}	1.08×10^{-2}
6.3	5.29	2.23×10^{-1}	1.03×10^{-2}
6.3	5.81	1.93×10^{-1}	9.61×10^{-3}
6.3	6.01	1.19×10^{-1}	7.81×10^{-3}
6.3	6.54	1.04×10^{-1}	7.49×10^{-3}
6.3	7.07	7.72×10^{-2}	6.60×10^{-3}
6.3	7.61	1.95×10^{-2}	3.94×10^{-3}
6.3	8.27	2.52×10^{-2}	2.06×10^{-3}
6.3	8.81	2.79×10^{-2}	2.17×10^{-3}
6.3	9.34	3.03×10^{-2}	2.26×10^{-3}
6.3	9.87	3.27×10^{-2}	2.34×10^{-3}
6.3	10.67	3.56×10^{-2}	2.78×10^{-3}
6.3	11.21	3.48×10^{-2}	2.75×10^{-3}
6.3	11.74	2.77×10^{-2}	2.45×10^{-3}
6.3	12.27	2.03×10^{-2}	2.10×10^{-3}
6.3	13.07	1.84×10^{-2}	1.95×10^{-3}
6.3	13.60	1.32×10^{-2}	1.66×10^{-3}
6.3	14.13	9.51×10^{-3}	1.41×10^{-3}
6.3	14.67	6.20×10^{-3}	1.14×10^{-3}
6.3	15.46	4.10×10^{-3}	1.06×10^{-3}
6.3	15.99	6.59×10^{-3}	1.35×10^{-3}
6.3	16.53	4.94×10^{-3}	1.17×10^{-3}
6.3	17.06	4.66×10^{-3}	1.14×10^{-3}
6.3	17.85	3.01×10^{-3}	8.40×10^{-4}
6.3	18.38	2.31×10^{-3}	7.37×10^{-4}
6.3	18.91	1.62×10^{-3}	6.18×10^{-4}

Table A.16: Continued.

E_x (MeV)	$\theta_{\text{c.m.}}$ (deg)	$d\sigma/d\Omega$ (mb/sr)	error (mb/sr)
6.3	20.77	1.51×10^{-3}	1.51×10^{-3}
6.3	21.30	1.00×10^{-5}	1.00×10^{-5}
6.3	21.83	1.00×10^{-5}	1.00×10^{-5}
6.3	22.62	1.00×10^{-5}	1.00×10^{-5}
6.3	23.15	1.00×10^{-5}	1.00×10^{-5}
6.3	23.67	1.00×10^{-5}	1.00×10^{-5}
6.3	24.20	1.00×10^{-5}	1.00×10^{-5}
6.3	24.99	1.00×10^{-5}	1.00×10^{-5}
6.3	25.52	1.00×10^{-5}	1.00×10^{-5}
6.3	26.05	1.00×10^{-5}	1.00×10^{-5}
6.3	26.57	1.00×10^{-5}	1.00×10^{-5}
6.5	0.41	1.26	1.47×10^{-1}
6.5	1.24	9.46×10^{-1}	7.20×10^{-2}
6.5	2.67	2.91×10^{-1}	5.67×10^{-3}
6.5	3.19	2.94×10^{-1}	5.70×10^{-3}
6.5	3.71	2.79×10^{-1}	5.55×10^{-3}
6.5	4.23	2.93×10^{-1}	5.69×10^{-3}
6.5	4.23	3.27×10^{-1}	1.25×10^{-2}
6.5	4.75	3.09×10^{-1}	1.22×10^{-2}
6.5	5.29	2.35×10^{-1}	1.07×10^{-2}
6.5	5.81	2.06×10^{-1}	9.96×10^{-3}
6.5	6.01	1.43×10^{-1}	8.49×10^{-3}
6.5	6.54	7.88×10^{-2}	6.70×10^{-3}
6.5	7.08	5.35×10^{-2}	6.13×10^{-3}
6.5	7.61	3.77×10^{-2}	4.74×10^{-3}
6.5	8.28	2.38×10^{-2}	2.00×10^{-3}
6.5	8.81	3.09×10^{-2}	2.28×10^{-3}
6.5	9.34	3.21×10^{-2}	2.32×10^{-3}
6.5	9.88	3.63×10^{-2}	2.47×10^{-3}

Table A.16: Continued.

E_x (MeV)	$\theta_{\text{c.m.}}$ (deg)	$d\sigma/d\Omega$ (mb/sr)	error (mb/sr)
6.5	11.74	3.29×10^{-2}	2.67×10^{-3}
6.5	12.27	1.99×10^{-2}	2.08×10^{-3}
6.5	13.07	1.57×10^{-2}	1.80×10^{-3}
6.5	13.60	1.45×10^{-2}	1.73×10^{-3}
6.5	14.14	1.12×10^{-2}	1.52×10^{-3}
6.5	14.67	9.53×10^{-3}	1.41×10^{-3}
6.5	15.46	4.92×10^{-3}	1.17×10^{-3}
6.5	16.00	5.48×10^{-3}	1.23×10^{-3}
6.5	16.53	5.77×10^{-3}	1.26×10^{-3}
6.5	17.06	4.67×10^{-3}	1.14×10^{-3}
6.5	17.85	3.48×10^{-3}	9.02×10^{-4}
6.5	18.38	3.49×10^{-3}	9.03×10^{-4}
6.5	18.92	3.02×10^{-3}	8.41×10^{-4}
6.5	19.45	1.63×10^{-3}	6.18×10^{-4}
6.5	20.24	1.51×10^{-3}	1.51×10^{-3}
6.5	20.77	1.00×10^{-5}	1.00×10^{-5}
6.5	21.30	3.02×10^{-3}	2.14×10^{-3}
6.5	21.83	1.00×10^{-5}	1.00×10^{-5}
6.5	22.62	1.25×10^{-3}	1.26×10^{-3}
6.5	23.15	1.25×10^{-3}	1.26×10^{-3}
6.5	23.68	1.00×10^{-5}	1.00×10^{-5}
6.5	24.20	1.00×10^{-5}	1.00×10^{-5}
6.5	25.00	1.00×10^{-5}	1.00×10^{-5}
6.5	25.52	7.44×10^{-4}	7.49×10^{-4}
6.5	26.05	1.00×10^{-5}	1.00×10^{-5}
6.5	26.58	1.00×10^{-5}	1.00×10^{-5}
6.7	0.41	1.37	1.46×10^{-1}
6.7	1.24	9.40×10^{-1}	6.79×10^{-2}
6.7	2.67	3.45×10^{-1}	6.20×10^{-3}

Table A.16: Continued.

E_x (MeV)	$\theta_{\text{c.m.}}$ (deg)	$d\sigma/d\Omega$ (mb/sr)	error (mb/sr)
6.7	4.23	3.33×10^{-1}	6.15×10^{-3}
6.7	4.23	3.55×10^{-1}	1.32×10^{-2}
6.7	4.75	3.06×10^{-1}	1.23×10^{-2}
6.7	5.29	3.00×10^{-1}	1.23×10^{-2}
6.7	5.81	2.38×10^{-1}	1.10×10^{-2}
6.7	6.01	2.09×10^{-1}	1.07×10^{-2}
6.7	6.54	1.30×10^{-1}	8.72×10^{-3}
6.7	7.08	1.02×10^{-1}	7.51×10^{-3}
6.7	7.61	8.39×10^{-2}	6.88×10^{-3}
6.7	8.28	4.49×10^{-2}	2.75×10^{-3}
6.7	8.81	4.66×10^{-2}	2.80×10^{-3}
6.7	9.34	4.78×10^{-2}	2.83×10^{-3}
6.7	9.88	5.10×10^{-2}	2.93×10^{-3}
6.7	10.68	6.38×10^{-2}	3.72×10^{-3}
6.7	11.21	5.28×10^{-2}	3.38×10^{-3}
6.7	11.74	4.54×10^{-2}	3.14×10^{-3}
6.7	12.27	3.29×10^{-2}	2.67×10^{-3}
6.7	13.07	2.66×10^{-2}	2.35×10^{-3}
6.7	13.60	1.86×10^{-2}	1.97×10^{-3}
6.7	14.14	1.53×10^{-2}	1.78×10^{-3}
6.7	14.67	1.22×10^{-2}	1.59×10^{-3}
6.7	15.47	9.59×10^{-3}	1.63×10^{-3}
6.7	16.00	1.01×10^{-2}	1.67×10^{-3}
6.7	16.53	8.51×10^{-3}	1.53×10^{-3}
6.7	17.06	9.08×10^{-3}	1.58×10^{-3}
6.7	17.86	5.35×10^{-3}	1.12×10^{-3}
6.7	18.39	3.73×10^{-3}	9.33×10^{-4}
6.7	18.92	3.95×10^{-3}	9.62×10^{-4}
6.7	19.45	3.49×10^{-3}	9.05×10^{-4}

Table A.16: Continued.

E_x (MeV)	$\theta_{\text{c.m.}}$ (deg)	$d\sigma/d\Omega$ (mb/sr)	error (mb/sr)
6.7	21.30	4.53×10^{-3}	2.62×10^{-3}
6.7	21.83	3.02×10^{-3}	2.15×10^{-3}
6.7	22.62	1.00×10^{-5}	1.00×10^{-5}
6.7	23.15	2.50×10^{-3}	1.78×10^{-3}
6.7	23.68	2.50×10^{-3}	1.78×10^{-3}
6.7	24.21	1.25×10^{-3}	1.26×10^{-3}
6.7	25.00	1.00×10^{-5}	1.00×10^{-5}
6.7	25.52	7.44×10^{-4}	7.49×10^{-4}
6.7	26.05	1.00×10^{-5}	1.00×10^{-5}
6.7	26.58	7.46×10^{-4}	7.51×10^{-4}
6.9	0.41	1.64	1.62×10^{-1}
6.9	1.24	1.12	7.51×10^{-2}
6.9	2.67	4.60×10^{-1}	7.20×10^{-3}
6.9	3.19	4.24×10^{-1}	6.94×10^{-3}
6.9	3.71	4.58×10^{-1}	7.23×10^{-3}
6.9	4.23	4.75×10^{-1}	7.37×10^{-3}
6.9	4.23	4.33×10^{-1}	1.47×10^{-2}
6.9	4.75	5.23×10^{-1}	1.61×10^{-2}
6.9	5.29	4.91×10^{-1}	1.56×10^{-2}
6.9	5.81	4.81×10^{-1}	1.53×10^{-2}
6.9	6.01	4.24×10^{-1}	1.47×10^{-2}
6.9	6.54	3.51×10^{-1}	1.35×10^{-2}
6.9	7.08	3.00×10^{-1}	1.23×10^{-2}
6.9	7.61	2.49×10^{-1}	1.11×10^{-2}
6.9	8.28	1.86×10^{-1}	5.59×10^{-3}
6.9	8.81	1.89×10^{-1}	5.64×10^{-3}
6.9	9.34	2.05×10^{-1}	5.88×10^{-3}
6.9	9.88	1.96×10^{-1}	5.74×10^{-3}
6.9	10.68	1.63×10^{-1}	5.96×10^{-3}

Table A.16: Continued.

E_x (MeV)	$\theta_{\text{c.m.}}$ (deg)	$d\sigma/d\Omega$ (mb/sr)	error (mb/sr)
6.9	12.27	1.02×10^{-1}	4.71×10^{-3}
6.9	13.07	7.67×10^{-2}	3.99×10^{-3}
6.9	13.61	5.77×10^{-2}	3.46×10^{-3}
6.9	14.14	4.39×10^{-2}	3.02×10^{-3}
6.9	14.67	3.77×10^{-2}	2.80×10^{-3}
6.9	15.47	2.23×10^{-2}	2.48×10^{-3}
6.9	16.00	2.01×10^{-2}	2.35×10^{-3}
6.9	16.53	1.95×10^{-2}	2.32×10^{-3}
6.9	17.06	1.43×10^{-2}	1.99×10^{-3}
6.9	17.86	7.91×10^{-3}	1.36×10^{-3}
6.9	18.39	6.74×10^{-3}	1.26×10^{-3}
6.9	18.92	8.15×10^{-3}	1.38×10^{-3}
6.9	19.45	4.42×10^{-3}	1.02×10^{-3}
6.9	20.24	4.52×10^{-3}	2.62×10^{-3}
6.9	20.77	3.02×10^{-3}	2.14×10^{-3}
6.9	21.30	1.51×10^{-3}	1.52×10^{-3}
6.9	21.83	3.02×10^{-3}	2.15×10^{-3}
6.9	22.62	3.75×10^{-3}	2.19×10^{-3}
6.9	23.15	1.25×10^{-3}	1.26×10^{-3}
6.9	23.68	1.25×10^{-3}	1.26×10^{-3}
6.9	24.21	1.25×10^{-3}	1.26×10^{-3}
6.9	25.00	1.00×10^{-5}	1.00×10^{-5}
6.9	25.53	7.44×10^{-4}	7.49×10^{-4}
6.9	26.05	1.00×10^{-5}	1.00×10^{-5}
6.9	26.58	7.46×10^{-4}	7.51×10^{-4}
7.1	0.41	1.66	1.62×10^{-1}
7.1	1.24	1.39	8.27×10^{-2}
7.1	2.67	4.50×10^{-1}	7.05×10^{-3}
7.1	3.19	3.63×10^{-1}	6.34×10^{-3}

Table A.16: Continued.

E_x (MeV)	$\theta_{\text{c.m.}}$ (deg)	$d\sigma/d\Omega$ (mb/sr)	error (mb/sr)
7.1	4.23	3.86×10^{-1}	1.36×10^{-2}
7.1	4.75	3.73×10^{-1}	1.33×10^{-2}
7.1	5.29	3.27×10^{-1}	1.25×10^{-2}
7.1	5.81	2.96×10^{-1}	1.18×10^{-2}
7.1	6.01	2.46×10^{-1}	1.11×10^{-2}
7.1	6.54	1.85×10^{-1}	9.56×10^{-3}
7.1	7.08	1.07×10^{-1}	7.37×10^{-3}
7.1	7.61	3.69×10^{-2}	4.79×10^{-3}
7.1	8.28	3.46×10^{-2}	2.39×10^{-3}
7.1	8.81	3.65×10^{-2}	2.46×10^{-3}
7.1	9.34	4.05×10^{-2}	2.59×10^{-3}
7.1	9.88	5.42×10^{-2}	2.99×10^{-3}
7.1	10.68	5.06×10^{-2}	3.31×10^{-3}
7.1	11.21	5.08×10^{-2}	3.32×10^{-3}
7.1	11.74	4.65×10^{-2}	3.18×10^{-3}
7.1	12.28	3.46×10^{-2}	2.74×10^{-3}
7.1	13.07	2.14×10^{-2}	2.11×10^{-3}
7.1	13.61	1.86×10^{-2}	1.96×10^{-3}
7.1	14.14	1.34×10^{-2}	1.67×10^{-3}
7.1	14.67	1.35×10^{-2}	1.67×10^{-3}
7.1	15.47	9.85×10^{-3}	1.65×10^{-3}
7.1	16.00	8.23×10^{-3}	1.51×10^{-3}
7.1	16.53	7.69×10^{-3}	1.46×10^{-3}
7.1	17.06	7.97×10^{-3}	1.48×10^{-3}
7.1	17.86	6.17×10^{-3}	1.21×10^{-3}
7.1	18.39	7.84×10^{-3}	1.37×10^{-3}
7.1	18.92	4.03×10^{-3}	9.83×10^{-4}
7.1	19.45	4.28×10^{-3}	1.01×10^{-3}
7.1	20.24	5.68×10^{-3}	2.85×10^{-3}

Table A.16: Continued.

E_x (MeV)	$\theta_{\text{c.m.}}$ (deg)	$d\sigma/d\Omega$ (mb/sr)	error (mb/sr)
7.1	21.83	1.42×10^{-3}	1.43×10^{-3}
7.1	22.63	1.18×10^{-3}	1.20×10^{-3}
7.1	23.15	1.00×10^{-5}	1.00×10^{-5}
7.1	23.68	2.36×10^{-3}	1.70×10^{-3}
7.1	24.21	1.00×10^{-5}	1.00×10^{-5}
7.1	25.00	2.89×10^{-3}	1.78×10^{-3}
7.1	25.53	1.93×10^{-3}	1.42×10^{-3}
7.1	26.05	9.67×10^{-4}	1.01×10^{-3}
7.1	26.58	1.00×10^{-5}	1.00×10^{-5}
7.3	0.41	2.25	1.84×10^{-1}
7.3	1.24	1.98	9.65×10^{-2}
7.3	2.67	7.35×10^{-1}	8.98×10^{-3}
7.3	3.19	6.76×10^{-1}	8.61×10^{-3}
7.3	3.71	7.28×10^{-1}	8.94×10^{-3}
7.3	4.23	7.89×10^{-1}	9.31×10^{-3}
7.3	4.23	5.91×10^{-1}	1.68×10^{-2}
7.3	4.75	5.76×10^{-1}	1.66×10^{-2}
7.3	5.29	6.02×10^{-1}	1.70×10^{-2}
7.3	5.81	6.76×10^{-1}	1.80×10^{-2}
7.3	6.01	6.21×10^{-1}	1.75×10^{-2}
7.3	6.54	5.63×10^{-1}	1.66×10^{-2}
7.3	7.08	4.22×10^{-1}	1.45×10^{-2}
7.3	7.61	3.59×10^{-1}	1.33×10^{-2}
7.3	8.28	1.83×10^{-1}	5.57×10^{-3}
7.3	8.81	1.24×10^{-1}	4.58×10^{-3}
7.3	9.35	1.02×10^{-1}	4.16×10^{-3}
7.3	9.88	1.05×10^{-1}	4.23×10^{-3}
7.3	10.68	9.79×10^{-2}	4.61×10^{-3}
7.3	11.21	8.74×10^{-2}	4.36×10^{-3}

Table A.16: Continued.

E_x (MeV)	$\theta_{\text{c.m.}}$ (deg)	$d\sigma/d\Omega$ (mb/sr)	error (mb/sr)
7.3	13.08	1.42×10^{-1}	5.43×10^{-3}
7.3	13.61	9.70×10^{-2}	4.49×10^{-3}
7.3	14.14	7.60×10^{-2}	3.97×10^{-3}
7.3	14.67	5.10×10^{-2}	3.25×10^{-3}
7.3	15.47	7.69×10^{-2}	4.61×10^{-3}
7.3	16.00	5.80×10^{-2}	4.00×10^{-3}
7.3	16.53	5.12×10^{-2}	3.76×10^{-3}
7.3	17.06	3.17×10^{-2}	2.96×10^{-3}
7.3	17.86	4.03×10^{-2}	3.03×10^{-3}
7.3	18.39	3.30×10^{-2}	2.75×10^{-3}
7.3	18.92	2.78×10^{-2}	2.52×10^{-3}
7.3	19.45	2.78×10^{-2}	2.52×10^{-3}
7.3	20.25	3.64×10^{-2}	7.30×10^{-3}
7.3	20.78	3.94×10^{-2}	7.59×10^{-3}
7.3	21.30	1.90×10^{-2}	5.27×10^{-3}
7.3	21.83	2.05×10^{-2}	5.48×10^{-3}
7.3	22.63	1.18×10^{-2}	3.74×10^{-3}
7.3	23.16	1.65×10^{-2}	4.44×10^{-3}
7.3	23.68	2.37×10^{-2}	5.31×10^{-3}
7.3	24.21	9.48×10^{-3}	3.35×10^{-3}
7.3	25.00	5.19×10^{-3}	1.97×10^{-3}
7.3	25.53	4.46×10^{-3}	1.83×10^{-3}
7.3	26.06	6.69×10^{-3}	2.24×10^{-3}
7.3	26.58	7.45×10^{-3}	2.37×10^{-3}
7.5	1.24	2.20×10^{1}	3.28×10^{-1}
7.5	2.67	1.84×10^{1}	4.59×10^{-2}
7.5	3.19	1.93×10^{1}	4.71×10^{-2}
7.5	3.71	2.25×10^{1}	5.09×10^{-2}
7.5	4.23	2.39×10^{1}	5.27×10^{-2}

Table A.16: Continued.

E_x (MeV)	$\theta_{\text{c.m.}}$ (deg)	$d\sigma/d\Omega$ (mb/sr)	error (mb/sr)
7.5	5.29	3.00×10^{1}	1.25×10^{-1}
7.5	5.81	3.00×10^{1}	1.25×10^{-1}
7.5	6.01	3.28×10^{1}	1.28×10^{-1}
7.5	6.54	2.84×10^{1}	1.19×10^{-1}
7.5	7.08	2.61×10^{1}	1.14×10^{-1}
7.5	7.61	2.01×10^{1}	9.99×10^{-2}
7.5	8.28	1.00×10^{1}	4.55×10^{-2}
7.5	8.81	7.10	3.74×10^{-2}
7.5	9.35	5.09	3.11×10^{-2}
7.5	9.88	4.32	2.85×10^{-2}
7.5	10.68	4.22	3.01×10^{-2}
7.5	11.21	4.79	3.21×10^{-2}
7.5	11.74	5.45	3.44×10^{-2}
7.5	12.28	5.77	3.53×10^{-2}
7.5	13.08	5.69	3.62×10^{-2}
7.5	13.61	5.20	3.46×10^{-2}
7.5	14.14	4.48	3.19×10^{-2}
7.5	14.67	3.56	2.82×10^{-2}
7.5	15.47	2.12	2.53×10^{-2}
7.5	16.00	1.57	2.15×10^{-2}
7.5	16.53	1.13	1.81×10^{-2}
7.5	17.06	8.75×10^{-1}	1.58×10^{-2}
7.5	17.86	5.06×10^{-1}	1.08×10^{-2}
7.5	18.39	4.62×10^{-1}	1.03×10^{-2}
7.5	18.92	4.29×10^{-1}	9.92×10^{-3}
7.5	19.45	4.17×10^{-1}	9.78×10^{-3}
7.5	20.25	3.34×10^{-1}	2.25×10^{-2}
7.5	20.78	2.85×10^{-1}	2.08×10^{-2}
7.5	21.31	2.07×10^{-1}	1.77×10^{-2}

Table A.16: Continued.

E_x (MeV)	$\theta_{\text{c.m.}}$ (deg)	$d\sigma/d\Omega$ (mb/sr)	error (mb/sr)
7.5	23.16	8.91×10^{-2}	1.07×10^{-2}
7.5	23.69	7.39×10^{-2}	9.73×10^{-3}
7.5	24.21	7.02×10^{-2}	9.49×10^{-3}
7.5	25.00	3.35×10^{-2}	4.85×10^{-3}
7.5	25.53	3.00×10^{-2}	4.59×10^{-3}
7.5	26.06	2.38×10^{-2}	4.09×10^{-3}
7.5	26.59	2.45×10^{-2}	4.15×10^{-3}
7.7	1.24	1.16×10^{1}	2.38×10^{-1}
7.7	2.67	5.62	2.62×10^{-2}
7.7	3.19	5.11	2.46×10^{-2}
7.7	3.71	4.62	2.31×10^{-2}
7.7	4.23	6.01	2.64×10^{-2}
7.7	4.23	5.46	5.08×10^{-2}
7.7	4.76	5.93	5.29×10^{-2}
7.7	5.29	6.10	5.39×10^{-2}
7.7	5.81	5.66	5.22×10^{-2}
7.7	6.01	7.16	6.16×10^{-2}
7.7	6.54	6.56	5.91×10^{-2}
7.7	7.08	4.10	4.69×10^{-2}
7.7	7.61	2.98	3.99×10^{-2}
7.7	8.28	1.67	1.79×10^{-2}
7.7	8.81	1.04	1.38×10^{-2}
7.7	9.35	7.24×10^{-1}	1.14×10^{-2}
7.7	9.88	6.79×10^{-1}	1.10×10^{-2}
7.7	10.68	1.25	1.65×10^{-2}
7.7	11.21	1.65	1.89×10^{-2}
7.7	11.75	1.72	1.93×10^{-2}
7.7	12.28	1.84	2.00×10^{-2}
7.7	13.08	1.77	1.96×10^{-2}

Table A.16: Continued.

E_x (MeV)	$\theta_{\text{c.m.}}$ (deg)	$d\sigma/d\Omega$ (mb/sr)	error (mb/sr)
7.7	14.67	1.11	1.55×10^{-2}
7.7	15.47	8.93×10^{-1}	1.61×10^{-2}
7.7	16.00	6.32×10^{-1}	1.35×10^{-2}
7.7	16.53	4.13×10^{-1}	1.08×10^{-2}
7.7	17.07	2.93×10^{-1}	9.09×10^{-3}
7.7	17.86	2.35×10^{-1}	7.52×10^{-3}
7.7	18.39	1.98×10^{-1}	6.89×10^{-3}
7.7	18.92	1.92×10^{-1}	6.78×10^{-3}
7.7	19.45	1.76×10^{-1}	6.49×10^{-3}
7.7	20.25	1.36×10^{-1}	1.41×10^{-2}
7.7	20.78	1.42×10^{-1}	1.45×10^{-2}
7.7	21.31	1.35×10^{-1}	1.41×10^{-2}
7.7	21.84	7.12×10^{-2}	1.02×10^{-2}
7.7	22.63	6.51×10^{-2}	8.90×10^{-3}
7.7	23.16	5.19×10^{-2}	7.94×10^{-3}
7.7	23.69	3.63×10^{-2}	6.64×10^{-3}
7.7	24.22	3.03×10^{-2}	6.07×10^{-3}
7.7	25.01	2.37×10^{-2}	4.01×10^{-3}
7.7	25.53	1.76×10^{-2}	3.46×10^{-3}
7.7	26.06	1.70×10^{-2}	3.40×10^{-3}
7.7	26.59	1.63×10^{-2}	3.33×10^{-3}
7.9	0.41	2.66	1.97×10^{-1}
7.9	1.24	2.62	1.09×10^{-1}
7.9	2.67	1.30	1.21×10^{-2}
7.9	3.19	1.02	1.07×10^{-2}
7.9	3.71	7.69×10^{-1}	9.26×10^{-3}
7.9	4.24	6.58×10^{-1}	8.56×10^{-3}
7.9	4.24	6.30×10^{-1}	1.72×10^{-2}
7.9	4.76	5.50×10^{-1}	1.61×10^{-2}

Table A.16: Continued.

E_x (MeV)	$\theta_{\text{c.m.}}$ (deg)	$d\sigma/d\Omega$ (mb/sr)	error (mb/sr)
7.9	6.01	4.72×10^{-1}	1.56×10^{-2}
7.9	6.55	4.17×10^{-1}	1.47×10^{-2}
7.9	7.08	3.96×10^{-1}	1.43×10^{-2}
7.9	7.61	2.97×10^{-1}	1.27×10^{-2}
7.9	8.28	1.76×10^{-1}	5.68×10^{-3}
7.9	8.81	1.32×10^{-1}	4.93×10^{-3}
7.9	9.35	1.10×10^{-1}	4.51×10^{-3}
7.9	9.88	1.09×10^{-1}	4.58×10^{-3}
7.9	10.68	1.15×10^{-1}	5.64×10^{-3}
7.9	11.21	1.12×10^{-1}	5.78×10^{-3}
7.9	11.75	9.71×10^{-2}	5.57×10^{-3}
7.9	12.28	9.45×10^{-2}	5.48×10^{-3}
7.9	13.08	8.98×10^{-2}	5.00×10^{-3}
7.9	13.61	7.28×10^{-2}	4.42×10^{-3}
7.9	14.14	5.90×10^{-2}	3.83×10^{-3}
7.9	14.68	4.90×10^{-2}	3.36×10^{-3}
7.9	15.47	3.37×10^{-2}	3.11×10^{-3}
7.9	16.00	3.14×10^{-2}	2.96×10^{-3}
7.9	16.54	2.10×10^{-2}	2.42×10^{-3}
7.9	17.07	1.53×10^{-2}	2.06×10^{-3}
7.9	17.86	1.42×10^{-2}	1.82×10^{-3}
7.9	18.39	1.17×10^{-2}	1.65×10^{-3}
7.9	18.93	1.20×10^{-2}	1.67×10^{-3}
7.9	19.46	9.42×10^{-3}	1.48×10^{-3}
7.9	20.25	7.08×10^{-3}	3.20×10^{-3}
7.9	20.78	1.28×10^{-2}	4.27×10^{-3}
7.9	21.31	8.51×10^{-3}	3.52×10^{-3}
7.9	21.84	4.26×10^{-3}	2.47×10^{-3}
7.9	22.63	4.37×10^{-3}	2.20×10^{-3}

Table A.16: Continued.

E_x (MeV)	$\theta_{\text{c.m.}}$ (deg)	$d\sigma/d\Omega$ (mb/sr)	error (mb/sr)
7.9	24.22	1.10×10^{-3}	1.10×10^{-3}
7.9	25.01	3.98×10^{-3}	1.79×10^{-3}
7.9	25.54	5.58×10^{-3}	2.13×10^{-3}
7.9	26.06	2.40×10^{-3}	1.40×10^{-3}
7.9	26.59	1.60×10^{-3}	1.14×10^{-3}
8.1	0.41	2.95	2.09×10^{-1}
8.1	1.24	2.19	1.01×10^{-1}
8.1	2.67	1.10	1.10×10^{-2}
8.1	3.19	9.00×10^{-1}	9.99×10^{-3}
8.1	3.71	7.25×10^{-1}	8.97×10^{-3}
8.1	4.24	6.19×10^{-1}	8.28×10^{-3}
8.1	4.24	6.50×10^{-1}	1.78×10^{-2}
8.1	4.76	5.63×10^{-1}	1.65×10^{-2}
8.1	5.29	5.35×10^{-1}	1.61×10^{-2}
8.1	5.81	4.56×10^{-1}	1.49×10^{-2}
8.1	6.01	4.33×10^{-1}	1.47×10^{-2}
8.1	6.55	3.52×10^{-1}	1.34×10^{-2}
8.1	7.08	3.00×10^{-1}	1.24×10^{-2}
8.1	7.61	2.89×10^{-1}	1.20×10^{-2}
8.1	8.28	1.60×10^{-1}	5.19×10^{-3}
8.1	8.81	1.34×10^{-1}	4.75×10^{-3}
8.1	9.35	1.14×10^{-1}	4.39×10^{-3}
8.1	9.88	1.05×10^{-1}	4.21×10^{-3}
8.1	10.68	1.03×10^{-1}	4.82×10^{-3}
8.1	11.21	9.26×10^{-2}	4.59×10^{-3}
8.1	11.75	8.63×10^{-2}	4.47×10^{-3}
8.1	12.28	8.30×10^{-2}	4.43×10^{-3}
8.1	13.08	6.71×10^{-2}	4.01×10^{-3}
8.1	13.61	5.92×10^{-2}	3.83×10^{-3}

Table A.16: Continued.

E_x (MeV)	$\theta_{\text{c.m.}}$ (deg)	$d\sigma/d\Omega$ (mb/sr)	error (mb/sr)
8.1	15.47	1.85×10^{-2}	2.61×10^{-3}
8.1	16.01	1.31×10^{-2}	2.22×10^{-3}
8.1	16.54	1.30×10^{-2}	2.15×10^{-3}
8.1	17.07	8.18×10^{-3}	1.81×10^{-3}
8.1	17.87	1.10×10^{-2}	1.78×10^{-3}
8.1	18.40	7.58×10^{-3}	1.46×10^{-3}
8.1	18.93	7.08×10^{-3}	1.38×10^{-3}
8.1	19.46	6.92×10^{-3}	1.34×10^{-3}
8.1	20.25	9.25×10^{-3}	4.21×10^{-3}
8.1	20.78	5.56×10^{-3}	3.25×10^{-3}
8.1	21.31	1.85×10^{-3}	1.88×10^{-3}
8.1	21.84	3.71×10^{-3}	2.66×10^{-3}
8.1	22.63	4.81×10^{-3}	3.57×10^{-3}
8.1	23.16	2.41×10^{-3}	2.53×10^{-3}
8.1	23.69	1.00×10^{-5}	1.00×10^{-5}
8.1	24.22	1.00×10^{-5}	1.00×10^{-5}
8.1	25.01	5.62×10^{-4}	5.62×10^{-4}
8.1	25.54	1.00×10^{-5}	1.00×10^{-5}
8.1	26.06	1.69×10^{-3}	9.77×10^{-4}
8.1	26.59	1.00×10^{-5}	1.00×10^{-5}
8.3	0.41	2.60	1.94×10^{-1}
8.3	1.24	2.35	1.04×10^{-1}
8.3	2.67	9.75×10^{-1}	1.04×10^{-2}
8.3	3.19	7.71×10^{-1}	9.26×10^{-3}
8.3	3.71	6.55×10^{-1}	8.52×10^{-3}
8.3	4.24	5.92×10^{-1}	8.10×10^{-3}
8.3	4.24	6.31×10^{-1}	1.73×10^{-2}
8.3	4.76	5.58×10^{-1}	1.63×10^{-2}
8.3	5.29	5.23×10^{-1}	1.58×10^{-2}

Table A.16: Continued.

E_x (MeV)	$\theta_{\text{c.m.}}$ (deg)	$d\sigma/d\Omega$ (mb/sr)	error (mb/sr)
8.3	6.55	3.88×10^{-1}	1.40×10^{-2}
8.3	7.08	3.25×10^{-1}	1.28×10^{-2}
8.3	7.61	2.11×10^{-1}	1.04×10^{-2}
8.3	8.28	1.49×10^{-1}	4.97×10^{-3}
8.3	8.82	1.24×10^{-1}	4.54×10^{-3}
8.3	9.35	1.26×10^{-1}	4.56×10^{-3}
8.3	9.88	1.03×10^{-1}	4.13×10^{-3}
8.3	10.68	1.06×10^{-1}	4.84×10^{-3}
8.3	11.22	9.67×10^{-2}	4.63×10^{-3}
8.3	11.75	8.64×10^{-2}	4.38×10^{-3}
8.3	12.28	7.44×10^{-2}	4.06×10^{-3}
8.3	13.08	5.62×10^{-2}	3.42×10^{-3}
8.3	13.61	4.60×10^{-2}	3.10×10^{-3}
8.3	14.15	3.63×10^{-2}	2.75×10^{-3}
8.3	14.68	2.79×10^{-2}	2.42×10^{-3}
8.3	15.48	1.76×10^{-2}	2.23×10^{-3}
8.3	16.01	1.39×10^{-2}	2.00×10^{-3}
8.3	16.54	1.30×10^{-2}	1.97×10^{-3}
8.3	17.07	1.40×10^{-2}	2.08×10^{-3}
8.3	17.87	1.18×10^{-2}	1.82×10^{-3}
8.3	18.40	8.46×10^{-3}	1.63×10^{-3}
8.3	18.93	6.15×10^{-3}	1.45×10^{-3}
8.3	19.46	8.30×10^{-3}	1.60×10^{-3}
8.3	20.25	7.62×10^{-3}	3.11×10^{-3}
8.3	20.78	5.09×10^{-3}	2.54×10^{-3}
8.3	21.31	2.55×10^{-3}	1.80×10^{-3}
8.3	21.84	3.82×10^{-3}	2.21×10^{-3}
8.3	22.64	9.80×10^{-4}	9.80×10^{-4}
8.3	23.16	1.96×10^{-3}	1.39×10^{-3}

Table A.16: Continued.

E_x (MeV)	$\theta_{\text{c.m.}}$ (deg)	$d\sigma/d\Omega$ (mb/sr)	error (mb/sr)
8.3	25.01	1.00×10^{-5}	1.00×10^{-5}
8.3	25.54	2.70×10^{-3}	2.17×10^{-3}
8.3	26.07	1.00×10^{-5}	1.00×10^{-5}
8.3	26.59	1.00×10^{-5}	1.00×10^{-5}
8.5	0.41	4.88	2.65×10^{-1}
8.5	1.24	3.50	1.26×10^{-1}
8.5	2.67	1.11	1.11×10^{-2}
8.5	3.19	7.71×10^{-1}	9.28×10^{-3}
8.5	3.71	5.97×10^{-1}	8.15×10^{-3}
8.5	4.24	5.73×10^{-1}	7.97×10^{-3}
8.5	4.24	5.80×10^{-1}	1.67×10^{-2}
8.5	4.76	5.58×10^{-1}	1.64×10^{-2}
8.5	5.29	5.57×10^{-1}	1.64×10^{-2}
8.5	5.81	5.52×10^{-1}	1.63×10^{-2}
8.5	6.01	5.62×10^{-1}	1.68×10^{-2}
8.5	6.55	4.48×10^{-1}	1.50×10^{-2}
8.5	7.08	3.64×10^{-1}	1.37×10^{-2}
8.5	7.61	2.82×10^{-1}	1.20×10^{-2}
8.5	8.28	1.46×10^{-1}	4.97×10^{-3}
8.5	8.82	1.07×10^{-1}	4.25×10^{-3}
8.5	9.35	1.08×10^{-1}	4.26×10^{-3}
8.5	9.88	1.15×10^{-1}	4.39×10^{-3}
8.5	10.68	1.12×10^{-1}	4.99×10^{-3}
8.5	11.22	1.04×10^{-1}	4.81×10^{-3}
8.5	11.75	1.06×10^{-1}	4.85×10^{-3}
8.5	12.28	9.11×10^{-2}	4.51×10^{-3}
8.5	13.08	6.58×10^{-2}	3.70×10^{-3}
8.5	13.61	5.33×10^{-2}	3.34×10^{-3}
8.5	14.15	3.68×10^{-2}	2.77×10^{-3}

Table A.16: Continued.

E_x (MeV)	$\theta_{\text{c.m.}}$ (deg)	$d\sigma/d\Omega$ (mb/sr)	error (mb/sr)
8.5	16.01	1.92×10^{-2}	2.30×10^{-3}
8.5	16.54	1.62×10^{-2}	2.11×10^{-3}
8.5	17.07	1.40×10^{-2}	1.97×10^{-3}
8.5	17.87	1.68×10^{-2}	1.98×10^{-3}
8.5	18.40	1.23×10^{-2}	1.70×10^{-3}
8.5	18.93	8.78×10^{-3}	1.45×10^{-3}
8.5	19.46	8.60×10^{-3}	1.46×10^{-3}
8.5	20.26	7.40×10^{-3}	3.33×10^{-3}
8.5	20.79	1.19×10^{-2}	4.23×10^{-3}
8.5	21.31	1.48×10^{-3}	1.49×10^{-3}
8.5	21.84	1.48×10^{-3}	1.49×10^{-3}
8.5	22.64	1.60×10^{-3}	1.70×10^{-3}
8.5	23.17	1.60×10^{-3}	1.70×10^{-3}
8.5	23.69	3.21×10^{-3}	2.41×10^{-3}
8.5	24.22	1.00×10^{-5}	1.00×10^{-5}
8.5	25.01	6.56×10^{-4}	6.62×10^{-4}
8.5	25.54	6.57×10^{-4}	6.63×10^{-4}
8.5	26.07	6.58×10^{-4}	6.64×10^{-4}
8.5	26.60	1.00×10^{-5}	1.00×10^{-5}
8.7	0.41	1.23×10^{1}	4.22×10^{-1}
8.7	1.24	1.02×10^{1}	2.16×10^{-1}
8.7	2.67	2.75	1.76×10^{-2}
8.7	3.19	1.48	1.29×10^{-2}
8.7	3.72	8.18×10^{-1}	9.57×10^{-3}
8.7	4.24	6.30×10^{-1}	8.39×10^{-3}
8.7	4.24	6.62×10^{-1}	1.78×10^{-2}
8.7	4.76	6.65×10^{-1}	1.78×10^{-2}
8.7	5.29	8.39×10^{-1}	2.00×10^{-2}
8.7	5.81	9.36×10^{-1}	2.12×10^{-2}

Table A.16: Continued.

E_x (MeV)	$\theta_{\text{c.m.}}$ (deg)	$d\sigma/d\Omega$ (mb/sr)	error (mb/sr)
8.7	7.08	8.68×10^{-1}	2.08×10^{-2}
8.7	7.62	6.26×10^{-1}	1.77×10^{-2}
8.7	8.28	2.63×10^{-1}	6.72×10^{-3}
8.7	8.82	1.79×10^{-1}	5.53×10^{-3}
8.7	9.35	1.39×10^{-1}	4.88×10^{-3}
8.7	9.88	1.73×10^{-1}	5.44×10^{-3}
8.7	10.68	2.10×10^{-1}	6.73×10^{-3}
8.7	11.22	2.54×10^{-1}	7.40×10^{-3}
8.7	11.75	2.53×10^{-1}	7.39×10^{-3}
8.7	12.28	2.29×10^{-1}	7.02×10^{-3}
8.7	13.08	1.90×10^{-1}	6.30×10^{-3}
8.7	13.62	1.64×10^{-1}	5.85×10^{-3}
8.7	14.15	1.10×10^{-1}	4.78×10^{-3}
8.7	14.68	7.73×10^{-2}	4.01×10^{-3}
8.7	15.48	4.29×10^{-2}	3.44×10^{-3}
8.7	16.01	3.01×10^{-2}	2.88×10^{-3}
8.7	16.54	2.94×10^{-2}	2.85×10^{-3}
8.7	17.07	3.68×10^{-2}	3.19×10^{-3}
8.7	17.87	3.30×10^{-2}	2.76×10^{-3}
8.7	18.40	3.44×10^{-2}	2.82×10^{-3}
8.7	18.93	3.00×10^{-2}	2.63×10^{-3}
8.7	19.46	2.73×10^{-2}	2.51×10^{-3}
8.7	20.26	2.65×10^{-2}	6.47×10^{-3}
8.7	20.79	1.25×10^{-2}	4.43×10^{-3}
8.7	21.32	7.81×10^{-3}	3.51×10^{-3}
8.7	21.85	9.38×10^{-3}	3.85×10^{-3}
8.7	22.64	3.99×10^{-3}	2.34×10^{-3}
8.7	23.17	5.33×10^{-3}	2.69×10^{-3}
8.7	23.70	2.67×10^{-3}	1.90×10^{-3}

Table A.16: Continued.

E_x (MeV)	$\theta_{\text{c.m.}}$ (deg)	$d\sigma/d\Omega$ (mb/sr)	error (mb/sr)
8.7	25.54	1.43×10^{-3}	1.02×10^{-3}
8.7	26.07	2.14×10^{-3}	1.25×10^{-3}
8.7	26.60	1.43×10^{-3}	1.02×10^{-3}
8.9	0.41	1.62×10^{1}	4.82×10^{-1}
8.9	1.24	1.48×10^{1}	2.60×10^{-1}
8.9	2.67	4.68	2.30×10^{-2}
8.9	3.19	2.59	1.71×10^{-2}
8.9	3.72	1.31	1.21×10^{-2}
8.9	4.24	7.66×10^{-1}	9.27×10^{-3}
8.9	4.24	8.84×10^{-1}	2.06×10^{-2}
8.9	4.76	7.68×10^{-1}	1.92×10^{-2}
8.9	5.29	9.88×10^{-1}	2.18×10^{-2}
8.9	5.81	1.27	2.47×10^{-2}
8.9	6.01	1.55	2.79×10^{-2}
8.9	6.55	1.60	2.84×10^{-2}
8.9	7.08	1.38	2.63×10^{-2}
8.9	7.62	1.04	2.29×10^{-2}
8.9	8.28	4.26×10^{-1}	8.39×10^{-3}
8.9	8.82	2.74×10^{-1}	6.72×10^{-3}
8.9	9.35	2.03×10^{-1}	5.77×10^{-3}
8.9	9.88	1.96×10^{-1}	5.68×10^{-3}
8.9	10.68	2.90×10^{-1}	7.88×10^{-3}
8.9	11.22	3.85×10^{-1}	9.08×10^{-3}
8.9	11.75	4.05×10^{-1}	9.32×10^{-3}
8.9	12.28	3.91×10^{-1}	9.16×10^{-3}
8.9	13.08	3.02×10^{-1}	7.93×10^{-3}
8.9	13.62	2.50×10^{-1}	7.21×10^{-3}
8.9	14.15	1.90×10^{-1}	6.28×10^{-3}
8.9	14.68	1.05×10^{-1}	4.68×10^{-3}

Table A.16: Continued.

E_x (MeV)	$\theta_{\text{c.m.}}$ (deg)	$d\sigma/d\Omega$ (mb/sr)	error (mb/sr)
8.9	16.54	4.20×10^{-2}	3.40×10^{-3}
8.9	17.07	4.55×10^{-2}	3.55×10^{-3}
8.9	17.87	3.94×10^{-2}	3.08×10^{-3}
8.9	18.40	4.35×10^{-2}	3.23×10^{-3}
8.9	18.93	3.66×10^{-2}	2.97×10^{-3}
8.9	19.46	3.50×10^{-2}	2.90×10^{-3}
8.9	20.26	6.88×10^{-3}	3.08×10^{-3}
8.9	20.79	1.51×10^{-2}	4.58×10^{-3}
8.9	21.32	9.65×10^{-3}	3.66×10^{-3}
8.9	21.85	1.24×10^{-2}	4.15×10^{-3}
8.9	22.64	3.88×10^{-3}	2.25×10^{-3}
8.9	23.17	3.88×10^{-3}	2.27×10^{-3}
8.9	23.70	1.30×10^{-3}	1.30×10^{-3}
8.9	24.23	2.60×10^{-3}	1.85×10^{-3}
8.9	25.02	3.05×10^{-3}	1.55×10^{-3}
8.9	25.55	7.63×10^{-4}	7.69×10^{-4}
8.9	26.07	3.05×10^{-3}	1.55×10^{-3}
8.9	26.60	1.53×10^{-3}	1.09×10^{-3}
9.1	0.41	4.36	2.48×10^{-1}
9.1	1.24	4.03	1.34×10^{-1}
9.1	2.67	1.41	1.27×10^{-2}
9.1	3.19	1.06	1.10×10^{-2}
9.1	3.72	7.24×10^{-1}	9.05×10^{-3}
9.1	4.24	5.49×10^{-1}	7.88×10^{-3}
9.1	4.24	6.41×10^{-1}	1.76×10^{-2}
9.1	4.76	4.90×10^{-1}	1.54×10^{-2}
9.1	5.29	4.48×10^{-1}	1.47×10^{-2}
9.1	5.81	4.36×10^{-1}	1.46×10^{-2}
9.1	6.01	5.25×10^{-1}	1.64×10^{-2}

Table A.16: Continued.

E_x (MeV)	$\theta_{\text{c.m.}}$ (deg)	$d\sigma/d\Omega$ (mb/sr)	error (mb/sr)
9.1	7.62	3.14×10^{-1}	1.27×10^{-2}
9.1	8.28	1.81×10^{-1}	5.52×10^{-3}
9.1	8.82	1.26×10^{-1}	4.60×10^{-3}
9.1	9.35	9.36×10^{-2}	3.96×10^{-3}
9.1	9.89	8.24×10^{-2}	3.72×10^{-3}
9.1	10.69	9.35×10^{-2}	4.58×10^{-3}
9.1	11.22	1.14×10^{-1}	5.07×10^{-3}
9.1	11.75	1.04×10^{-1}	4.83×10^{-3}
9.1	12.29	1.07×10^{-1}	4.92×10^{-3}
9.1	13.08	9.61×10^{-2}	4.49×10^{-3}
9.1	13.62	7.75×10^{-2}	4.03×10^{-3}
9.1	14.15	5.49×10^{-2}	3.39×10^{-3}
9.1	14.68	3.64×10^{-2}	2.76×10^{-3}
9.1	15.48	2.19×10^{-2}	2.47×10^{-3}
9.1	16.01	1.55×10^{-2}	2.07×10^{-3}
9.1	16.54	1.47×10^{-2}	2.02×10^{-3}
9.1	17.08	7.30×10^{-3}	1.43×10^{-3}
9.1	17.87	1.47×10^{-2}	1.92×10^{-3}
9.1	18.40	1.09×10^{-2}	1.64×10^{-3}
9.1	18.93	1.36×10^{-2}	1.84×10^{-3}
9.1	19.46	9.46×10^{-3}	1.53×10^{-3}
9.1	20.26	8.04×10^{-3}	3.64×10^{-3}
9.1	20.79	9.66×10^{-3}	3.98×10^{-3}
9.1	21.32	4.83×10^{-3}	2.81×10^{-3}
9.1	21.85	3.23×10^{-3}	2.30×10^{-3}
9.1	22.64	2.61×10^{-3}	1.92×10^{-3}
9.1	23.17	1.31×10^{-3}	1.36×10^{-3}
9.1	23.70	1.31×10^{-3}	1.36×10^{-3}
9.1	24.23	1.00×10^{-5}	1.00×10^{-5}

Table A.16: Continued.

E_x (MeV)	$\theta_{\text{c.m.}}$ (deg)	$d\sigma/d\Omega$ (mb/sr)	error (mb/sr)
9.1	26.07	1.38×10^{-3}	9.84×10^{-4}
9.1	26.60	1.38×10^{-3}	9.85×10^{-4}
9.3	0.41	1.52	1.45×10^{-1}
9.3	1.24	1.10	6.95×10^{-2}
9.3	2.67	5.66×10^{-1}	8.17×10^{-3}
9.3	3.19	5.69×10^{-1}	8.15×10^{-3}
9.3	3.72	5.39×10^{-1}	7.88×10^{-3}
9.3	4.24	4.88×10^{-1}	7.52×10^{-3}
9.3	4.24	4.79×10^{-1}	1.55×10^{-2}
9.3	4.76	4.43×10^{-1}	1.48×10^{-2}
9.3	5.29	3.81×10^{-1}	1.38×10^{-2}
9.3	5.81	3.24×10^{-1}	1.28×10^{-2}
9.3	6.01	2.84×10^{-1}	1.23×10^{-2}
9.3	6.55	2.33×10^{-1}	1.13×10^{-2}
9.3	7.08	1.86×10^{-1}	1.03×10^{-2}
9.3	7.62	1.58×10^{-1}	9.16×10^{-3}
9.3	8.28	1.00×10^{-1}	4.14×10^{-3}
9.3	8.82	8.44×10^{-2}	3.78×10^{-3}
9.3	9.35	7.37×10^{-2}	3.53×10^{-3}
9.3	9.89	6.37×10^{-2}	3.27×10^{-3}
9.3	10.69	6.33×10^{-2}	3.76×10^{-3}
9.3	11.22	5.09×10^{-2}	3.39×10^{-3}
9.3	11.75	4.69×10^{-2}	3.26×10^{-3}
9.3	12.29	4.32×10^{-2}	3.14×10^{-3}
9.3	13.09	4.31×10^{-2}	3.04×10^{-3}
9.3	13.62	2.84×10^{-2}	2.48×10^{-3}
9.3	14.15	2.85×10^{-2}	2.47×10^{-3}
9.3	14.68	2.17×10^{-2}	2.15×10^{-3}
9.3	15.48	2.06×10^{-2}	2.39×10^{-3}

Table A.16: Continued.

E_x (MeV)	$\theta_{\text{c.m.}}$ (deg)	$d\sigma/d\Omega$ (mb/sr)	error (mb/sr)
9.3	17.08	1.58×10^{-2}	2.10×10^{-3}
9.3	17.87	8.96×10^{-3}	1.46×10^{-3}
9.3	18.40	9.93×10^{-3}	1.53×10^{-3}
9.3	18.94	5.49×10^{-3}	1.15×10^{-3}
9.3	19.47	4.81×10^{-3}	1.07×10^{-3}
9.3	20.26	3.60×10^{-3}	2.57×10^{-3}
9.3	20.79	1.00×10^{-5}	1.00×10^{-5}
9.3	21.32	1.00×10^{-5}	1.00×10^{-5}
9.3	21.85	1.00×10^{-5}	1.00×10^{-5}
9.3	22.64	1.00×10^{-5}	1.00×10^{-5}
9.3	23.17	1.63×10^{-3}	1.71×10^{-3}
9.3	23.70	1.64×10^{-3}	1.72×10^{-3}
9.3	24.23	1.64×10^{-3}	1.72×10^{-3}
9.3	25.02	1.38×10^{-3}	9.86×10^{-4}
9.3	25.55	6.92×10^{-4}	6.98×10^{-4}
9.3	26.08	2.08×10^{-3}	1.21×10^{-3}
9.3	26.60	1.39×10^{-3}	9.90×10^{-4}
9.5	0.41	1.17	1.28×10^{-1}
9.5	1.24	9.91×10^{-1}	6.60×10^{-2}
9.5	2.67	4.54×10^{-1}	7.65×10^{-3}
9.5	3.20	4.83×10^{-1}	7.83×10^{-3}
9.5	3.72	5.19×10^{-1}	8.03×10^{-3}
9.5	4.24	4.89×10^{-1}	7.79×10^{-3}
9.5	4.24	5.15×10^{-1}	1.66×10^{-2}
9.5	4.76	5.05×10^{-1}	1.64×10^{-2}
9.5	5.29	4.59×10^{-1}	1.58×10^{-2}
9.5	5.81	4.19×10^{-1}	1.51×10^{-2}
9.5	6.01	4.13×10^{-1}	1.56×10^{-2}
9.5	6.55	4.19×10^{-1}	1.55×10^{-2}

Table A.16: Continued.

E_x (MeV)	$\theta_{\text{c.m.}}$ (deg)	$d\sigma/d\Omega$ (mb/sr)	error (mb/sr)
9.5	8.29	4.16×10^{-1}	8.51×10^{-3}
9.5	8.82	4.38×10^{-1}	8.69×10^{-3}
9.5	9.35	4.56×10^{-1}	8.84×10^{-3}
9.5	9.89	4.54×10^{-1}	8.81×10^{-3}
9.5	10.69	4.07×10^{-1}	9.37×10^{-3}
9.5	11.22	3.87×10^{-1}	9.14×10^{-3}
9.5	11.75	3.87×10^{-1}	9.15×10^{-3}
9.5	12.29	3.50×10^{-1}	8.70×10^{-3}
9.5	13.09	3.03×10^{-1}	7.96×10^{-3}
9.5	13.62	2.66×10^{-1}	7.45×10^{-3}
9.5	14.15	2.36×10^{-1}	7.01×10^{-3}
9.5	14.68	2.08×10^{-1}	6.58×10^{-3}
9.5	15.48	1.54×10^{-1}	6.53×10^{-3}
9.5	16.01	1.16×10^{-1}	5.67×10^{-3}
9.5	16.55	1.04×10^{-1}	5.36×10^{-3}
9.5	17.08	7.62×10^{-2}	4.59×10^{-3}
9.5	17.88	4.04×10^{-2}	3.10×10^{-3}
9.5	18.41	2.90×10^{-2}	2.62×10^{-3}
9.5	18.94	2.50×10^{-2}	2.44×10^{-3}
9.5	19.47	1.75×10^{-2}	2.04×10^{-3}
9.5	20.26	1.40×10^{-2}	4.70×10^{-3}
9.5	20.79	1.09×10^{-2}	4.16×10^{-3}
9.5	21.32	7.80×10^{-3}	3.51×10^{-3}
9.5	21.85	6.25×10^{-3}	3.14×10^{-3}
9.5	22.65	6.07×10^{-3}	2.74×10^{-3}
9.5	23.18	2.43×10^{-3}	1.73×10^{-3}
9.5	23.70	6.08×10^{-3}	2.74×10^{-3}
9.5	24.23	6.09×10^{-3}	2.74×10^{-3}
9.5	25.02	1.35×10^{-3}	9.66×10^{-4}

Table A.16: Continued.

E_x (MeV)	$\theta_{\text{c.m.}}$ (deg)	$d\sigma/d\Omega$ (mb/sr)	error (mb/sr)
9.5	26.61	6.79×10^{-4}	6.82×10^{-4}
9.7	0.41	1.35	1.37×10^{-1}
9.7	1.24	9.95×10^{-1}	6.63×10^{-2}
9.7	2.67	4.55×10^{-1}	8.19×10^{-3}
9.7	3.20	4.43×10^{-1}	8.26×10^{-3}
9.7	3.72	4.50×10^{-1}	8.60×10^{-3}
9.7	4.24	4.48×10^{-1}	8.96×10^{-3}
9.7	4.24	4.50×10^{-1}	1.81×10^{-2}
9.7	4.76	4.54×10^{-1}	1.91×10^{-2}
9.7	5.29	4.24×10^{-1}	1.95×10^{-2}
9.7	5.81	3.43×10^{-1}	1.94×10^{-2}
9.7	6.02	3.35×10^{-1}	2.23×10^{-2}
9.7	6.55	2.53×10^{-1}	2.16×10^{-2}
9.7	7.08	2.02×10^{-1}	2.12×10^{-2}
9.7	7.62	1.45×10^{-1}	1.95×10^{-2}
9.7	8.29	1.02×10^{-1}	7.64×10^{-3}
9.7	8.82	7.05×10^{-2}	6.46×10^{-3}
9.7	9.35	6.36×10^{-2}	5.32×10^{-3}
9.7	9.89	7.59×10^{-2}	4.72×10^{-3}
9.7	10.69	6.41×10^{-2}	4.57×10^{-3}
9.7	11.22	6.74×10^{-2}	4.34×10^{-3}
9.7	11.75	6.47×10^{-2}	4.11×10^{-3}
9.7	12.29	5.31×10^{-2}	3.68×10^{-3}
9.7	13.09	6.62×10^{-2}	3.88×10^{-3}
9.7	13.62	5.96×10^{-2}	3.64×10^{-3}
9.7	14.15	5.15×10^{-2}	3.35×10^{-3}
9.7	14.69	3.67×10^{-2}	2.82×10^{-3}
9.7	15.48	4.13×10^{-2}	3.41×10^{-3}
9.7	16.02	3.92×10^{-2}	3.31×10^{-3}

Table A.16: Continued.

E_x (MeV)	$\theta_{\text{c.m.}}$ (deg)	$d\sigma/d\Omega$ (mb/sr)	error (mb/sr)
9.7	17.88	1.62×10^{-2}	1.96×10^{-3}
9.7	18.41	1.50×10^{-2}	1.89×10^{-3}
9.7	18.94	7.12×10^{-3}	1.31×10^{-3}
9.7	19.47	4.77×10^{-3}	1.08×10^{-3}
9.7	20.26	7.35×10^{-3}	3.30×10^{-3}
9.7	20.80	4.42×10^{-3}	2.56×10^{-3}
9.7	21.32	4.42×10^{-3}	2.56×10^{-3}
9.7	21.85	5.90×10^{-3}	2.96×10^{-3}
9.7	22.65	6.18×10^{-3}	2.53×10^{-3}
9.7	23.18	4.13×10^{-3}	2.07×10^{-3}
9.7	23.71	4.13×10^{-3}	2.07×10^{-3}
9.7	24.23	2.07×10^{-3}	1.46×10^{-3}
9.7	25.03	2.17×10^{-3}	1.58×10^{-3}
9.7	25.55	2.17×10^{-3}	1.59×10^{-3}
9.7	26.08	1.09×10^{-3}	1.12×10^{-3}
9.7	26.61	2.17×10^{-3}	1.59×10^{-3}
9.9	0.41	1.90	1.63×10^{-1}
9.9	1.24	1.70	8.71×10^{-2}
9.9	2.67	9.82×10^{-1}	1.07×10^{-2}
9.9	3.20	1.01	1.08×10^{-2}
9.9	3.72	1.09	1.12×10^{-2}
9.9	4.24	1.09	1.13×10^{-2}
9.9	4.24	1.13	2.37×10^{-2}
9.9	4.76	1.14	2.39×10^{-2}
9.9	5.29	1.13	2.39×10^{-2}
9.9	5.82	1.11	2.38×10^{-2}
9.9	6.02	1.23	2.59×10^{-2}
9.9	6.55	1.10	2.48×10^{-2}
9.9	7.08	9.49×10^{-1}	2.33×10^{-2}

Table A.16: Continued.

E_x (MeV)	$\theta_{\text{c.m.}}$ (deg)	$d\sigma/d\Omega$ (mb/sr)	error (mb/sr)
9.9	8.82	3.45×10^{-1}	8.77×10^{-3}
9.9	9.35	2.65×10^{-1}	7.90×10^{-3}
9.9	9.89	2.21×10^{-1}	7.27×10^{-3}
9.9	10.69	1.78×10^{-1}	7.17×10^{-3}
9.9	11.22	1.97×10^{-1}	7.40×10^{-3}
9.9	11.76	1.89×10^{-1}	7.29×10^{-3}
9.9	12.29	2.18×10^{-1}	7.77×10^{-3}
9.9	13.09	2.08×10^{-1}	7.48×10^{-3}
9.9	13.62	1.97×10^{-1}	7.28×10^{-3}
9.9	14.15	1.75×10^{-1}	6.77×10^{-3}
9.9	14.69	1.46×10^{-1}	6.09×10^{-3}
9.9	15.49	9.68×10^{-2}	5.55×10^{-3}
9.9	16.02	6.70×10^{-2}	4.53×10^{-3}
9.9	16.55	6.02×10^{-2}	4.19×10^{-3}
9.9	17.08	3.89×10^{-2}	3.34×10^{-3}
9.9	17.88	2.25×10^{-2}	2.26×10^{-3}
9.9	18.41	2.24×10^{-2}	2.25×10^{-3}
9.9	18.94	2.01×10^{-2}	2.13×10^{-3}
9.9	19.47	2.04×10^{-2}	2.14×10^{-3}
9.9	20.27	2.12×10^{-2}	5.94×10^{-3}
9.9	20.80	1.15×10^{-2}	4.35×10^{-3}
9.9	21.33	9.83×10^{-3}	4.03×10^{-3}
9.9	21.86	8.20×10^{-3}	3.68×10^{-3}
9.9	22.65	1.21×10^{-2}	3.86×10^{-3}
9.9	23.18	1.21×10^{-3}	1.21×10^{-3}
9.9	23.71	2.42×10^{-3}	1.72×10^{-3}
9.9	24.24	1.21×10^{-3}	1.22×10^{-3}
9.9	25.03	2.81×10^{-3}	1.26×10^{-3}
9.9	25.56	1.12×10^{-3}	7.95×10^{-4}

Table A.16: Continued.

E_x (MeV)	$\theta_{\text{c.m.}}$ (deg)	$d\sigma/d\Omega$ (mb/sr)	error (mb/sr)
10.1	0.41	1.76	1.55×10^{-1}
10.1	1.24	1.42	7.84×10^{-2}
10.1	2.67	7.18×10^{-1}	9.19×10^{-3}
10.1	3.20	7.52×10^{-1}	9.34×10^{-3}
10.1	3.72	7.97×10^{-1}	9.59×10^{-3}
10.1	4.24	8.58×10^{-1}	9.93×10^{-3}
10.1	4.24	8.12×10^{-1}	2.00×10^{-2}
10.1	4.76	8.61×10^{-1}	2.06×10^{-2}
10.1	5.29	8.87×10^{-1}	2.09×10^{-2}
10.1	5.82	7.93×10^{-1}	1.98×10^{-2}
10.1	6.02	7.61×10^{-1}	2.01×10^{-2}
10.1	6.55	6.74×10^{-1}	1.90×10^{-2}
10.1	7.09	4.87×10^{-1}	1.61×10^{-2}
10.1	7.62	3.50×10^{-1}	1.39×10^{-2}
10.1	8.29	1.96×10^{-1}	5.96×10^{-3}
10.1	8.82	1.52×10^{-1}	5.26×10^{-3}
10.1	9.36	1.21×10^{-1}	4.70×10^{-3}
10.1	9.89	1.06×10^{-1}	4.38×10^{-3}
10.1	10.69	9.52×10^{-2}	4.77×10^{-3}
10.1	11.22	1.02×10^{-1}	4.92×10^{-3}
10.1	11.76	9.44×10^{-2}	4.78×10^{-3}
10.1	12.29	9.55×10^{-2}	4.86×10^{-3}
10.1	13.09	8.82×10^{-2}	4.99×10^{-3}
10.1	13.62	7.98×10^{-2}	4.99×10^{-3}
10.1	14.16	8.58×10^{-2}	5.29×10^{-3}
10.1	14.69	5.66×10^{-2}	4.77×10^{-3}
10.1	15.49	4.45×10^{-2}	4.85×10^{-3}
10.1	16.02	2.88×10^{-2}	4.17×10^{-3}
10.1	16.55	2.02×10^{-2}	3.56×10^{-3}

Table A.16: Continued.

E_x (MeV)	$\theta_{\text{c.m.}}$ (deg)	$d\sigma/d\Omega$ (mb/sr)	error (mb/sr)
10.1	18.41	9.27×10^{-3}	1.63×10^{-3}
10.1	18.94	8.81×10^{-3}	1.52×10^{-3}
10.1	19.47	8.97×10^{-3}	1.48×10^{-3}
10.1	20.27	1.01×10^{-2}	3.85×10^{-3}
10.1	20.80	5.76×10^{-3}	2.94×10^{-3}
10.1	21.33	8.65×10^{-3}	3.55×10^{-3}
10.1	21.86	4.33×10^{-3}	2.52×10^{-3}
10.1	22.65	9.79×10^{-4}	9.79×10^{-4}
10.1	23.18	1.96×10^{-3}	1.39×10^{-3}
10.1	23.71	1.96×10^{-3}	1.39×10^{-3}
10.1	24.24	9.82×10^{-4}	9.82×10^{-4}
10.1	25.03	1.70×10^{-3}	1.23×10^{-3}
10.1	25.56	8.54×10^{-4}	8.68×10^{-4}
10.1	26.09	1.00×10^{-5}	1.00×10^{-5}
10.1	26.61	3.43×10^{-3}	1.74×10^{-3}
10.3	0.41	1.95	1.66×10^{-1}
10.3	1.24	1.57	8.35×10^{-2}
10.3	2.67	7.36×10^{-1}	9.28×10^{-3}
10.3	3.20	7.55×10^{-1}	9.35×10^{-3}
10.3	3.72	7.77×10^{-1}	9.45×10^{-3}
10.3	4.24	8.36×10^{-1}	9.78×10^{-3}
10.3	4.24	8.16×10^{-1}	2.00×10^{-2}
10.3	4.76	8.75×10^{-1}	2.07×10^{-2}
10.3	5.30	8.35×10^{-1}	2.03×10^{-2}
10.3	5.82	8.00×10^{-1}	1.99×10^{-2}
10.3	6.02	7.83×10^{-1}	2.02×10^{-2}
10.3	6.55	7.04×10^{-1}	1.92×10^{-2}
10.3	7.09	5.49×10^{-1}	1.70×10^{-2}
10.3	7.62	3.74×10^{-1}	1.42×10^{-2}

Table A.16: Continued.

E_x (MeV)	$\theta_{\text{c.m.}}$ (deg)	$d\sigma/d\Omega$ (mb/sr)	error (mb/sr)
10.3	9.36	1.46×10^{-1}	5.05×10^{-3}
10.3	9.89	1.16×10^{-1}	4.51×10^{-3}
10.3	10.69	8.92×10^{-2}	4.55×10^{-3}
10.3	11.22	8.47×10^{-2}	4.44×10^{-3}
10.3	11.76	8.20×10^{-2}	4.38×10^{-3}
10.3	12.29	7.56×10^{-2}	4.21×10^{-3}
10.3	13.09	6.39×10^{-2}	3.83×10^{-3}
10.3	13.62	5.71×10^{-2}	3.64×10^{-3}
10.3	14.16	5.50×10^{-2}	3.58×10^{-3}
10.3	14.69	5.38×10^{-2}	3.54×10^{-3}
10.3	15.49	4.56×10^{-2}	3.78×10^{-3}
10.3	16.02	3.16×10^{-2}	3.26×10^{-3}
10.3	16.55	2.47×10^{-2}	2.95×10^{-3}
10.3	17.08	1.95×10^{-2}	2.68×10^{-3}
10.3	17.88	1.61×10^{-2}	2.18×10^{-3}
10.3	18.41	9.07×10^{-3}	1.73×10^{-3}
10.3	18.94	1.13×10^{-2}	1.84×10^{-3}
10.3	19.47	8.29×10^{-3}	1.62×10^{-3}
10.3	20.27	4.31×10^{-3}	2.50×10^{-3}
10.3	20.80	8.64×10^{-3}	3.55×10^{-3}
10.3	21.33	1.44×10^{-3}	1.45×10^{-3}
10.3	21.86	7.22×10^{-3}	3.24×10^{-3}
10.3	22.65	1.35×10^{-3}	1.37×10^{-3}
10.3	23.18	4.04×10^{-3}	2.39×10^{-3}
10.3	23.71	1.00×10^{-5}	1.00×10^{-5}
10.3	24.24	5.40×10^{-3}	2.78×10^{-3}
10.3	25.03	8.19×10^{-4}	8.60×10^{-4}
10.3	25.56	1.00×10^{-5}	1.00×10^{-5}
10.3	26.09	1.64×10^{-3}	1.22×10^{-3}

Table A.16: Continued.

E_x (MeV)	$\theta_{\text{c.m.}}$ (deg)	$d\sigma/d\Omega$ (mb/sr)	error (mb/sr)
10.5	1.24	1.67	8.45×10^{-2}
10.5	2.67	8.51×10^{-1}	9.92×10^{-3}
10.5	3.20	8.62×10^{-1}	9.93×10^{-3}
10.5	3.72	8.94×10^{-1}	1.01×10^{-2}
10.5	4.24	9.66×10^{-1}	1.04×10^{-2}
10.5	4.24	9.55×10^{-1}	2.17×10^{-2}
10.5	4.76	9.59×10^{-1}	2.17×10^{-2}
10.5	5.30	9.48×10^{-1}	2.16×10^{-2}
10.5	5.82	9.04×10^{-1}	2.11×10^{-2}
10.5	6.02	9.24×10^{-1}	2.19×10^{-2}
10.5	6.55	8.42×10^{-1}	2.09×10^{-2}
10.5	7.09	7.11×10^{-1}	1.91×10^{-2}
10.5	7.62	5.82×10^{-1}	1.74×10^{-2}
10.5	8.29	3.44×10^{-1}	7.69×10^{-3}
10.5	8.82	2.74×10^{-1}	6.85×10^{-3}
10.5	9.36	2.00×10^{-1}	5.87×10^{-3}
10.5	9.89	1.53×10^{-1}	5.14×10^{-3}
10.5	10.69	1.25×10^{-1}	5.29×10^{-3}
10.5	11.23	1.01×10^{-1}	4.77×10^{-3}
10.5	11.76	1.03×10^{-1}	4.81×10^{-3}
10.5	12.29	9.41×10^{-2}	4.61×10^{-3}
10.5	13.09	8.35×10^{-2}	4.24×10^{-3}
10.5	13.62	8.45×10^{-2}	4.26×10^{-3}
10.5	14.16	7.47×10^{-2}	4.01×10^{-3}
10.5	14.69	6.45×10^{-2}	3.73×10^{-3}
10.5	15.49	5.87×10^{-2}	4.09×10^{-3}
10.5	16.02	3.86×10^{-2}	3.33×10^{-3}
10.5	16.55	3.35×10^{-2}	3.10×10^{-3}
10.5	17.08	3.40×10^{-2}	3.11×10^{-3}

Table A.16: Continued.

E_x (MeV)	$\theta_{\text{c.m.}}$ (deg)	$d\sigma/d\Omega$ (mb/sr)	error (mb/sr)
10.5	18.94	1.08×10^{-2}	1.65×10^{-3}
10.5	19.48	8.66×10^{-3}	1.50×10^{-3}
10.5	20.27	6.02×10^{-3}	3.02×10^{-3}
10.5	20.80	1.36×10^{-2}	4.54×10^{-3}
10.5	21.33	7.54×10^{-3}	3.38×10^{-3}
10.5	21.86	4.53×10^{-3}	2.62×10^{-3}
10.5	22.66	9.67×10^{-3}	3.47×10^{-3}
10.5	23.18	3.63×10^{-3}	2.11×10^{-3}
10.5	23.71	1.00×10^{-5}	1.00×10^{-5}
10.5	24.24	4.85×10^{-3}	2.44×10^{-3}
10.5	25.03	2.73×10^{-3}	1.60×10^{-3}
10.5	25.56	3.64×10^{-3}	1.85×10^{-3}
10.5	26.09	9.12×10^{-4}	9.26×10^{-4}
10.5	26.62	9.13×10^{-4}	9.27×10^{-4}
10.7	0.41	2.68	1.89×10^{-1}
10.7	1.24	1.91	8.95×10^{-2}
10.7	2.68	1.21	1.18×10^{-2}
10.7	3.20	1.27	1.21×10^{-2}
10.7	3.72	1.36	1.24×10^{-2}
10.7	4.24	1.32	1.22×10^{-2}
10.7	4.24	1.35	2.56×10^{-2}
10.7	4.76	1.38	2.58×10^{-2}
10.7	5.30	1.38	2.58×10^{-2}
10.7	5.82	1.38	2.58×10^{-2}
10.7	6.02	1.50	2.76×10^{-2}
10.7	6.55	1.45	2.71×10^{-2}
10.7	7.09	1.25	2.53×10^{-2}
10.7	7.62	1.04	2.28×10^{-2}
10.7	8.29	6.28×10^{-1}	1.04×10^{-2}

Table A.16: Continued.

E_x (MeV)	$\theta_{\text{c.m.}}$ (deg)	$d\sigma/d\Omega$ (mb/sr)	error (mb/sr)
10.7	9.89	2.55×10^{-1}	6.62×10^{-3}
10.7	10.69	2.11×10^{-1}	6.80×10^{-3}
10.7	11.23	1.87×10^{-1}	6.41×10^{-3}
10.7	11.76	1.81×10^{-1}	6.30×10^{-3}
10.7	12.29	1.74×10^{-1}	6.20×10^{-3}
10.7	13.09	1.68×10^{-1}	5.96×10^{-3}
10.7	13.63	1.56×10^{-1}	5.74×10^{-3}
10.7	14.16	1.46×10^{-1}	5.53×10^{-3}
10.7	14.69	1.22×10^{-1}	5.07×10^{-3}
10.7	15.49	9.65×10^{-2}	5.19×10^{-3}
10.7	16.02	7.42×10^{-2}	4.56×10^{-3}
10.7	16.55	6.22×10^{-2}	4.17×10^{-3}
10.7	17.09	5.67×10^{-2}	3.98×10^{-3}
10.7	17.88	2.71×10^{-2}	2.54×10^{-3}
10.7	18.42	1.95×10^{-2}	2.16×10^{-3}
10.7	18.95	1.51×10^{-2}	1.90×10^{-3}
10.7	19.48	1.42×10^{-2}	1.85×10^{-3}
10.7	20.27	1.32×10^{-2}	4.40×10^{-3}
10.7	20.80	8.78×10^{-3}	4.15×10^{-3}
10.7	21.33	4.39×10^{-3}	2.54×10^{-3}
10.7	21.86	1.32×10^{-2}	4.41×10^{-3}
10.7	22.66	2.37×10^{-3}	1.69×10^{-3}
10.7	23.19	7.11×10^{-3}	2.92×10^{-3}
10.7	23.72	8.31×10^{-3}	3.16×10^{-3}
10.7	24.24	7.13×10^{-3}	2.92×10^{-3}
10.7	25.04	2.98×10^{-3}	1.51×10^{-3}
10.7	25.56	1.49×10^{-3}	1.06×10^{-3}
10.7	26.09	1.49×10^{-3}	1.06×10^{-3}
10.7	26.62	7.47×10^{-4}	7.54×10^{-4}

Table A.16: Continued.

E_x (MeV)	$\theta_{\text{c.m.}}$ (deg)	$d\sigma/d\Omega$ (mb/sr)	error (mb/sr)
10.9	2.68	1.78	1.43×10^{-2}
10.9	3.20	1.59	1.36×10^{-2}
10.9	3.72	1.60	1.36×10^{-2}
10.9	4.24	1.75	1.41×10^{-2}
10.9	4.24	1.64	2.82×10^{-2}
10.9	4.76	1.72	2.89×10^{-2}
10.9	5.30	1.87	3.01×10^{-2}
10.9	5.82	1.82	2.97×10^{-2}
10.9	6.02	1.88	3.09×10^{-2}
10.9	6.55	1.65	2.90×10^{-2}
10.9	7.09	1.42	2.70×10^{-2}
10.9	7.62	1.13	2.42×10^{-2}
10.9	8.29	6.45×10^{-1}	1.05×10^{-2}
10.9	8.82	5.04×10^{-1}	9.27×10^{-3}
10.9	9.36	3.92×10^{-1}	8.17×10^{-3}
10.9	9.89	3.05×10^{-1}	7.20×10^{-3}
10.9	10.69	2.60×10^{-1}	7.54×10^{-3}
10.9	11.23	2.51×10^{-1}	7.41×10^{-3}
10.9	11.76	2.27×10^{-1}	7.07×10^{-3}
10.9	12.29	2.25×10^{-1}	7.04×10^{-3}
10.9	13.09	2.15×10^{-1}	6.82×10^{-3}
10.9	13.63	2.10×10^{-1}	6.72×10^{-3}
10.9	14.16	1.90×10^{-1}	6.39×10^{-3}
10.9	14.69	1.63×10^{-1}	5.92×10^{-3}
10.9	15.49	1.19×10^{-1}	5.77×10^{-3}
10.9	16.02	9.85×10^{-2}	5.24×10^{-3}
10.9	16.56	6.90×10^{-2}	4.39×10^{-3}
10.9	17.09	6.44×10^{-2}	4.23×10^{-3}
10.9	17.89	3.75×10^{-2}	2.95×10^{-3}

Table A.16: Continued.

E_x (MeV)	$\theta_{\text{c.m.}}$ (deg)	$d\sigma/d\Omega$ (mb/sr)	error (mb/sr)
10.9	19.48	1.90×10^{-2}	2.10×10^{-3}
10.9	20.27	2.40×10^{-2}	5.83×10^{-3}
10.9	20.80	2.54×10^{-2}	6.00×10^{-3}
10.9	21.33	1.13×10^{-2}	4.00×10^{-3}
10.9	21.86	5.66×10^{-3}	2.83×10^{-3}
10.9	22.66	4.63×10^{-3}	2.33×10^{-3}
10.9	23.19	5.80×10^{-3}	2.60×10^{-3}
10.9	23.72	1.28×10^{-2}	3.87×10^{-3}
10.9	24.25	4.65×10^{-3}	2.33×10^{-3}
10.9	25.04	2.98×10^{-3}	1.34×10^{-3}
10.9	25.57	4.18×10^{-3}	1.58×10^{-3}
10.9	26.09	1.20×10^{-3}	8.47×10^{-4}
10.9	26.62	1.00×10^{-5}	1.00×10^{-5}
11.1	1.24	1.38×10^{1}	2.48×10^{-1}
11.1	2.68	4.45	2.25×10^{-2}
11.1	3.20	2.65	1.73×10^{-2}
11.1	3.72	1.69	1.39×10^{-2}
11.1	4.24	1.45	1.28×10^{-2}
11.1	4.24	1.40	2.59×10^{-2}
11.1	4.76	1.43	2.63×10^{-2}
11.1	5.30	1.76	2.90×10^{-2}
11.1	5.82	1.98	3.08×10^{-2}
11.1	6.02	2.35	3.45×10^{-2}
11.1	6.55	2.26	3.39×10^{-2}
11.1	7.09	1.97	3.17×10^{-2}
11.1	7.62	1.53	2.80×10^{-2}
11.1	8.29	7.55×10^{-1}	1.13×10^{-2}
11.1	8.82	5.56×10^{-1}	9.67×10^{-3}
11.1	9.36	4.50×10^{-1}	8.70×10^{-3}

Table A.16: Continued.

E_x (MeV)	$\theta_{\text{c.m.}}$ (deg)	$d\sigma/d\Omega$ (mb/sr)	error (mb/sr)
11.1	11.23	5.20×10^{-1}	1.06×10^{-2}
11.1	11.76	5.13×10^{-1}	1.05×10^{-2}
11.1	12.29	5.00×10^{-1}	1.04×10^{-2}
11.1	13.09	4.10×10^{-1}	9.29×10^{-3}
11.1	13.63	3.52×10^{-1}	8.61×10^{-3}
11.1	14.16	2.72×10^{-1}	7.58×10^{-3}
11.1	14.69	2.20×10^{-1}	6.80×10^{-3}
11.1	15.49	1.48×10^{-1}	6.44×10^{-3}
11.1	16.02	1.40×10^{-1}	6.25×10^{-3}
11.1	16.56	1.22×10^{-1}	5.84×10^{-3}
11.1	17.09	1.00×10^{-1}	5.28×10^{-3}
11.1	17.89	7.54×10^{-2}	4.17×10^{-3}
11.1	18.42	5.99×10^{-2}	3.72×10^{-3}
11.1	18.95	5.12×10^{-2}	3.44×10^{-3}
11.1	19.48	4.57×10^{-2}	3.25×10^{-3}
11.1	20.28	9.55×10^{-3}	3.92×10^{-3}
11.1	20.81	2.07×10^{-2}	5.81×10^{-3}
11.1	21.34	1.28×10^{-2}	4.54×10^{-3}
11.1	21.87	1.44×10^{-2}	4.82×10^{-3}
11.1	22.66	1.11×10^{-2}	3.51×10^{-3}
11.1	23.19	1.11×10^{-2}	3.52×10^{-3}
11.1	23.72	1.11×10^{-2}	3.52×10^{-3}
11.1	24.25	1.00×10^{-2}	3.34×10^{-3}
11.1	25.04	3.50×10^{-3}	1.57×10^{-3}
11.1	25.57	1.40×10^{-3}	9.95×10^{-4}
11.1	26.10	2.11×10^{-3}	1.22×10^{-3}
11.1	26.62	2.81×10^{-3}	1.41×10^{-3}
11.3	0.41	4.36	2.48×10^{-1}
11.3	1.24	3.54	1.26×10^{-1}

Table A.16: Continued.

E_x (MeV)	$\theta_{\text{c.m.}}$ (deg)	$d\sigma/d\Omega$ (mb/sr)	error (mb/sr)
11.3	3.72	1.10	1.12×10^{-2}
11.3	4.24	1.09	1.11×10^{-2}
11.3	4.24	1.08	2.30×10^{-2}
11.3	4.76	1.12	2.33×10^{-2}
11.3	5.30	1.19	2.41×10^{-2}
11.3	5.82	1.14	2.36×10^{-2}
11.3	6.02	1.16	2.43×10^{-2}
11.3	6.55	1.19	2.46×10^{-2}
11.3	7.09	1.01	2.28×10^{-2}
11.3	7.62	8.65×10^{-1}	2.11×10^{-2}
11.3	8.29	5.29×10^{-1}	9.40×10^{-3}
11.3	8.83	3.93×10^{-1}	8.11×10^{-3}
11.3	9.36	3.00×10^{-1}	7.09×10^{-3}
11.3	9.89	2.56×10^{-1}	6.55×10^{-3}
11.3	10.69	1.94×10^{-1}	6.51×10^{-3}
11.3	11.23	1.68×10^{-1}	6.08×10^{-3}
11.3	11.76	1.60×10^{-1}	5.94×10^{-3}
11.3	12.30	1.64×10^{-1}	6.03×10^{-3}
11.3	13.10	1.72×10^{-1}	6.00×10^{-3}
11.3	13.63	1.58×10^{-1}	5.77×10^{-3}
11.3	14.16	1.63×10^{-1}	5.85×10^{-3}
11.3	14.69	1.46×10^{-1}	5.53×10^{-3}
11.3	15.49	1.07×10^{-1}	5.50×10^{-3}
11.3	16.03	9.39×10^{-2}	5.15×10^{-3}
11.3	16.56	7.45×10^{-2}	4.58×10^{-3}
11.3	17.09	5.70×10^{-2}	4.00×10^{-3}
11.3	17.89	2.31×10^{-2}	2.30×10^{-3}
11.3	18.42	2.79×10^{-2}	2.52×10^{-3}
11.3	18.95	2.03×10^{-2}	2.16×10^{-3}

Table A.16: Continued.

E_x (MeV)	$\theta_{\text{c.m.}}$ (deg)	$d\sigma/d\Omega$ (mb/sr)	error (mb/sr)
11.3	20.81	9.39×10^{-3}	3.56×10^{-3}
11.3	21.34	9.40×10^{-3}	3.56×10^{-3}
11.3	21.87	8.07×10^{-3}	3.30×10^{-3}
11.3	22.66	1.05×10^{-2}	3.77×10^{-3}
11.3	23.19	6.58×10^{-3}	2.96×10^{-3}
11.3	23.72	2.63×10^{-3}	1.87×10^{-3}
11.3	24.25	2.64×10^{-3}	1.88×10^{-3}
11.3	25.04	1.00×10^{-5}	1.00×10^{-5}
11.3	25.57	3.62×10^{-3}	1.83×10^{-3}
11.3	26.10	4.53×10^{-3}	2.06×10^{-3}
11.3	26.62	9.08×10^{-4}	9.18×10^{-4}
11.5	0.41	3.42	2.17×10^{-1}
11.5	1.24	2.83	1.12×10^{-1}
11.5	2.68	1.35	1.23×10^{-2}
11.5	3.20	1.37	1.24×10^{-2}
11.5	3.72	1.39	1.25×10^{-2}
11.5	4.24	1.36	1.24×10^{-2}
11.5	4.24	1.23	2.45×10^{-2}
11.5	4.76	1.38	2.59×10^{-2}
11.5	5.30	1.43	2.63×10^{-2}
11.5	5.82	1.50	2.70×10^{-2}
11.5	6.02	1.54	2.78×10^{-2}
11.5	6.55	1.47	2.72×10^{-2}
11.5	7.09	1.53	2.78×10^{-2}
11.5	7.62	1.38	2.63×10^{-2}
11.5	8.29	8.38×10^{-1}	1.19×10^{-2}
11.5	8.83	6.24×10^{-1}	1.02×10^{-2}
11.5	9.36	4.58×10^{-1}	8.78×10^{-3}
11.5	9.89	3.71×10^{-1}	7.90×10^{-3}

Table A.16: Continued.

E_x (MeV)	$\theta_{\text{c.m.}}$ (deg)	$d\sigma/d\Omega$ (mb/sr)	error (mb/sr)
11.5	11.76	2.46×10^{-1}	7.31×10^{-3}
11.5	12.30	2.56×10^{-1}	7.47×10^{-3}
11.5	13.10	2.58×10^{-1}	7.24×10^{-3}
11.5	13.63	2.71×10^{-1}	7.42×10^{-3}
11.5	14.16	2.37×10^{-1}	6.94×10^{-3}
11.5	14.70	2.37×10^{-1}	6.94×10^{-3}
11.5	15.50	1.64×10^{-1}	6.77×10^{-3}
11.5	16.03	1.37×10^{-1}	6.18×10^{-3}
11.5	16.56	1.14×10^{-1}	5.63×10^{-3}
11.5	17.09	8.90×10^{-2}	4.98×10^{-3}
11.5	17.89	4.57×10^{-2}	3.29×10^{-3}
11.5	18.42	3.84×10^{-2}	3.01×10^{-3}
11.5	18.95	2.43×10^{-2}	2.41×10^{-3}
11.5	19.48	1.97×10^{-2}	2.17×10^{-3}
11.5	20.28	1.20×10^{-2}	4.24×10^{-3}
11.5	20.81	1.80×10^{-2}	5.20×10^{-3}
11.5	21.34	1.05×10^{-2}	3.97×10^{-3}
11.5	21.87	1.50×10^{-2}	4.75×10^{-3}
11.5	22.66	1.13×10^{-2}	3.60×10^{-3}
11.5	23.19	9.09×10^{-3}	3.22×10^{-3}
11.5	23.72	2.28×10^{-3}	1.61×10^{-3}
11.5	24.25	6.83×10^{-3}	2.80×10^{-3}
11.5	25.04	1.56×10^{-3}	1.12×10^{-3}
11.5	25.57	3.12×10^{-3}	1.58×10^{-3}
11.5	26.10	7.81×10^{-4}	7.86×10^{-4}
11.5	26.63	5.47×10^{-3}	2.10×10^{-3}
11.7	0.41	4.52	2.47×10^{-1}
11.7	1.24	4.07	1.32×10^{-1}
11.7	2.68	2.71	1.74×10^{-2}

Table A.16: Continued.

E_x (MeV)	$\theta_{\text{c.m.}}$ (deg)	$d\sigma/d\Omega$ (mb/sr)	error (mb/sr)
11.7	4.24	2.69	1.74×10^{-2}
11.7	4.24	2.98	3.80×10^{-2}
11.7	4.76	2.81	3.69×10^{-2}
11.7	5.30	3.24	3.96×10^{-2}
11.7	5.82	3.75	4.26×10^{-2}
11.7	6.02	4.44	4.71×10^{-2}
11.7	6.55	4.57	4.78×10^{-2}
11.7	7.09	4.18	4.57×10^{-2}
11.7	7.62	4.34	4.66×10^{-2}
11.7	8.29	2.63	2.13×10^{-2}
11.7	8.83	2.04	1.87×10^{-2}
11.7	9.36	1.44	1.57×10^{-2}
11.7	9.90	9.08×10^{-1}	1.24×10^{-2}
11.7	10.70	9.56×10^{-1}	1.43×10^{-2}
11.7	11.23	7.99×10^{-1}	1.31×10^{-2}
11.7	11.76	7.95×10^{-1}	1.31×10^{-2}
11.7	12.30	8.82×10^{-1}	1.38×10^{-2}
11.7	13.10	9.04×10^{-1}	1.37×10^{-2}
11.7	13.63	9.30×10^{-1}	1.39×10^{-2}
11.7	14.16	9.14×10^{-1}	1.38×10^{-2}
11.7	14.70	8.92×10^{-1}	1.36×10^{-2}
11.7	15.50	5.32×10^{-1}	1.22×10^{-2}
11.7	16.03	4.74×10^{-1}	1.15×10^{-2}
11.7	16.56	3.71×10^{-1}	1.02×10^{-2}
11.7	17.09	3.15×10^{-1}	9.37×10^{-3}
11.7	17.89	1.38×10^{-1}	5.63×10^{-3}
11.7	18.42	1.11×10^{-1}	5.04×10^{-3}
11.7	18.95	7.77×10^{-2}	4.23×10^{-3}
11.7	19.48	7.69×10^{-2}	4.21×10^{-3}

Table A.16: Continued.

E_x (MeV)	$\theta_{\text{c.m.}}$ (deg)	$d\sigma/d\Omega$ (mb/sr)	error (mb/sr)
11.7	21.34	3.74×10^{-2}	7.49×10^{-3}
11.7	21.87	5.09×10^{-2}	8.75×10^{-3}
11.7	22.67	4.00×10^{-2}	7.10×10^{-3}
11.7	23.20	2.75×10^{-2}	5.88×10^{-3}
11.7	23.72	2.25×10^{-2}	5.32×10^{-3}
11.7	24.25	1.76×10^{-2}	4.70×10^{-3}
11.7	25.05	9.57×10^{-3}	2.57×10^{-3}
11.7	25.57	3.42×10^{-3}	1.54×10^{-3}
11.7	26.10	5.49×10^{-3}	1.94×10^{-3}
11.7	26.63	4.81×10^{-3}	1.82×10^{-3}
11.9	0.41	6.33	2.95×10^{-1}
11.9	1.24	5.67	1.57×10^{-1}
11.9	2.68	4.13	2.16×10^{-2}
11.9	3.20	3.91	2.10×10^{-2}
11.9	3.72	4.27	2.19×10^{-2}
11.9	4.24	5.18	2.42×10^{-2}
11.9	4.24	4.64	4.71×10^{-2}
11.9	4.76	5.55	5.15×10^{-2}
11.9	5.30	6.30	5.49×10^{-2}
11.9	5.82	7.47	5.98×10^{-2}
11.9	6.02	8.49	6.52×10^{-2}
11.9	6.56	9.00	6.72×10^{-2}
11.9	7.09	8.22	6.42×10^{-2}
11.9	7.62	7.52	6.14×10^{-2}
11.9	8.29	5.20	3.06×10^{-2}
11.9	8.83	4.19	2.73×10^{-2}
11.9	9.36	3.23	2.39×10^{-2}
11.9	9.90	2.30	2.00×10^{-2}
11.9	10.70	1.18	1.60×10^{-2}

Table A.16: Continued.

E_x (MeV)	$\theta_{\text{c.m.}}$ (deg)	$d\sigma/d\Omega$ (mb/sr)	error (mb/sr)
11.9	12.30	1.18	1.60×10^{-2}
11.9	13.10	1.27	1.66×10^{-2}
11.9	13.63	1.34	1.71×10^{-2}
11.9	14.17	1.35	1.72×10^{-2}
11.9	14.70	1.16	1.59×10^{-2}
11.9	15.50	9.72×10^{-1}	1.66×10^{-2}
11.9	16.03	7.52×10^{-1}	1.46×10^{-2}
11.9	16.56	5.48×10^{-1}	1.24×10^{-2}
11.9	17.09	3.41×10^{-1}	9.75×10^{-3}
11.9	17.89	1.80×10^{-1}	6.43×10^{-3}
11.9	18.42	1.24×10^{-1}	5.33×10^{-3}
11.9	18.96	1.01×10^{-1}	4.81×10^{-3}
11.9	19.49	8.56×10^{-2}	4.44×10^{-3}
11.9	20.28	9.34×10^{-2}	1.17×10^{-2}
11.9	20.81	6.14×10^{-2}	9.50×10^{-3}
11.9	21.34	7.17×10^{-2}	1.03×10^{-2}
11.9	21.87	5.86×10^{-2}	9.29×10^{-3}
11.9	22.67	4.99×10^{-2}	7.64×10^{-3}
11.9	23.20	2.56×10^{-2}	5.47×10^{-3}
11.9	23.73	1.98×10^{-2}	4.81×10^{-3}
11.9	24.26	1.28×10^{-2}	3.87×10^{-3}
11.9	25.05	1.05×10^{-2}	2.73×10^{-3}
11.9	25.58	1.34×10^{-2}	3.08×10^{-3}
11.9	26.10	7.05×10^{-3}	2.24×10^{-3}
11.9	26.63	4.24×10^{-3}	1.73×10^{-3}
12.1	0.41	6.44	2.98×10^{-1}
12.1	1.24	5.98	1.62×10^{-1}
12.1	2.68	2.82	1.78×10^{-2}
12.1	3.20	2.52	1.68×10^{-2}

Table A.16: Continued.

E_x (MeV)	$\theta_{\text{c.m.}}$ (deg)	$d\sigma/d\Omega$ (mb/sr)	error (mb/sr)
12.1	4.24	2.37	3.36×10^{-2}
12.1	4.76	2.66	3.57×10^{-2}
12.1	5.30	2.79	3.65×10^{-2}
12.1	5.82	2.76	3.63×10^{-2}
12.1	6.02	2.89	3.83×10^{-2}
12.1	6.56	2.63	3.65×10^{-2}
12.1	7.09	2.29	3.41×10^{-2}
12.1	7.63	1.68	2.92×10^{-2}
12.1	8.29	1.05	1.35×10^{-2}
12.1	8.83	7.81×10^{-1}	1.16×10^{-2}
12.1	9.36	6.48×10^{-1}	1.06×10^{-2}
12.1	9.90	5.88×10^{-1}	1.00×10^{-2}
12.1	10.70	3.97×10^{-1}	9.33×10^{-3}
12.1	11.23	4.00×10^{-1}	9.36×10^{-3}
12.1	11.77	3.87×10^{-1}	9.20×10^{-3}
12.1	12.30	3.84×10^{-1}	9.17×10^{-3}
12.1	13.10	4.12×10^{-1}	9.49×10^{-3}
12.1	13.63	3.40×10^{-1}	8.62×10^{-3}
12.1	14.17	3.46×10^{-1}	8.69×10^{-3}
12.1	14.70	2.43×10^{-1}	7.29×10^{-3}
12.1	15.50	2.38×10^{-1}	8.14×10^{-3}
12.1	16.03	1.74×10^{-1}	6.96×10^{-3}
12.1	16.56	1.15×10^{-1}	5.66×10^{-3}
12.1	17.10	8.56×10^{-2}	4.88×10^{-3}
12.1	17.89	5.33×10^{-2}	3.52×10^{-3}
12.1	18.43	4.39×10^{-2}	3.20×10^{-3}
12.1	18.96	3.69×10^{-2}	2.93×10^{-3}
12.1	19.49	3.49×10^{-2}	2.85×10^{-3}
12.1	20.28	2.74×10^{-2}	6.50×10^{-3}

Table A.16: Continued.

E_x (MeV)	$\theta_{\text{c.m.}}$ (deg)	$d\sigma/d\Omega$ (mb/sr)	error (mb/sr)
12.1	21.88	2.29×10^{-2}	5.95×10^{-3}
12.1	22.67	1.67×10^{-2}	4.33×10^{-3}
12.1	23.20	1.34×10^{-2}	3.88×10^{-3}
12.1	23.73	4.47×10^{-3}	2.24×10^{-3}
12.1	24.26	7.84×10^{-3}	2.97×10^{-3}
12.1	25.05	3.50×10^{-3}	1.58×10^{-3}
12.1	25.58	8.42×10^{-3}	2.45×10^{-3}
12.1	26.11	2.81×10^{-3}	1.41×10^{-3}
12.1	26.63	1.41×10^{-3}	9.99×10^{-4}
12.3	1.24	7.83	1.84×10^{-1}
12.3	2.68	2.70	1.75×10^{-2}
12.3	3.20	1.79	1.42×10^{-2}
12.3	3.72	1.18	1.16×10^{-2}
12.3	4.24	1.06	1.10×10^{-2}
12.3	4.24	1.02	2.22×10^{-2}
12.3	4.76	9.83×10^{-1}	2.18×10^{-2}
12.3	5.30	1.13	2.33×10^{-2}
12.3	5.82	1.08	2.28×10^{-2}
12.3	6.02	1.28	2.55×10^{-2}
12.3	6.56	1.23	2.50×10^{-2}
12.3	7.09	1.15	2.41×10^{-2}
12.3	7.63	8.85×10^{-1}	2.13×10^{-2}
12.3	8.29	4.38×10^{-1}	8.68×10^{-3}
12.3	8.83	3.11×10^{-1}	7.32×10^{-3}
12.3	9.36	2.44×10^{-1}	6.49×10^{-3}
12.3	9.90	2.04×10^{-1}	5.93×10^{-3}
12.3	10.70	2.17×10^{-1}	6.88×10^{-3}
12.3	11.23	2.66×10^{-1}	7.60×10^{-3}
12.3	11.77	2.46×10^{-1}	7.32×10^{-3}

Table A.16: Continued.

E_x (MeV)	$\theta_{\text{c.m.}}$ (deg)	$d\sigma/d\Omega$ (mb/sr)	error (mb/sr)
12.3	13.63	2.13×10^{-1}	6.79×10^{-3}
12.3	14.17	1.71×10^{-1}	6.09×10^{-3}
12.3	14.70	1.48×10^{-1}	5.66×10^{-3}
12.3	15.50	1.22×10^{-1}	5.85×10^{-3}
12.3	16.03	8.63×10^{-2}	4.92×10^{-3}
12.3	16.56	7.39×10^{-2}	4.55×10^{-3}
12.3	17.10	4.98×10^{-2}	3.74×10^{-3}
12.3	17.90	3.74×10^{-2}	2.94×10^{-3}
12.3	18.43	3.05×10^{-2}	2.65×10^{-3}
12.3	18.96	2.90×10^{-2}	2.59×10^{-3}
12.3	19.49	2.84×10^{-2}	2.56×10^{-3}
12.3	20.29	2.83×10^{-2}	6.70×10^{-3}
12.3	20.82	1.10×10^{-2}	4.17×10^{-3}
12.3	21.35	1.89×10^{-2}	5.48×10^{-3}
12.3	21.88	1.74×10^{-2}	5.25×10^{-3}
12.3	22.67	1.00×10^{-2}	3.55×10^{-3}
12.3	23.20	8.76×10^{-3}	3.33×10^{-3}
12.3	23.73	7.52×10^{-3}	3.08×10^{-3}
12.3	24.26	5.02×10^{-3}	2.52×10^{-3}
12.3	25.05	4.41×10^{-3}	1.67×10^{-3}
12.3	25.58	6.31×10^{-3}	2.00×10^{-3}
12.3	26.11	1.89×10^{-3}	1.10×10^{-3}
12.3	26.64	3.80×10^{-3}	1.55×10^{-3}
12.5	1.24	8.25	1.90×10^{-1}
12.5	2.68	2.97	1.83×10^{-2}
12.5	3.20	1.92	1.47×10^{-2}
12.5	3.72	1.25	1.19×10^{-2}
12.5	4.24	8.38×10^{-1}	9.76×10^{-3}
12.5	4.24	9.75×10^{-1}	2.18×10^{-2}

Table A.16: Continued.

E_x (MeV)	$\theta_{\text{c.m.}}$ (deg)	$d\sigma/d\Omega$ (mb/sr)	error (mb/sr)
12.5	5.82	9.98×10^{-1}	2.21×10^{-2}
12.5	6.02	1.14	2.41×10^{-2}
12.5	6.56	1.17	2.43×10^{-2}
12.5	7.09	9.69×10^{-1}	2.22×10^{-2}
12.5	7.63	7.77×10^{-1}	1.99×10^{-2}
12.5	8.30	3.73×10^{-1}	7.97×10^{-3}
12.5	8.83	2.70×10^{-1}	6.78×10^{-3}
12.5	9.36	2.01×10^{-1}	5.86×10^{-3}
12.5	9.90	1.64×10^{-1}	5.29×10^{-3}
12.5	10.70	1.85×10^{-1}	6.38×10^{-3}
12.5	11.23	2.24×10^{-1}	7.00×10^{-3}
12.5	11.77	2.36×10^{-1}	7.19×10^{-3}
12.5	12.30	2.42×10^{-1}	7.28×10^{-3}
12.5	13.10	2.13×10^{-1}	6.85×10^{-3}
12.5	13.64	2.16×10^{-1}	6.90×10^{-3}
12.5	14.17	1.65×10^{-1}	6.05×10^{-3}
12.5	14.70	1.30×10^{-1}	5.36×10^{-3}
12.5	15.50	9.64×10^{-2}	5.19×10^{-3}
12.5	16.03	7.46×10^{-2}	4.57×10^{-3}
12.5	16.57	5.82×10^{-2}	4.04×10^{-3}
12.5	17.10	4.85×10^{-2}	3.68×10^{-3}
12.5	17.90	3.39×10^{-2}	2.81×10^{-3}
12.5	18.43	2.74×10^{-2}	2.53×10^{-3}
12.5	18.96	2.77×10^{-2}	2.54×10^{-3}
12.5	19.49	1.86×10^{-2}	2.08×10^{-3}
12.5	20.29	2.37×10^{-2}	5.79×10^{-3}
12.5	20.82	2.24×10^{-2}	5.62×10^{-3}
12.5	21.35	1.26×10^{-2}	4.21×10^{-3}
12.5	21.88	1.12×10^{-2}	3.98×10^{-3}

Table A.16: Continued.

E_x (MeV)	$\theta_{\text{c.m.}}$ (deg)	$d\sigma/d\Omega$ (mb/sr)	error (mb/sr)
12.5	23.73	6.43×10^{-3}	2.92×10^{-3}
12.5	24.26	2.57×10^{-3}	1.83×10^{-3}
12.5	25.05	4.08×10^{-3}	1.67×10^{-3}
12.5	25.58	2.72×10^{-3}	1.37×10^{-3}
12.5	26.11	6.14×10^{-3}	2.06×10^{-3}
12.5	26.64	2.73×10^{-3}	1.37×10^{-3}
12.7	0.41	5.09	2.67×10^{-1}
12.7	1.24	4.82	1.46×10^{-1}
12.7	2.68	2.05	1.53×10^{-2}
12.7	3.20	1.54	1.33×10^{-2}
12.7	3.72	1.16	1.16×10^{-2}
12.7	4.24	9.08×10^{-1}	1.03×10^{-2}
12.7	4.24	9.80×10^{-1}	2.22×10^{-2}
12.7	4.76	8.87×10^{-1}	2.11×10^{-2}
12.7	5.30	8.36×10^{-1}	2.05×10^{-2}
12.7	5.82	8.68×10^{-1}	2.08×10^{-2}
12.7	6.02	8.93×10^{-1}	2.17×10^{-2}
12.7	6.56	8.09×10^{-1}	2.06×10^{-2}
12.7	7.09	7.07×10^{-1}	1.91×10^{-2}
12.7	7.63	6.43×10^{-1}	1.81×10^{-2}
12.7	8.30	3.04×10^{-1}	7.24×10^{-3}
12.7	8.83	2.20×10^{-1}	6.16×10^{-3}
12.7	9.37	1.61×10^{-1}	5.28×10^{-3}
12.7	9.90	1.36×10^{-1}	4.85×10^{-3}
12.7	10.70	1.25×10^{-1}	5.31×10^{-3}
12.7	11.23	1.38×10^{-1}	5.57×10^{-3}
12.7	11.77	1.48×10^{-1}	5.76×10^{-3}
12.7	12.30	1.50×10^{-1}	5.80×10^{-3}
12.7	13.10	1.46×10^{-1}	5.67×10^{-3}

Table A.16: Continued.

E_x (MeV)	$\theta_{\text{c.m.}}$ (deg)	$d\sigma/d\Omega$ (mb/sr)	error (mb/sr)
12.7	14.70	8.82×10^{-2}	4.44×10^{-3}
12.7	15.50	5.65×10^{-2}	4.02×10^{-3}
12.7	16.04	5.37×10^{-2}	3.91×10^{-3}
12.7	16.57	4.05×10^{-2}	3.39×10^{-3}
12.7	17.10	2.91×10^{-2}	2.88×10^{-3}
12.7	17.90	2.10×10^{-2}	2.23×10^{-3}
12.7	18.43	1.55×10^{-2}	1.92×10^{-3}
12.7	18.96	1.39×10^{-2}	1.82×10^{-3}
12.7	19.49	1.21×10^{-2}	1.70×10^{-3}
12.7	20.29	8.47×10^{-3}	3.82×10^{-3}
12.7	20.82	1.53×10^{-2}	5.14×10^{-3}
12.7	21.35	1.70×10^{-3}	1.71×10^{-3}
12.7	21.88	5.10×10^{-3}	2.96×10^{-3}
12.7	22.68	7.54×10^{-3}	3.41×10^{-3}
12.7	23.20	7.54×10^{-3}	3.42×10^{-3}
12.7	23.73	3.02×10^{-3}	2.16×10^{-3}
12.7	24.26	1.51×10^{-3}	1.53×10^{-3}
12.7	25.06	1.64×10^{-3}	1.17×10^{-3}
12.7	25.58	8.20×10^{-4}	8.31×10^{-4}
12.7	26.11	1.64×10^{-3}	1.18×10^{-3}
12.7	26.64	1.64×10^{-3}	1.18×10^{-3}
12.9	0.42	3.51	2.21×10^{-1}
12.9	1.25	3.11	1.17×10^{-1}
12.9	2.68	1.59	1.34×10^{-2}
12.9	3.20	1.36	1.24×10^{-2}
12.9	3.72	1.19	1.16×10^{-2}
12.9	4.24	1.05	1.09×10^{-2}
12.9	4.24	1.08	2.30×10^{-2}
12.9	4.77	1.00	2.22×10^{-2}

Table A.16: Continued.

E_x (MeV)	$\theta_{\text{c.m.}}$ (deg)	$d\sigma/d\Omega$ (mb/sr)	error (mb/sr)
12.9	6.02	9.28×10^{-1}	2.20×10^{-2}
12.9	6.56	8.83×10^{-1}	2.14×10^{-2}
12.9	7.09	7.33×10^{-1}	1.94×10^{-2}
12.9	7.63	5.59×10^{-1}	1.70×10^{-2}
12.9	8.30	3.22×10^{-1}	7.49×10^{-3}
12.9	8.83	2.30×10^{-1}	6.35×10^{-3}
12.9	9.37	1.61×10^{-1}	5.32×10^{-3}
12.9	9.90	1.41×10^{-1}	4.99×10^{-3}
12.9	10.70	1.29×10^{-1}	5.42×10^{-3}
12.9	11.24	1.34×10^{-1}	5.51×10^{-3}
12.9	11.77	1.38×10^{-1}	5.61×10^{-3}
12.9	12.30	1.32×10^{-1}	5.47×10^{-3}
12.9	13.10	1.18×10^{-1}	5.19×10^{-3}
12.9	13.64	1.08×10^{-1}	4.95×10^{-3}
12.9	14.17	1.00×10^{-1}	4.77×10^{-3}
12.9	14.70	8.61×10^{-2}	4.42×10^{-3}
12.9	15.50	5.48×10^{-2}	3.97×10^{-3}
12.9	16.04	3.65×10^{-2}	3.25×10^{-3}
12.9	16.57	3.89×10^{-2}	3.34×10^{-3}
12.9	17.10	2.85×10^{-2}	2.85×10^{-3}
12.9	17.90	1.59×10^{-2}	1.91×10^{-3}
12.9	18.43	1.62×10^{-2}	1.92×10^{-3}
12.9	18.96	1.36×10^{-2}	1.76×10^{-3}
12.9	19.49	1.20×10^{-2}	1.66×10^{-3}
12.9	20.29	5.53×10^{-3}	3.23×10^{-3}
12.9	20.82	1.48×10^{-2}	5.33×10^{-3}
12.9	21.35	7.39×10^{-3}	3.74×10^{-3}
12.9	21.88	3.70×10^{-3}	2.64×10^{-3}
12.9	22.68	4.41×10^{-3}	2.22×10^{-3}

Table A.16: Continued.

E_x (MeV)	$\theta_{\text{c.m.}}$ (deg)	$d\sigma/d\Omega$ (mb/sr)	error (mb/sr)
12.9	24.26	1.11×10^{-3}	1.11×10^{-3}
12.9	25.06	2.80×10^{-3}	1.25×10^{-3}
12.9	25.59	5.61×10^{-4}	5.61×10^{-4}
12.9	26.11	1.00×10^{-5}	1.00×10^{-5}
12.9	26.64	1.69×10^{-3}	9.74×10^{-4}
13.1	0.42	3.39	2.19×10^{-1}
13.1	1.25	2.72	1.10×10^{-1}
13.1	2.68	1.61	1.34×10^{-2}
13.1	3.20	1.51	1.30×10^{-2}
13.1	3.72	1.43	1.27×10^{-2}
13.1	4.24	1.27	1.20×10^{-2}
13.1	4.24	1.33	2.54×10^{-2}
13.1	4.77	1.22	2.43×10^{-2}
13.1	5.30	1.16	2.37×10^{-2}
13.1	5.82	1.15	2.36×10^{-2}
13.1	6.02	1.16	2.44×10^{-2}
13.1	6.56	9.88×10^{-1}	2.25×10^{-2}
13.1	7.09	8.10×10^{-1}	2.05×10^{-2}
13.1	7.63	6.88×10^{-1}	1.88×10^{-2}
13.1	8.30	3.47×10^{-1}	7.73×10^{-3}
13.1	8.83	2.85×10^{-1}	7.01×10^{-3}
13.1	9.37	2.02×10^{-1}	5.91×10^{-3}
13.1	9.90	1.63×10^{-1}	5.32×10^{-3}
13.1	10.70	1.61×10^{-1}	5.98×10^{-3}
13.1	11.24	1.49×10^{-1}	5.76×10^{-3}
13.1	11.77	1.55×10^{-1}	5.86×10^{-3}
13.1	12.30	1.68×10^{-1}	6.10×10^{-3}
13.1	13.11	1.46×10^{-1}	5.74×10^{-3}
13.1	13.64	1.42×10^{-1}	5.67×10^{-3}

Table A.16: Continued.

E_x (MeV)	$\theta_{\text{c.m.}}$ (deg)	$d\sigma/d\Omega$ (mb/sr)	error (mb/sr)
13.1	15.50	6.85×10^{-2}	4.46×10^{-3}
13.1	16.04	4.05×10^{-2}	3.47×10^{-3}
13.1	16.57	3.97×10^{-2}	3.40×10^{-3}
13.1	17.10	3.84×10^{-2}	3.33×10^{-3}
13.1	17.90	2.54×10^{-2}	2.54×10^{-3}
13.1	18.43	1.77×10^{-2}	2.13×10^{-3}
13.1	18.96	1.69×10^{-2}	2.07×10^{-3}
13.1	19.50	9.84×10^{-3}	1.58×10^{-3}
13.1	20.29	4.40×10^{-3}	2.55×10^{-3}
13.1	20.82	7.35×10^{-3}	3.30×10^{-3}
13.1	21.35	8.83×10^{-3}	3.61×10^{-3}
13.1	21.88	1.03×10^{-2}	3.91×10^{-3}
13.1	22.68	5.85×10^{-3}	2.95×10^{-3}
13.1	23.21	1.46×10^{-3}	1.48×10^{-3}
13.1	23.74	5.87×10^{-3}	2.96×10^{-3}
13.1	24.27	2.94×10^{-3}	2.10×10^{-3}
13.1	25.06	1.64×10^{-3}	1.17×10^{-3}
13.1	25.59	1.64×10^{-3}	1.17×10^{-3}
13.1	26.12	8.21×10^{-4}	8.30×10^{-4}
13.1	26.64	8.22×10^{-4}	8.31×10^{-4}
13.3	0.42	2.90	2.01×10^{-1}
13.3	1.25	2.71	1.09×10^{-1}
13.3	2.68	1.82	1.43×10^{-2}
13.3	3.20	1.76	1.40×10^{-2}
13.3	3.72	1.69	1.38×10^{-2}
13.3	4.24	1.58	1.33×10^{-2}
13.3	4.24	1.64	2.82×10^{-2}
13.3	4.77	1.57	2.76×10^{-2}
13.3	5.30	1.49	2.69×10^{-2}

Table A.16: Continued.

E_x (MeV)	$\theta_{\text{c.m.}}$ (deg)	$d\sigma/d\Omega$ (mb/sr)	error (mb/sr)
13.3	6.56	1.21	2.48×10^{-2}
13.3	7.09	1.01	2.27×10^{-2}
13.3	7.63	7.31×10^{-1}	1.93×10^{-2}
13.3	8.30	4.39×10^{-1}	8.72×10^{-3}
13.3	8.83	3.36×10^{-1}	7.63×10^{-3}
13.3	9.37	2.62×10^{-1}	6.74×10^{-3}
13.3	9.90	2.24×10^{-1}	6.24×10^{-3}
13.3	10.70	1.94×10^{-1}	6.58×10^{-3}
13.3	11.24	1.89×10^{-1}	6.51×10^{-3}
13.3	11.77	1.69×10^{-1}	6.16×10^{-3}
13.3	12.31	1.77×10^{-1}	6.29×10^{-3}
13.3	13.11	1.66×10^{-1}	6.06×10^{-3}
13.3	13.64	1.41×10^{-1}	5.60×10^{-3}
13.3	14.17	1.31×10^{-1}	5.39×10^{-3}
13.3	14.71	1.16×10^{-1}	5.07×10^{-3}
13.3	15.51	7.31×10^{-2}	4.57×10^{-3}
13.3	16.04	6.51×10^{-2}	4.31×10^{-3}
13.3	16.57	4.98×10^{-2}	3.77×10^{-3}
13.3	17.10	4.44×10^{-2}	3.56×10^{-3}
13.3	17.90	2.73×10^{-2}	2.59×10^{-3}
13.3	18.43	2.15×10^{-2}	2.30×10^{-3}
13.3	18.97	1.85×10^{-2}	2.14×10^{-3}
13.3	19.50	1.37×10^{-2}	1.84×10^{-3}
13.3	20.29	1.41×10^{-2}	4.47×10^{-3}
13.3	20.82	1.27×10^{-2}	4.26×10^{-3}
13.3	21.36	9.90×10^{-3}	3.75×10^{-3}
13.3	21.89	1.27×10^{-2}	4.26×10^{-3}
13.3	22.68	5.48×10^{-3}	2.46×10^{-3}
13.3	23.21	5.49×10^{-3}	2.46×10^{-3}

Table A.16: Continued.

E_x (MeV)	$\theta_{\text{c.m.}}$ (deg)	$d\sigma/d\Omega$ (mb/sr)	error (mb/sr)
13.3	25.06	3.87×10^{-3}	1.78×10^{-3}
13.3	25.59	3.88×10^{-3}	1.78×10^{-3}
13.3	26.12	1.00×10^{-5}	1.00×10^{-5}
13.3	26.65	1.00×10^{-5}	1.00×10^{-5}
13.5	1.25	2.31	1.00×10^{-1}
13.5	2.68	1.62	1.35×10^{-2}
13.5	3.20	1.57	1.33×10^{-2}
13.5	3.72	1.46	1.29×10^{-2}
13.5	4.24	1.50	1.30×10^{-2}
13.5	4.24	1.44	2.64×10^{-2}
13.5	4.77	1.40	2.61×10^{-2}
13.5	5.30	1.38	2.59×10^{-2}
13.5	5.82	1.26	2.47×10^{-2}
13.5	6.02	1.26	2.54×10^{-2}
13.5	6.56	1.05	2.32×10^{-2}
13.5	7.09	8.82×10^{-1}	2.13×10^{-2}
13.5	7.63	7.16×10^{-1}	1.92×10^{-2}
13.5	8.30	4.13×10^{-1}	8.40×10^{-3}
13.5	8.83	3.24×10^{-1}	7.45×10^{-3}
13.5	9.37	2.52×10^{-1}	6.58×10^{-3}
13.5	9.90	2.05×10^{-1}	5.94×10^{-3}
13.5	10.70	1.68×10^{-1}	6.19×10^{-3}
13.5	11.24	1.65×10^{-1}	6.13×10^{-3}
13.5	11.77	1.46×10^{-1}	5.77×10^{-3}
13.5	12.31	1.48×10^{-1}	5.81×10^{-3}
13.5	13.11	1.46×10^{-1}	5.68×10^{-3}
13.5	13.64	1.25×10^{-1}	5.28×10^{-3}
13.5	14.17	1.19×10^{-1}	5.15×10^{-3}
13.5	14.71	1.04×10^{-1}	4.82×10^{-3}

Table A.16: Continued.

E_x (MeV)	$\theta_{\text{c.m.}}$ (deg)	$d\sigma/d\Omega$ (mb/sr)	error (mb/sr)
13.5	16.57	5.03×10^{-2}	3.79×10^{-3}
13.5	17.11	3.48×10^{-2}	3.15×10^{-3}
13.5	17.90	2.23×10^{-2}	2.28×10^{-3}
13.5	18.44	1.68×10^{-2}	1.98×10^{-3}
13.5	18.97	1.66×10^{-2}	1.97×10^{-3}
13.5	19.50	1.24×10^{-2}	1.70×10^{-3}
13.5	20.30	1.27×10^{-2}	4.26×10^{-3}
13.5	20.83	1.27×10^{-2}	4.26×10^{-3}
13.5	21.36	1.13×10^{-2}	4.02×10^{-3}
13.5	21.89	8.50×10^{-3}	3.48×10^{-3}
13.5	22.68	5.36×10^{-3}	2.70×10^{-3}
13.5	23.21	4.03×10^{-3}	2.34×10^{-3}
13.5	23.74	2.69×10^{-3}	1.92×10^{-3}
13.5	24.27	4.04×10^{-3}	2.35×10^{-3}
13.5	25.06	1.91×10^{-3}	1.11×10^{-3}
13.5	25.59	1.91×10^{-3}	1.11×10^{-3}
13.5	26.12	1.28×10^{-3}	9.06×10^{-4}
13.5	26.65	2.56×10^{-3}	1.28×10^{-3}
13.7	0.42	2.45	1.82×10^{-1}
13.7	1.25	2.30	9.94×10^{-2}
13.7	2.68	1.63	1.35×10^{-2}
13.7	3.20	1.58	1.33×10^{-2}
13.7	3.72	1.56	1.33×10^{-2}
13.7	4.24	1.47	1.29×10^{-2}
13.7	4.24	1.49	2.69×10^{-2}
13.7	4.77	1.38	2.60×10^{-2}
13.7	5.30	1.37	2.58×10^{-2}
13.7	5.82	1.27	2.50×10^{-2}
13.7	6.02	1.23	2.50×10^{-2}

Table A.16: Continued.

E_x (MeV)	$\theta_{\text{c.m.}}$ (deg)	$d\sigma/d\Omega$ (mb/sr)	error (mb/sr)
13.7	7.63	7.88×10^{-1}	1.99×10^{-2}
13.7	8.30	4.41×10^{-1}	8.65×10^{-3}
13.7	8.83	3.51×10^{-1}	7.72×10^{-3}
13.7	9.37	2.84×10^{-1}	6.95×10^{-3}
13.7	9.90	2.25×10^{-1}	6.19×10^{-3}
13.7	10.71	1.81×10^{-1}	6.37×10^{-3}
13.7	11.24	1.79×10^{-1}	6.33×10^{-3}
13.7	11.77	1.51×10^{-1}	5.83×10^{-3}
13.7	12.31	1.52×10^{-1}	5.86×10^{-3}
13.7	13.11	1.45×10^{-1}	5.75×10^{-3}
13.7	13.64	1.29×10^{-1}	5.43×10^{-3}
13.7	14.18	1.22×10^{-1}	5.28×10^{-3}
13.7	14.71	1.05×10^{-1}	4.91×10^{-3}
13.7	15.51	7.46×10^{-2}	4.64×10^{-3}
13.7	16.04	5.62×10^{-2}	4.03×10^{-3}
13.7	16.57	4.14×10^{-2}	3.47×10^{-3}
13.7	17.11	3.44×10^{-2}	3.15×10^{-3}
13.7	17.91	2.41×10^{-2}	2.37×10^{-3}
13.7	18.44	1.72×10^{-2}	2.01×10^{-3}
13.7	18.97	1.67×10^{-2}	1.97×10^{-3}
13.7	19.50	1.22×10^{-2}	1.69×10^{-3}
13.7	20.30	7.66×10^{-3}	3.44×10^{-3}
13.7	20.83	7.67×10^{-3}	3.45×10^{-3}
13.7	21.36	6.14×10^{-3}	3.08×10^{-3}
13.7	21.89	6.15×10^{-3}	3.09×10^{-3}
13.7	22.68	4.64×10^{-3}	2.33×10^{-3}
13.7	23.21	3.48×10^{-3}	2.02×10^{-3}
13.7	23.74	3.49×10^{-3}	2.02×10^{-3}
13.7	24.27	4.65×10^{-3}	2.34×10^{-3}

Table A.16: Continued.

E_x (MeV)	$\theta_{\text{c.m.}}$ (deg)	$d\sigma/d\Omega$ (mb/sr)	error (mb/sr)
13.7	26.12	1.01×10^{-3}	1.03×10^{-3}
13.7	26.65	1.01×10^{-3}	1.03×10^{-3}
13.9	0.42	2.35	1.81×10^{-1}
13.9	1.25	2.37	1.02×10^{-1}
13.9	2.68	1.70	1.38×10^{-2}
13.9	3.20	1.67	1.37×10^{-2}
13.9	3.72	1.66	1.37×10^{-2}
13.9	4.25	1.62	1.35×10^{-2}
13.9	4.25	1.58	2.77×10^{-2}
13.9	4.77	1.51	2.71×10^{-2}
13.9	5.30	1.43	2.64×10^{-2}
13.9	5.82	1.33	2.55×10^{-2}
13.9	6.03	1.38	2.65×10^{-2}
13.9	6.56	1.15	2.44×10^{-2}
13.9	7.10	9.38×10^{-1}	2.19×10^{-2}
13.9	7.63	7.95×10^{-1}	2.02×10^{-2}
13.9	8.30	4.65×10^{-1}	8.93×10^{-3}
13.9	8.83	3.79×10^{-1}	8.06×10^{-3}
13.9	9.37	2.87×10^{-1}	7.02×10^{-3}
13.9	9.90	2.36×10^{-1}	6.38×10^{-3}
13.9	10.71	2.07×10^{-1}	6.79×10^{-3}
13.9	11.24	1.81×10^{-1}	6.36×10^{-3}
13.9	11.77	1.75×10^{-1}	6.26×10^{-3}
13.9	12.31	1.54×10^{-1}	5.88×10^{-3}
13.9	13.11	1.55×10^{-1}	5.82×10^{-3}
13.9	13.64	1.40×10^{-1}	5.55×10^{-3}
13.9	14.18	1.20×10^{-1}	5.13×10^{-3}
13.9	14.71	9.40×10^{-2}	4.56×10^{-3}
13.9	15.51	6.94×10^{-2}	4.48×10^{-3}

Table A.16: Continued.

E_x (MeV)	$\theta_{\text{c.m.}}$ (deg)	$d\sigma/d\Omega$ (mb/sr)	error (mb/sr)
13.9	17.11	3.72×10^{-2}	3.27×10^{-3}
13.9	17.91	2.30×10^{-2}	2.32×10^{-3}
13.9	18.44	1.85×10^{-2}	2.08×10^{-3}
13.9	18.97	1.61×10^{-2}	1.94×10^{-3}
13.9	19.50	1.37×10^{-2}	1.79×10^{-3}
13.9	20.30	6.97×10^{-3}	3.13×10^{-3}
13.9	20.83	8.38×10^{-3}	3.43×10^{-3}
13.9	21.36	8.39×10^{-3}	3.43×10^{-3}
13.9	21.89	7.00×10^{-3}	3.13×10^{-3}
13.9	22.69	5.73×10^{-3}	2.58×10^{-3}
13.9	23.22	3.44×10^{-3}	1.99×10^{-3}
13.9	23.75	4.59×10^{-3}	2.31×10^{-3}
13.9	24.27	1.15×10^{-3}	1.15×10^{-3}
13.9	25.07	5.60×10^{-4}	5.60×10^{-4}
13.9	25.60	2.24×10^{-3}	1.12×10^{-3}
13.9	26.12	5.61×10^{-4}	5.61×10^{-4}
13.9	26.65	5.62×10^{-4}	5.62×10^{-4}
14.1	0.42	2.49	1.89×10^{-1}
14.1	1.25	2.32	1.02×10^{-1}
14.1	2.68	1.75	1.41×10^{-2}
14.1	3.20	1.72	1.39×10^{-2}
14.1	3.72	1.70	1.38×10^{-2}
14.1	4.25	1.61	1.35×10^{-2}
14.1	4.25	1.62	2.81×10^{-2}
14.1	4.77	1.64	2.83×10^{-2}
14.1	5.30	1.54	2.74×10^{-2}
14.1	5.83	1.41	2.63×10^{-2}
14.1	6.03	1.31	2.59×10^{-2}
14.1	6.56	1.18	2.46×10^{-2}

Table A.16: Continued.

E_x (MeV)	$\theta_{\text{c.m.}}$ (deg)	$d\sigma/d\Omega$ (mb/sr)	error (mb/sr)
14.1	8.30	4.92×10^{-1}	9.27×10^{-3}
14.1	8.84	3.94×10^{-1}	8.30×10^{-3}
14.1	9.37	3.32×10^{-1}	7.62×10^{-3}
14.1	9.91	2.78×10^{-1}	6.97×10^{-3}
14.1	10.71	2.43×10^{-1}	7.38×10^{-3}
14.1	11.24	2.12×10^{-1}	6.91×10^{-3}
14.1	11.78	2.05×10^{-1}	6.79×10^{-3}
14.1	12.31	1.94×10^{-1}	6.63×10^{-3}
14.1	13.11	1.58×10^{-1}	5.84×10^{-3}
14.1	13.64	1.65×10^{-1}	5.96×10^{-3}
14.1	14.18	1.39×10^{-1}	5.48×10^{-3}
14.1	14.71	1.36×10^{-1}	5.42×10^{-3}
14.1	15.51	9.54×10^{-2}	5.24×10^{-3}
14.1	16.04	7.01×10^{-2}	4.49×10^{-3}
14.1	16.58	5.46×10^{-2}	3.96×10^{-3}
14.1	17.11	4.74×10^{-2}	3.68×10^{-3}
14.1	17.91	3.02×10^{-2}	2.70×10^{-3}
14.1	18.44	2.64×10^{-2}	2.53×10^{-3}
14.1	18.97	2.02×10^{-2}	2.21×10^{-3}
14.1	19.50	1.65×10^{-2}	2.00×10^{-3}
14.1	20.30	1.09×10^{-2}	3.85×10^{-3}
14.1	20.83	1.22×10^{-2}	4.09×10^{-3}
14.1	21.36	1.09×10^{-2}	3.85×10^{-3}
14.1	21.89	1.50×10^{-2}	4.53×10^{-3}
14.1	22.69	6.09×10^{-3}	2.74×10^{-3}
14.1	23.22	7.32×10^{-3}	3.01×10^{-3}
14.1	23.75	3.66×10^{-3}	2.12×10^{-3}
14.1	24.28	3.67×10^{-3}	2.13×10^{-3}
14.1	25.07	4.46×10^{-3}	1.86×10^{-3}

Table A.16: Continued.

E_x (MeV)	$\theta_{\text{c.m.}}$ (deg)	$d\sigma/d\Omega$ (mb/sr)	error (mb/sr)
14.1	26.65	4.48×10^{-3}	1.85×10^{-3}
14.3	0.42	2.84	1.98×10^{-1}
14.3	1.25	2.81	1.11×10^{-1}
14.3	2.68	2.11	1.54×10^{-2}
14.3	3.20	2.05	1.52×10^{-2}
14.3	3.72	1.95	1.48×10^{-2}
14.3	4.25	1.82	1.43×10^{-2}
14.3	4.25	1.91	3.06×10^{-2}
14.3	4.77	1.73	2.91×10^{-2}
14.3	5.30	1.62	2.82×10^{-2}
14.3	5.83	1.51	2.73×10^{-2}
14.3	6.03	1.55	2.82×10^{-2}
14.3	6.56	1.35	2.63×10^{-2}
14.3	7.10	1.21	2.50×10^{-2}
14.3	7.63	1.02	2.28×10^{-2}
14.3	8.30	6.05×10^{-1}	1.02×10^{-2}
14.3	8.84	4.70×10^{-1}	8.99×10^{-3}
14.3	9.37	4.06×10^{-1}	8.36×10^{-3}
14.3	9.91	3.14×10^{-1}	7.37×10^{-3}
14.3	10.71	2.88×10^{-1}	7.94×10^{-3}
14.3	11.24	2.78×10^{-1}	7.82×10^{-3}
14.3	11.78	2.77×10^{-1}	7.80×10^{-3}
14.3	12.31	2.86×10^{-1}	7.93×10^{-3}
14.3	13.11	2.48×10^{-1}	7.29×10^{-3}
14.3	13.65	2.33×10^{-1}	7.08×10^{-3}
14.3	14.18	2.02×10^{-1}	6.62×10^{-3}
14.3	14.71	1.95×10^{-1}	6.50×10^{-3}
14.3	15.51	1.28×10^{-1}	6.09×10^{-3}
14.3	16.05	1.15×10^{-1}	5.76×10^{-3}

Table A.16: Continued.

E_x (MeV)	$\theta_{\text{c.m.}}$ (deg)	$d\sigma/d\Omega$ (mb/sr)	error (mb/sr)
14.3	17.91	3.94×10^{-2}	3.05×10^{-3}
14.3	18.44	3.63×10^{-2}	2.92×10^{-3}
14.3	18.97	2.71×10^{-2}	2.52×10^{-3}
14.3	19.51	2.76×10^{-2}	2.55×10^{-3}
14.3	20.30	1.12×10^{-2}	3.95×10^{-3}
14.3	20.83	1.40×10^{-2}	4.42×10^{-3}
14.3	21.36	1.40×10^{-2}	4.42×10^{-3}
14.3	21.89	1.82×10^{-2}	5.05×10^{-3}
14.3	22.69	6.79×10^{-3}	3.05×10^{-3}
14.3	23.22	8.15×10^{-3}	3.35×10^{-3}
14.3	23.75	6.80×10^{-3}	3.06×10^{-3}
14.3	24.28	2.72×10^{-3}	1.94×10^{-3}
14.3	25.07	4.82×10^{-3}	2.00×10^{-3}
14.3	25.60	2.41×10^{-3}	1.41×10^{-3}
14.3	26.13	8.06×10^{-4}	8.13×10^{-4}
14.3	26.66	1.61×10^{-3}	1.15×10^{-3}
14.5	1.25	3.17	1.17×10^{-1}
14.5	2.68	2.64	1.72×10^{-2}
14.5	3.20	2.64	1.73×10^{-2}
14.5	3.72	2.59	1.71×10^{-2}
14.5	4.25	2.37	1.64×10^{-2}
14.5	4.25	2.41	3.43×10^{-2}
14.5	4.77	2.31	3.36×10^{-2}
14.5	5.30	2.14	3.23×10^{-2}
14.5	5.83	2.09	3.20×10^{-2}
14.5	6.03	2.12	3.28×10^{-2}
14.5	6.56	1.88	3.10×10^{-2}
14.5	7.10	1.75	2.99×10^{-2}
14.5	7.63	1.55	2.81×10^{-2}

Table A.16: Continued.

E_x (MeV)	$\theta_{\text{c.m.}}$ (deg)	$d\sigma/d\Omega$ (mb/sr)	error (mb/sr)
14.5	9.37	5.99×10^{-1}	1.01×10^{-2}
14.5	9.91	4.68×10^{-1}	8.97×10^{-3}
14.5	10.71	4.23×10^{-1}	9.63×10^{-3}
14.5	11.24	4.10×10^{-1}	9.49×10^{-3}
14.5	11.78	4.09×10^{-1}	9.48×10^{-3}
14.5	12.31	4.04×10^{-1}	9.42×10^{-3}
14.5	13.11	3.66×10^{-1}	8.77×10^{-3}
14.5	13.65	3.50×10^{-1}	8.59×10^{-3}
14.5	14.18	3.31×10^{-1}	8.36×10^{-3}
14.5	14.71	2.82×10^{-1}	7.73×10^{-3}
14.5	15.51	1.95×10^{-1}	7.47×10^{-3}
14.5	16.05	1.46×10^{-1}	6.48×10^{-3}
14.5	16.58	1.24×10^{-1}	5.96×10^{-3}
14.5	17.11	1.00×10^{-1}	5.35×10^{-3}
14.5	17.91	5.23×10^{-2}	3.53×10^{-3}
14.5	18.44	4.72×10^{-2}	3.34×10^{-3}
14.5	18.97	3.55×10^{-2}	2.90×10^{-3}
14.5	19.51	3.61×10^{-2}	2.92×10^{-3}
14.5	20.30	2.49×10^{-2}	6.05×10^{-3}
14.5	20.83	3.08×10^{-2}	6.74×10^{-3}
14.5	21.37	2.64×10^{-2}	6.24×10^{-3}
14.5	21.90	8.81×10^{-3}	3.60×10^{-3}
14.5	22.69	1.62×10^{-2}	4.74×10^{-3}
14.5	23.22	1.08×10^{-2}	3.86×10^{-3}
14.5	23.75	1.36×10^{-3}	1.36×10^{-3}
14.5	24.28	5.43×10^{-3}	2.74×10^{-3}
14.5	25.07	6.16×10^{-3}	2.19×10^{-3}
14.5	25.60	3.09×10^{-3}	1.55×10^{-3}
14.5	26.13	3.09×10^{-3}	1.55×10^{-3}

Table A.16: Continued.

E_x (MeV)	$\theta_{\text{c.m.}}$ (deg)	$d\sigma/d\Omega$ (mb/sr)	error (mb/sr)
14.7	1.25	3.27	1.18×10^{-1}
14.7	2.68	2.70	1.75×10^{-2}
14.7	3.20	2.73	1.76×10^{-2}
14.7	3.72	2.79	1.78×10^{-2}
14.7	4.25	2.80	1.79×10^{-2}
14.7	4.25	2.80	3.70×10^{-2}
14.7	4.77	2.79	3.69×10^{-2}
14.7	5.30	2.70	3.63×10^{-2}
14.7	5.83	2.61	3.57×10^{-2}
14.7	6.03	2.73	3.77×10^{-2}
14.7	6.56	2.58	3.65×10^{-2}
14.7	7.10	2.20	3.38×10^{-2}
14.7	7.63	1.81	3.06×10^{-2}
14.7	8.30	1.06	1.35×10^{-2}
14.7	8.84	9.50×10^{-1}	1.28×10^{-2}
14.7	9.37	7.81×10^{-1}	1.16×10^{-2}
14.7	9.91	6.06×10^{-1}	1.02×10^{-2}
14.7	10.71	4.70×10^{-1}	1.01×10^{-2}
14.7	11.24	4.46×10^{-1}	9.86×10^{-3}
14.7	11.78	4.16×10^{-1}	9.53×10^{-3}
14.7	12.31	3.90×10^{-1}	9.23×10^{-3}
14.7	13.11	3.72×10^{-1}	8.87×10^{-3}
14.7	13.65	3.38×10^{-1}	8.46×10^{-3}
14.7	14.18	3.12×10^{-1}	8.14×10^{-3}
14.7	14.71	2.72×10^{-1}	7.60×10^{-3}
14.7	15.51	2.05×10^{-1}	7.60×10^{-3}
14.7	16.05	1.65×10^{-1}	6.81×10^{-3}
14.7	16.58	1.34×10^{-1}	6.13×10^{-3}
14.7	17.11	1.05×10^{-1}	5.44×10^{-3}

Table A.16: Continued.

E_x (MeV)	$\theta_{\text{c.m.}}$ (deg)	$d\sigma/d\Omega$ (mb/sr)	error (mb/sr)
14.7	18.98	3.81×10^{-2}	2.97×10^{-3}
14.7	19.51	3.05×10^{-2}	2.66×10^{-3}
14.7	20.31	2.42×10^{-2}	5.87×10^{-3}
14.7	20.84	4.13×10^{-2}	7.69×10^{-3}
14.7	21.37	2.14×10^{-2}	5.53×10^{-3}
14.7	21.90	1.43×10^{-2}	4.51×10^{-3}
14.7	22.69	8.67×10^{-3}	3.29×10^{-3}
14.7	23.22	1.12×10^{-2}	3.74×10^{-3}
14.7	23.75	1.12×10^{-2}	3.74×10^{-3}
14.7	24.28	8.70×10^{-3}	3.31×10^{-3}
14.7	25.08	5.96×10^{-3}	2.12×10^{-3}
14.7	25.60	2.98×10^{-3}	1.50×10^{-3}
14.7	26.13	4.48×10^{-3}	1.85×10^{-3}
14.7	26.66	2.99×10^{-3}	1.50×10^{-3}
14.9	0.42	3.17	2.07×10^{-1}
14.9	1.25	3.06	1.14×10^{-1}
14.9	2.68	2.68	1.75×10^{-2}
14.9	3.20	2.95	1.84×10^{-2}
14.9	3.72	3.08	1.88×10^{-2}
14.9	4.25	3.09	1.88×10^{-2}
14.9	4.25	2.82	3.70×10^{-2}
14.9	4.77	3.20	3.95×10^{-2}
14.9	5.30	3.03	3.84×10^{-2}
14.9	5.83	2.91	3.77×10^{-2}
14.9	6.03	2.73	3.78×10^{-2}
14.9	6.56	2.82	3.82×10^{-2}
14.9	7.10	2.45	3.56×10^{-2}
14.9	7.63	1.93	3.17×10^{-2}
14.9	8.30	1.13	1.40×10^{-2}

Table A.16: Continued.

E_x (MeV)	$\theta_{\text{c.m.}}$ (deg)	$d\sigma/d\Omega$ (mb/sr)	error (mb/sr)
14.9	9.91	6.28×10^{-1}	1.04×10^{-2}
14.9	10.71	5.84×10^{-1}	1.13×10^{-2}
14.9	11.24	5.66×10^{-1}	1.12×10^{-2}
14.9	11.78	5.40×10^{-1}	1.09×10^{-2}
14.9	12.31	4.97×10^{-1}	1.05×10^{-2}
14.9	13.11	4.48×10^{-1}	9.77×10^{-3}
14.9	13.65	3.88×10^{-1}	9.09×10^{-3}
14.9	14.18	3.45×10^{-1}	8.57×10^{-3}
14.9	14.72	3.23×10^{-1}	8.29×10^{-3}
14.9	15.52	1.99×10^{-1}	7.46×10^{-3}
14.9	16.05	1.66×10^{-1}	6.81×10^{-3}
14.9	16.58	1.34×10^{-1}	6.13×10^{-3}
14.9	17.12	8.90×10^{-2}	4.99×10^{-3}
14.9	17.91	6.42×10^{-2}	3.92×10^{-3}
14.9	18.45	5.03×10^{-2}	3.47×10^{-3}
14.9	18.98	3.94×10^{-2}	3.07×10^{-3}
14.9	19.51	3.59×10^{-2}	2.94×10^{-3}
14.9	20.31	1.70×10^{-2}	5.16×10^{-3}
14.9	20.84	2.17×10^{-2}	5.82×10^{-3}
14.9	21.37	1.55×10^{-2}	4.93×10^{-3}
14.9	21.90	2.18×10^{-2}	5.84×10^{-3}
14.9	22.70	1.00×10^{-2}	3.34×10^{-3}
14.9	23.23	7.79×10^{-3}	2.95×10^{-3}
14.9	23.75	1.00×10^{-2}	3.35×10^{-3}
14.9	24.28	1.00×10^{-2}	3.35×10^{-3}
14.9	25.08	6.29×10^{-3}	2.00×10^{-3}
14.9	25.61	1.26×10^{-3}	8.94×10^{-4}
14.9	26.14	3.15×10^{-3}	1.41×10^{-3}
14.9	26.66	4.42×10^{-3}	1.68×10^{-3}

Table A.16: Continued.

E_x (MeV)	$\theta_{\text{c.m.}}$ (deg)	$d\sigma/d\Omega$ (mb/sr)	error (mb/sr)
15.1	2.68	2.48	1.69×10^{-2}
15.1	3.20	2.88	1.82×10^{-2}
15.1	3.72	3.01	1.86×10^{-2}
15.1	4.25	3.30	1.95×10^{-2}
15.1	4.25	3.01	3.85×10^{-2}
15.1	4.77	3.30	4.04×10^{-2}
15.1	5.31	3.48	4.15×10^{-2}
15.1	5.83	3.12	3.93×10^{-2}
15.1	6.03	3.19	4.08×10^{-2}
15.1	6.56	2.44	3.58×10^{-2}
15.1	7.10	2.44	3.57×10^{-2}
15.1	7.63	1.90	3.15×10^{-2}
15.1	8.30	1.11	1.38×10^{-2}
15.1	8.84	9.28×10^{-1}	1.26×10^{-2}
15.1	9.37	7.45×10^{-1}	1.13×10^{-2}
15.1	9.91	6.63×10^{-1}	1.06×10^{-2}
15.1	10.71	5.47×10^{-1}	1.10×10^{-2}
15.1	11.25	5.06×10^{-1}	1.06×10^{-2}
15.1	11.78	4.81×10^{-1}	1.03×10^{-2}
15.1	12.31	4.11×10^{-1}	9.57×10^{-3}
15.1	13.12	3.79×10^{-1}	9.00×10^{-3}
15.1	13.65	3.25×10^{-1}	8.34×10^{-3}
15.1	14.18	2.82×10^{-1}	7.76×10^{-3}
15.1	14.72	2.23×10^{-1}	6.91×10^{-3}
15.1	15.52	1.90×10^{-1}	7.36×10^{-3}
15.1	16.05	1.26×10^{-1}	6.01×10^{-3}
15.1	16.58	1.15×10^{-1}	5.73×10^{-3}
15.1	17.12	8.57×10^{-2}	4.94×10^{-3}
15.1	17.92	5.07×10^{-2}	3.41×10^{-3}

Table A.16: Continued.

E_x (MeV)	$\theta_{\text{c.m.}}$ (deg)	$d\sigma/d\Omega$ (mb/sr)	error (mb/sr)
15.1	19.51	3.05×10^{-2}	2.64×10^{-3}
15.1	20.31	3.26×10^{-2}	7.34×10^{-3}
15.1	20.84	2.28×10^{-2}	6.13×10^{-3}
15.1	21.37	2.78×10^{-2}	6.77×10^{-3}
15.1	21.90	9.81×10^{-3}	4.02×10^{-3}
15.1	22.70	1.03×10^{-2}	3.93×10^{-3}
15.1	23.23	8.87×10^{-3}	3.64×10^{-3}
15.1	23.76	7.40×10^{-3}	3.33×10^{-3}
15.1	24.29	8.90×10^{-3}	3.65×10^{-3}
15.1	25.08	9.76×10^{-3}	2.85×10^{-3}
15.1	25.61	4.89×10^{-3}	2.01×10^{-3}
15.1	26.14	3.26×10^{-3}	1.64×10^{-3}
15.1	26.67	8.17×10^{-4}	8.21×10^{-4}
15.3	0.42	2.95	2.01×10^{-1}
15.3	1.25	2.43	1.03×10^{-1}
15.3	2.68	1.98	1.51×10^{-2}
15.3	3.20	1.94	1.50×10^{-2}
15.3	3.73	2.25	1.61×10^{-2}
15.3	4.25	2.43	1.68×10^{-2}
15.3	4.25	2.11	3.25×10^{-2}
15.3	4.77	2.27	3.37×10^{-2}
15.3	5.31	2.46	3.50×10^{-2}
15.3	5.83	2.27	3.37×10^{-2}
15.3	6.03	2.20	3.40×10^{-2}
15.3	6.56	1.91	3.16×10^{-2}
15.3	7.10	1.39	2.71×10^{-2}
15.3	7.64	1.26	2.56×10^{-2}
15.3	8.30	7.51×10^{-1}	1.14×10^{-2}
15.3	8.84	6.48×10^{-1}	1.05×10^{-2}

Table A.16: Continued.

E_x (MeV)	$\theta_{\text{c.m.}}$ (deg)	$d\sigma/d\Omega$ (mb/sr)	error (mb/sr)
15.3	10.71	3.89×10^{-1}	9.44×10^{-3}
15.3	11.25	4.26×10^{-1}	9.88×10^{-3}
15.3	11.78	4.21×10^{-1}	9.82×10^{-3}
15.3	12.32	3.42×10^{-1}	8.87×10^{-3}
15.3	13.12	3.00×10^{-1}	8.10×10^{-3}
15.3	13.65	2.59×10^{-1}	7.52×10^{-3}
15.3	14.18	2.20×10^{-1}	6.93×10^{-3}
15.3	14.72	1.80×10^{-1}	6.28×10^{-3}
15.3	15.52	1.41×10^{-1}	6.28×10^{-3}
15.3	16.05	1.08×10^{-1}	5.49×10^{-3}
15.3	16.59	8.32×10^{-2}	4.83×10^{-3}
15.3	17.12	6.88×10^{-2}	4.39×10^{-3}
15.3	17.92	3.75×10^{-2}	2.99×10^{-3}
15.3	18.45	3.61×10^{-2}	2.92×10^{-3}
15.3	18.98	2.93×10^{-2}	2.63×10^{-3}
15.3	19.51	2.40×10^{-2}	2.39×10^{-3}
15.3	20.31	1.83×10^{-2}	5.30×10^{-3}
15.3	20.84	1.99×10^{-2}	5.53×10^{-3}
15.3	21.37	1.68×10^{-2}	5.09×10^{-3}
15.3	21.90	1.38×10^{-2}	4.61×10^{-3}
15.3	22.70	1.31×10^{-2}	3.98×10^{-3}
15.3	23.23	4.78×10^{-3}	2.40×10^{-3}
15.3	23.76	5.98×10^{-3}	2.69×10^{-3}
15.3	24.29	4.79×10^{-3}	2.41×10^{-3}
15.3	25.08	2.42×10^{-3}	1.41×10^{-3}
15.3	25.61	3.24×10^{-3}	1.63×10^{-3}
15.3	26.14	1.62×10^{-3}	1.16×10^{-3}
15.3	26.67	1.00×10^{-5}	1.00×10^{-5}
15.5	1.25	2.12	9.51×10^{-2}

Table A.16: Continued.

E_x (MeV)	$\theta_{\text{c.m.}}$ (deg)	$d\sigma/d\Omega$ (mb/sr)	error (mb/sr)
15.5	3.73	1.84	1.46×10^{-2}
15.5	4.25	2.05	1.54×10^{-2}
15.5	4.25	1.87	3.06×10^{-2}
15.5	4.77	2.00	3.16×10^{-2}
15.5	5.31	1.92	3.09×10^{-2}
15.5	5.83	1.91	3.09×10^{-2}
15.5	6.03	1.88	3.15×10^{-2}
15.5	6.56	1.66	2.96×10^{-2}
15.5	7.10	1.40	2.70×10^{-2}
15.5	7.64	1.08	2.38×10^{-2}
15.5	8.31	7.11×10^{-1}	1.11×10^{-2}
15.5	8.84	6.01×10^{-1}	1.02×10^{-2}
15.5	9.38	5.21×10^{-1}	9.50×10^{-3}
15.5	9.91	4.81×10^{-1}	9.13×10^{-3}
15.5	10.71	3.69×10^{-1}	9.12×10^{-3}
15.5	11.25	3.54×10^{-1}	8.93×10^{-3}
15.5	11.78	3.28×10^{-1}	8.60×10^{-3}
15.5	12.32	3.24×10^{-1}	8.54×10^{-3}
15.5	13.12	2.78×10^{-1}	7.68×10^{-3}
15.5	13.65	2.45×10^{-1}	7.21×10^{-3}
15.5	14.19	2.10×10^{-1}	6.68×10^{-3}
15.5	14.72	1.78×10^{-1}	6.13×10^{-3}
15.5	15.52	1.21×10^{-1}	5.94×10^{-3}
15.5	16.05	1.06×10^{-1}	5.54×10^{-3}
15.5	16.59	9.03×10^{-2}	5.11×10^{-3}
15.5	17.12	5.82×10^{-2}	4.12×10^{-3}
15.5	17.92	3.45×10^{-2}	2.88×10^{-3}
15.5	18.45	2.95×10^{-2}	2.66×10^{-3}
15.5	18.98	2.59×10^{-2}	2.49×10^{-3}

Table A.16: Continued.

E_x (MeV)	$\theta_{\text{c.m.}}$ (deg)	$d\sigma/d\Omega$ (mb/sr)	error (mb/sr)
15.5	20.84	2.85×10^{-2}	6.76×10^{-3}
15.5	21.37	1.75×10^{-2}	5.28×10^{-3}
15.5	21.91	1.11×10^{-2}	4.22×10^{-3}
15.5	22.70	8.76×10^{-3}	3.33×10^{-3}
15.5	23.23	1.00×10^{-2}	3.57×10^{-3}
15.5	23.76	1.13×10^{-2}	3.79×10^{-3}
15.5	24.29	2.51×10^{-3}	1.78×10^{-3}
15.5	25.08	1.45×10^{-3}	1.03×10^{-3}
15.5	25.61	3.63×10^{-3}	1.63×10^{-3}
15.5	26.14	1.45×10^{-3}	1.03×10^{-3}
15.5	26.67	7.27×10^{-4}	7.33×10^{-4}
15.7	0.42	2.48	1.83×10^{-1}
15.7	1.25	2.17	9.55×10^{-2}
15.7	2.68	1.70	1.40×10^{-2}
15.7	3.20	1.76	1.43×10^{-2}
15.7	3.73	1.79	1.44×10^{-2}
15.7	4.25	1.91	1.49×10^{-2}
15.7	4.25	1.91	3.09×10^{-2}
15.7	4.77	1.93	3.11×10^{-2}
15.7	5.31	1.83	3.03×10^{-2}
15.7	5.83	1.80	3.01×10^{-2}
15.7	6.03	1.68	2.97×10^{-2}
15.7	6.57	1.51	2.81×10^{-2}
15.7	7.10	1.24	2.55×10^{-2}
15.7	7.64	8.36×10^{-1}	2.10×10^{-2}
15.7	8.31	6.11×10^{-1}	1.03×10^{-2}
15.7	8.84	5.23×10^{-1}	9.51×10^{-3}
15.7	9.38	4.78×10^{-1}	9.08×10^{-3}
15.7	9.91	4.36×10^{-1}	8.68×10^{-3}

Table A.16: Continued.

E_x (MeV)	$\theta_{\text{c.m.}}$ (deg)	$d\sigma/d\Omega$ (mb/sr)	error (mb/sr)
15.7	11.78	3.35×10^{-1}	8.68×10^{-3}
15.7	12.32	2.77×10^{-1}	7.90×10^{-3}
15.7	13.12	2.36×10^{-1}	7.10×10^{-3}
15.7	13.65	1.99×10^{-1}	6.52×10^{-3}
15.7	14.19	1.81×10^{-1}	6.22×10^{-3}
15.7	14.72	1.55×10^{-1}	5.75×10^{-3}
15.7	15.52	1.13×10^{-1}	5.88×10^{-3}
15.7	16.05	8.99×10^{-2}	5.24×10^{-3}
15.7	16.59	8.29×10^{-2}	5.02×10^{-3}
15.7	17.12	5.96×10^{-2}	4.26×10^{-3}
15.7	17.92	3.65×10^{-2}	2.94×10^{-3}
15.7	18.45	2.78×10^{-2}	2.57×10^{-3}
15.7	18.98	2.57×10^{-2}	2.47×10^{-3}
15.7	19.52	2.11×10^{-2}	2.23×10^{-3}
15.7	20.31	2.11×10^{-2}	5.66×10^{-3}
15.7	20.84	1.05×10^{-2}	4.00×10^{-3}
15.7	21.38	6.03×10^{-3}	3.03×10^{-3}
15.7	21.91	9.06×10^{-3}	3.71×10^{-3}
15.7	22.70	1.14×10^{-2}	3.62×10^{-3}
15.7	23.23	5.70×10^{-3}	2.56×10^{-3}
15.7	23.76	3.43×10^{-3}	1.98×10^{-3}
15.7	24.29	5.72×10^{-3}	2.57×10^{-3}
15.7	25.09	3.13×10^{-3}	1.59×10^{-3}
15.7	25.61	3.92×10^{-3}	1.78×10^{-3}
15.7	26.14	7.85×10^{-4}	7.92×10^{-4}
15.7	26.67	1.57×10^{-3}	1.12×10^{-3}
15.9	0.42	2.38	1.79×10^{-1}
15.9	1.25	2.27	9.79×10^{-2}
15.9	2.68	1.83	1.45×10^{-2}

Table A.16: Continued.

E_x (MeV)	$\theta_{\text{c.m.}}$ (deg)	$d\sigma/d\Omega$ (mb/sr)	error (mb/sr)
15.9	4.25	2.02	1.53×10^{-2}
15.9	4.25	2.04	3.20×10^{-2}
15.9	4.77	2.05	3.21×10^{-2}
15.9	5.31	2.03	3.20×10^{-2}
15.9	5.83	1.91	3.10×10^{-2}
15.9	6.03	1.81	3.07×10^{-2}
15.9	6.57	1.56	2.86×10^{-2}
15.9	7.10	1.28	2.57×10^{-2}
15.9	7.64	1.01	2.29×10^{-2}
15.9	8.31	5.89×10^{-1}	1.01×10^{-2}
15.9	8.84	5.05×10^{-1}	9.32×10^{-3}
15.9	9.38	4.64×10^{-1}	8.93×10^{-3}
15.9	9.91	4.34×10^{-1}	8.64×10^{-3}
15.9	10.71	4.62×10^{-1}	1.01×10^{-2}
15.9	11.25	4.38×10^{-1}	9.85×10^{-3}
15.9	11.78	4.18×10^{-1}	9.63×10^{-3}
15.9	12.32	3.86×10^{-1}	9.26×10^{-3}
15.9	13.12	3.07×10^{-1}	8.14×10^{-3}
15.9	13.65	2.78×10^{-1}	7.73×10^{-3}
15.9	14.19	2.27×10^{-1}	7.00×10^{-3}
15.9	14.72	2.04×10^{-1}	6.62×10^{-3}
15.9	15.52	1.13×10^{-1}	5.69×10^{-3}
15.9	16.06	9.64×10^{-2}	5.25×10^{-3}
15.9	16.59	6.87×10^{-2}	4.44×10^{-3}
15.9	17.12	7.02×10^{-2}	4.48×10^{-3}
15.9	17.92	4.58×10^{-2}	3.29×10^{-3}
15.9	18.45	3.79×10^{-2}	2.99×10^{-3}
15.9	18.99	2.89×10^{-2}	2.61×10^{-3}
15.9	19.52	3.15×10^{-2}	2.73×10^{-3}

Table A.16: Continued.

E_x (MeV)	$\theta_{\text{c.m.}}$ (deg)	$d\sigma/d\Omega$ (mb/sr)	error (mb/sr)
15.9	21.38	9.79×10^{-3}	4.01×10^{-3}
15.9	21.91	1.31×10^{-2}	4.64×10^{-3}
15.9	22.70	3.89×10^{-3}	2.26×10^{-3}
15.9	23.23	1.04×10^{-2}	3.71×10^{-3}
15.9	23.76	6.49×10^{-3}	2.92×10^{-3}
15.9	24.29	2.60×10^{-3}	1.85×10^{-3}
15.9	25.09	1.37×10^{-3}	9.75×10^{-4}
15.9	25.62	6.85×10^{-4}	6.90×10^{-4}
15.9	26.15	6.86×10^{-4}	6.91×10^{-4}
15.9	26.67	6.87×10^{-4}	6.92×10^{-4}
16.1	1.25	2.94	1.13×10^{-1}
16.1	2.68	2.38	1.65×10^{-2}
16.1	3.20	2.55	1.71×10^{-2}
16.1	3.73	2.77	1.78×10^{-2}
16.1	4.25	2.62	1.74×10^{-2}
16.1	4.25	2.68	3.63×10^{-2}
16.1	4.77	2.69	3.64×10^{-2}
16.1	5.31	2.64	3.61×10^{-2}
16.1	5.83	2.59	3.57×10^{-2}
16.1	6.03	2.56	3.62×10^{-2}
16.1	6.57	2.27	3.41×10^{-2}
16.1	7.10	1.88	3.11×10^{-2}
16.1	7.64	1.39	2.66×10^{-2}
16.1	8.31	7.97×10^{-1}	1.16×10^{-2}
16.1	8.84	6.57×10^{-1}	1.06×10^{-2}
16.1	9.38	5.76×10^{-1}	9.88×10^{-3}
16.1	9.91	5.20×10^{-1}	9.40×10^{-3}
16.1	10.72	5.49×10^{-1}	1.10×10^{-2}
16.1	11.25	5.26×10^{-1}	1.08×10^{-2}

Table A.16: Continued.

E_x (MeV)	$\theta_{\text{c.m.}}$ (deg)	$d\sigma/d\Omega$ (mb/sr)	error (mb/sr)
16.1	13.12	3.99×10^{-1}	9.38×10^{-3}
16.1	13.66	3.51×10^{-1}	8.79×10^{-3}
16.1	14.19	3.00×10^{-1}	8.12×10^{-3}
16.1	14.72	2.29×10^{-1}	7.10×10^{-3}
16.1	15.52	1.56×10^{-1}	6.64×10^{-3}
16.1	16.06	1.22×10^{-1}	5.88×10^{-3}
16.1	16.59	1.02×10^{-1}	5.37×10^{-3}
16.1	17.12	8.24×10^{-2}	4.83×10^{-3}
16.1	17.92	4.32×10^{-2}	3.25×10^{-3}
16.1	18.46	3.84×10^{-2}	3.06×10^{-3}
16.1	18.99	4.02×10^{-2}	3.13×10^{-3}
16.1	19.52	3.03×10^{-2}	2.72×10^{-3}
16.1	20.32	3.01×10^{-2}	7.35×10^{-3}
16.1	20.85	2.84×10^{-2}	7.14×10^{-3}
16.1	21.38	8.88×10^{-3}	3.98×10^{-3}
16.1	21.91	1.24×10^{-2}	4.72×10^{-3}
16.1	22.71	5.56×10^{-3}	2.80×10^{-3}
16.1	23.24	2.78×10^{-3}	1.98×10^{-3}
16.1	23.77	9.76×10^{-3}	3.71×10^{-3}
16.1	24.30	6.98×10^{-3}	3.14×10^{-3}
16.1	25.09	4.95×10^{-3}	1.88×10^{-3}
16.1	25.62	1.42×10^{-3}	1.01×10^{-3}
16.1	26.15	4.25×10^{-3}	1.75×10^{-3}
16.1	26.68	2.13×10^{-3}	1.23×10^{-3}
16.3	0.42	3.60	2.25×10^{-1}
16.3	1.25	3.31	1.21×10^{-1}
16.3	2.68	2.22	1.59×10^{-2}
16.3	3.20	2.32	1.63×10^{-2}
16.3	3.73	2.42	1.66×10^{-2}

Table A.16: Continued.

E_x (MeV)	$\theta_{\text{c.m.}}$ (deg)	$d\sigma/d\Omega$ (mb/sr)	error (mb/sr)
16.3	4.77	2.90	3.78×10^{-2}
16.3	5.31	2.93	3.80×10^{-2}
16.3	5.83	2.66	3.62×10^{-2}
16.3	6.03	2.65	3.68×10^{-2}
16.3	6.57	2.34	3.46×10^{-2}
16.3	7.10	1.88	3.10×10^{-2}
16.3	7.64	1.44	2.71×10^{-2}
16.3	8.31	7.29×10^{-1}	1.11×10^{-2}
16.3	8.84	6.04×10^{-1}	1.01×10^{-2}
16.3	9.38	4.93×10^{-1}	9.14×10^{-3}
16.3	9.91	4.77×10^{-1}	8.98×10^{-3}
16.3	10.72	3.55×10^{-1}	8.98×10^{-3}
16.3	11.25	3.52×10^{-1}	8.96×10^{-3}
16.3	11.79	3.14×10^{-1}	8.47×10^{-3}
16.3	12.32	2.69×10^{-1}	7.84×10^{-3}
16.3	13.12	2.64×10^{-1}	7.69×10^{-3}
16.3	13.66	2.12×10^{-1}	6.89×10^{-3}
16.3	14.19	1.80×10^{-1}	6.36×10^{-3}
16.3	14.72	1.39×10^{-1}	5.58×10^{-3}
16.3	15.53	1.12×10^{-1}	5.81×10^{-3}
16.3	16.06	9.09×10^{-2}	5.23×10^{-3}
16.3	16.59	7.36×10^{-2}	4.70×10^{-3}
16.3	17.12	6.01×10^{-2}	4.25×10^{-3}
16.3	17.92	3.66×10^{-2}	3.00×10^{-3}
16.3	18.46	2.65×10^{-2}	2.55×10^{-3}
16.3	18.99	2.98×10^{-2}	2.70×10^{-3}
16.3	19.52	1.97×10^{-2}	2.19×10^{-3}
16.3	20.32	2.30×10^{-2}	5.76×10^{-3}
16.3	20.85	1.29×10^{-2}	4.33×10^{-3}

Table A.16: Continued.

E_x (MeV)	$\theta_{\text{c.m.}}$ (deg)	$d\sigma/d\Omega$ (mb/sr)	error (mb/sr)
16.3	22.71	9.30×10^{-3}	3.31×10^{-3}
16.3	23.24	8.15×10^{-3}	3.10×10^{-3}
16.3	23.77	1.17×10^{-3}	1.17×10^{-3}
16.3	24.30	1.00×10^{-5}	1.00×10^{-5}
16.3	25.09	2.14×10^{-3}	1.25×10^{-3}
16.3	25.62	2.15×10^{-3}	1.25×10^{-3}
16.3	26.15	1.43×10^{-3}	1.02×10^{-3}
16.3	26.68	2.15×10^{-3}	1.26×10^{-3}
16.5	0.42	3.00	2.05×10^{-1}
16.5	1.25	2.87	1.12×10^{-1}
16.5	2.68	1.72	1.40×10^{-2}
16.5	3.20	1.62	1.36×10^{-2}
16.5	3.73	1.64	1.37×10^{-2}
16.5	4.25	1.79	1.43×10^{-2}
16.5	4.25	1.67	2.88×10^{-2}
16.5	4.77	1.85	3.03×10^{-2}
16.5	5.31	1.82	3.00×10^{-2}
16.5	5.83	1.72	2.92×10^{-2}
16.5	6.03	1.62	2.88×10^{-2}
16.5	6.57	1.41	2.69×10^{-2}
16.5	7.10	1.13	2.43×10^{-2}
16.5	7.64	8.94×10^{-1}	2.15×10^{-2}
16.5	8.31	5.09×10^{-1}	9.28×10^{-3}
16.5	8.84	3.95×10^{-1}	8.17×10^{-3}
16.5	9.38	3.54×10^{-1}	7.73×10^{-3}
16.5	9.91	3.08×10^{-1}	7.22×10^{-3}
16.5	10.72	2.80×10^{-1}	7.92×10^{-3}
16.5	11.25	2.69×10^{-1}	7.77×10^{-3}
16.5	11.79	2.48×10^{-1}	7.48×10^{-3}

Table A.16: Continued.

E_x (MeV)	$\theta_{\text{c.m.}}$ (deg)	$d\sigma/d\Omega$ (mb/sr)	error (mb/sr)
16.5	13.66	1.71×10^{-1}	6.16×10^{-3}
16.5	14.19	1.40×10^{-1}	5.56×10^{-3}
16.5	14.73	1.24×10^{-1}	5.23×10^{-3}
16.5	15.53	8.49×10^{-2}	4.98×10^{-3}
16.5	16.06	8.05×10^{-2}	4.85×10^{-3}
16.5	16.59	5.64×10^{-2}	4.06×10^{-3}
16.5	17.13	4.89×10^{-2}	3.79×10^{-3}
16.5	17.93	3.61×10^{-2}	2.92×10^{-3}
16.5	18.46	2.88×10^{-2}	2.61×10^{-3}
16.5	18.99	2.56×10^{-2}	2.46×10^{-3}
16.5	19.52	2.22×10^{-2}	2.29×10^{-3}
16.5	20.32	1.06×10^{-2}	4.03×10^{-3}
16.5	20.85	1.67×10^{-2}	5.05×10^{-3}
16.5	21.38	6.08×10^{-3}	3.05×10^{-3}
16.5	21.91	6.09×10^{-3}	3.05×10^{-3}
16.5	22.71	1.11×10^{-2}	3.97×10^{-3}
16.5	23.24	6.95×10^{-3}	3.14×10^{-3}
16.5	23.77	1.39×10^{-3}	1.40×10^{-3}
16.5	24.30	5.57×10^{-3}	2.81×10^{-3}
16.5	25.09	4.70×10^{-3}	1.79×10^{-3}
16.5	25.62	1.35×10^{-3}	9.55×10^{-4}
16.5	26.15	1.35×10^{-3}	9.56×10^{-4}
16.5	26.68	6.74×10^{-4}	6.77×10^{-4}
16.7	0.42	3.21	2.10×10^{-1}
16.7	1.25	2.99	1.14×10^{-1}
16.7	2.68	1.87	1.46×10^{-2}
16.7	3.20	1.77	1.42×10^{-2}
16.7	3.73	1.79	1.43×10^{-2}
16.7	4.25	1.78	1.42×10^{-2}

Table A.16: Continued.

E_x (MeV)	$\theta_{\text{c.m.}}$ (deg)	$d\sigma/d\Omega$ (mb/sr)	error (mb/sr)
16.7	5.31	1.78	2.97×10^{-2}
16.7	5.83	1.69	2.89×10^{-2}
16.7	6.03	1.67	2.91×10^{-2}
16.7	6.57	1.37	2.65×10^{-2}
16.7	7.10	1.15	2.41×10^{-2}
16.7	7.64	8.82×10^{-1}	2.13×10^{-2}
16.7	8.31	5.11×10^{-1}	9.29×10^{-3}
16.7	8.84	4.04×10^{-1}	8.26×10^{-3}
16.7	9.38	3.49×10^{-1}	7.67×10^{-3}
16.7	9.92	3.07×10^{-1}	7.20×10^{-3}
16.7	10.72	3.18×10^{-1}	8.47×10^{-3}
16.7	11.25	3.13×10^{-1}	8.40×10^{-3}
16.7	11.79	2.83×10^{-1}	8.00×10^{-3}
16.7	12.32	2.78×10^{-1}	7.92×10^{-3}
16.7	13.12	2.11×10^{-1}	6.80×10^{-3}
16.7	13.66	1.90×10^{-1}	6.46×10^{-3}
16.7	14.19	1.57×10^{-1}	5.87×10^{-3}
16.7	14.73	1.30×10^{-1}	5.34×10^{-3}
16.7	15.53	9.77×10^{-2}	5.34×10^{-3}
16.7	16.06	7.89×10^{-2}	4.79×10^{-3}
16.7	16.59	6.46×10^{-2}	4.33×10^{-3}
16.7	17.13	7.05×10^{-2}	4.52×10^{-3}
16.7	17.93	2.68×10^{-2}	2.55×10^{-3}
16.7	18.46	3.00×10^{-2}	2.69×10^{-3}
16.7	18.99	2.64×10^{-2}	2.52×10^{-3}
16.7	19.52	2.48×10^{-2}	2.45×10^{-3}
16.7	20.32	1.26×10^{-2}	4.19×10^{-3}
16.7	20.85	1.95×10^{-2}	5.24×10^{-3}
16.7	21.38	8.39×10^{-3}	3.43×10^{-3}

Table A.16: Continued.

E_x (MeV)	$\theta_{\text{c.m.}}$ (deg)	$d\sigma/d\Omega$ (mb/sr)	error (mb/sr)
16.7	23.24	4.78×10^{-3}	2.40×10^{-3}
16.7	23.77	2.39×10^{-3}	1.70×10^{-3}
16.7	24.30	9.58×10^{-3}	3.41×10^{-3}
16.7	25.10	5.18×10^{-3}	1.98×10^{-3}
16.7	25.63	4.45×10^{-3}	1.83×10^{-3}
16.7	26.15	7.42×10^{-4}	7.47×10^{-4}
16.7	26.68	2.97×10^{-3}	1.50×10^{-3}
16.9	0.42	3.95	2.33×10^{-1}
16.9	1.25	3.52	1.23×10^{-1}
16.9	2.68	2.03	1.52×10^{-2}
16.9	3.20	1.89	1.47×10^{-2}
16.9	3.73	1.87	1.46×10^{-2}
16.9	4.25	1.94	1.48×10^{-2}
16.9	4.25	1.81	2.97×10^{-2}
16.9	4.77	1.90	3.04×10^{-2}
16.9	5.31	1.91	3.05×10^{-2}
16.9	5.83	1.79	2.96×10^{-2}
16.9	6.03	1.79	3.01×10^{-2}
16.9	6.57	1.56	2.82×10^{-2}
16.9	7.10	1.31	2.56×10^{-2}
16.9	7.64	9.56×10^{-1}	2.20×10^{-2}
16.9	8.31	5.49×10^{-1}	9.62×10^{-3}
16.9	8.85	4.43×10^{-1}	8.64×10^{-3}
16.9	9.38	3.77×10^{-1}	7.98×10^{-3}
16.9	9.92	3.49×10^{-1}	7.68×10^{-3}
16.9	10.72	3.31×10^{-1}	8.60×10^{-3}
16.9	11.25	3.03×10^{-1}	8.25×10^{-3}
16.9	11.79	3.06×10^{-1}	8.28×10^{-3}
16.9	12.32	2.63×10^{-1}	7.69×10^{-3}

Table A.16: Continued.

E_x (MeV)	$\theta_{\text{c.m.}}$ (deg)	$d\sigma/d\Omega$ (mb/sr)	error (mb/sr)
16.9	14.19	1.55×10^{-1}	5.83×10^{-3}
16.9	14.73	1.37×10^{-1}	5.47×10^{-3}
16.9	15.53	1.02×10^{-1}	5.58×10^{-3}
16.9	16.06	8.88×10^{-2}	5.21×10^{-3}
16.9	16.60	8.21×10^{-2}	5.00×10^{-3}
16.9	17.13	6.63×10^{-2}	4.50×10^{-3}
16.9	17.93	3.99×10^{-2}	3.09×10^{-3}
16.9	18.46	3.61×10^{-2}	2.94×10^{-3}
16.9	18.99	2.07×10^{-2}	2.23×10^{-3}
16.9	19.53	2.22×10^{-2}	2.31×10^{-3}
16.9	20.32	1.61×10^{-2}	4.87×10^{-3}
16.9	20.86	1.17×10^{-2}	4.15×10^{-3}
16.9	21.39	5.87×10^{-3}	2.94×10^{-3}
16.9	21.92	1.17×10^{-2}	4.17×10^{-3}
16.9	22.71	8.32×10^{-3}	3.41×10^{-3}
16.9	23.24	5.55×10^{-3}	2.80×10^{-3}
16.9	23.77	4.17×10^{-3}	2.43×10^{-3}
16.9	24.30	6.96×10^{-3}	3.15×10^{-3}
16.9	25.10	3.59×10^{-3}	1.62×10^{-3}
16.9	25.63	1.00×10^{-5}	1.00×10^{-5}
16.9	26.16	1.44×10^{-3}	1.02×10^{-3}
16.9	26.68	7.20×10^{-4}	7.25×10^{-4}
17.1	0.42	4.02	2.32×10^{-1}
17.1	1.25	3.64	1.24×10^{-1}
17.1	2.68	2.06	1.52×10^{-2}
17.1	3.20	1.86	1.45×10^{-2}
17.1	3.73	1.80	1.43×10^{-2}
17.1	4.25	1.85	1.44×10^{-2}
17.1	4.25	1.78	2.94×10^{-2}

Table A.16: Continued.

E_x (MeV)	$\theta_{\text{c.m.}}$ (deg)	$d\sigma/d\Omega$ (mb/sr)	error (mb/sr)
17.1	5.83	1.76	2.93×10^{-2}
17.1	6.03	1.76	2.97×10^{-2}
17.1	6.57	1.54	2.79×10^{-2}
17.1	7.11	1.27	2.54×10^{-2}
17.1	7.64	1.01	2.26×10^{-2}
17.1	8.31	5.89×10^{-1}	9.96×10^{-3}
17.1	8.85	4.66×10^{-1}	8.86×10^{-3}
17.1	9.38	3.77×10^{-1}	7.97×10^{-3}
17.1	9.92	3.43×10^{-1}	7.61×10^{-3}
17.1	10.72	3.27×10^{-1}	8.52×10^{-3}
17.1	11.26	3.28×10^{-1}	8.53×10^{-3}
17.1	11.79	3.19×10^{-1}	8.41×10^{-3}
17.1	12.32	2.83×10^{-1}	7.93×10^{-3}
17.1	13.13	2.20×10^{-1}	6.82×10^{-3}
17.1	13.66	1.91×10^{-1}	6.36×10^{-3}
17.1	14.20	1.60×10^{-1}	5.81×10^{-3}
17.1	14.73	1.29×10^{-1}	5.21×10^{-3}
17.1	15.53	1.07×10^{-1}	5.60×10^{-3}
17.1	16.06	9.23×10^{-2}	5.21×10^{-3}
17.1	16.60	7.84×10^{-2}	4.81×10^{-3}
17.1	17.13	7.49×10^{-2}	4.69×10^{-3}
17.1	17.93	4.38×10^{-2}	3.27×10^{-3}
17.1	18.46	3.25×10^{-2}	2.82×10^{-3}
17.1	19.00	2.85×10^{-2}	2.64×10^{-3}
17.1	19.53	2.41×10^{-2}	2.43×10^{-3}
17.1	20.33	1.89×10^{-2}	5.27×10^{-3}
17.1	20.86	7.28×10^{-3}	3.27×10^{-3}
17.1	21.39	1.17×10^{-2}	4.13×10^{-3}
17.1	21.92	1.46×10^{-2}	4.63×10^{-3}

Table A.16: Continued.

E_x (MeV)	$\theta_{\text{c.m.}}$ (deg)	$d\sigma/d\Omega$ (mb/sr)	error (mb/sr)
17.1	23.78	1.33×10^{-2}	4.50×10^{-3}
17.1	24.31	2.97×10^{-3}	2.11×10^{-3}
17.1	25.10	3.96×10^{-3}	1.79×10^{-3}
17.1	25.63	1.59×10^{-3}	1.13×10^{-3}
17.1	26.16	3.18×10^{-3}	1.60×10^{-3}
17.1	26.69	2.39×10^{-3}	1.40×10^{-3}
17.3	0.42	3.94	2.32×10^{-1}
17.3	1.25	3.97	1.31×10^{-1}
17.3	2.68	2.02	1.50×10^{-2}
17.3	3.21	1.87	1.45×10^{-2}
17.3	3.73	1.88	1.45×10^{-2}
17.3	4.25	1.83	1.44×10^{-2}
17.3	4.25	1.81	2.98×10^{-2}
17.3	4.77	1.89	3.04×10^{-2}
17.3	5.31	1.92	3.07×10^{-2}
17.3	5.83	1.80	2.97×10^{-2}
17.3	6.03	1.83	3.04×10^{-2}
17.3	6.57	1.62	2.86×10^{-2}
17.3	7.11	1.34	2.61×10^{-2}
17.3	7.64	1.03	2.27×10^{-2}
17.3	8.31	6.37×10^{-1}	1.04×10^{-2}
17.3	8.85	4.88×10^{-1}	9.09×10^{-3}
17.3	9.38	4.17×10^{-1}	8.40×10^{-3}
17.3	9.92	3.90×10^{-1}	8.13×10^{-3}
17.3	10.72	3.88×10^{-1}	9.24×10^{-3}
17.3	11.26	3.77×10^{-1}	9.11×10^{-3}
17.3	11.79	3.49×10^{-1}	8.76×10^{-3}
17.3	12.33	3.24×10^{-1}	8.45×10^{-3}
17.3	13.13	2.49×10^{-1}	7.19×10^{-3}

Table A.16: Continued.

E_x (MeV)	$\theta_{\text{c.m.}}$ (deg)	$d\sigma/d\Omega$ (mb/sr)	error (mb/sr)
17.3	14.73	1.57×10^{-1}	5.72×10^{-3}
17.3	15.53	1.19×10^{-1}	5.85×10^{-3}
17.3	16.07	1.04×10^{-1}	5.47×10^{-3}
17.3	16.60	8.45×10^{-2}	4.93×10^{-3}
17.3	17.13	7.58×10^{-2}	4.66×10^{-3}
17.3	17.93	4.17×10^{-2}	3.14×10^{-3}
17.3	18.46	3.90×10^{-2}	3.04×10^{-3}
17.3	19.00	3.02×10^{-2}	2.68×10^{-3}
17.3	19.53	2.84×10^{-2}	2.60×10^{-3}
17.3	20.33	2.32×10^{-2}	6.26×10^{-3}
17.3	20.86	1.16×10^{-2}	4.42×10^{-3}
17.3	21.39	2.00×10^{-2}	5.79×10^{-3}
17.3	21.92	1.00×10^{-2}	4.10×10^{-3}
17.3	22.72	8.71×10^{-3}	3.32×10^{-3}
17.3	23.25	2.49×10^{-3}	1.77×10^{-3}
17.3	23.78	2.49×10^{-3}	1.77×10^{-3}
17.3	24.31	4.99×10^{-3}	2.52×10^{-3}
17.3	25.10	3.75×10^{-3}	1.69×10^{-3}
17.3	25.63	2.25×10^{-3}	1.31×10^{-3}
17.3	26.16	3.76×10^{-3}	1.70×10^{-3}
17.3	26.69	7.53×10^{-4}	7.58×10^{-4}
17.5	0.42	3.83	2.27×10^{-1}
17.5	1.25	3.48	1.22×10^{-1}
17.5	2.68	2.09	1.53×10^{-2}
17.5	3.21	2.00	1.50×10^{-2}
17.5	3.73	2.00	1.50×10^{-2}
17.5	4.25	1.99	1.50×10^{-2}
17.5	4.25	2.05	3.15×10^{-2}
17.5	4.77	2.08	3.18×10^{-2}

Table A.16: Continued.

E_x (MeV)	$\theta_{\text{c.m.}}$ (deg)	$d\sigma/d\Omega$ (mb/sr)	error (mb/sr)
17.5	6.03	2.08	3.23×10^{-2}
17.5	6.57	1.84	3.05×10^{-2}
17.5	7.11	1.53	2.78×10^{-2}
17.5	7.64	1.24	2.50×10^{-2}
17.5	8.31	7.71×10^{-1}	1.14×10^{-2}
17.5	8.85	6.05×10^{-1}	1.01×10^{-2}
17.5	9.38	5.25×10^{-1}	9.40×10^{-3}
17.5	9.92	4.32×10^{-1}	8.53×10^{-3}
17.5	10.72	5.14×10^{-1}	1.06×10^{-2}
17.5	11.26	4.78×10^{-1}	1.02×10^{-2}
17.5	11.79	4.33×10^{-1}	9.73×10^{-3}
17.5	12.33	4.20×10^{-1}	9.59×10^{-3}
17.5	13.13	3.23×10^{-1}	8.26×10^{-3}
17.5	13.66	2.72×10^{-1}	7.58×10^{-3}
17.5	14.20	2.51×10^{-1}	7.27×10^{-3}
17.5	14.73	2.17×10^{-1}	6.77×10^{-3}
17.5	15.53	1.33×10^{-1}	6.10×10^{-3}
17.5	16.07	1.26×10^{-1}	5.94×10^{-3}
17.5	16.60	1.14×10^{-1}	5.63×10^{-3}
17.5	17.13	1.04×10^{-1}	5.38×10^{-3}
17.5	17.93	5.78×10^{-2}	3.75×10^{-3}
17.5	18.47	4.84×10^{-2}	3.43×10^{-3}
17.5	19.00	3.97×10^{-2}	3.11×10^{-3}
17.5	19.53	3.11×10^{-2}	2.75×10^{-3}
17.5	20.33	2.13×10^{-2}	5.94×10^{-3}
17.5	20.86	1.97×10^{-2}	5.71×10^{-3}
17.5	21.39	1.15×10^{-2}	4.36×10^{-3}
17.5	21.92	1.97×10^{-2}	5.72×10^{-3}
17.5	22.72	5.25×10^{-3}	2.64×10^{-3}

Table A.16: Continued.

E_x (MeV)	$\theta_{\text{c.m.}}$ (deg)	$d\sigma/d\Omega$ (mb/sr)	error (mb/sr)
17.5	24.31	1.18×10^{-2}	3.98×10^{-3}
17.5	25.10	7.25×10^{-3}	2.60×10^{-3}
17.5	25.63	1.82×10^{-3}	1.30×10^{-3}
17.5	26.16	1.82×10^{-3}	1.30×10^{-3}
17.5	26.69	9.10×10^{-4}	9.19×10^{-4}
17.7	0.42	3.42	2.16×10^{-1}
17.7	1.25	3.46	1.22×10^{-1}
17.7	2.68	2.42	1.65×10^{-2}
17.7	3.21	2.46	1.66×10^{-2}
17.7	3.73	2.56	1.70×10^{-2}
17.7	4.25	2.48	1.67×10^{-2}
17.7	4.25	2.57	3.53×10^{-2}
17.7	4.77	2.63	3.57×10^{-2}
17.7	5.31	2.60	3.55×10^{-2}
17.7	5.83	2.65	3.59×10^{-2}
17.7	6.03	2.65	3.66×10^{-2}
17.7	6.57	2.45	3.52×10^{-2}
17.7	7.11	2.14	3.30×10^{-2}
17.7	7.64	1.80	3.02×10^{-2}
17.7	8.31	1.15	1.40×10^{-2}
17.7	8.85	9.33×10^{-1}	1.26×10^{-2}
17.7	9.38	7.71×10^{-1}	1.14×10^{-2}
17.7	9.92	6.43×10^{-1}	1.04×10^{-2}
17.7	10.72	6.36×10^{-1}	1.18×10^{-2}
17.7	11.26	5.85×10^{-1}	1.13×10^{-2}
17.7	11.79	5.29×10^{-1}	1.08×10^{-2}
17.7	12.33	4.72×10^{-1}	1.02×10^{-2}
17.7	13.13	3.94×10^{-1}	9.04×10^{-3}
17.7	13.66	3.34×10^{-1}	8.32×10^{-3}

Table A.16: Continued.

E_x (MeV)	$\theta_{\text{c.m.}}$ (deg)	$d\sigma/d\Omega$ (mb/sr)	error (mb/sr)
17.7	15.53	1.71×10^{-1}	6.83×10^{-3}
17.7	16.07	1.40×10^{-1}	6.19×10^{-3}
17.7	16.60	1.31×10^{-1}	5.97×10^{-3}
17.7	17.13	1.08×10^{-1}	5.44×10^{-3}
17.7	17.93	6.09×10^{-2}	3.79×10^{-3}
17.7	18.47	4.79×10^{-2}	3.36×10^{-3}
17.7	19.00	4.02×10^{-2}	3.08×10^{-3}
17.7	19.53	3.77×10^{-2}	2.98×10^{-3}
17.7	20.33	3.33×10^{-2}	7.50×10^{-3}
17.7	20.86	2.67×10^{-2}	6.71×10^{-3}
17.7	21.39	5.01×10^{-3}	2.90×10^{-3}
17.7	21.92	1.51×10^{-2}	5.04×10^{-3}
17.7	22.72	1.10×10^{-2}	3.67×10^{-3}
17.7	23.25	4.87×10^{-3}	2.44×10^{-3}
17.7	23.78	8.54×10^{-3}	3.24×10^{-3}
17.7	24.31	6.11×10^{-3}	2.75×10^{-3}
17.7	25.11	4.47×10^{-3}	2.01×10^{-3}
17.7	25.64	3.58×10^{-3}	1.80×10^{-3}
17.7	26.16	4.48×10^{-3}	2.03×10^{-3}
17.7	26.69	3.59×10^{-3}	1.82×10^{-3}
17.9	0.42	3.47	2.16×10^{-1}
17.9	1.25	3.21	1.17×10^{-1}
17.9	2.68	2.46	1.66×10^{-2}
17.9	3.21	2.54	1.69×10^{-2}
17.9	3.73	2.70	1.74×10^{-2}
17.9	4.25	2.85	1.79×10^{-2}
17.9	4.25	2.65	3.58×10^{-2}
17.9	4.78	2.94	3.76×10^{-2}
17.9	5.31	3.01	3.81×10^{-2}

Table A.16: Continued.

E_x (MeV)	$\theta_{\text{c.m.}}$ (deg)	$d\sigma/d\Omega$ (mb/sr)	error (mb/sr)
17.9	6.57	2.62	3.65×10^{-2}
17.9	7.11	2.29	3.41×10^{-2}
17.9	7.64	1.85	3.06×10^{-2}
17.9	8.31	1.19	1.42×10^{-2}
17.9	8.85	9.95×10^{-1}	1.30×10^{-2}
17.9	9.38	8.51×10^{-1}	1.20×10^{-2}
17.9	9.92	7.35×10^{-1}	1.11×10^{-2}
17.9	10.72	6.20×10^{-1}	1.16×10^{-2}
17.9	11.26	5.68×10^{-1}	1.11×10^{-2}
17.9	11.79	5.04×10^{-1}	1.05×10^{-2}
17.9	12.33	4.38×10^{-1}	9.78×10^{-3}
17.9	13.13	3.97×10^{-1}	9.11×10^{-3}
17.9	13.67	3.34×10^{-1}	8.36×10^{-3}
17.9	14.20	2.82×10^{-1}	7.68×10^{-3}
17.9	14.73	2.33×10^{-1}	6.98×10^{-3}
17.9	15.54	1.79×10^{-1}	7.00×10^{-3}
17.9	16.07	1.58×10^{-1}	6.56×10^{-3}
17.9	16.60	1.35×10^{-1}	6.07×10^{-3}
17.9	17.14	8.55×10^{-2}	4.84×10^{-3}
17.9	17.94	6.86×10^{-2}	4.00×10^{-3}
17.9	18.47	4.59×10^{-2}	3.27×10^{-3}
17.9	19.00	3.84×10^{-2}	2.99×10^{-3}
17.9	19.53	3.64×10^{-2}	2.91×10^{-3}
17.9	20.33	2.68×10^{-2}	6.33×10^{-3}
17.9	20.86	2.53×10^{-2}	6.16×10^{-3}
17.9	21.40	1.34×10^{-2}	4.48×10^{-3}
17.9	21.93	8.95×10^{-3}	3.66×10^{-3}
17.9	22.72	9.08×10^{-3}	3.46×10^{-3}
17.9	23.25	3.90×10^{-3}	2.26×10^{-3}

Table A.16: Continued.

E_x (MeV)	$\theta_{\text{c.m.}}$ (deg)	$d\sigma/d\Omega$ (mb/sr)	error (mb/sr)
17.9	25.11	4.58×10^{-3}	1.74×10^{-3}
17.9	25.64	1.31×10^{-3}	9.30×10^{-4}
17.9	26.17	1.97×10^{-3}	1.14×10^{-3}
17.9	26.70	1.97×10^{-3}	1.14×10^{-3}
18.1	0.42	3.38	2.11×10^{-1}
18.1	1.25	3.46	1.21×10^{-1}
18.1	2.68	2.39	1.65×10^{-2}
18.1	3.21	2.51	1.69×10^{-2}
18.1	3.73	2.68	1.75×10^{-2}
18.1	4.25	2.79	1.79×10^{-2}
18.1	4.25	2.58	3.55×10^{-2}
18.1	4.78	2.92	3.77×10^{-2}
18.1	5.31	2.87	3.74×10^{-2}
18.1	5.83	2.84	3.72×10^{-2}
18.1	6.04	2.85	3.83×10^{-2}
18.1	6.57	2.59	3.65×10^{-2}
18.1	7.11	2.26	3.40×10^{-2}
18.1	7.64	1.80	3.04×10^{-2}
18.1	8.31	1.15	1.40×10^{-2}
18.1	8.85	9.03×10^{-1}	1.24×10^{-2}
18.1	9.39	7.75×10^{-1}	1.15×10^{-2}
18.1	9.92	6.97×10^{-1}	1.09×10^{-2}
18.1	10.72	5.83×10^{-1}	1.13×10^{-2}
18.1	11.26	5.28×10^{-1}	1.07×10^{-2}
18.1	11.79	4.85×10^{-1}	1.03×10^{-2}
18.1	12.33	4.17×10^{-1}	9.55×10^{-3}
18.1	13.13	3.69×10^{-1}	8.84×10^{-3}
18.1	13.67	3.06×10^{-1}	8.05×10^{-3}
18.1	14.20	2.70×10^{-1}	7.56×10^{-3}

Table A.16: Continued.

E_x (MeV)	$\theta_{\text{c.m.}}$ (deg)	$d\sigma/d\Omega$ (mb/sr)	error (mb/sr)
18.1	16.07	1.39×10^{-1}	6.15×10^{-3}
18.1	16.60	1.17×10^{-1}	5.64×10^{-3}
18.1	17.14	1.01×10^{-1}	5.24×10^{-3}
18.1	17.94	6.38×10^{-2}	3.85×10^{-3}
18.1	18.47	5.39×10^{-2}	3.54×10^{-3}
18.1	19.00	4.23×10^{-2}	3.14×10^{-3}
18.1	19.54	3.58×10^{-2}	2.89×10^{-3}
18.1	20.33	1.83×10^{-2}	5.10×10^{-3}
18.1	20.87	1.27×10^{-2}	4.24×10^{-3}
18.1	21.40	2.12×10^{-2}	5.49×10^{-3}
18.1	21.93	1.41×10^{-2}	4.48×10^{-3}
18.1	22.72	1.06×10^{-2}	3.54×10^{-3}
18.1	23.26	8.24×10^{-3}	3.12×10^{-3}
18.1	23.79	5.89×10^{-3}	2.64×10^{-3}
18.1	24.32	9.44×10^{-3}	3.35×10^{-3}
18.1	25.11	4.68×10^{-3}	1.93×10^{-3}
18.1	25.64	3.90×10^{-3}	1.76×10^{-3}
18.1	26.17	2.35×10^{-3}	1.36×10^{-3}
18.1	26.70	7.83×10^{-4}	7.88×10^{-4}
18.3	0.42	4.78	2.55×10^{-1}
18.3	1.25	3.96	1.30×10^{-1}
18.3	2.68	2.67	1.74×10^{-2}
18.3	3.21	2.68	1.75×10^{-2}
18.3	3.73	2.87	1.81×10^{-2}
18.3	4.25	2.95	1.84×10^{-2}
18.3	4.25	2.83	3.73×10^{-2}
18.3	4.78	2.96	3.82×10^{-2}
18.3	5.31	3.16	3.95×10^{-2}
18.3	5.84	3.07	3.90×10^{-2}

Table A.16: Continued.

E_x (MeV)	$\theta_{\text{c.m.}}$ (deg)	$d\sigma/d\Omega$ (mb/sr)	error (mb/sr)
18.3	7.11	2.45	3.57×10^{-2}
18.3	7.64	2.03	3.26×10^{-2}
18.3	8.31	1.21	1.45×10^{-2}
18.3	8.85	9.06×10^{-1}	1.25×10^{-2}
18.3	9.39	7.83×10^{-1}	1.16×10^{-2}
18.3	9.92	6.28×10^{-1}	1.04×10^{-2}
18.3	10.73	5.82×10^{-1}	1.14×10^{-2}
18.3	11.26	5.40×10^{-1}	1.10×10^{-2}
18.3	11.80	4.83×10^{-1}	1.04×10^{-2}
18.3	12.33	4.50×10^{-1}	1.00×10^{-2}
18.3	13.13	3.54×10^{-1}	8.67×10^{-3}
18.3	13.67	3.20×10^{-1}	8.25×10^{-3}
18.3	14.20	2.73×10^{-1}	7.62×10^{-3}
18.3	14.74	2.51×10^{-1}	7.29×10^{-3}
18.3	15.54	1.70×10^{-1}	6.84×10^{-3}
18.3	16.07	1.36×10^{-1}	6.11×10^{-3}
18.3	16.61	1.25×10^{-1}	5.85×10^{-3}
18.3	17.14	1.06×10^{-1}	5.41×10^{-3}
18.3	17.94	6.76×10^{-2}	3.95×10^{-3}
18.3	18.47	5.88×10^{-2}	3.68×10^{-3}
18.3	19.00	4.73×10^{-2}	3.31×10^{-3}
18.3	19.54	4.04×10^{-2}	3.06×10^{-3}
18.3	20.34	2.56×10^{-2}	6.04×10^{-3}
18.3	20.87	2.84×10^{-2}	6.37×10^{-3}
18.3	21.40	2.14×10^{-2}	5.52×10^{-3}
18.3	21.93	1.57×10^{-2}	4.73×10^{-3}
18.3	22.73	1.03×10^{-2}	3.45×10^{-3}
18.3	23.26	3.44×10^{-3}	1.99×10^{-3}
18.3	23.79	9.20×10^{-3}	3.26×10^{-3}

Table A.16: Continued.

E_x (MeV)	$\theta_{\text{c.m.}}$ (deg)	$d\sigma/d\Omega$ (mb/sr)	error (mb/sr)
18.3	25.64	3.07×10^{-3}	1.38×10^{-3}
18.3	26.17	2.46×10^{-3}	1.23×10^{-3}
18.3	26.70	2.46×10^{-3}	1.23×10^{-3}
18.5	0.42	4.43	2.46×10^{-1}
18.5	1.25	4.13	1.33×10^{-1}
18.5	2.68	2.84	1.80×10^{-2}
18.5	3.21	2.96	1.83×10^{-2}
18.5	3.73	3.20	1.91×10^{-2}
18.5	4.25	3.30	1.94×10^{-2}
18.5	4.25	3.25	3.99×10^{-2}
18.5	4.78	3.39	4.08×10^{-2}
18.5	5.31	3.55	4.18×10^{-2}
18.5	5.84	3.54	4.18×10^{-2}
18.5	6.04	3.46	4.22×10^{-2}
18.5	6.57	3.27	4.11×10^{-2}
18.5	7.11	2.82	3.82×10^{-2}
18.5	7.65	2.28	3.44×10^{-2}
18.5	8.32	1.38	1.54×10^{-2}
18.5	8.85	1.08	1.36×10^{-2}
18.5	9.39	8.60×10^{-1}	1.22×10^{-2}
18.5	9.92	6.97×10^{-1}	1.09×10^{-2}
18.5	10.73	5.94×10^{-1}	1.15×10^{-2}
18.5	11.26	5.47×10^{-1}	1.10×10^{-2}
18.5	11.80	5.07×10^{-1}	1.06×10^{-2}
18.5	12.33	4.42×10^{-1}	9.88×10^{-3}
18.5	13.13	3.72×10^{-1}	8.87×10^{-3}
18.5	13.67	3.19×10^{-1}	8.22×10^{-3}
18.5	14.20	2.74×10^{-1}	7.63×10^{-3}
18.5	14.74	2.27×10^{-1}	6.96×10^{-3}

Table A.16: Continued.

E_x (MeV)	$\theta_{\text{c.m.}}$ (deg)	$d\sigma/d\Omega$ (mb/sr)	error (mb/sr)
18.5	16.61	1.35×10^{-1}	6.14×10^{-3}
18.5	17.14	1.01×10^{-1}	5.33×10^{-3}
18.5	17.94	7.17×10^{-2}	4.14×10^{-3}
18.5	18.47	4.76×10^{-2}	3.38×10^{-3}
18.5	19.01	4.06×10^{-2}	3.12×10^{-3}
18.5	19.54	3.62×10^{-2}	2.94×10^{-3}
18.5	20.34	2.86×10^{-2}	6.59×10^{-3}
18.5	20.87	1.81×10^{-2}	5.24×10^{-3}
18.5	21.40	1.06×10^{-2}	4.00×10^{-3}
18.5	21.93	1.66×10^{-2}	5.03×10^{-3}
18.5	22.73	1.13×10^{-2}	3.79×10^{-3}
18.5	23.26	6.30×10^{-3}	2.83×10^{-3}
18.5	23.79	7.57×10^{-3}	3.10×10^{-3}
18.5	24.32	5.05×10^{-3}	2.53×10^{-3}
18.5	25.11	6.48×10^{-3}	2.31×10^{-3}
18.5	25.64	2.43×10^{-3}	1.42×10^{-3}
18.5	26.17	4.06×10^{-3}	1.83×10^{-3}
18.5	26.70	2.44×10^{-3}	1.42×10^{-3}
18.7	0.42	3.64	2.20×10^{-1}
18.7	1.25	3.41	1.19×10^{-1}
18.7	2.68	2.72	1.75×10^{-2}
18.7	3.21	2.96	1.83×10^{-2}
18.7	3.73	3.19	1.90×10^{-2}
18.7	4.25	3.54	2.00×10^{-2}
18.7	4.25	3.21	3.95×10^{-2}
18.7	4.78	3.60	4.18×10^{-2}
18.7	5.31	3.74	4.26×10^{-2}
18.7	5.84	3.57	4.17×10^{-2}
18.7	6.04	3.65	4.32×10^{-2}

Table A.16: Continued.

E_x (MeV)	$\theta_{\text{c.m.}}$ (deg)	$d\sigma/d\Omega$ (mb/sr)	error (mb/sr)
18.7	7.65	2.29	3.43×10^{-2}
18.7	8.32	1.40	1.55×10^{-2}
18.7	8.85	1.15	1.40×10^{-2}
18.7	9.39	9.05×10^{-1}	1.25×10^{-2}
18.7	9.92	7.59×10^{-1}	1.14×10^{-2}
18.7	10.73	5.67×10^{-1}	1.12×10^{-2}
18.7	11.26	5.34×10^{-1}	1.09×10^{-2}
18.7	11.80	4.78×10^{-1}	1.03×10^{-2}
18.7	12.33	4.46×10^{-1}	9.95×10^{-3}
18.7	13.14	3.42×10^{-1}	8.50×10^{-3}
18.7	13.67	3.08×10^{-1}	8.08×10^{-3}
18.7	14.20	2.68×10^{-1}	7.53×10^{-3}
18.7	14.74	2.25×10^{-1}	6.91×10^{-3}
18.7	15.54	1.63×10^{-1}	6.83×10^{-3}
18.7	16.07	1.38×10^{-1}	6.29×10^{-3}
18.7	16.61	1.12×10^{-1}	5.68×10^{-3}
18.7	17.14	1.12×10^{-1}	5.65×10^{-3}
18.7	17.94	5.74×10^{-2}	3.70×10^{-3}
18.7	18.47	4.78×10^{-2}	3.38×10^{-3}
18.7	19.01	3.91×10^{-2}	3.05×10^{-3}
18.7	19.54	3.83×10^{-2}	3.02×10^{-3}
18.7	20.34	2.20×10^{-2}	5.69×10^{-3}
18.7	20.87	1.61×10^{-2}	4.87×10^{-3}
18.7	21.40	2.35×10^{-2}	5.89×10^{-3}
18.7	21.93	1.76×10^{-2}	5.11×10^{-3}
18.7	22.73	4.44×10^{-3}	2.23×10^{-3}
18.7	23.26	1.00×10^{-2}	3.35×10^{-3}
18.7	23.79	1.11×10^{-2}	3.53×10^{-3}
18.7	24.32	6.69×10^{-3}	2.74×10^{-3}

Table A.16: Continued.

E_x (MeV)	$\theta_{\text{c.m.}}$ (deg)	$d\sigma/d\Omega$ (mb/sr)	error (mb/sr)
18.7	26.18	2.25×10^{-3}	1.30×10^{-3}
18.7	26.70	3.00×10^{-3}	1.51×10^{-3}
18.9	0.42	3.59	2.18×10^{-1}
18.9	1.25	3.72	1.25×10^{-1}
18.9	2.68	2.69	1.74×10^{-2}
18.9	3.21	2.79	1.77×10^{-2}
18.9	3.73	2.97	1.83×10^{-2}
18.9	4.25	3.25	1.91×10^{-2}
18.9	4.25	3.09	3.87×10^{-2}
18.9	4.78	3.32	4.01×10^{-2}
18.9	5.31	3.42	4.08×10^{-2}
18.9	5.84	3.32	4.02×10^{-2}
18.9	6.04	3.37	4.14×10^{-2}
18.9	6.57	2.98	3.90×10^{-2}
18.9	7.11	2.55	3.60×10^{-2}
18.9	7.65	2.05	3.23×10^{-2}
18.9	8.32	1.25	1.46×10^{-2}
18.9	8.85	9.58×10^{-1}	1.28×10^{-2}
18.9	9.39	7.75×10^{-1}	1.15×10^{-2}
18.9	9.92	6.44×10^{-1}	1.05×10^{-2}
18.9	10.73	5.89×10^{-1}	1.14×10^{-2}
18.9	11.26	5.49×10^{-1}	1.10×10^{-2}
18.9	11.80	5.24×10^{-1}	1.08×10^{-2}
18.9	12.33	4.70×10^{-1}	1.02×10^{-2}
18.9	13.14	3.78×10^{-1}	8.91×10^{-3}
18.9	13.67	3.30×10^{-1}	8.33×10^{-3}
18.9	14.21	2.79×10^{-1}	7.65×10^{-3}
18.9	14.74	2.60×10^{-1}	7.39×10^{-3}
18.9	15.54	1.70×10^{-1}	6.92×10^{-3}

Table A.16: Continued.

E_x (MeV)	$\theta_{\text{c.m.}}$ (deg)	$d\sigma/d\Omega$ (mb/sr)	error (mb/sr)
18.9	17.14	9.98×10^{-2}	5.31×10^{-3}
18.9	17.94	6.86×10^{-2}	4.02×10^{-3}
18.9	18.48	5.28×10^{-2}	3.53×10^{-3}
18.9	19.01	4.56×10^{-2}	3.28×10^{-3}
18.9	19.54	3.98×10^{-2}	3.06×10^{-3}
18.9	20.34	1.80×10^{-2}	5.21×10^{-3}
18.9	20.87	1.50×10^{-2}	4.76×10^{-3}
18.9	21.40	1.95×10^{-2}	5.43×10^{-3}
18.9	21.94	1.80×10^{-2}	5.22×10^{-3}
18.9	22.73	1.15×10^{-2}	3.85×10^{-3}
18.9	23.26	1.40×10^{-2}	4.26×10^{-3}
18.9	23.79	1.02×10^{-2}	3.64×10^{-3}
18.9	24.32	6.40×10^{-3}	2.87×10^{-3}
18.9	25.12	4.01×10^{-3}	1.64×10^{-3}
18.9	25.65	2.68×10^{-3}	1.35×10^{-3}
18.9	26.18	2.68×10^{-3}	1.35×10^{-3}
18.9	26.71	2.69×10^{-3}	1.35×10^{-3}
19.1	0.42	4.26	2.40×10^{-1}
19.1	1.25	4.01	1.31×10^{-1}
19.1	2.68	2.83	1.79×10^{-2}
19.1	3.21	2.90	1.81×10^{-2}
19.1	3.73	3.09	1.87×10^{-2}
19.1	4.25	3.30	1.93×10^{-2}
19.1	4.25	3.17	3.91×10^{-2}
19.1	4.78	3.42	4.06×10^{-2}
19.1	5.31	3.47	4.10×10^{-2}
19.1	5.84	3.49	4.11×10^{-2}
19.1	6.04	3.48	4.19×10^{-2}
19.1	6.57	3.24	4.04×10^{-2}

Table A.16: Continued.

E_x (MeV)	$\theta_{\text{c.m.}}$ (deg)	$d\sigma/d\Omega$ (mb/sr)	error (mb/sr)
19.1	8.32	1.31	1.49×10^{-2}
19.1	8.85	1.00	1.31×10^{-2}
19.1	9.39	8.14×10^{-1}	1.18×10^{-2}
19.1	9.93	6.87×10^{-1}	1.08×10^{-2}
19.1	10.73	6.06×10^{-1}	1.16×10^{-2}
19.1	11.26	5.82×10^{-1}	1.13×10^{-2}
19.1	11.80	5.49×10^{-1}	1.10×10^{-2}
19.1	12.33	4.95×10^{-1}	1.05×10^{-2}
19.1	13.14	3.99×10^{-1}	9.11×10^{-3}
19.1	13.67	3.50×10^{-1}	8.52×10^{-3}
19.1	14.21	2.89×10^{-1}	7.75×10^{-3}
19.1	14.74	2.62×10^{-1}	7.38×10^{-3}
19.1	15.54	1.68×10^{-1}	6.86×10^{-3}
19.1	16.08	1.48×10^{-1}	6.44×10^{-3}
19.1	16.61	1.34×10^{-1}	6.12×10^{-3}
19.1	17.14	9.39×10^{-2}	5.13×10^{-3}
19.1	17.94	6.10×10^{-2}	3.81×10^{-3}
19.1	18.48	5.61×10^{-2}	3.65×10^{-3}
19.1	19.01	5.32×10^{-2}	3.56×10^{-3}
19.1	19.54	3.51×10^{-2}	2.89×10^{-3}
19.1	20.34	3.02×10^{-2}	7.17×10^{-3}
19.1	20.87	1.85×10^{-2}	5.60×10^{-3}
19.1	21.41	8.42×10^{-3}	3.78×10^{-3}
19.1	21.94	1.85×10^{-2}	5.61×10^{-3}
19.1	22.73	5.50×10^{-3}	2.77×10^{-3}
19.1	23.27	5.50×10^{-3}	2.77×10^{-3}
19.1	23.80	4.13×10^{-3}	2.41×10^{-3}
19.1	24.33	4.14×10^{-3}	2.40×10^{-3}
19.1	25.12	3.68×10^{-3}	1.51×10^{-3}

Table A.16: Continued.

E_x (MeV)	$\theta_{\text{c.m.}}$ (deg)	$d\sigma/d\Omega$ (mb/sr)	error (mb/sr)
19.1	26.71	3.08×10^{-3}	1.38×10^{-3}
19.3	0.42	4.78	2.53×10^{-1}
19.3	1.25	4.55	1.39×10^{-1}
19.3	2.68	2.85	1.80×10^{-2}
19.3	3.21	2.90	1.81×10^{-2}
19.3	3.73	3.02	1.85×10^{-2}
19.3	4.25	3.24	1.91×10^{-2}
19.3	4.25	2.98	3.79×10^{-2}
19.3	4.78	3.32	4.00×10^{-2}
19.3	5.31	3.43	4.07×10^{-2}
19.3	5.84	3.32	4.00×10^{-2}
19.3	6.04	3.28	4.08×10^{-2}
19.3	6.58	3.09	3.95×10^{-2}
19.3	7.11	2.62	3.64×10^{-2}
19.3	7.65	2.10	3.26×10^{-2}
19.3	8.32	1.25	1.46×10^{-2}
19.3	8.85	9.75×10^{-1}	1.29×10^{-2}
19.3	9.39	8.08×10^{-1}	1.18×10^{-2}
19.3	9.93	6.92×10^{-1}	1.09×10^{-2}
19.3	10.73	5.69×10^{-1}	1.12×10^{-2}
19.3	11.27	5.61×10^{-1}	1.11×10^{-2}
19.3	11.80	5.30×10^{-1}	1.08×10^{-2}
19.3	12.34	4.81×10^{-1}	1.03×10^{-2}
19.3	13.14	4.06×10^{-1}	9.27×10^{-3}
19.3	13.67	3.53×10^{-1}	8.65×10^{-3}
19.3	14.21	3.09×10^{-1}	8.10×10^{-3}
19.3	14.74	2.56×10^{-1}	7.37×10^{-3}
19.3	15.54	1.75×10^{-1}	6.95×10^{-3}
19.3	16.08	1.51×10^{-1}	6.45×10^{-3}

Table A.16: Continued.

E_x (MeV)	$\theta_{\text{c.m.}}$ (deg)	$d\sigma/d\Omega$ (mb/sr)	error (mb/sr)
19.3	17.95	6.96×10^{-2}	4.02×10^{-3}
19.3	18.48	5.11×10^{-2}	3.45×10^{-3}
19.3	19.01	4.41×10^{-2}	3.20×10^{-3}
19.3	19.54	3.10×10^{-2}	2.69×10^{-3}
19.3	20.34	2.26×10^{-2}	5.67×10^{-3}
19.3	20.88	1.84×10^{-2}	5.12×10^{-3}
19.3	21.41	1.13×10^{-2}	4.02×10^{-3}
19.3	21.94	1.28×10^{-2}	4.27×10^{-3}
19.3	22.74	1.36×10^{-2}	4.88×10^{-3}
19.3	23.27	1.70×10^{-2}	5.44×10^{-3}
19.3	23.80	8.50×10^{-3}	3.85×10^{-3}
19.3	24.33	5.11×10^{-3}	2.98×10^{-3}
19.3	25.12	3.74×10^{-3}	1.68×10^{-3}
19.3	25.65	3.74×10^{-3}	1.68×10^{-3}
19.3	26.18	3.75×10^{-3}	1.68×10^{-3}
19.3	26.71	1.00×10^{-5}	1.00×10^{-5}
19.5	0.42	5.14	2.62×10^{-1}
19.5	1.25	4.52	1.38×10^{-1}
19.5	2.68	2.79	1.78×10^{-2}
19.5	3.21	2.76	1.76×10^{-2}
19.5	3.73	2.84	1.79×10^{-2}
19.5	4.25	3.04	1.85×10^{-2}
19.5	4.25	2.84	3.71×10^{-2}
19.5	4.78	3.06	3.85×10^{-2}
19.5	5.31	3.13	3.89×10^{-2}
19.5	5.84	3.11	3.88×10^{-2}
19.5	6.04	3.10	3.97×10^{-2}
19.5	6.58	2.88	3.83×10^{-2}
19.5	7.11	2.50	3.56×10^{-2}

Table A.16: Continued.

E_x (MeV)	$\theta_{\text{c.m.}}$ (deg)	$d\sigma/d\Omega$ (mb/sr)	error (mb/sr)
19.5	8.86	9.31×10^{-1}	1.26×10^{-2}
19.5	9.39	7.57×10^{-1}	1.14×10^{-2}
19.5	9.93	6.49×10^{-1}	1.05×10^{-2}
19.5	10.73	5.60×10^{-1}	1.11×10^{-2}
19.5	11.27	5.38×10^{-1}	1.09×10^{-2}
19.5	11.80	5.29×10^{-1}	1.08×10^{-2}
19.5	12.34	4.55×10^{-1}	1.00×10^{-2}
19.5	13.14	4.16×10^{-1}	9.41×10^{-3}
19.5	13.67	3.64×10^{-1}	8.79×10^{-3}
19.5	14.21	3.14×10^{-1}	8.17×10^{-3}
19.5	14.74	2.49×10^{-1}	7.28×10^{-3}
19.5	15.55	1.85×10^{-1}	7.19×10^{-3}
19.5	16.08	1.44×10^{-1}	6.37×10^{-3}
19.5	16.61	1.12×10^{-1}	5.62×10^{-3}
19.5	17.15	9.42×10^{-2}	5.14×10^{-3}
19.5	17.95	6.54×10^{-2}	3.96×10^{-3}
19.5	18.48	5.53×10^{-2}	3.64×10^{-3}
19.5	19.01	4.47×10^{-2}	3.27×10^{-3}
19.5	19.55	3.83×10^{-2}	3.03×10^{-3}
19.5	20.35	2.83×10^{-2}	6.52×10^{-3}
19.5	20.88	1.94×10^{-2}	5.40×10^{-3}
19.5	21.41	2.09×10^{-2}	5.60×10^{-3}
19.5	21.94	1.05×10^{-2}	3.96×10^{-3}
19.5	22.74	6.73×10^{-3}	2.76×10^{-3}
19.5	23.27	6.74×10^{-3}	2.76×10^{-3}
19.5	23.80	7.87×10^{-3}	2.98×10^{-3}
19.5	24.33	2.25×10^{-3}	1.60×10^{-3}
19.5	25.13	3.74×10^{-3}	1.53×10^{-3}
19.5	25.65	4.99×10^{-3}	1.77×10^{-3}

Table A.16: Continued.

E_x (MeV)	$\theta_{\text{c.m.}}$ (deg)	$d\sigma/d\Omega$ (mb/sr)	error (mb/sr)
19.7	0.42	4.87	2.55×10^{-1}
19.7	1.25	4.77	1.42×10^{-1}
19.7	2.68	2.84	1.79×10^{-2}
19.7	3.21	2.70	1.75×10^{-2}
19.7	3.73	2.68	1.74×10^{-2}
19.7	4.26	2.90	1.81×10^{-2}
19.7	4.26	2.64	3.57×10^{-2}
19.7	4.78	2.88	3.73×10^{-2}
19.7	5.32	3.03	3.82×10^{-2}
19.7	5.84	2.99	3.80×10^{-2}
19.7	6.04	2.95	3.86×10^{-2}
19.7	6.58	2.69	3.69×10^{-2}
19.7	7.11	2.36	3.46×10^{-2}
19.7	7.65	1.94	3.14×10^{-2}
19.7	8.32	1.12	1.38×10^{-2}
19.7	8.86	8.99×10^{-1}	1.23×10^{-2}
19.7	9.39	7.17×10^{-1}	1.10×10^{-2}
19.7	9.93	6.08×10^{-1}	1.02×10^{-2}
19.7	10.73	5.52×10^{-1}	1.11×10^{-2}
19.7	11.27	5.35×10^{-1}	1.09×10^{-2}
19.7	11.80	4.78×10^{-1}	1.03×10^{-2}
19.7	12.34	4.56×10^{-1}	1.01×10^{-2}
19.7	13.14	3.84×10^{-1}	9.09×10^{-3}
19.7	13.68	3.57×10^{-1}	8.77×10^{-3}
19.7	14.21	3.03×10^{-1}	8.08×10^{-3}
19.7	14.75	2.51×10^{-1}	7.36×10^{-3}
19.7	15.55	1.64×10^{-1}	6.67×10^{-3}
19.7	16.08	1.42×10^{-1}	6.20×10^{-3}
19.7	16.61	1.16×10^{-1}	5.60×10^{-3}

Table A.16: Continued.

E_x (MeV)	$\theta_{\text{c.m.}}$ (deg)	$d\sigma/d\Omega$ (mb/sr)	error (mb/sr)
19.7	18.48	4.89×10^{-2}	3.39×10^{-3}
19.7	19.02	4.43×10^{-2}	3.22×10^{-3}
19.7	19.55	3.73×10^{-2}	2.96×10^{-3}
19.7	20.35	4.17×10^{-2}	8.07×10^{-3}
19.7	20.88	2.48×10^{-2}	6.21×10^{-3}
19.7	21.41	1.55×10^{-2}	4.92×10^{-3}
19.7	21.94	1.24×10^{-2}	4.40×10^{-3}
19.7	22.74	1.62×10^{-2}	4.50×10^{-3}
19.7	23.27	1.37×10^{-2}	4.15×10^{-3}
19.7	23.80	1.37×10^{-2}	4.15×10^{-3}
19.7	24.33	7.49×10^{-3}	3.07×10^{-3}
19.7	25.13	3.98×10^{-3}	1.79×10^{-3}
19.7	25.66	3.19×10^{-3}	1.61×10^{-3}
19.7	26.19	3.99×10^{-3}	1.80×10^{-3}
19.7	26.72	4.00×10^{-3}	1.80×10^{-3}
19.9	0.42	5.47	2.72×10^{-1}
19.9	1.25	4.90	1.44×10^{-1}
19.9	2.69	2.91	1.82×10^{-2}
19.9	3.21	2.71	1.75×10^{-2}
19.9	3.73	2.69	1.75×10^{-2}
19.9	4.26	2.78	1.77×10^{-2}
19.9	4.26	2.53	3.49×10^{-2}
19.9	4.78	2.79	3.67×10^{-2}
19.9	5.32	2.87	3.72×10^{-2}
19.9	5.84	2.94	3.77×10^{-2}
19.9	6.04	2.95	3.86×10^{-2}
19.9	6.58	2.71	3.70×10^{-2}
19.9	7.11	2.35	3.44×10^{-2}
19.9	7.65	1.91	3.10×10^{-2}

Table A.16: Continued.

E_x (MeV)	$\theta_{\text{c.m.}}$ (deg)	$d\sigma/d\Omega$ (mb/sr)	error (mb/sr)
19.9	9.39	7.24×10^{-1}	1.11×10^{-2}
19.9	9.93	6.13×10^{-1}	1.02×10^{-2}
19.9	10.73	5.49×10^{-1}	1.10×10^{-2}
19.9	11.27	4.94×10^{-1}	1.04×10^{-2}
19.9	11.80	4.56×10^{-1}	1.00×10^{-2}
19.9	12.34	4.29×10^{-1}	9.71×10^{-3}
19.9	13.14	3.65×10^{-1}	8.80×10^{-3}
19.9	13.68	3.26×10^{-1}	8.32×10^{-3}
19.9	14.21	2.80×10^{-1}	7.70×10^{-3}
19.9	14.75	2.32×10^{-1}	7.01×10^{-3}
19.9	15.55	1.75×10^{-1}	7.00×10^{-3}
19.9	16.08	1.54×10^{-1}	6.58×10^{-3}
19.9	16.62	1.16×10^{-1}	5.71×10^{-3}
19.9	17.15	9.70×10^{-2}	5.22×10^{-3}
19.9	17.95	5.65×10^{-2}	3.65×10^{-3}
19.9	18.48	4.82×10^{-2}	3.37×10^{-3}
19.9	19.02	3.45×10^{-2}	2.86×10^{-3}
19.9	19.55	3.19×10^{-2}	2.74×10^{-3}
19.9	20.35	2.83×10^{-2}	6.51×10^{-3}
19.9	20.88	2.53×10^{-2}	6.15×10^{-3}
19.9	21.41	2.09×10^{-2}	5.59×10^{-3}
19.9	21.94	1.49×10^{-2}	4.73×10^{-3}
19.9	22.74	1.04×10^{-2}	3.98×10^{-3}
19.9	23.27	8.94×10^{-3}	3.70×10^{-3}
19.9	23.80	5.97×10^{-3}	3.02×10^{-3}
19.9	24.33	1.00×10^{-5}	1.00×10^{-5}
19.9	25.13	4.60×10^{-3}	1.75×10^{-3}
19.9	25.66	3.95×10^{-3}	1.62×10^{-3}
19.9	26.19	3.30×10^{-3}	1.48×10^{-3}

Table A.16: Continued.

E_x (MeV)	$\theta_{\text{c.m.}}$ (deg)	$d\sigma/d\Omega$ (mb/sr)	error (mb/sr)
20.1	2.69	2.84	1.80×10^{-2}
20.1	3.21	2.65	1.73×10^{-2}
20.1	3.73	2.54	1.70×10^{-2}
20.1	4.26	2.67	1.74×10^{-2}
20.1	4.26	2.44	3.44×10^{-2}
20.1	4.78	2.69	3.61×10^{-2}
20.1	5.32	2.74	3.64×10^{-2}
20.1	5.84	2.83	3.70×10^{-2}
20.1	6.04	2.70	3.70×10^{-2}
20.1	6.58	2.58	3.62×10^{-2}
20.1	7.11	2.21	3.36×10^{-2}
20.1	7.65	1.85	3.06×10^{-2}
20.1	8.32	1.11	1.37×10^{-2}
20.1	8.86	8.98×10^{-1}	1.23×10^{-2}
20.1	9.39	7.19×10^{-1}	1.10×10^{-2}
20.1	9.93	6.08×10^{-1}	1.02×10^{-2}
20.1	10.73	4.96×10^{-1}	1.05×10^{-2}
20.1	11.27	4.59×10^{-1}	1.01×10^{-2}
20.1	11.80	4.37×10^{-1}	9.82×10^{-3}
20.1	12.34	3.84×10^{-1}	9.21×10^{-3}
20.1	13.14	3.44×10^{-1}	8.60×10^{-3}
20.1	13.68	3.08×10^{-1}	8.14×10^{-3}
20.1	14.21	2.58×10^{-1}	7.45×10^{-3}
20.1	14.75	2.15×10^{-1}	6.81×10^{-3}
20.1	15.55	1.46×10^{-1}	6.42×10^{-3}
20.1	16.08	1.27×10^{-1}	5.98×10^{-3}
20.1	16.62	1.11×10^{-1}	5.59×10^{-3}
20.1	17.15	8.27×10^{-2}	4.83×10^{-3}
20.1	17.95	5.15×10^{-2}	3.50×10^{-3}

Table A.16: Continued.

E_x (MeV)	$\theta_{\text{c.m.}}$ (deg)	$d\sigma/d\Omega$ (mb/sr)	error (mb/sr)
20.1	19.55	2.84×10^{-2}	2.60×10^{-3}
20.1	20.35	3.13×10^{-2}	6.69×10^{-3}
20.1	20.88	1.71×10^{-2}	4.94×10^{-3}
20.1	21.41	1.57×10^{-2}	4.73×10^{-3}
20.1	21.95	1.85×10^{-2}	5.15×10^{-3}
20.1	22.74	1.40×10^{-2}	4.49×10^{-3}
20.1	23.27	8.39×10^{-3}	3.45×10^{-3}
20.1	23.81	4.20×10^{-3}	2.45×10^{-3}
20.1	24.34	8.41×10^{-3}	3.48×10^{-3}
20.1	25.13	5.97×10^{-3}	2.13×10^{-3}
20.1	25.66	4.48×10^{-3}	1.85×10^{-3}
20.1	26.19	4.49×10^{-3}	1.84×10^{-3}
20.1	26.72	1.50×10^{-3}	1.06×10^{-3}
20.3	0.42	5.91	2.82×10^{-1}
20.3	1.25	5.41	1.52×10^{-1}
20.3	2.69	2.78	1.78×10^{-2}
20.3	3.21	2.49	1.68×10^{-2}
20.3	3.73	2.37	1.64×10^{-2}
20.3	4.26	2.43	1.66×10^{-2}
20.3	4.26	2.27	3.31×10^{-2}
20.3	4.78	2.46	3.44×10^{-2}
20.3	5.32	2.52	3.49×10^{-2}
20.3	5.84	2.53	3.49×10^{-2}
20.3	6.04	2.47	3.54×10^{-2}
20.3	6.58	2.33	3.45×10^{-2}
20.3	7.11	2.08	3.26×10^{-2}
20.3	7.65	1.64	2.89×10^{-2}
20.3	8.32	9.83×10^{-1}	1.30×10^{-2}
20.3	8.86	8.15×10^{-1}	1.18×10^{-2}

Table A.16: Continued.

E_x (MeV)	$\theta_{\text{c.m.}}$ (deg)	$d\sigma/d\Omega$ (mb/sr)	error (mb/sr)
20.3	10.73	4.64×10^{-1}	1.01×10^{-2}
20.3	11.27	4.23×10^{-1}	9.65×10^{-3}
20.3	11.81	4.11×10^{-1}	9.52×10^{-3}
20.3	12.34	3.78×10^{-1}	9.14×10^{-3}
20.3	13.14	2.90×10^{-1}	7.85×10^{-3}
20.3	13.68	2.76×10^{-1}	7.66×10^{-3}
20.3	14.21	2.34×10^{-1}	7.05×10^{-3}
20.3	14.75	1.92×10^{-1}	6.38×10^{-3}
20.3	15.55	1.43×10^{-1}	6.34×10^{-3}
20.3	16.09	1.20×10^{-1}	5.81×10^{-3}
20.3	16.62	9.51×10^{-2}	5.17×10^{-3}
20.3	17.15	7.94×10^{-2}	4.73×10^{-3}
20.3	17.95	4.55×10^{-2}	3.28×10^{-3}
20.3	18.49	4.60×10^{-2}	3.29×10^{-3}
20.3	19.02	3.76×10^{-2}	2.98×10^{-3}
20.3	19.55	2.86×10^{-2}	2.59×10^{-3}
20.3	20.35	1.75×10^{-2}	4.87×10^{-3}
20.3	20.88	1.35×10^{-2}	4.28×10^{-3}
20.3	21.42	1.49×10^{-2}	4.49×10^{-3}
20.3	21.95	1.35×10^{-2}	4.30×10^{-3}
20.3	22.75	2.46×10^{-3}	1.74×10^{-3}
20.3	23.28	7.37×10^{-3}	3.03×10^{-3}
20.3	23.81	9.84×10^{-3}	3.50×10^{-3}
20.3	24.34	3.70×10^{-3}	2.14×10^{-3}
20.3	25.13	2.68×10^{-3}	1.35×10^{-3}
20.3	25.66	1.34×10^{-3}	9.53×10^{-4}
20.3	26.19	3.36×10^{-3}	1.51×10^{-3}
20.3	26.72	1.00×10^{-5}	1.00×10^{-5}
20.5	0.42	6.31	2.94×10^{-1}

Table A.16: Continued.

E_x (MeV)	$\theta_{\text{c.m.}}$ (deg)	$d\sigma/d\Omega$ (mb/sr)	error (mb/sr)
20.5	3.21	2.41	1.65×10^{-2}
20.5	3.73	2.27	1.61×10^{-2}
20.5	4.26	2.26	1.60×10^{-2}
20.5	4.26	2.13	3.22×10^{-2}
20.5	4.78	2.26	3.31×10^{-2}
20.5	5.32	2.35	3.38×10^{-2}
20.5	5.84	2.25	3.31×10^{-2}
20.5	6.04	2.26	3.40×10^{-2}
20.5	6.58	2.14	3.31×10^{-2}
20.5	7.12	1.89	3.12×10^{-2}
20.5	7.65	1.52	2.79×10^{-2}
20.5	8.32	8.99×10^{-1}	1.24×10^{-2}
20.5	8.86	7.63×10^{-1}	1.14×10^{-2}
20.5	9.39	5.96×10^{-1}	1.01×10^{-2}
20.5	9.93	5.01×10^{-1}	9.27×10^{-3}
20.5	10.74	4.31×10^{-1}	9.79×10^{-3}
20.5	11.27	4.54×10^{-1}	1.00×10^{-2}
20.5	11.81	3.98×10^{-1}	9.41×10^{-3}
20.5	12.34	3.70×10^{-1}	9.09×10^{-3}
20.5	13.15	3.10×10^{-1}	8.13×10^{-3}
20.5	13.68	2.69×10^{-1}	7.58×10^{-3}
20.5	14.22	2.28×10^{-1}	6.98×10^{-3}
20.5	14.75	1.98×10^{-1}	6.51×10^{-3}
20.5	15.55	1.28×10^{-1}	6.06×10^{-3}
20.5	16.09	1.11×10^{-1}	5.64×10^{-3}
20.5	16.62	9.86×10^{-2}	5.32×10^{-3}
20.5	17.15	8.06×10^{-2}	4.81×10^{-3}
20.5	17.96	4.74×10^{-2}	3.38×10^{-3}
20.5	18.49	4.30×10^{-2}	3.21×10^{-3}

Table A.16: Continued.

E_x (MeV)	$\theta_{\text{c.m.}}$ (deg)	$d\sigma/d\Omega$ (mb/sr)	error (mb/sr)
20.5	20.35	1.17×10^{-2}	4.42×10^{-3}
20.5	20.89	1.83×10^{-2}	5.55×10^{-3}
20.5	21.42	1.50×10^{-2}	5.02×10^{-3}
20.5	21.95	5.01×10^{-3}	2.90×10^{-3}
20.5	22.75	8.70×10^{-3}	3.31×10^{-3}
20.5	23.28	3.73×10^{-3}	2.17×10^{-3}
20.5	23.81	9.97×10^{-3}	3.55×10^{-3}
20.5	24.34	1.25×10^{-3}	1.25×10^{-3}
20.5	25.14	1.88×10^{-3}	1.34×10^{-3}
20.5	25.67	5.64×10^{-3}	2.32×10^{-3}
20.5	26.19	9.41×10^{-4}	9.51×10^{-4}
20.5	26.72	4.71×10^{-3}	2.14×10^{-3}
20.7	0.42	5.85	2.81×10^{-1}
20.7	1.25	5.34	1.51×10^{-1}
20.7	2.69	2.66	1.74×10^{-2}
20.7	3.21	2.36	1.64×10^{-2}
20.7	3.73	2.19	1.58×10^{-2}
20.7	4.26	2.17	1.58×10^{-2}
20.7	4.26	1.99	3.13×10^{-2}
20.7	4.78	2.21	3.29×10^{-2}
20.7	5.32	2.23	3.31×10^{-2}
20.7	5.84	2.14	3.24×10^{-2}
20.7	6.04	2.15	3.33×10^{-2}
20.7	6.58	2.02	3.22×10^{-2}
20.7	7.12	1.67	2.93×10^{-2}
20.7	7.65	1.41	2.70×10^{-2}
20.7	8.32	8.42×10^{-1}	1.21×10^{-2}
20.7	8.86	6.85×10^{-1}	1.09×10^{-2}
20.7	9.40	5.55×10^{-1}	9.80×10^{-3}

Table A.16: Continued.

E_x (MeV)	$\theta_{\text{c.m.}}$ (deg)	$d\sigma/d\Omega$ (mb/sr)	error (mb/sr)
20.7	11.27	4.55×10^{-1}	1.01×10^{-2}
20.7	11.81	4.22×10^{-1}	9.69×10^{-3}
20.7	12.34	4.07×10^{-1}	9.51×10^{-3}
20.7	13.15	3.31×10^{-1}	8.37×10^{-3}
20.7	13.68	3.11×10^{-1}	8.11×10^{-3}
20.7	14.22	2.43×10^{-1}	7.18×10^{-3}
20.7	14.75	2.12×10^{-1}	6.71×10^{-3}
20.7	15.55	1.21×10^{-1}	5.88×10^{-3}
20.7	16.09	1.21×10^{-1}	5.86×10^{-3}
20.7	16.62	1.06×10^{-1}	5.47×10^{-3}
20.7	17.16	8.88×10^{-2}	5.02×10^{-3}
20.7	17.96	4.94×10^{-2}	3.43×10^{-3}
20.7	18.49	4.24×10^{-2}	3.17×10^{-3}
20.7	19.02	3.19×10^{-2}	2.76×10^{-3}
20.7	19.56	2.43×10^{-2}	2.41×10^{-3}
20.7	20.36	2.29×10^{-2}	5.93×10^{-3}
20.7	20.89	1.37×10^{-2}	4.60×10^{-3}
20.7	21.42	9.17×10^{-3}	3.75×10^{-3}
20.7	21.95	1.99×10^{-2}	5.54×10^{-3}
20.7	22.75	9.50×10^{-3}	3.37×10^{-3}
20.7	23.28	1.07×10^{-2}	3.58×10^{-3}
20.7	23.81	7.14×10^{-3}	2.93×10^{-3}
20.7	24.34	5.96×10^{-3}	2.68×10^{-3}
20.7	25.14	2.91×10^{-3}	1.47×10^{-3}
20.7	25.67	3.64×10^{-3}	1.64×10^{-3}
20.7	26.20	1.46×10^{-3}	1.04×10^{-3}
20.7	26.73	2.19×10^{-3}	1.28×10^{-3}
20.9	0.42	5.61	2.73×10^{-1}
20.9	1.25	4.84	1.43×10^{-1}

Table A.16: Continued.

E_x (MeV)	$\theta_{\text{c.m.}}$ (deg)	$d\sigma/d\Omega$ (mb/sr)	error (mb/sr)
20.9	3.73	2.12	1.56×10^{-2}
20.9	4.26	2.13	1.57×10^{-2}
20.9	4.26	1.99	3.11×10^{-2}
20.9	4.78	2.07	3.18×10^{-2}
20.9	5.32	2.14	3.23×10^{-2}
20.9	5.84	2.11	3.20×10^{-2}
20.9	6.04	2.04	3.25×10^{-2}
20.9	6.58	1.98	3.19×10^{-2}
20.9	7.12	1.65	2.92×10^{-2}
20.9	7.65	1.38	2.68×10^{-2}
20.9	8.32	8.07×10^{-1}	1.18×10^{-2}
20.9	8.86	6.67×10^{-1}	1.07×10^{-2}
20.9	9.40	5.77×10^{-1}	9.97×10^{-3}
20.9	9.93	4.89×10^{-1}	9.18×10^{-3}
20.9	10.74	5.09×10^{-1}	1.05×10^{-2}
20.9	11.27	4.95×10^{-1}	1.04×10^{-2}
20.9	11.81	4.60×10^{-1}	1.00×10^{-2}
20.9	12.34	4.21×10^{-1}	9.60×10^{-3}
20.9	13.15	3.68×10^{-1}	8.83×10^{-3}
20.9	13.68	3.10×10^{-1}	8.12×10^{-3}
20.9	14.22	2.80×10^{-1}	7.70×10^{-3}
20.9	14.75	2.36×10^{-1}	7.08×10^{-3}
20.9	15.55	1.53×10^{-1}	6.59×10^{-3}
20.9	16.09	1.15×10^{-1}	5.72×10^{-3}
20.9	16.62	1.00×10^{-1}	5.34×10^{-3}
20.9	17.16	8.55×10^{-2}	4.92×10^{-3}
20.9	17.96	4.47×10^{-2}	3.27×10^{-3}
20.9	18.49	4.16×10^{-2}	3.15×10^{-3}
20.9	19.02	3.64×10^{-2}	2.95×10^{-3}

Table A.16: Continued.

E_x (MeV)	$\theta_{\text{c.m.}}$ (deg)	$d\sigma/d\Omega$ (mb/sr)	error (mb/sr)
20.9	20.89	1.93×10^{-2}	5.61×10^{-3}
20.9	21.42	1.61×10^{-2}	5.12×10^{-3}
20.9	21.95	1.13×10^{-2}	4.28×10^{-3}
20.9	22.75	5.73×10^{-3}	2.88×10^{-3}
20.9	23.28	1.29×10^{-2}	4.34×10^{-3}
20.9	23.81	4.30×10^{-3}	2.50×10^{-3}
20.9	24.34	7.18×10^{-3}	3.25×10^{-3}
20.9	25.14	9.08×10^{-3}	3.28×10^{-3}
20.9	25.67	7.96×10^{-3}	3.12×10^{-3}
20.9	26.20	1.14×10^{-3}	1.16×10^{-3}
20.9	26.73	4.56×10^{-3}	2.34×10^{-3}
21.1	0.42	5.85	2.81×10^{-1}
21.1	1.25	4.90	1.44×10^{-1}
21.1	2.69	2.55	1.71×10^{-2}
21.1	3.21	2.25	1.61×10^{-2}
21.1	3.73	2.15	1.57×10^{-2}
21.1	4.26	2.08	1.55×10^{-2}
21.1	4.26	1.96	3.11×10^{-2}
21.1	4.78	2.02	3.16×10^{-2}
21.1	5.32	2.08	3.21×10^{-2}
21.1	5.84	2.07	3.21×10^{-2}
21.1	6.04	1.95	3.17×10^{-2}
21.1	6.58	1.86	3.09×10^{-2}
21.1	7.12	1.62	2.89×10^{-2}
21.1	7.65	1.38	2.66×10^{-2}
21.1	8.32	8.56×10^{-1}	1.21×10^{-2}
21.1	8.86	7.41×10^{-1}	1.13×10^{-2}
21.1	9.40	6.03×10^{-1}	1.02×10^{-2}
21.1	9.93	5.28×10^{-1}	9.52×10^{-3}

Table A.16: Continued.

E_x (MeV)	$\theta_{\text{c.m.}}$ (deg)	$d\sigma/d\Omega$ (mb/sr)	error (mb/sr)
21.1	11.81	4.83×10^{-1}	1.03×10^{-2}
21.1	12.35	4.46×10^{-1}	9.91×10^{-3}
21.1	13.15	3.72×10^{-1}	8.88×10^{-3}
21.1	13.68	3.29×10^{-1}	8.36×10^{-3}
21.1	14.22	2.81×10^{-1}	7.72×10^{-3}
21.1	14.75	2.41×10^{-1}	7.16×10^{-3}
21.1	15.56	1.61×10^{-1}	6.72×10^{-3}
21.1	16.09	1.48×10^{-1}	6.44×10^{-3}
21.1	16.62	1.14×10^{-1}	5.66×10^{-3}
21.1	17.16	8.77×10^{-2}	4.96×10^{-3}
21.1	17.96	5.38×10^{-2}	3.58×10^{-3}
21.1	18.49	4.75×10^{-2}	3.37×10^{-3}
21.1	19.03	3.93×10^{-2}	3.06×10^{-3}
21.1	19.56	3.08×10^{-2}	2.71×10^{-3}
21.1	20.36	1.98×10^{-2}	5.31×10^{-3}
21.1	20.89	1.42×10^{-2}	4.49×10^{-3}
21.1	21.42	9.94×10^{-3}	3.76×10^{-3}
21.1	21.96	1.85×10^{-2}	5.14×10^{-3}
21.1	22.75	7.67×10^{-3}	2.90×10^{-3}
21.1	23.28	7.68×10^{-3}	2.91×10^{-3}
21.1	23.82	3.29×10^{-3}	1.91×10^{-3}
21.1	24.35	7.70×10^{-3}	2.91×10^{-3}
21.1	25.14	4.94×10^{-3}	1.88×10^{-3}
21.1	25.67	4.95×10^{-3}	1.88×10^{-3}
21.1	26.20	2.13×10^{-3}	1.23×10^{-3}
21.1	26.73	1.42×10^{-3}	1.01×10^{-3}
21.3	0.42	5.24	2.68×10^{-1}
21.3	1.25	4.58	1.41×10^{-1}
21.3	2.69	2.51	1.70×10^{-2}

Table A.16: Continued.

E_x (MeV)	$\theta_{\text{c.m.}}$ (deg)	$d\sigma/d\Omega$ (mb/sr)	error (mb/sr)
21.3	4.26	2.16	1.58×10^{-2}
21.3	4.26	2.03	3.17×10^{-2}
21.3	4.78	1.98	3.14×10^{-2}
21.3	5.32	2.05	3.19×10^{-2}
21.3	5.84	2.09	3.23×10^{-2}
21.3	6.04	2.09	3.29×10^{-2}
21.3	6.58	2.00	3.21×10^{-2}
21.3	7.12	1.74	3.00×10^{-2}
21.3	7.65	1.43	2.71×10^{-2}
21.3	8.33	9.01×10^{-1}	1.25×10^{-2}
21.3	8.86	7.91×10^{-1}	1.17×10^{-2}
21.3	9.40	6.58×10^{-1}	1.07×10^{-2}
21.3	9.93	5.59×10^{-1}	9.84×10^{-3}
21.3	10.74	5.72×10^{-1}	1.13×10^{-2}
21.3	11.27	5.35×10^{-1}	1.09×10^{-2}
21.3	11.81	5.53×10^{-1}	1.11×10^{-2}
21.3	12.35	5.02×10^{-1}	1.06×10^{-2}
21.3	13.15	3.92×10^{-1}	9.14×10^{-3}
21.3	13.68	3.47×10^{-1}	8.59×10^{-3}
21.3	14.22	3.00×10^{-1}	7.99×10^{-3}
21.3	14.76	2.49×10^{-1}	7.28×10^{-3}
21.3	15.56	1.52×10^{-1}	6.52×10^{-3}
21.3	16.09	1.42×10^{-1}	6.29×10^{-3}
21.3	16.63	1.15×10^{-1}	5.67×10^{-3}
21.3	17.16	9.45×10^{-2}	5.13×10^{-3}
21.3	17.96	6.26×10^{-2}	3.90×10^{-3}
21.3	18.49	4.71×10^{-2}	3.38×10^{-3}
21.3	19.03	4.24×10^{-2}	3.21×10^{-3}
21.3	19.56	3.54×10^{-2}	2.93×10^{-3}

Table A.16: Continued.

E_x (MeV)	$\theta_{\text{c.m.}}$ (deg)	$d\sigma/d\Omega$ (mb/sr)	error (mb/sr)
21.3	21.43	3.10×10^{-2}	7.15×10^{-3}
21.3	21.96	1.63×10^{-2}	5.19×10^{-3}
21.3	22.75	3.95×10^{-3}	2.29×10^{-3}
21.3	23.29	5.27×10^{-3}	2.65×10^{-3}
21.3	23.82	5.28×10^{-3}	2.65×10^{-3}
21.3	24.35	3.96×10^{-3}	2.30×10^{-3}
21.3	25.14	3.74×10^{-3}	1.68×10^{-3}
21.3	25.67	3.00×10^{-3}	1.50×10^{-3}
21.3	26.20	5.25×10^{-3}	2.00×10^{-3}
21.3	26.73	2.25×10^{-3}	1.31×10^{-3}
21.5	0.42	4.89	2.57×10^{-1}
21.5	1.25	4.79	1.43×10^{-1}
21.5	2.69	2.62	1.74×10^{-2}
21.5	3.21	2.41	1.67×10^{-2}
21.5	3.73	2.29	1.63×10^{-2}
21.5	4.26	2.27	1.62×10^{-2}
21.5	4.26	2.18	3.29×10^{-2}
21.5	4.78	2.20	3.30×10^{-2}
21.5	5.32	2.18	3.30×10^{-2}
21.5	5.84	2.19	3.30×10^{-2}
21.5	6.04	2.15	3.35×10^{-2}
21.5	6.58	2.06	3.26×10^{-2}
21.5	7.12	1.83	3.07×10^{-2}
21.5	7.65	1.46	2.75×10^{-2}
21.5	8.33	9.38×10^{-1}	1.27×10^{-2}
21.5	8.86	8.04×10^{-1}	1.18×10^{-2}
21.5	9.40	6.76×10^{-1}	1.08×10^{-2}
21.5	9.94	6.15×10^{-1}	1.03×10^{-2}
21.5	10.74	5.91×10^{-1}	1.15×10^{-2}

Table A.16: Continued.

E_x (MeV)	$\theta_{\text{c.m.}}$ (deg)	$d\sigma/d\Omega$ (mb/sr)	error (mb/sr)
21.5	12.35	4.80×10^{-1}	1.04×10^{-2}
21.5	13.15	4.17×10^{-1}	9.51×10^{-3}
21.5	13.69	3.74×10^{-1}	9.01×10^{-3}
21.5	14.22	3.13×10^{-1}	8.24×10^{-3}
21.5	14.76	2.56×10^{-1}	7.45×10^{-3}
21.5	15.56	1.76×10^{-1}	6.95×10^{-3}
21.5	16.09	1.62×10^{-1}	6.67×10^{-3}
21.5	16.63	1.22×10^{-1}	5.78×10^{-3}
21.5	17.16	1.04×10^{-1}	5.36×10^{-3}
21.5	17.96	5.84×10^{-2}	3.74×10^{-3}
21.5	18.50	5.42×10^{-2}	3.60×10^{-3}
21.5	19.03	3.87×10^{-2}	3.05×10^{-3}
21.5	19.56	4.04×10^{-2}	3.11×10^{-3}
21.5	20.36	2.25×10^{-2}	5.63×10^{-3}
21.5	20.89	1.97×10^{-2}	5.28×10^{-3}
21.5	21.43	1.55×10^{-2}	4.68×10^{-3}
21.5	21.96	1.69×10^{-2}	4.89×10^{-3}
21.5	22.76	1.06×10^{-2}	4.04×10^{-3}
21.5	23.29	9.08×10^{-3}	3.74×10^{-3}
21.5	23.82	7.58×10^{-3}	3.41×10^{-3}
21.5	24.35	1.06×10^{-2}	4.05×10^{-3}
21.5	25.15	3.66×10^{-3}	1.65×10^{-3}
21.5	25.68	7.33×10^{-3}	2.34×10^{-3}
21.5	26.21	4.41×10^{-3}	1.81×10^{-3}
21.5	26.74	1.47×10^{-3}	1.04×10^{-3}
21.7	0.42	5.09	2.62×10^{-1}
21.7	1.25	4.55	1.39×10^{-1}
21.7	2.69	2.73	1.78×10^{-2}
21.7	3.21	2.59	1.73×10^{-2}

Table A.16: Continued.

E_x (MeV)	$\theta_{\text{c.m.}}$ (deg)	$d\sigma/d\Omega$ (mb/sr)	error (mb/sr)
21.7	4.26	2.29	3.39×10^{-2}
21.7	4.78	2.30	3.39×10^{-2}
21.7	5.32	2.42	3.48×10^{-2}
21.7	5.84	2.27	3.38×10^{-2}
21.7	6.04	2.30	3.46×10^{-2}
21.7	6.58	2.14	3.34×10^{-2}
21.7	7.12	1.88	3.13×10^{-2}
21.7	7.66	1.58	2.87×10^{-2}
21.7	8.33	1.01	1.33×10^{-2}
21.7	8.86	8.66×10^{-1}	1.23×10^{-2}
21.7	9.40	7.38×10^{-1}	1.13×10^{-2}
21.7	9.94	6.17×10^{-1}	1.04×10^{-2}
21.7	10.74	6.01×10^{-1}	1.16×10^{-2}
21.7	11.28	5.62×10^{-1}	1.13×10^{-2}
21.7	11.81	5.15×10^{-1}	1.08×10^{-2}
21.7	12.35	4.76×10^{-1}	1.04×10^{-2}
21.7	13.15	3.79×10^{-1}	9.04×10^{-3}
21.7	13.69	3.56×10^{-1}	8.76×10^{-3}
21.7	14.22	2.94×10^{-1}	7.96×10^{-3}
21.7	14.76	2.59×10^{-1}	7.47×10^{-3}
21.7	15.56	1.80×10^{-1}	7.13×10^{-3}
21.7	16.09	1.46×10^{-1}	6.42×10^{-3}
21.7	16.63	1.22×10^{-1}	5.86×10^{-3}
21.7	17.16	1.09×10^{-1}	5.54×10^{-3}
21.7	17.96	5.54×10^{-2}	3.65×10^{-3}
21.7	18.50	5.46×10^{-2}	3.62×10^{-3}
21.7	19.03	4.26×10^{-2}	3.20×10^{-3}
21.7	19.56	4.14×10^{-2}	3.15×10^{-3}
21.7	20.36	3.50×10^{-2}	6.88×10^{-3}

Table A.16: Continued.

E_x (MeV)	$\theta_{\text{c.m.}}$ (deg)	$d\sigma/d\Omega$ (mb/sr)	error (mb/sr)
21.7	21.96	1.08×10^{-2}	3.82×10^{-3}
21.7	22.76	1.76×10^{-2}	4.57×10^{-3}
21.7	23.29	9.41×10^{-3}	3.34×10^{-3}
21.7	23.82	5.89×10^{-3}	2.64×10^{-3}
21.7	24.35	5.90×10^{-3}	2.64×10^{-3}
21.7	25.15	6.61×10^{-3}	2.37×10^{-3}
21.7	25.68	8.28×10^{-3}	2.65×10^{-3}
21.7	26.21	3.32×10^{-3}	1.68×10^{-3}
21.7	26.74	1.66×10^{-3}	1.18×10^{-3}
21.9	0.42	4.75	2.52×10^{-1}
21.9	1.25	4.54	1.39×10^{-1}
21.9	2.69	2.79	1.80×10^{-2}
21.9	3.21	2.66	1.76×10^{-2}
21.9	3.74	2.58	1.73×10^{-2}
21.9	4.26	2.51	1.71×10^{-2}
21.9	4.26	2.36	3.43×10^{-2}
21.9	4.78	2.52	3.54×10^{-2}
21.9	5.32	2.43	3.48×10^{-2}
21.9	5.84	2.44	3.49×10^{-2}
21.9	6.05	2.42	3.56×10^{-2}
21.9	6.58	2.23	3.41×10^{-2}
21.9	7.12	1.99	3.22×10^{-2}
21.9	7.66	1.67	2.95×10^{-2}
21.9	8.33	1.03	1.33×10^{-2}
21.9	8.86	9.12×10^{-1}	1.25×10^{-2}
21.9	9.40	7.49×10^{-1}	1.14×10^{-2}
21.9	9.94	6.53×10^{-1}	1.06×10^{-2}
21.9	10.74	5.59×10^{-1}	1.12×10^{-2}
21.9	11.28	5.62×10^{-1}	1.12×10^{-2}

Table A.16: Continued.

E_x (MeV)	$\theta_{\text{c.m.}}$ (deg)	$d\sigma/d\Omega$ (mb/sr)	error (mb/sr)
21.9	13.15	3.88×10^{-1}	9.16×10^{-3}
21.9	13.69	3.31×10^{-1}	8.47×10^{-3}
21.9	14.22	2.85×10^{-1}	7.85×10^{-3}
21.9	14.76	2.34×10^{-1}	7.12×10^{-3}
21.9	15.56	1.82×10^{-1}	7.14×10^{-3}
21.9	16.10	1.27×10^{-1}	5.99×10^{-3}
21.9	16.63	1.17×10^{-1}	5.74×10^{-3}
21.9	17.16	1.00×10^{-1}	5.30×10^{-3}
21.9	17.97	6.59×10^{-2}	4.02×10^{-3}
21.9	18.50	4.84×10^{-2}	3.45×10^{-3}
21.9	19.03	4.87×10^{-2}	3.45×10^{-3}
21.9	19.57	3.39×10^{-2}	2.89×10^{-3}
21.9	20.37	1.88×10^{-2}	5.23×10^{-3}
21.9	20.90	2.46×10^{-2}	5.99×10^{-3}
21.9	21.43	2.90×10^{-2}	6.51×10^{-3}
21.9	21.96	1.31×10^{-2}	4.37×10^{-3}
21.9	22.76	1.28×10^{-2}	4.29×10^{-3}
21.9	23.29	1.28×10^{-2}	4.30×10^{-3}
21.9	23.82	8.53×10^{-3}	3.52×10^{-3}
21.9	24.35	1.14×10^{-2}	4.06×10^{-3}
21.9	25.15	5.77×10^{-3}	2.20×10^{-3}
21.9	25.68	3.30×10^{-3}	1.66×10^{-3}
21.9	26.21	4.13×10^{-3}	1.86×10^{-3}
21.9	26.74	2.48×10^{-3}	1.45×10^{-3}
22.1	0.42	4.84	2.54×10^{-1}
22.1	1.25	4.53	1.38×10^{-1}
22.1	2.69	2.83	1.81×10^{-2}
22.1	3.21	2.67	1.76×10^{-2}
22.1	3.74	2.68	1.76×10^{-2}

Table A.16: Continued.

E_x (MeV)	$\theta_{\text{c.m.}}$ (deg)	$d\sigma/d\Omega$ (mb/sr)	error (mb/sr)
22.1	4.78	2.48	3.52×10^{-2}
22.1	5.32	2.65	3.64×10^{-2}
22.1	5.84	2.47	3.51×10^{-2}
22.1	6.05	2.46	3.59×10^{-2}
22.1	6.58	2.29	3.45×10^{-2}
22.1	7.12	2.03	3.25×10^{-2}
22.1	7.66	1.72	2.99×10^{-2}
22.1	8.33	1.04	1.35×10^{-2}
22.1	8.86	8.78×10^{-1}	1.24×10^{-2}
22.1	9.40	7.43×10^{-1}	1.14×10^{-2}
22.1	9.94	6.66×10^{-1}	1.08×10^{-2}
22.1	10.74	5.81×10^{-1}	1.14×10^{-2}
22.1	11.28	5.57×10^{-1}	1.11×10^{-2}
22.1	11.81	5.36×10^{-1}	1.09×10^{-2}
22.1	12.35	4.78×10^{-1}	1.03×10^{-2}
22.1	13.15	3.84×10^{-1}	9.13×10^{-3}
22.1	13.69	3.58×10^{-1}	8.80×10^{-3}
22.1	14.22	2.88×10^{-1}	7.90×10^{-3}
22.1	14.76	2.43×10^{-1}	7.26×10^{-3}
22.1	15.56	1.73×10^{-1}	7.03×10^{-3}
22.1	16.10	1.40×10^{-1}	6.34×10^{-3}
22.1	16.63	1.23×10^{-1}	5.92×10^{-3}
22.1	17.17	9.75×10^{-2}	5.27×10^{-3}
22.1	17.97	5.86×10^{-2}	3.74×10^{-3}
22.1	18.50	4.59×10^{-2}	3.31×10^{-3}
22.1	19.03	4.23×10^{-2}	3.18×10^{-3}
22.1	19.57	3.55×10^{-2}	2.92×10^{-3}
22.1	20.37	2.95×10^{-2}	7.00×10^{-3}
22.1	20.90	3.77×10^{-2}	7.92×10^{-3}

Table A.16: Continued.

E_x (MeV)	$\theta_{\text{c.m.}}$ (deg)	$d\sigma/d\Omega$ (mb/sr)	error (mb/sr)
22.1	22.76	1.02×10^{-2}	3.62×10^{-3}
22.1	23.29	1.53×10^{-2}	4.45×10^{-3}
22.1	23.83	5.11×10^{-3}	2.56×10^{-3}
22.1	24.36	1.02×10^{-2}	3.64×10^{-3}
22.1	25.15	3.21×10^{-3}	1.61×10^{-3}
22.1	25.68	5.62×10^{-3}	2.14×10^{-3}
22.1	26.21	3.22×10^{-3}	1.62×10^{-3}
22.1	26.74	5.64×10^{-3}	2.15×10^{-3}
22.3	0.42	4.57	2.48×10^{-1}
22.3	1.25	4.43	1.37×10^{-1}
22.3	2.69	2.92	1.83×10^{-2}
22.3	3.21	2.81	1.80×10^{-2}
22.3	3.74	2.74	1.78×10^{-2}
22.3	4.26	2.69	1.76×10^{-2}
22.3	4.26	2.58	3.58×10^{-2}
22.3	4.78	2.73	3.68×10^{-2}
22.3	5.32	2.63	3.62×10^{-2}
22.3	5.84	2.55	3.56×10^{-2}
22.3	6.05	2.53	3.63×10^{-2}
22.3	6.58	2.24	3.42×10^{-2}
22.3	7.12	1.97	3.21×10^{-2}
22.3	7.66	1.68	2.94×10^{-2}
22.3	8.33	1.01	1.32×10^{-2}
22.3	8.87	8.74×10^{-1}	1.23×10^{-2}
22.3	9.40	7.22×10^{-1}	1.12×10^{-2}
22.3	9.94	6.39×10^{-1}	1.05×10^{-2}
22.3	10.74	5.88×10^{-1}	1.15×10^{-2}
22.3	11.28	5.76×10^{-1}	1.14×10^{-2}
22.3	11.82	5.34×10^{-1}	1.09×10^{-2}

Table A.16: Continued.

E_x (MeV)	$\theta_{\text{c.m.}}$ (deg)	$d\sigma/d\Omega$ (mb/sr)	error (mb/sr)
22.3	13.69	3.45×10^{-1}	8.61×10^{-3}
22.3	14.23	2.98×10^{-1}	8.00×10^{-3}
22.3	14.76	2.39×10^{-1}	7.17×10^{-3}
22.3	15.56	1.64×10^{-1}	6.86×10^{-3}
22.3	16.10	1.42×10^{-1}	6.37×10^{-3}
22.3	16.63	9.96×10^{-2}	5.36×10^{-3}
22.3	17.17	9.37×10^{-2}	5.19×10^{-3}
22.3	17.97	6.62×10^{-2}	3.93×10^{-3}
22.3	18.50	5.23×10^{-2}	3.50×10^{-3}
22.3	19.04	4.34×10^{-2}	3.19×10^{-3}
22.3	19.57	3.72×10^{-2}	2.95×10^{-3}
22.3	20.37	2.06×10^{-2}	5.52×10^{-3}
22.3	20.90	1.62×10^{-2}	4.90×10^{-3}
22.3	21.43	1.77×10^{-2}	5.12×10^{-3}
22.3	21.97	1.18×10^{-2}	4.18×10^{-3}
22.3	22.76	4.48×10^{-3}	2.24×10^{-3}
22.3	23.30	8.97×10^{-3}	3.18×10^{-3}
22.3	23.83	8.98×10^{-3}	3.19×10^{-3}
22.3	24.36	8.99×10^{-3}	3.19×10^{-3}
22.3	25.15	3.09×10^{-3}	1.55×10^{-3}
22.3	25.68	1.55×10^{-3}	1.10×10^{-3}
22.3	26.21	2.32×10^{-3}	1.35×10^{-3}
22.3	26.74	3.88×10^{-3}	1.75×10^{-3}
22.5	0.42	4.70	2.52×10^{-1}
22.5	1.25	4.41	1.37×10^{-1}
22.5	2.69	2.94	1.84×10^{-2}
22.5	3.21	2.93	1.84×10^{-2}
22.5	3.74	2.88	1.82×10^{-2}
22.5	4.26	2.85	1.81×10^{-2}

Table A.16: Continued.

E_x (MeV)	$\theta_{\text{c.m.}}$ (deg)	$d\sigma/d\Omega$ (mb/sr)	error (mb/sr)
22.5	5.32	2.76	3.69×10^{-2}
22.5	5.85	2.64	3.61×10^{-2}
22.5	6.05	2.51	3.59×10^{-2}
22.5	6.58	2.31	3.45×10^{-2}
22.5	7.12	2.03	3.24×10^{-2}
22.5	7.66	1.67	2.93×10^{-2}
22.5	8.33	1.03	1.33×10^{-2}
22.5	8.87	8.79×10^{-1}	1.23×10^{-2}
22.5	9.40	7.41×10^{-1}	1.13×10^{-2}
22.5	9.94	6.45×10^{-1}	1.06×10^{-2}
22.5	10.74	5.57×10^{-1}	1.12×10^{-2}
22.5	11.28	5.52×10^{-1}	1.11×10^{-2}
22.5	11.82	5.00×10^{-1}	1.06×10^{-2}
22.5	12.35	4.84×10^{-1}	1.04×10^{-2}
22.5	13.16	4.08×10^{-1}	9.32×10^{-3}
22.5	13.69	3.37×10^{-1}	8.48×10^{-3}
22.5	14.23	2.82×10^{-1}	7.76×10^{-3}
22.5	14.76	2.28×10^{-1}	6.98×10^{-3}
22.5	15.57	1.62×10^{-1}	6.83×10^{-3}
22.5	16.10	1.33×10^{-1}	6.18×10^{-3}
22.5	16.63	1.12×10^{-1}	5.68×10^{-3}
22.5	17.17	9.48×10^{-2}	5.22×10^{-3}
22.5	17.97	6.73×10^{-2}	4.07×10^{-3}
22.5	18.50	5.36×10^{-2}	3.64×10^{-3}
22.5	19.04	4.74×10^{-2}	3.42×10^{-3}
22.5	19.57	3.79×10^{-2}	3.06×10^{-3}
22.5	20.37	3.02×10^{-2}	6.78×10^{-3}
22.5	20.90	2.12×10^{-2}	5.68×10^{-3}
22.5	21.44	1.21×10^{-2}	4.29×10^{-3}

Table A.16: Continued.

E_x (MeV)	$\theta_{\text{c.m.}}$ (deg)	$d\sigma/d\Omega$ (mb/sr)	error (mb/sr)
22.5	23.30	8.50×10^{-3}	3.01×10^{-3}
22.5	23.83	9.57×10^{-3}	3.20×10^{-3}
22.5	24.36	4.26×10^{-3}	2.13×10^{-3}
22.5	25.16	2.14×10^{-3}	1.24×10^{-3}
22.5	25.69	4.28×10^{-3}	1.75×10^{-3}
22.5	26.22	2.86×10^{-3}	1.43×10^{-3}
22.5	26.75	5.01×10^{-3}	1.90×10^{-3}
22.7	0.42	4.87	2.57×10^{-1}
22.7	1.25	4.45	1.37×10^{-1}
22.7	2.69	3.00	1.86×10^{-2}
22.7	3.21	2.97	1.85×10^{-2}
22.7	3.74	3.02	1.86×10^{-2}
22.7	4.26	2.93	1.84×10^{-2}
22.7	4.26	2.77	3.70×10^{-2}
22.7	4.78	2.78	3.71×10^{-2}
22.7	5.32	2.76	3.69×10^{-2}
22.7	5.85	2.69	3.64×10^{-2}
22.7	6.05	2.56	3.63×10^{-2}
22.7	6.58	2.42	3.53×10^{-2}
22.7	7.12	2.05	3.25×10^{-2}
22.7	7.66	1.68	2.94×10^{-2}
22.7	8.33	9.88×10^{-1}	1.31×10^{-2}
22.7	8.87	8.40×10^{-1}	1.20×10^{-2}
22.7	9.40	7.37×10^{-1}	1.13×10^{-2}
22.7	9.94	6.51×10^{-1}	1.06×10^{-2}
22.7	10.74	5.88×10^{-1}	1.14×10^{-2}
22.7	11.28	5.57×10^{-1}	1.11×10^{-2}
22.7	11.82	5.21×10^{-1}	1.08×10^{-2}
22.7	12.35	4.86×10^{-1}	1.04×10^{-2}

Table A.16: Continued.

E_x (MeV)	$\theta_{\text{c.m.}}$ (deg)	$d\sigma/d\Omega$ (mb/sr)	error (mb/sr)
22.7	14.23	2.87×10^{-1}	7.82×10^{-3}
22.7	14.76	2.40×10^{-1}	7.14×10^{-3}
22.7	15.57	1.57×10^{-1}	6.58×10^{-3}
22.7	16.10	1.19×10^{-1}	5.73×10^{-3}
22.7	16.64	1.15×10^{-1}	5.62×10^{-3}
22.7	17.17	1.03×10^{-1}	5.31×10^{-3}
22.7	17.97	6.22×10^{-2}	3.85×10^{-3}
22.7	18.51	5.29×10^{-2}	3.55×10^{-3}
22.7	19.04	4.42×10^{-2}	3.25×10^{-3}
22.7	19.57	3.29×10^{-2}	2.81×10^{-3}
22.7	20.37	3.81×10^{-2}	7.82×10^{-3}
22.7	20.91	1.59×10^{-2}	5.04×10^{-3}
22.7	21.44	1.91×10^{-2}	5.53×10^{-3}
22.7	21.97	1.27×10^{-2}	4.51×10^{-3}
22.7	22.77	1.61×10^{-2}	4.49×10^{-3}
22.7	23.30	1.36×10^{-2}	4.13×10^{-3}
22.7	23.83	8.69×10^{-3}	3.30×10^{-3}
22.7	24.36	7.46×10^{-3}	3.06×10^{-3}
22.7	25.16	3.25×10^{-3}	1.64×10^{-3}
22.7	25.69	3.25×10^{-3}	1.64×10^{-3}
22.7	26.22	7.32×10^{-3}	2.47×10^{-3}
22.7	26.75	4.08×10^{-3}	1.84×10^{-3}
22.9	0.42	4.84	2.55×10^{-1}
22.9	1.25	4.40	1.37×10^{-1}
22.9	2.69	3.11	1.89×10^{-2}
22.9	3.21	3.06	1.88×10^{-2}
22.9	3.74	3.00	1.86×10^{-2}
22.9	4.26	3.01	1.86×10^{-2}
22.9	4.26	2.83	3.72×10^{-2}

Table A.16: Continued.

E_x (MeV)	$\theta_{\text{c.m.}}$ (deg)	$d\sigma/d\Omega$ (mb/sr)	error (mb/sr)
22.9	5.85	2.72	3.65×10^{-2}
22.9	6.05	2.57	3.66×10^{-2}
22.9	6.59	2.36	3.49×10^{-2}
22.9	7.12	2.05	3.25×10^{-2}
22.9	7.66	1.75	3.00×10^{-2}
22.9	8.33	9.38×10^{-1}	1.27×10^{-2}
22.9	8.87	8.29×10^{-1}	1.20×10^{-2}
22.9	9.40	7.04×10^{-1}	1.10×10^{-2}
22.9	9.94	6.21×10^{-1}	1.04×10^{-2}
22.9	10.75	5.91×10^{-1}	1.14×10^{-2}
22.9	11.28	5.66×10^{-1}	1.12×10^{-2}
22.9	11.82	5.13×10^{-1}	1.06×10^{-2}
22.9	12.35	5.00×10^{-1}	1.05×10^{-2}
22.9	13.16	3.97×10^{-1}	9.21×10^{-3}
22.9	13.69	3.53×10^{-1}	8.68×10^{-3}
22.9	14.23	2.91×10^{-1}	7.88×10^{-3}
22.9	14.76	2.38×10^{-1}	7.12×10^{-3}
22.9	15.57	1.67×10^{-1}	6.86×10^{-3}
22.9	16.10	1.37×10^{-1}	6.21×10^{-3}
22.9	16.64	1.21×10^{-1}	5.85×10^{-3}
22.9	17.17	9.94×10^{-2}	5.30×10^{-3}
22.9	17.97	6.13×10^{-2}	3.82×10^{-3}
22.9	18.51	5.27×10^{-2}	3.54×10^{-3}
22.9	19.04	4.74×10^{-2}	3.36×10^{-3}
22.9	19.57	4.49×10^{-2}	3.27×10^{-3}
22.9	20.37	3.40×10^{-2}	7.28×10^{-3}
22.9	20.91	3.40×10^{-2}	7.30×10^{-3}
22.9	21.44	1.55×10^{-2}	4.91×10^{-3}
22.9	21.97	1.55×10^{-2}	4.92×10^{-3}

Table A.16: Continued.

E_x (MeV)	$\theta_{\text{c.m.}}$ (deg)	$d\sigma/d\Omega$ (mb/sr)	error (mb/sr)
22.9	23.83	4.56×10^{-3}	2.28×10^{-3}
22.9	24.36	6.84×10^{-3}	2.80×10^{-3}
22.9	25.16	3.68×10^{-3}	1.51×10^{-3}
22.9	25.69	3.69×10^{-3}	1.51×10^{-3}
22.9	26.22	3.08×10^{-3}	1.38×10^{-3}
22.9	26.75	6.17×10^{-4}	6.18×10^{-4}
23.1	0.42	4.48	2.47×10^{-1}
23.1	1.25	4.39	1.37×10^{-1}
23.1	2.69	3.01	1.86×10^{-2}
23.1	3.21	3.05	1.87×10^{-2}
23.1	3.74	3.05	1.87×10^{-2}
23.1	4.26	3.01	1.86×10^{-2}
23.1	4.26	2.74	3.67×10^{-2}
23.1	4.79	2.87	3.76×10^{-2}
23.1	5.32	2.86	3.75×10^{-2}
23.1	5.85	2.65	3.61×10^{-2}
23.1	6.05	2.62	3.67×10^{-2}
23.1	6.59	2.26	3.41×10^{-2}
23.1	7.12	1.97	3.19×10^{-2}
23.1	7.66	1.59	2.86×10^{-2}
23.1	8.33	9.64×10^{-1}	1.29×10^{-2}
23.1	8.87	8.20×10^{-1}	1.19×10^{-2}
23.1	9.41	6.90×10^{-1}	1.09×10^{-2}
23.1	9.94	6.08×10^{-1}	1.03×10^{-2}
23.1	10.75	5.70×10^{-1}	1.12×10^{-2}
23.1	11.28	5.65×10^{-1}	1.12×10^{-2}
23.1	11.82	5.47×10^{-1}	1.10×10^{-2}
23.1	12.36	5.14×10^{-1}	1.07×10^{-2}
23.1	13.16	4.11×10^{-1}	9.37×10^{-3}

Table A.16: Continued.

E_x (MeV)	$\theta_{\text{c.m.}}$ (deg)	$d\sigma/d\Omega$ (mb/sr)	error (mb/sr)
23.1	14.77	2.59×10^{-1}	7.44×10^{-3}
23.1	15.57	1.74×10^{-1}	7.00×10^{-3}
23.1	16.10	1.33×10^{-1}	6.11×10^{-3}
23.1	16.64	1.14×10^{-1}	5.66×10^{-3}
23.1	17.17	9.40×10^{-2}	5.15×10^{-3}
23.1	17.97	6.13×10^{-2}	3.84×10^{-3}
23.1	18.51	5.64×10^{-2}	3.69×10^{-3}
23.1	19.04	4.19×10^{-2}	3.18×10^{-3}
23.1	19.58	4.24×10^{-2}	3.20×10^{-3}
23.1	20.38	2.40×10^{-2}	6.21×10^{-3}
23.1	20.91	1.92×10^{-2}	5.56×10^{-3}
23.1	21.44	1.60×10^{-2}	5.08×10^{-3}
23.1	21.97	1.76×10^{-2}	5.33×10^{-3}
23.1	22.77	1.51×10^{-2}	4.21×10^{-3}
23.1	23.30	6.98×10^{-3}	2.86×10^{-3}
23.1	23.84	9.32×10^{-3}	3.31×10^{-3}
23.1	24.37	7.00×10^{-3}	2.86×10^{-3}
23.1	25.16	2.93×10^{-3}	1.47×10^{-3}
23.1	25.69	4.40×10^{-3}	1.80×10^{-3}
23.1	26.22	7.34×10^{-3}	2.33×10^{-3}
23.1	26.75	2.94×10^{-3}	1.47×10^{-3}
23.3	0.42	4.24	2.39×10^{-1}
23.3	1.25	4.24	1.34×10^{-1}
23.3	2.69	3.02	1.87×10^{-2}
23.3	3.21	2.95	1.84×10^{-2}
23.3	3.74	3.03	1.86×10^{-2}
23.3	4.26	3.04	1.87×10^{-2}
23.3	4.26	2.86	3.75×10^{-2}
23.3	4.79	2.84	3.74×10^{-2}

Table A.16: Continued.

E_x (MeV)	$\theta_{\text{c.m.}}$ (deg)	$d\sigma/d\Omega$ (mb/sr)	error (mb/sr)
23.3	6.05	2.56	3.62×10^{-2}
23.3	6.59	2.28	3.42×10^{-2}
23.3	7.12	2.00	3.20×10^{-2}
23.3	7.66	1.59	2.85×10^{-2}
23.3	8.33	9.47×10^{-1}	1.27×10^{-2}
23.3	8.87	7.98×10^{-1}	1.17×10^{-2}
23.3	9.41	6.95×10^{-1}	1.09×10^{-2}
23.3	9.94	6.03×10^{-1}	1.02×10^{-2}
23.3	10.75	5.88×10^{-1}	1.15×10^{-2}
23.3	11.28	5.77×10^{-1}	1.13×10^{-2}
23.3	11.82	5.42×10^{-1}	1.10×10^{-2}
23.3	12.36	5.36×10^{-1}	1.09×10^{-2}
23.3	13.16	4.20×10^{-1}	9.49×10^{-3}
23.3	13.70	3.58×10^{-1}	8.77×10^{-3}
23.3	14.23	3.31×10^{-1}	8.43×10^{-3}
23.3	14.77	2.57×10^{-1}	7.42×10^{-3}
23.3	15.57	1.59×10^{-1}	6.68×10^{-3}
23.3	16.11	1.36×10^{-1}	6.16×10^{-3}
23.3	16.64	1.15×10^{-1}	5.68×10^{-3}
23.3	17.17	1.02×10^{-1}	5.34×10^{-3}
23.3	17.98	6.49×10^{-2}	3.99×10^{-3}
23.3	18.51	5.55×10^{-2}	3.68×10^{-3}
23.3	19.04	4.49×10^{-2}	3.31×10^{-3}
23.3	19.58	3.89×10^{-2}	3.09×10^{-3}
23.3	20.38	3.03×10^{-2}	7.18×10^{-3}
23.3	20.91	1.86×10^{-2}	5.61×10^{-3}
23.3	21.44	2.20×10^{-2}	6.12×10^{-3}
23.3	21.98	1.52×10^{-2}	5.08×10^{-3}
23.3	22.77	1.29×10^{-2}	4.11×10^{-3}

Table A.16: Continued.

E_x (MeV)	$\theta_{\text{c.m.}}$ (deg)	$d\sigma/d\Omega$ (mb/sr)	error (mb/sr)
23.3	24.37	1.17×10^{-2}	3.91×10^{-3}
23.3	25.16	4.91×10^{-3}	2.02×10^{-3}
23.3	25.70	7.38×10^{-3}	2.48×10^{-3}
23.3	26.23	5.75×10^{-3}	2.19×10^{-3}
23.3	26.76	3.29×10^{-3}	1.65×10^{-3}
23.5	0.42	4.73	2.54×10^{-1}
23.5	1.25	4.13	1.33×10^{-1}
23.5	2.69	3.09	1.89×10^{-2}
23.5	3.21	3.05	1.87×10^{-2}
23.5	3.74	3.05	1.87×10^{-2}
23.5	4.26	3.02	1.86×10^{-2}
23.5	4.26	2.90	3.78×10^{-2}
23.5	4.79	2.87	3.76×10^{-2}
23.5	5.32	2.81	3.72×10^{-2}
23.5	5.85	2.71	3.65×10^{-2}
23.5	6.05	2.66	3.71×10^{-2}
23.5	6.59	2.34	3.46×10^{-2}
23.5	7.12	2.00	3.21×10^{-2}
23.5	7.66	1.66	2.92×10^{-2}
23.5	8.33	9.69×10^{-1}	1.29×10^{-2}
23.5	8.87	8.04×10^{-1}	1.17×10^{-2}
23.5	9.41	7.08×10^{-1}	1.10×10^{-2}
23.5	9.94	5.94×10^{-1}	1.01×10^{-2}
23.5	10.75	6.23×10^{-1}	1.19×10^{-2}
23.5	11.29	6.27×10^{-1}	1.19×10^{-2}
23.5	11.82	5.85×10^{-1}	1.15×10^{-2}
23.5	12.36	5.41×10^{-1}	1.11×10^{-2}
23.5	13.16	4.14×10^{-1}	9.40×10^{-3}
23.5	13.70	3.98×10^{-1}	9.21×10^{-3}

Table A.16: Continued.

E_x (MeV)	$\theta_{\text{c.m.}}$ (deg)	$d\sigma/d\Omega$ (mb/sr)	error (mb/sr)
23.5	15.57	1.83×10^{-1}	7.19×10^{-3}
23.5	16.11	1.58×10^{-1}	6.68×10^{-3}
23.5	16.64	1.26×10^{-1}	5.96×10^{-3}
23.5	17.18	1.16×10^{-1}	5.73×10^{-3}
23.5	17.98	6.70×10^{-2}	3.99×10^{-3}
23.5	18.51	5.34×10^{-2}	3.56×10^{-3}
23.5	19.05	5.05×10^{-2}	3.46×10^{-3}
23.5	19.58	4.36×10^{-2}	3.22×10^{-3}
23.5	20.38	1.96×10^{-2}	5.69×10^{-3}
23.5	20.91	1.96×10^{-2}	5.70×10^{-3}
23.5	21.45	2.29×10^{-2}	6.15×10^{-3}
23.5	21.98	1.97×10^{-2}	5.70×10^{-3}
23.5	22.78	1.25×10^{-2}	3.98×10^{-3}
23.5	23.31	8.79×10^{-3}	3.34×10^{-3}
23.5	23.84	1.13×10^{-2}	3.79×10^{-3}
23.5	24.37	7.55×10^{-3}	3.09×10^{-3}
23.5	25.17	4.40×10^{-3}	1.81×10^{-3}
23.5	25.70	5.88×10^{-3}	2.09×10^{-3}
23.5	26.23	3.68×10^{-3}	1.65×10^{-3}
23.5	26.76	2.21×10^{-3}	1.28×10^{-3}
23.7	0.42	4.64	2.51×10^{-1}
23.7	1.25	4.36	1.37×10^{-1}
23.7	2.69	3.17	1.91×10^{-2}
23.7	3.21	3.15	1.91×10^{-2}
23.7	3.74	3.14	1.90×10^{-2}
23.7	4.26	3.09	1.89×10^{-2}
23.7	4.26	2.96	3.82×10^{-2}
23.7	4.79	2.93	3.80×10^{-2}
23.7	5.32	2.89	3.77×10^{-2}

Table A.16: Continued.

E_x (MeV)	$\theta_{\text{c.m.}}$ (deg)	$d\sigma/d\Omega$ (mb/sr)	error (mb/sr)
23.7	6.59	2.37	3.51×10^{-2}
23.7	7.12	2.00	3.22×10^{-2}
23.7	7.66	1.71	2.97×10^{-2}
23.7	8.33	9.68×10^{-1}	1.29×10^{-2}
23.7	8.87	8.29×10^{-1}	1.19×10^{-2}
23.7	9.41	7.15×10^{-1}	1.11×10^{-2}
23.7	9.94	6.13×10^{-1}	1.03×10^{-2}
23.7	10.75	6.32×10^{-1}	1.19×10^{-2}
23.7	11.29	6.17×10^{-1}	1.18×10^{-2}
23.7	11.82	5.91×10^{-1}	1.15×10^{-2}
23.7	12.36	5.57×10^{-1}	1.12×10^{-2}
23.7	13.16	4.57×10^{-1}	9.91×10^{-3}
23.7	13.70	3.96×10^{-1}	9.23×10^{-3}
23.7	14.23	3.38×10^{-1}	8.52×10^{-3}
23.7	14.77	2.90×10^{-1}	7.89×10^{-3}
23.7	15.57	1.68×10^{-1}	6.93×10^{-3}
23.7	16.11	1.51×10^{-1}	6.56×10^{-3}
23.7	16.64	1.36×10^{-1}	6.23×10^{-3}
23.7	17.18	1.14×10^{-1}	5.69×10^{-3}
23.7	17.98	6.81×10^{-2}	4.04×10^{-3}
23.7	18.51	6.18×10^{-2}	3.84×10^{-3}
23.7	19.05	5.66×10^{-2}	3.68×10^{-3}
23.7	19.58	4.05×10^{-2}	3.12×10^{-3}
23.7	20.38	3.19×10^{-2}	7.34×10^{-3}
23.7	20.91	2.85×10^{-2}	6.95×10^{-3}
23.7	21.45	1.68×10^{-2}	5.33×10^{-3}
23.7	21.98	1.51×10^{-2}	5.60×10^{-3}
23.7	22.78	1.38×10^{-2}	4.42×10^{-3}
23.7	23.31	1.39×10^{-2}	4.41×10^{-3}

Table A.16: Continued.

E_x (MeV)	$\theta_{\text{c.m.}}$ (deg)	$d\sigma/d\Omega$ (mb/sr)	error (mb/sr)
23.7	25.17	4.88×10^{-3}	1.86×10^{-3}
23.7	25.70	4.89×10^{-3}	1.86×10^{-3}
23.7	26.23	3.50×10^{-3}	1.59×10^{-3}
23.7	26.76	2.10×10^{-3}	1.22×10^{-3}
23.9	0.42	4.35	2.44×10^{-1}
23.9	1.25	4.28	1.36×10^{-1}
23.9	2.69	3.23	1.93×10^{-2}
23.9	3.21	3.26	1.94×10^{-2}
23.9	3.74	3.21	1.92×10^{-2}
23.9	4.26	3.19	1.92×10^{-2}
23.9	4.26	3.10	3.93×10^{-2}
23.9	4.79	3.07	3.91×10^{-2}
23.9	5.32	3.02	3.87×10^{-2}
23.9	5.85	2.96	3.83×10^{-2}
23.9	6.05	2.70	3.73×10^{-2}
23.9	6.59	2.49	3.58×10^{-2}
23.9	7.13	2.17	3.34×10^{-2}
23.9	7.66	1.65	2.91×10^{-2}
23.9	8.33	1.01	1.32×10^{-2}
23.9	8.87	8.50×10^{-1}	1.21×10^{-2}
23.9	9.41	7.63×10^{-1}	1.15×10^{-2}
23.9	9.95	6.21×10^{-1}	1.04×10^{-2}
23.9	10.75	6.37×10^{-1}	1.19×10^{-2}
23.9	11.29	6.45×10^{-1}	1.20×10^{-2}
23.9	11.82	6.14×10^{-1}	1.17×10^{-2}
23.9	12.36	5.82×10^{-1}	1.14×10^{-2}
23.9	13.16	4.65×10^{-1}	9.98×10^{-3}
23.9	13.70	4.12×10^{-1}	9.38×10^{-3}
23.9	14.24	3.49×10^{-1}	8.64×10^{-3}

Table A.16: Continued.

E_x (MeV)	$\theta_{\text{c.m.}}$ (deg)	$d\sigma/d\Omega$ (mb/sr)	error (mb/sr)
23.9	16.11	1.52×10^{-1}	6.60×10^{-3}
23.9	16.64	1.39×10^{-1}	6.32×10^{-3}
23.9	17.18	1.14×10^{-1}	5.72×10^{-3}
23.9	17.98	6.92×10^{-2}	4.09×10^{-3}
23.9	18.51	6.23×10^{-2}	3.88×10^{-3}
23.9	19.05	5.15×10^{-2}	3.53×10^{-3}
23.9	19.58	4.75×10^{-2}	3.40×10^{-3}
23.9	20.38	2.46×10^{-2}	5.97×10^{-3}
23.9	20.92	1.88×10^{-2}	5.22×10^{-3}
23.9	21.45	2.46×10^{-2}	5.99×10^{-3}
23.9	21.98	2.61×10^{-2}	6.17×10^{-3}
23.9	22.78	1.46×10^{-2}	4.25×10^{-3}
23.9	23.31	1.22×10^{-2}	3.88×10^{-3}
23.9	23.84	2.45×10^{-3}	1.73×10^{-3}
23.9	24.37	6.13×10^{-3}	2.75×10^{-3}
23.9	25.17	3.26×10^{-3}	1.46×10^{-3}
23.9	25.70	3.26×10^{-3}	1.46×10^{-3}
23.9	26.23	3.27×10^{-3}	1.46×10^{-3}
23.9	26.76	1.96×10^{-3}	1.14×10^{-3}
24.1	0.42	4.54	2.46×10^{-1}
24.1	1.25	4.23	1.34×10^{-1}
24.1	2.69	3.25	1.94×10^{-2}
24.1	3.21	3.28	1.95×10^{-2}
24.1	3.74	3.27	1.94×10^{-2}
24.1	4.26	3.26	1.94×10^{-2}
24.1	4.26	3.08	3.91×10^{-2}
24.1	4.79	3.12	3.94×10^{-2}
24.1	5.33	3.13	3.94×10^{-2}
24.1	5.85	2.94	3.82×10^{-2}

Table A.16: Continued.

E_x (MeV)	$\theta_{\text{c.m.}}$ (deg)	$d\sigma/d\Omega$ (mb/sr)	error (mb/sr)
24.1	7.13	2.16	3.34×10^{-2}
24.1	7.66	1.76	3.00×10^{-2}
24.1	8.34	1.04	1.33×10^{-2}
24.1	8.87	8.34×10^{-1}	1.19×10^{-2}
24.1	9.41	7.41×10^{-1}	1.13×10^{-2}
24.1	9.95	6.31×10^{-1}	1.04×10^{-2}
24.1	10.75	6.55×10^{-1}	1.21×10^{-2}
24.1	11.29	6.23×10^{-1}	1.18×10^{-2}
24.1	11.82	6.11×10^{-1}	1.17×10^{-2}
24.1	12.36	5.85×10^{-1}	1.14×10^{-2}
24.1	13.17	4.81×10^{-1}	1.02×10^{-2}
24.1	13.70	4.46×10^{-1}	9.78×10^{-3}
24.1	14.24	3.70×10^{-1}	8.91×10^{-3}
24.1	14.77	2.84×10^{-1}	7.81×10^{-3}
24.1	15.58	2.09×10^{-1}	7.78×10^{-3}
24.1	16.11	1.79×10^{-1}	7.20×10^{-3}
24.1	16.65	1.26×10^{-1}	6.03×10^{-3}
24.1	17.18	1.11×10^{-1}	5.66×10^{-3}
24.1	17.98	7.08×10^{-2}	4.20×10^{-3}
24.1	18.52	6.83×10^{-2}	4.12×10^{-3}
24.1	19.05	5.14×10^{-2}	3.58×10^{-3}
24.1	19.58	4.93×10^{-2}	3.50×10^{-3}
24.1	20.38	2.18×10^{-2}	5.84×10^{-3}
24.1	20.92	3.27×10^{-2}	7.16×10^{-3}
24.1	21.45	1.87×10^{-2}	5.42×10^{-3}
24.1	21.98	2.18×10^{-2}	5.86×10^{-3}
24.1	22.78	9.33×10^{-3}	3.31×10^{-3}
24.1	23.31	8.18×10^{-3}	3.10×10^{-3}
24.1	23.85	4.68×10^{-3}	2.34×10^{-3}

Table A.16: Continued.

E_x (MeV)	$\theta_{\text{c.m.}}$ (deg)	$d\sigma/d\Omega$ (mb/sr)	error (mb/sr)
24.1	25.70	2.24×10^{-3}	1.30×10^{-3}
24.1	26.23	5.23×10^{-3}	1.99×10^{-3}
24.1	26.76	6.73×10^{-3}	2.26×10^{-3}
24.3	0.42	4.38	2.43×10^{-1}
24.3	1.25	4.51	1.39×10^{-1}
24.3	2.69	3.27	1.94×10^{-2}
24.3	3.21	3.33	1.96×10^{-2}
24.3	3.74	3.30	1.95×10^{-2}
24.3	4.26	3.32	1.96×10^{-2}
24.3	4.26	3.07	3.90×10^{-2}
24.3	4.79	3.24	4.00×10^{-2}
24.3	5.33	3.11	3.92×10^{-2}
24.3	5.85	2.94	3.82×10^{-2}
24.3	6.05	2.82	3.82×10^{-2}
24.3	6.59	2.52	3.61×10^{-2}
24.3	7.13	2.22	3.39×10^{-2}
24.3	7.66	1.80	3.06×10^{-2}
24.3	8.34	1.09	1.37×10^{-2}
24.3	8.87	8.57×10^{-1}	1.22×10^{-2}
24.3	9.41	7.62×10^{-1}	1.15×10^{-2}
24.3	9.95	6.59×10^{-1}	1.07×10^{-2}
24.3	10.75	6.53×10^{-1}	1.21×10^{-2}
24.3	11.29	6.34×10^{-1}	1.19×10^{-2}
24.3	11.83	6.03×10^{-1}	1.16×10^{-2}
24.3	12.36	5.76×10^{-1}	1.14×10^{-2}
24.3	13.17	4.74×10^{-1}	9.99×10^{-3}
24.3	13.70	4.12×10^{-1}	9.32×10^{-3}
24.3	14.24	3.65×10^{-1}	8.76×10^{-3}
24.3	14.77	2.99×10^{-1}	7.94×10^{-3}

Table A.16: Continued.

E_x (MeV)	$\theta_{\text{c.m.}}$ (deg)	$d\sigma/d\Omega$ (mb/sr)	error (mb/sr)
24.3	16.65	1.42×10^{-1}	6.28×10^{-3}
24.3	17.18	1.03×10^{-1}	5.35×10^{-3}
24.3	17.98	7.61×10^{-2}	4.29×10^{-3}
24.3	18.52	5.92×10^{-2}	3.79×10^{-3}
24.3	19.05	5.44×10^{-2}	3.63×10^{-3}
24.3	19.59	4.53×10^{-2}	3.31×10^{-3}
24.3	20.39	2.87×10^{-2}	6.78×10^{-3}
24.3	20.92	2.55×10^{-2}	6.40×10^{-3}
24.3	21.45	2.39×10^{-2}	6.20×10^{-3}
24.3	21.99	1.28×10^{-2}	4.53×10^{-3}
24.3	22.78	1.18×10^{-2}	3.96×10^{-3}
24.3	23.32	6.57×10^{-3}	2.96×10^{-3}
24.3	23.85	1.45×10^{-2}	4.39×10^{-3}
24.3	24.38	5.27×10^{-3}	2.64×10^{-3}
24.3	25.18	4.57×10^{-3}	1.73×10^{-3}
24.3	25.71	5.89×10^{-3}	1.97×10^{-3}
24.3	26.24	3.28×10^{-3}	1.47×10^{-3}
24.3	26.77	5.25×10^{-3}	1.86×10^{-3}
24.5	0.42	4.13	2.34×10^{-1}
24.5	1.25	4.19	1.33×10^{-1}
24.5	2.69	3.27	1.93×10^{-2}
24.5	3.21	3.26	1.93×10^{-2}
24.5	3.74	3.34	1.96×10^{-2}
24.5	4.26	3.26	1.93×10^{-2}
24.5	4.26	3.09	3.90×10^{-2}
24.5	4.79	3.12	3.92×10^{-2}
24.5	5.33	3.13	3.92×10^{-2}
24.5	5.85	2.98	3.83×10^{-2}
24.5	6.05	2.86	3.83×10^{-2}

Table A.16: Continued.

E_x (MeV)	$\theta_{\text{c.m.}}$ (deg)	$d\sigma/d\Omega$ (mb/sr)	error (mb/sr)
24.5	7.66	1.81	3.04×10^{-2}
24.5	8.34	1.08	1.37×10^{-2}
24.5	8.87	8.95×10^{-1}	1.24×10^{-2}
24.5	9.41	7.68×10^{-1}	1.15×10^{-2}
24.5	9.95	6.73×10^{-1}	1.08×10^{-2}
24.5	10.75	6.62×10^{-1}	1.21×10^{-2}
24.5	11.29	6.14×10^{-1}	1.16×10^{-2}
24.5	11.83	6.05×10^{-1}	1.15×10^{-2}
24.5	12.36	5.30×10^{-1}	1.08×10^{-2}
24.5	13.17	4.69×10^{-1}	1.00×10^{-2}
24.5	13.70	4.21×10^{-1}	9.49×10^{-3}
24.5	14.24	3.29×10^{-1}	8.40×10^{-3}
24.5	14.77	2.84×10^{-1}	7.80×10^{-3}
24.5	15.58	2.03×10^{-1}	7.58×10^{-3}
24.5	16.11	1.74×10^{-1}	7.02×10^{-3}
24.5	16.65	1.41×10^{-1}	6.32×10^{-3}
24.5	17.18	9.68×10^{-2}	5.24×10^{-3}
24.5	17.99	6.88×10^{-2}	4.13×10^{-3}
24.5	18.52	6.33×10^{-2}	3.96×10^{-3}
24.5	19.05	5.34×10^{-2}	3.64×10^{-3}
24.5	19.59	5.13×10^{-2}	3.56×10^{-3}
24.5	20.39	4.77×10^{-2}	8.21×10^{-3}
24.5	20.92	2.67×10^{-2}	6.14×10^{-3}
24.5	21.45	2.81×10^{-2}	6.31×10^{-3}
24.5	21.99	1.55×10^{-2}	4.68×10^{-3}
24.5	22.79	1.68×10^{-2}	4.70×10^{-3}
24.5	23.32	7.78×10^{-3}	3.19×10^{-3}
24.5	23.85	7.79×10^{-3}	3.19×10^{-3}
24.5	24.38	5.20×10^{-3}	2.61×10^{-3}

Table A.16: Continued.

E_x (MeV)	$\theta_{\text{c.m.}}$ (deg)	$d\sigma/d\Omega$ (mb/sr)	error (mb/sr)
24.5	26.24	6.27×10^{-3}	2.10×10^{-3}
24.5	26.77	1.39×10^{-3}	9.90×10^{-4}
24.7	0.42	4.80	2.54×10^{-1}
24.7	1.25	4.31	1.35×10^{-1}
24.7	2.69	3.35	1.96×10^{-2}
24.7	3.22	3.30	1.95×10^{-2}
24.7	3.74	3.34	1.96×10^{-2}
24.7	4.26	3.32	1.95×10^{-2}
24.7	4.26	3.19	3.95×10^{-2}
24.7	4.79	3.15	3.93×10^{-2}
24.7	5.33	3.19	3.96×10^{-2}
24.7	5.85	2.94	3.79×10^{-2}
24.7	6.05	2.89	3.86×10^{-2}
24.7	6.59	2.66	3.70×10^{-2}
24.7	7.13	2.20	3.37×10^{-2}
24.7	7.67	1.84	3.09×10^{-2}
24.7	8.34	1.07	1.35×10^{-2}
24.7	8.87	8.82×10^{-1}	1.23×10^{-2}
24.7	9.41	7.97×10^{-1}	1.17×10^{-2}
24.7	9.95	6.68×10^{-1}	1.07×10^{-2}
24.7	10.75	6.32×10^{-1}	1.18×10^{-2}
24.7	11.29	6.33×10^{-1}	1.18×10^{-2}
24.7	11.83	5.92×10^{-1}	1.15×10^{-2}
24.7	12.36	5.50×10^{-1}	1.11×10^{-2}
24.7	13.17	4.61×10^{-1}	9.96×10^{-3}
24.7	13.70	4.14×10^{-1}	9.44×10^{-3}
24.7	14.24	3.43×10^{-1}	8.59×10^{-3}
24.7	14.78	2.70×10^{-1}	7.63×10^{-3}
24.7	15.58	1.87×10^{-1}	7.22×10^{-3}

Table A.16: Continued.

E_x (MeV)	$\theta_{\text{c.m.}}$ (deg)	$d\sigma/d\Omega$ (mb/sr)	error (mb/sr)
24.7	17.18	9.85×10^{-2}	5.25×10^{-3}
24.7	17.99	6.55×10^{-2}	4.00×10^{-3}
24.7	18.52	6.08×10^{-2}	3.85×10^{-3}
24.7	19.06	5.02×10^{-2}	3.50×10^{-3}
24.7	19.59	3.81×10^{-2}	3.05×10^{-3}
24.7	20.39	4.73×10^{-2}	9.53×10^{-3}
24.7	20.92	3.03×10^{-2}	7.61×10^{-3}
24.7	21.46	2.08×10^{-2}	6.32×10^{-3}
24.7	21.99	3.04×10^{-2}	7.63×10^{-3}
24.7	22.79	1.30×10^{-2}	3.94×10^{-3}
24.7	23.32	1.18×10^{-2}	3.76×10^{-3}
24.7	23.85	1.42×10^{-2}	4.12×10^{-3}
24.7	24.38	7.12×10^{-3}	2.92×10^{-3}
24.7	25.18	4.28×10^{-3}	1.76×10^{-3}
24.7	25.71	5.00×10^{-3}	1.90×10^{-3}
24.7	26.24	5.01×10^{-3}	1.91×10^{-3}
24.7	26.77	1.43×10^{-3}	1.02×10^{-3}
24.9	0.42	4.29	2.40×10^{-1}
24.9	1.25	4.53	1.38×10^{-1}
24.9	2.69	3.43	1.99×10^{-2}
24.9	3.22	3.36	1.97×10^{-2}
24.9	3.74	3.34	1.96×10^{-2}
24.9	4.26	3.33	1.96×10^{-2}
24.9	4.26	3.17	3.94×10^{-2}
24.9	4.79	3.23	3.98×10^{-2}
24.9	5.33	3.07	3.88×10^{-2}
24.9	5.85	2.97	3.81×10^{-2}
24.9	6.05	2.88	3.85×10^{-2}
24.9	6.59	2.58	3.64×10^{-2}

Table A.16: Continued.

E_x (MeV)	$\theta_{\text{c.m.}}$ (deg)	$d\sigma/d\Omega$ (mb/sr)	error (mb/sr)
24.9	8.34	1.05	1.34×10^{-2}
24.9	8.88	8.83×10^{-1}	1.23×10^{-2}
24.9	9.41	7.81×10^{-1}	1.16×10^{-2}
24.9	9.95	6.75×10^{-1}	1.08×10^{-2}
24.9	10.76	6.18×10^{-1}	1.17×10^{-2}
24.9	11.29	6.11×10^{-1}	1.16×10^{-2}
24.9	11.83	5.77×10^{-1}	1.13×10^{-2}
24.9	12.37	5.26×10^{-1}	1.08×10^{-2}
24.9	13.17	4.55×10^{-1}	9.91×10^{-3}
24.9	13.71	3.87×10^{-1}	9.14×10^{-3}
24.9	14.24	3.18×10^{-1}	8.29×10^{-3}
24.9	14.78	2.75×10^{-1}	7.71×10^{-3}
24.9	15.58	1.92×10^{-1}	7.35×10^{-3}
24.9	16.12	1.57×10^{-1}	6.64×10^{-3}
24.9	16.65	1.31×10^{-1}	6.05×10^{-3}
24.9	17.19	1.08×10^{-1}	5.51×10^{-3}
24.9	17.99	7.24×10^{-2}	4.19×10^{-3}
24.9	18.52	5.50×10^{-2}	3.65×10^{-3}
24.9	19.06	4.92×10^{-2}	3.46×10^{-3}
24.9	19.59	3.99×10^{-2}	3.11×10^{-3}
24.9	20.39	3.07×10^{-2}	6.89×10^{-3}
24.9	20.92	2.30×10^{-2}	5.97×10^{-3}
24.9	21.46	2.00×10^{-2}	5.57×10^{-3}
24.9	21.99	1.69×10^{-2}	5.12×10^{-3}
24.9	22.79	1.67×10^{-2}	4.32×10^{-3}
24.9	23.32	1.23×10^{-2}	3.70×10^{-3}
24.9	23.85	5.58×10^{-3}	2.50×10^{-3}
24.9	24.39	2.23×10^{-3}	1.58×10^{-3}
24.9	25.18	5.61×10^{-3}	1.99×10^{-3}

Table A.16: Continued.

E_x (MeV)	$\theta_{\text{c.m.}}$ (deg)	$d\sigma/d\Omega$ (mb/sr)	error (mb/sr)
24.9	26.77	2.11×10^{-3}	1.22×10^{-3}

Bibliography

[1] M. G. Mayer, Phys. Rev. **75**, 1969 (1949).

[2] M. G. Mayer, Phys. Rev. **78**, 16 (1950).

[3] O. Haxel, J. H. D. Jensen, and H. E Suess, Phys. Rev. **75**, 1766 (1949).

[4] O. Haxel, J. H. D. Jensen, and H. E Suess, Z. Physik **128**, 295 (1950).

[5] J. Chadwick C. D. Ellis G. Gamow R. H. Fowler O. W. Richardson Ernest Rutherford, F. W. Aston and D. R. Hartree, Roy. Soc. Proc. **123**, 373 (1929).

[6] W. Wefelmeier, Z. Physik **107**, 332 (1937).

[7] L. R. Hafstad and E. Teller, Phys. Rev. **54**, 681 (1938).

[8] D. Brink, Proc. international school of physics "enrico fermi" course **36** (1965), ed. by C. Bloch, (Academic Press, 1966) p. 247.

[9] Y. Fujiwara, H. Horiuchi, K. Ikeda, M. Kamimura, K. Kato, Y. Suzuki, and E. Uegaki, Prog. Theor. Phys. Suppl. **68**, 29 (1980).

[10] E. Uegaki, S. Okabe, Y. Abe, and H. Tanaka, Prog. Theor. Phys. **57**, 1262 (1977).

[11] M. Kamimura, Nucl. Phys. A **351**, 456 (1981).

[12] V. Gillet and N. V. Mau, Nuclear Physics **54**, 321 (1964).

[13] S. Cohen and D. Kurath, Nuclear Physics **73**, 1 (1965).

[14] M. Bouten, P. V. Leuven, and H. Depuydt, Nucl. Phys. A **94**, 687 (1967).

[15] H. Horiuchi, K. Ikeda, and N. Takigawa, Prog. Theor. Phys. Suppl. **E68**, 464 (1968).

[16] W. von Oertzen, M. Freer, and Y. Kanada-En'yo, Phys. Rep. **432**, 43 (2006).

[17] M. Freer, H. Horiuchi, Y. Kanada-En'yo, D. Lee, and Ulf-G. Meißner, Rev. Mod. Phys. **90**, 035004 (2018).

[18] M. Freer and H. O. U. Fynbo, Prog. Part. Nucl. Phys. **78**, 1 (2014).

[19] F. Hoyle, Astrophys. J. Suppl. Ser. **1**, 121 (1954).

[20] D.N.F Dunbar, R.E. Pixley, W.A. Wenzel, and W. Whaling, Phys. Rev. **92**, 649 (1953).

[21] C.W. Cook, W.A. Fowler, C.C. Lauritsen, and T. Lane, Phys. Rev. **107**, 508 (1957).

[22] S. Kubono, Z. Phys. A **349**, 237 (1994).

[23] S. Kubono, AIP Conf. Proc. **1213**, 107 (2010).

[24] H. Morinaga, Phys. Rev. **101**, 254 (1956).

[25] H. Morinaga, Phys. Lett. **21**, 78 (1966).

[26] A. Tohsaki, H. Horiuchi, P. Schuck, and G. Röpke, Phys. Rev. Lett. **87**, 192501 (2001).

[27] Y. Funaki, A. Tohsaki, H. Horiuchi, P. Schuck, and G. Röpke, Phys. Rev. C **67**, 051306 (2003).

[28] T. Yamada and P. Schuck, Euro. Phys. J. A **26**, 185 (2005).

[29] T Yamada and P Schuck, Phys. Rev. C **69**, 024309 (2004).

[30] M. Chernykh, H. Feldmeier, T. Neff, P. von Neumann-Cosel, and A. Richter, Phys. Rev. Lett. **98**, 032501 (2007).

[31] Ad R. Raduta, B. Borderie, E. Geraci, N. Le Neindre, P. Napolitani, M. F. Rivet, R. Alba, F. Amorini, G. Cardella, M. Chatterjee, E. De Filippo, D. Guinet, P. Lautesse, E. La Guidara, G. Lanzalone, G. Lanzano, I. Lombardo, O. Lopez, C. Maiolino, A. Pagano, S. Pirrone, G. Politi, F. Porto, F. Rizzo, P. Russotto, and J. P. Wieleczko, Phys. Lett. B **705**, 65 (2011).

[32] M. Itoh, H. Akimune, M. Fujiwara, U. Garg, H. Hashimoto, T. Kawabata, K. Kawase, S. Kishi, T. Murakami, K. Nakanishi, Y. Nakatsugawa, B. K. Nayak, H. Sakaguchi, S. Terashima, M. Uchida, Y. Yasuda, M. Yosoi, and J. Zenihiro, Journal of Physics: Conference Series **569** (2014).

[33] R. Smith, Tz Kokalova, C. Wheldon, J. E. Bishop, M. Freer, N. Curtis, and D. J. Parker, Phys. Rev. Lett. **119**, 1 (2017).

[34] T. Wakasa, E. Ihara, K. Fujita, Y. Funaki, K. Hatanaka, H. Horiuchi, M. Itoh, J. Kamiya, G. Röpke, H. Sakaguchi, N. Sakamoto, Y. Sakemi, P. Schuck, Y. Shimizu, M. Takashina, S. Terashima, A. Tohsaki, M. Uchida, H. P. Yoshida, and M. Yosoi, Phys. Lett. B **653**, 173 (2007).

[35] T. Hayamizu A. Oikawa Y. Sakemi M. Itoh, T. Takahashi and H. Yoshida, Mod. Phys. Lett. A **25**, 1935 (2010).

[36] A. A. Ogloblin, A. N. Danilov, A. S. Demyanova, S. A. Goncharov, and T. L. Belyaeva, Phys. Rev. C **94**, 051602 (2016).

[37] K. C. W. Li, R. Neveling, P. Adsley, P. Papka, F. D. Smit, J. W. Brümmer, C. Aa. Diget, M. Freer, M. N. Harakeh, Tz. Kokalova, F. Nemulodi, L. Pellegri, B. Rebeiro, J. A. Swartz, S. Triambak, J. J. van Zyl, and C. Wheldon, Phys. Rev. C **95**, 031302 (2017).

[38] S. Adachi, Y. Fujikawa, T. Kawabata, H. Akimune, T. Doi, T. Furuno, T. Harada, K. Inaba, S. Ishida, M. Itoh, C. Iwamoto, N. Kobayashi, Y. Maeda, Y. Matsuda, M. Murata, S. Okamoto, A. Sakaue, R. Sekiya, A. Tamii, and M. Tsumura, Phys. Lett. B **819**, 136411 (2021).

[39] T. Kawabata, T. Adachi, M. Fujiwara, K. Hatanaka, Y. Ishiguro, M. Itoh, Y. Maeda, H. Matsubara, H. Miyasako, Y. Nozawa, T. Saito, S. Sakaguchi, Y. Sasamoto, Y. Shimizu, T. Takahashi, A. Tamii, S. Terashima, H. Tokieda, N. Tomida, T. Uesaka, M. Uchida, Y. Yasuda, N. Yokota, H. P. Yoshida, and J. Zenihiro, Few-Body Systems **54**, 93 (2013).

[40] M. Freer L. Acosta M. Assié S. Bailey G. Cardella N. Curtis E. De Filippo D. Dell' Aquila S. De Luca L. Francalanza B. Gnoffo G. Lanzalone I. Lombardo N.S. Martorana S. Norella A. Pagano E.V. Pagano M. Papa S. Pirrone G. Politi F. Rizzo P. Russotto L. Quattrocchi R. Smith I. Stefan A. Trifirò M. Trimarchì G. Verde M. Vigilante J. Bishop, Tz. Kokalova and C. Wheldon, Phys. Rev. C **100**, 034320 (2019).

[41] L. M. Satarov, I. N. Mishustin, A. Motornenko, V. Vovchenko, M. I. Gorenstein, and H. Stoecker, Phys. Rev. C **99**, 024909 (2019).

[42] Z. Zhang and L. Chen, Phys. Rev. C **100**, 054304 (2019).

[43] L. M. Satarov, M. I. Gorenstein, I. N. Mishustin, and H. Stoecker, Phys. Rev. C **101**, 024913 (2020).

[44] L. M. Satarov, R. V. Poberezhnyuk, I. N. Mishustin, and H. Stoecker, Phys. Rev. C **103**, 024301 (2021).

[45] S. Typel, G. Röpke, T. Klähn, D. Blaschke, and H. H. Wolter, Phys. Rev. C **81**, 015803 (2010).

[46] T. Kawabata, H. Akimune, H. Fujimura, H. Fujita, Y. Fujita, M. Fujiwara, K. Hara, K. Y. Hara, K. Hatanaka, T. Ishikawa, M. Itoh, J. Kamiya, S. Kishi, M. Nakmura, K. Nakanishi, T. Noro, H. Sakaguchi, Y. Shimbara, H. Takeda, A. Tamii, S. Terashima, H. Toyokawa, M. Uchida, H. Ueno, T. Wakasa, Y. Yasuda, H. P. Yoshida, and M. Yosoi, Phys. Rev. C **70**, 034318 (2004).

[47] T. Kawabata, H. Akimune, H. Fujita, Y. Fujita, M. Fujiwara, K. Hara, K. Hatanaka, M. Itoh, Y. Kanada-En'yo, S. Kishi, K. Nakanishi, H. Sakaguchi, Y. Shimbara, A. Tamii, S. Terashima, M. Uchida, T. Wakasa, Y. Yasuda, H. P. Yoshida, and M. Yosoi, Phys. Lett. B **646**, 6 (2007).

[48] F. Ajzenberg-Selove, Nucl. Phys. A **523**, 1 (1991).

[49] T. Yamada and Y. Funaki, Phys. Rev. C **82**, 064315 (2010).

[50] Y. Kanada-En'Yo and T. Suhara, Phys. Rev. C **91**, 014316 (2015).

[51] B. Zhou and M. Kimura, Phys. Rev. C **98**, 054323 (2018).

[52] T. Yamada and Y. Funaki, Phys. Rev. C **92**, 034326 (2015).

[53] Y. Chiba and M. Kimura, Phys. Rev. C **101**, 024317 (2020).

[54] T. Yamada, Y. Funaki, H. Horiuchi, K. Ikeda, and A. Tohsaki, Prog. Theor. Phys. **120**, 1139 (2009).

[55] B. F. Bayman and A. Bohr, Nucl. Phys. **9**, 596 (1958/1959).

[56] Y. Chiba, M. Kimura, and Y. Taniguchi, Phys. Rev. C **93**, 034319 (2016).

[57] Y. Kanada-En'Yo, Phys. Rev. C **93**, 024322 (2016).

[58] Y. Chiba, Y. Taniguchi, and M. Kimura, Phys. Rev. C **95**, 044328 (2017).

[59] S. Adachi, T. Kawabata, K. Minomo, T. Kadoya, N. Yokota, H. Akimune, T. Baba, H. Fujimura, M. Fujiwara, Y. Funaki, T. Furuno, T. Hashimoto, K. Hatanaka, K. Inaba, Y. Ishii, M. Itoh, C. Iwamoto, K. Kawase, Y. Maeda, H. Matsubara, Y. Matsuda, H. Matsuno, T. Morimoto, H. Morita, M. Murata, T. Nanamura, I. Ou, S. Sakaguchi, Y. Sasamoto, R. Sawada, Y. Shimizu, K. Suda, A. Tamii, Y. Tameshige, M. Tsumura, M. Uchida, T. Uesaka, H. P. Yoshida, and S. Yoshida, Phys. Rev. C **97**, 014601 (2018).

[60] H. J. Lu, S. Brandenburg, R. De Leo, M. N. Harakeh, T. D. Poelhekken, and A. van der Woude, Phys. Rev. C **33**, 1116 (1986).

[61] D. H. Youngblood, Y.-W. Lui, and H. L. Clark, Phys. Rev. C **60**, 014304 (1999).

[62] M. Itoh, H. Sakaguchi, M. Uchida, T. Ishikawa, T. Kawabata, T. Murakami, H. Takeda, T. Taki, S. Terashima, N. Tsukahara, Y. Yasuda, M. Yosoi, U. Garg, M. Hedden, B. Kharraja, M. Koss, B.K. Nayak, S. Zhu, H. Fujimura, M. Fujiwara, K. Hara, H.P. Yoshida, H. Akimune, M.N. Harakeh, and M. Volkerts, Phys. Lett. B **549**, 58 (2002).

[63] M. Uchida, H. Sakaguchi, M. Itoh, M. Yosoi, T. Kawabata, H. Takeda, Y. Yasuda, T. Murakami, T. Ishikawa, T. Taki, N. Tsukahara, S. Terashima, U. Garg, M. Hedden, B. Kharraja, M. Koss, B.K. Nayak, S. Zhu, M. Fujiwara, H. Fujimura, K. Hara, E. Obayashi, H.P. Yoshida, H. Akimune, M.N. Harakeh, and M. Volkerts, Phys. Lett. B **557**, 12 (2003).

[64] M. Itoh, H. Sakaguchi, M. Uchida, T. Ishikawa, T. Kawabata, T. Murakami, H. Takeda, T. Taki, S. Terashima, N. Tsukahara, Y. Yasuda, M. Yosoi, U. Garg, M. Hedden, B. Kharraja, M. Koss, B. K. Nayak, S. Zhu, H. Fujimura, M. Fujiwara, K. Hara, H. P. Yoshida, H. Akimune, M. N. Harakeh, and M. Volkerts, Phys. Rev. C **68**, 064602 (2003).

[65] M. Uchida, H. Sakaguchi, M. Itoh, M. Yosoi, T. Kawabata, Y. Yasuda, H. Takeda, T. Murakami, S. Terashima, S. Kishi, U. Garg, P. Boutachkov, M. Hedden, B. Kharraja, M. Koss, B. K. Nayak, S. Zhu, M. Fujiwara, H. Fujimura, H. P. Yoshida, K. Hara, H. Akimune, and M. N. Harakeh, Phys. Rev. C **69**, 051301 (2004).

[66] T. Li, U. Garg, Y. Liu, R. Marks, B. K. Nayak, P. V. Madhusudhana Rao, M. Fujiwara, H. Hashimoto, K. Kawase, K. Nakanishi, S. Okumura, M. Yosoi, M. Itoh, M. Ichikawa, R. Matsuo, T. Terazono, M. Uchida, T. Kawabata, H. Akimune, Y. Iwao, T. Murakami, H. Sakaguchi, S. Terashima, Y. Yasuda, J. Zenihiro, and M. N. Harakeh, Phys. Rev. Lett. **99**, 162503 (2007).

[67] M. Itoh, H. Akimune, M. Fujiwara, U. Garg, N. Hashimoto, T. Kawabata, K. Kawase, S. Kishi, T. Murakami, K. Nakanishi, Y. Nakatsugawa, B. K. Nayak, S. Okumura, H. Sakaguchi, H. Takeda, S. Terashima, M. Uchida, Y. Yasuda, M. Yosoi, and J. Zenihiro, Phys. Rev. C **84**, 054308 (2011).

[68] M. Itoh, S. Kishi, H. Sakaguchi, H. Akimune, M. Fujiwara, U. Garg, K. Hara, H. Hashimoto, J. Hoffman, T. Kawabata, K. Kawase, T. Murakami, K. Nakanishi, B. K. Nayak, S. Terashima, M. Uchida, Y. Yasuda, and M. Yosoi, Phys. Rev. C **88**, 064313 (2013).

[69] Y. K. Gupta, U. Garg, J. Hoffman, J. Matta, P. V. Madhusudhana Rao, D. Patel, T. Peach, K. Yoshida, M. Itoh, M. Fujiwara, K. Hara, H. Hashimoto, K. Nakanishi, M. Yosoi, H. Sakaguchi, S. Terashima, S. Kishi, T. Murakami, M. Uchida, Y. Yasuda, H. Akimune, T. Kawabata, and M. N. Harakeh, Phys. Rev. C **93**, 044324 (2016).

[70] T. Peach, U. Garg, Y. K. Gupta, J. Hoffman, J. T. Matta, D. Patel, P. V. Madhusudhana Rao, K. Yoshida, M. Itoh, M. Fujiwara, K. Hara, H. Hashimoto, K. Nakanishi, M. Yosoi, H. Sakaguchi, S. Terashima, S. Kishi, T. Murakami, M. Uchida, Y. Yasuda, H. Akimune, T. Kawabata, M. N. Harakeh, and G. Colò, Phys. Rev. C **93**, 064325 (2016).

[71] M. N. Harakeh and A. van der Woude, *Giant Resonances*, (Oxford University Press, 2001).

[72] M. Fujiwara, H. Akimune, I. Daito, H. Fujimura, Y. Fujita, K. Hatanaka, H. Ikegami, I. Katayama, K. Nagayama, N. Matsuoka, S. Morinobu, T. Noro, M. Yoshimura, H. Sakaguchi, Y. Sakemi, A. Tamii, and M. Yosoi, Nucl. Instrum. Methods Phys. Res. Sect. A **422**, 484 (1999).

[73] T Wakasa, K Hatanaka, Y Fujita, G.P.A Berg, H Fujimura, H Fujita, M Itoh, J Kamiya, T Kawabata, K Nagayama, T Noro, H Sakaguchi, Y Shimbara, H Takeda, K Tamura,

H Ueno, M Uchida, M Uraki, and M Yosoi, Nucl. Instrum. Methods Phys. Res. Sect. A **482**, 79 (2002).

[74] I. Sugai, Y. Takeda, H. Makii, K. Sano, and Y. Nagai, Nucl. Instrum. Methods Phys. Res. Sect. A **521**, 227 (2004).

[75] T. Kawabata, H. Sakaguchi, A. Tamii, H. Takeda, T. Taki, and H Yoshida, Rcnp annual report 1996, p.161 (1996).

[76] W.R. Leo, *Techniques for Nuclear an Particle Physics Experiments*, (Springer-Verlag, 1993).

[77] J. Raynel, ECIS-95 computer program (1995) [old version of ECIS-12, NEA-0850/19].

[78] H. De Vries, C. W. De Jager, and C. De Vries, At. Data Nucl. Data Tables **36**, 495 (1987).

[79] G. R. Satchler and Dao T. Khoa, Phys. Rev. C **55**, 285 (1997).

[80] Y. Kanada-En'yo and K. Ogata, Phys. Rev. C **99**, 064601 (2019).

[81] Y. Kanada-En'yo and K. Ogata, Phys. Rev. C **99**, 064608 (2019).

[82] Y. Kanada-En'yo and K. Ogata, Phys. Rev. C **101**, 064308 (2020).

[83] Y. Kanada-En'yo and K. Ogata, Phys. Rev. C **101**, 064607 (2020).

[84] Y. Kanada-En'yo and K. Ogata, Phys. Rev. C **103**, 024603 (2021).

[85] M. N. Harakeh and A. E.L. Dieperink, Phys. Rev. C **23**, 2329 (1981).

[86] G. R. Satchler, Nucl. Phys. A **472**, 215 (1987).

[87] P. M. Endt, At. Data Nucl. Data Tables **55**, 171 (1993).

[88] J. W. Jury, B. L. Berman, D. D. Faul, P. Meyer, K. G. McNeill, and J. G. Woodworth, Phys. Rev. C, **19** (1979).

[89] D. Zubanov, R. A. Sutton, M. N. Thompson, and J. W. Jury, Phys. Rev. C **27**, 1957 (1983).

[90] G. R. Satchler and Dao T. Khoa, Phys. Rev. C **55**, 285 (1997).

[91] J. Zenihiro, H. Sakaguchi, T. Murakami, M. Yosoi, Y. Yasuda, S. Terashima, Y. Iwao, H. Takeda, M. Itoh, H. P. Yoshida, and M. Uchida, Phys. Rev. C **82**, 1 (2010).

[92] M. Milin and W. von Oertzen, Eur. Phys. J. A **14**, 295 (2002).

[93] P. R. Wrean, C. R. Brune, and R. W. Kavanagh, Phys. Rev. C **49**, 1205 (1994).

[94] R. Kunz, S. Barth, A. Denker, H. W. Drotleff, J. W. Hammer, H. Knee, and A. Mayer, Phys. Rev. C **53**, 2486 (1996).

[95] C. Wheldon, N. I. Ashwood, M. Barr, N. Curtis, M. Freer, Tz. Kokalova, J. D. Malcolm, V. A. Ziman, Th. Faestermann, H.-F. Wirth, R. Hertenberger, and R. Lutter, Phys. Rev. C **86**, 044328 (2012).

[96] T. Suzuki, R. Fujimoto, and T. Otsuka, Phys. Rev. C **67**, 15 (2003).

[97] B. A. Brown and W. D. M. Rae, Nucl. Data Sheets **120**, 115 (2014).

[98] H. Fujimura, H. Akimune, I. Daito, M. Fujiwara, K. Hara, K. Y. Hara, M. N. Harakeh, F. Ihara, T. Inomata, K. Ishibashi, T. Ishikawa, T. Kawabata, A. Tamii, M. Tanaka, H. Toyokawa, T. Yamanaka, and M. Yosoi, Phys. Rev. C **69**, 1 (2004).

[99] Y. Funaki, A. Tohsaki, H. Horiuchi, P. Schuck, and G. Röpke, Euro. Phys. J. A **24**, 321 (2005).

[100] H. Kanada, T. Kaneko, S. Nagata, and M. Nomoto, Prog. Theor. Phys. **61**, 1327 (1979).